DISSERTATION

PART I: DEVELOPMENT OF PLASMA SURFACE MODIFICATION AND CHARACTERIZATION STRATEGIES FOR THREE-DIMENSIONAL POLYMER CONSTRUCTS USED IN BIOLOGICAL APPLICATIONS

AND

PART II: EXPLORING GENERAL CHEMISTRY STUDENTS' METACOGNITIVE MONITORING ON EXAMINATIONS

Submitted by

Morgan Johanna Hawker

Department of Chemistry

In partial fulfillment of the requirements

For the Degree of Doctor of Philosophy

Colorado State University

Fort Collins, Colorado

Fall 2016

Doctoral Committee:

Advisor: Ellen R. Fisher

Dawn Rickey
Carmen S. Menoni
George Barisas
Matthew G. Rhodes

ABSTRACT

PART I: DEVELOPMENT OF PLASMA SURFACE MODIFICATION AND CHARACTERIZATION STRATEGIES FOR THREE-DIMENSIONAL POLYMER CONSTRUCTS USED IN BIOLOGICAL APPLICATIONS

AND

PART II: EXPLORING GENERAL CHEMISTRY STUDENTS' METACOGNITIVE MONITORING ON EXAMINATIONS

Synthetic polymeric biomaterials have enormous potential for use in biomedical devices designed for regenerative tissue engineering, wound healing, and controlled-release drug delivery. A comprehensive understanding of interactions between biological species and the material of interest is critical for developing biomedical constructs for a targeted application. Constructs with intricate porous architectures are often suitable as biomedical devices because they mimic the structure of the extracellular matrix (ECM). Surface properties (i.e., chemical functionality and wettability), however, must typically be customized depending on the desired function. Disentangling the role surface and bulk properties play in controlling interactions between the synthetic construct and a specific biological system, however, represents a significant challenge for the advancement of such biomedical applications.

Part I of this dissertation addresses this challenge through the fabrication, plasma modification, and characterization of polymer constructs, including porogen-leached scaffolds, electrospun fibers, and polymer films, fabricated using polycaprolactone (PCL), polylactic acid (PLA), Tygon®, and a polylactic-co-glycolic acid-based polymer (PLGH). Plasma processing –

an attractive tool for tuning surface properties of delicate polymeric materials with complex architectures – provides a low-temperature, sterile environment for construct modification, where a variety of precursors were selected to impart specific surface properties. Following plasma treatment, materials were characterized using multiple methods including contact angle goniometry, X-ray photoelectron spectroscopy (XPS), and scanning electron microscopy (SEM) to assess changes in wettability, chemical functionality, and construct architecture relative to unmodified materials. Interactions between plasma-modified materials and model biological systems, including human dermal fibroblasts (HDF), *Escherichia coli* (*E. coli*), and blood plasma, were evaluated as a means of assessing bioreactivity.

Part I begins with a review of state-of-the-art of wettability measurements for plasma-modified three-dimensional porous polymeric materials. Specifically, inherent challenges associated with evaluating the wettability of these complex constructs are evaluated. Issues associated with expanding contact angle goniometry-based techniques from two-dimensional to three-dimensional substrates are discussed, including the collection of both static and dynamic contact angle data. The importance of contextualizing wettability data by concurrently characterizing material surface chemistry and roughness is emphasized. This assessment strategy provides a holistic approach to evaluating the wettability behavior of three-dimensional materials, which persists throughout Part I of this dissertation as an essential piece of the research.

As one example, this analysis process was utilized when assessing two different nitric oxide (NO) releasing polymer films fabricated using PLGH and Tygon® before and after water vapor (H_2O) plasma modification. Film surface properties for both polymer systems, including wettability and chemistry, were altered dramatically upon plasma treatment while bulk properties

were maintained. Specifically, H_2O plasma treatment rendered PLGH films more wettable than unmodified films, and XPS characterization suggested plasma treatment resulted in polymer rearrangement and implantation of oxygen-containing functional groups. Similar results were observed for NO-releasing Tygon® films, where H_2O plasma treatment enhanced film wettability, doubled film oxygen content, and maintained surface roughness.

Fluorocarbon (FC) plasma precursors, octofluoropropane (C_3F_8) and hexafluoropropylene oxide (HFPO), were used to deposit conformal FC films on PCL scaffolds using plasma enhanced chemical vapor deposition (PECVD) with the goal of customizing scaffold bioreactivity. Cross-sectional XPS data demonstrated that FC film deposition occurred both on the outer scaffold surface and throughout the 3D structure. SEM images confirmed that FC film deposition yielded conformal rather than blanket coatings as the porous scaffold structure was maintained after plasma treatment. After 72 h, HDF cells do not attach to modified, seeded scaffolds; moreover viability studies demonstrated the scaffolds are non-cytotoxic.

Plasma copolymerization of allylamine (allylNH) and allyl alcohol (allylOH) on PCL scaffolds was utilized to expand upon the work with FC PECVD systems. Films with customizable and predictable nitrogen and oxygen content, as well as wettability, were deposited on PCL scaffolds using multiple allylNH/OH feedgas mixtures. Additionally, the bioreactivity of plasma-modified materials was evaluated using both HDF and *E. coli* attachment studies. Plasma-treated scaffolds showed enhanced HDF viability over unmodified scaffolds, demonstrating that both wettability and nitrogen content play a role in promoting cell attachment.

The coagulation response of blood plasma in the presence of PCL scaffolds was evaluated as a means of expanding to more complex biological systems using thromboelastography (TEG). In this work, modified TEG cups (with 50% more volume than

commercial consumables) were fabricated to accommodate 3D constructs. Proof-of-concept experiments using polymer scaffolds with a range of wettabilities and chemistries demonstrated that variations in surface properties resulted in differences in blood plasma coagulation dynamics. For example, maximum rate of thrombus generation ranged from 22.2 ± 2.2 (dyne/cm^2)/s for FC coated scaffolds to 8.7 ± 1.0 (dyne/cm^2)/s for nitrogen-containing scaffolds.

Part I of this dissertation concludes by describing progress toward developing a repertoire of constructs with differing surface and bulk properties, highlighting the plasma modification of polymer films, scaffolds, and electrospun fiber mats. Initial exploration of assessment strategies (e.g., use of imaging analysis software such as DiameterJ for characterizing differences in fiber mat geometry), and a parameter space exploration of 1,7-octadiene (OD) plasmas are included. One key finding from the OD parameter space study is that substrates treated further downstream at lower applied rf powers are more hydrophilic, suggesting the absence of a hydrocarbon film. When applied power is increased, however, substrates placed downstream of the coil are more hydrophobic, indicative of film deposition. Altogether, Part I demonstrates that construct properties, and thus bioreactivity, can be customized depending on the choice of plasma parameters.

Part II of this dissertation includes chemistry education-focused research that targets metacognition in general chemistry courses, and begins with an investigation of students' postdiction accuracies for a series of exams within a two-semester general chemistry course. Four of the research questions addressed are: How accurate are general chemistry students at postdicting their exam scores? Are there gender differences in postdiction accuracy? How do general chemistry students' postdiction accuracies relate to their exam performance? How do

general chemistry students' postdiction accuracies and metacognitive monitoring of their exam performance change over time? Results indicated that most general chemistry students are not accurate in their exam score postdictions and that higher-performing students make more accurate postdictions than lower-performing students.

These findings inspired the design and creation of an intervention aimed at improving metacognitive monitoring on general chemistry exams. Part II of this dissertation concludes by presenting the protocol developed for such an intervention and a description of an initial implementation. The goal of this intervention was to explore relationships between general chemistry student participation in metacognition-based exam preparation workshops and different factors related to metacognition, including metacognitive monitoring and metacognitive awareness. Results from a pilot study conducted with a small cohort of students in the Fall 2014 semester suggest there may be a difference in metacognitive awareness for exam preparation workshop participants when compared to test-taking strategy participants. Part II concludes with considerations for future studies related to the proposed intervention.

ACKNOWLEDGMENTS

This dissertation research would not have been possible without the infallible support of many people. You have helped tremendously throughout the ups and downs of my PhD work, and for that, I am exceptionally grateful.

First, I would like to thank Dr. Ellen Fisher for her mentorship throughout the research process. I am thankful for all you have taught me, including how to tackle challenging scientific questions, methods for effectively communicating science, and that drinking champagne when positive things happen ensures that positive things will continue to happen. You have continuously encouraged me to not sweat the small stuff and to celebrate every victory, no matter how minor it seems at the time. The supportive research community you have created allowed me to flourish both as a scientist and as a person, and for that, I am immensely appreciative.

I want to acknowledge members of the Fisher Group for their camaraderie throughout my time in graduate school. You are the best coworkers I could ask for, and you have taught me so much. You are my Colorado family, and I am deeply indebted to you for your assistance and encouragement in navigating the challenging graduate school landscape.

I must also thank Dr. Dawn Rickey and Dr. Lisa Dysleski for their guidance in chemistry education research. You have taught me how to develop high-quality research standards, which I will continue to use throughout all of my future research endeavors. Our valuable research meetings throughout my first year of graduate school gave me a sense of belonging in the CSU community, and for that, I am grateful.

To my research collaborators, including the CSU Compatible Polymer Network team members – for teaching me valuable lessons about multidisciplinary research and the benefits of collaboration. It was a privilege to work with each of you.

To all of the CSU chemistry department staff – for always pointing me in the right direction. You are not recognized enough for all that you do for our department, and I appreciate your support in multiple areas of my graduate student career. I am also grateful to members of the CSU faculty both in and out of the chemistry department, including my committee members, who have introduced me to new perspectives and broadened my horizons as a researcher.

I want to acknowledge my undergraduate research advisor Dr. Jin Zhang for guidance throughout my first experience working in the fast-paced world of research. The lessons you taught me have helped me to become the scientist that I am today. To my high school chemistry teachers Loreen and Roger Ruegg – your passion both for the subject and for high-quality science teaching was truly inspirational.

My friends and family have continued to serve as an amazing support system through the good and not so good times. To my roommates throughout the years – for always agreeing to listen to practice talks and helping to create environments that made me feel like I was at home. To my family, especially my parents and sister – for supporting me every step of the way and for being the best cheerleaders. I must also thank my grandma for always asking me about my research and the entertaining conversations about science that ensued. I love and appreciate all of you more than words can express.

For all of my mentors, teachers, coworkers, family, and friends – this dissertation is dedicated to you. Thank you.

TABLE OF CONTENTS

ABSTRACT ii

ACKNOWLEDGMENTS vii

TABLE OF CONTENTS ix

LIST OF TABLES xiv

LIST OF FIGURES xvi

PART I: DEVELOPMENT OF PLASMA SURFACE MODIFICATION AND CHARACTERIZATION STRATEGIES FOR THREE-DIMENSIONAL POLYMER CONSTRUCTS USED IN BIOLOGICAL APPLICATIONS

CHAPTER 1 – MATERIALS CHEMISTRY-FOCUSED RESEARCH: AN INTRODUCTION 2
1.1 Three-dimensional Polymeric Materials for Biomedical Device Applications 3
1.2 Fundamentals of Plasma Modification 5
1.3 Plasma Processing of Polymeric Materials for Biologically-relevant Applications 7
1.4 Overview of Research 9
REFERENCES 12

CHAPTER 2 – EXPERIMENTAL METHODS 15
2.1 Plasma Reactor Set-up and Treatment Conditions 15
2.1.1 Plasma reactor set-up 15
2.1.2 Plasma treatments 15
2.2 Substrate Preparation and Fabrication 20
2.2.1 Polymer scaffold fabrication 20
2.2.2 Polymer electrospun fiber fabrication 22
2.2.3 Polymer film fabrication 24
2.2.4 Nitric oxide releasing film fabrication 24
2.3 Material Characterization Techniques 25
2.3.1 Wettability analysis 25
2.3.2 Composition analysis 27
2.3.3 Morphological analysis 28
2.3.4 Additional surface analysis 31
2.4 Biological Assessment Strategies 32
2.4.1 Cell attachment and growth on fluorocarbon plasma-modified constructs 32
2.4.2 Cell attachment, growth, and viability on allylNH and allylOH plasma-modified substrates 33
2.4.3 Bacteria attachment and growth on allylNH and allylOH plasma-modified substrates 33

2.4.4 Thromboelastography (TEG) analyses 35
REFERENCES 40

CHAPTER 3 – INNOVATIVE APPLICATIONS OF SURFACE WETTABILITY MEASUREMENTS FOR PLASMA MODIFIED THREE-DIMENSIONAL POROUS POLYMERIC MATERIALS 42
3.1 Introduction 43
3.2 Background 46
3.2.1 Contact angle goniometry to measure wettability 47
3.2.2 Challenges of measuring wettability on 2D and 3D substrates 51
3.2.3 Simulations of drop dynamics on porous and rough substrates 57
3.3 Plasma-treated 3D Material Wettability Measurements 59
3.3.1 Plasma treated 3D materials that do not exhibit absorption behavior 60
3.3.2 Plasma treated 3D materials that exhibit absorption behavior 69
3.3.3 Adapting alternate CA techniques to 3D substrates 76
3.4 Recommendations for Best Practices and Future Vision 80
REFERENCES 83

CHAPTER 4 – CHARACTERIZATION OF H_2O PLASMA-MODIFIED NITRIC OXIDE-RELEASING POLYMERIC MATERIALS 88
4.1 Introduction 89
4.2. Results and Discussion: NO-releasing PLGH 92
4.2.1 Effect of plasma treatment on composition of S-nitrosated PLGH-cysteine films 92
4.2.2 Effect of prolonged treatment time on surface composition 103
4.2.3 Effect of plasma treatment on surface wettability 105
4.2.4 Effect of plasma treatment on surface morphology 106
4.2.5 Stability of the plasma treatment 112
4.3 Results and Discussion: NO-releasing Tygon® 114
4.3.1 Effect of plasma treatment on composition of Tygon® and NO-releasing films 114
4.3.2 Effect of plasma treatment on NO-releasing Tygon® film wettability and roughness 120
4.4 Summary: Comparison of Plasma-modified NO-releasing PLGH and Tygon® Films 121
REFERENCES 124

CHAPTER 5 – CONFORMAL ENCAPSULATION OF THREE-DIMENSIONAL, BIORESORBABLE POLYMERIC SCAFFOLDS USING PLASMA-ENHANCED CHEMICAL VAPOR DEPOSITION 128
5.1 Introduction 129
5.2 Results 130
5.2.1 Surface analysis 130
5.2.2 Cell attachment and growth 137
5.3 Discussion 142
5.4 Summary 146
REFERENCES 148

CHAPTER 6 – ALLYLAMINE AND ALLYL ALCOHOL PLASMA COPOLYMERIZATION: FABRICATION OF CUSTOMIZABLE BIOLOGICALLY-REACTIVE 3D SCAFFOLDS ...150
6.1 Introduction ...151
6.2 Results ...155
6.2.1 Plasma copolymerization on Si wafers: surface characterization ...155
6.2.2 Film deposition on 3D scaffolds ...158
6.2.3 Cell attachment, growth, and viability ...162
6.3 Discussion ...169
6.3.1 Characterization of plasma copolymerized allylNH/OH films: 2D and 3D substrates ...169
6.3.2 Bioreactivity assessment of plasma-modified materials using E. coli and HDF ...172
6.4 Summary ...174
REFERENCES ...176

CHAPTER 7 – MODIFCATION OF A COMMERCIAL THROMBOELASTOGRAPHY INSTRUMENT TO MEASURE COAGULATION DYNAMICS WITH THREE-DIMENSIONAL BIOMATERIALS ...180
7.1 Introduction ...181
7.2 Results ...185
7.2.1 PCL scaffold characterization ...185
7.2.2 Design optimization for TEG analysis of solid materials ...187
7.2.3 TEG analysis of polymer scaffolds with different surface properties ...189
7.3 Discussion ...189
7.4 Summary ...197
REFERENCES ...199

CHAPTER 8 – BUILDING A LIBRARY OF POLYMER CONSTRUCTS FOR EVALUATION AS SYNTHETIC BIOMATERIALS ...203
8.1 Introduction ...203
8.2 Plasma Modification of Electrospun Fibers: Expanding on Work with PCL ...204
8.3 DiameterJ as a Fiber Analysis Tool ...206
8.3.1 Image processing procedure ...208
8.3.2 Troubleshooting and future work ...210
8.4 Plasma-modified PCL/PLA Construct Surface Properties ...211
8.5 1,7-octadiene PECVD System: Parameter Space Exploration ...221
8.6 Summary ...232
REFERENCES ...233

CHAPTER 9 – RESEARCH SUMMARY AND FUTURE DIRECTIONS ...234
9.1 Research Summary ...234
9.1.1 Emergent themes ...234
9.1.2 Broader impact and outlook ...235
9.2 Future Directions ...236
9.2.1 Evaluation of construct library in complex biological systems ...236
9.2.2 Expanding plasma modification strategies ...237

9.2.3 Developing fabrication methods for three-dimensional porous polymer materials 238
9.2.4 Developing characterization methods for three-dimensional porous polymer materials 240
REFERENCES 245

PART II: EXPLORING GENERAL CHEMISTRY STUDENTS' METACOGNITIVE MONITORING ON EXAMINATIONS

CHAPTER 1 – INTRODUCTION OF CHEMISTRY EDUCATION FOCUSED RESEARCH 248
1.1 Motivation: Metacognitive Skillfulness and Judgment Accuracy 248
1.2 Metrics for Evaluating Metacognitive Monitoring 249
1.3 Overview of Research 250
REFERENCES 253

CHAPTER 2 – INVESTIGATING GENERAL CHEMISTRY STUDENTS' METACOGNITIVE MONITORING OF THEIR EXAM PERFORMANCE BY MEASURING POSTDICTION ACCURACIES OVER TIME 255
2.1 Introduction 256
2.2 Methods 257
2.3 Results and Discussion 262
2.3.1 Postdiction accuracy 262
2.3.2 Relationships between student exam postdiction accuracy and performance 267
2.3.3 Changes in postdiction accuracy and metacognitive monitoring over time 269
2.4 Limitations 274
2.5 Conclusions and Implications 275
REFERENCES 278

CHAPTER 3 – DESIGN OF METACOGNTIVE-BASED EXAM AND STUDY PREPARATION WORKSHOPS TO PROMOTE GENERAL CHEMISTRY STUDENT METACOGNITIVE AWARENESS 280
3.1 Introduction 281
3.2 Intervention Design and Implementation 284
3.2.1. Overview of the proposed study design 284
3.2.2. Test-taking strategies group activities 287
3.2.3. Exam preparation strategies group activities 289
3.2.4. Student exam data and postdiction data collection 291
3.2.5. Student recruitment plan 291
3.2.6. Procedures to maintain confidentiality 293
3.3 Pilot Study Summary 293
3.4 Reflections and Alterations for Future Studies 298
REFERENCES 300

APPENDIX I – TABLES CORRESPONDING TO PART I1, CHAPTER 2 302

APPENDIX II – SUPPLEMENTAL MATERIAL CORRESPONDING TO PART I1, CHAPTER 3 314
Metacognitive Awareness Inventory (MAI) 315
Multiple Choice Question Sets 318
Reflection Activity: Test taking strategies 322
Writing Assignment: Workshop #1 322
Study session template for test-taking strategies group 323
Study session template for exam preparation strategies group 324
Research Flyer 325
Recruitment E-mail 326

LIST OF ABBREVIATIONS 327

LIST OF TABLES

PART I

2.1 Summary of plasma precursors....17
2.2 Summary of plasma treatment conditions....18
2.3 Summary of electrospinning parameters....23

3.1 WCA and XPS elemental data for untreated and plasma-treated materials....64

4.1 XPS atomic composition ratios of *S*-nitrosated PLGH-cysteine films....94
4.2 Binding environment ratios for untreated and treated films....100
4.3 Water droplet spreading times associated with plasma treated samples....108
4.4 Surface roughness of *S*-nitrosated PLGH-cysteine films....110
4.5 Elemental Composition and WCA Values for Tygon® Films....118

7.1 Elemental composition and wettability of 3D polymeric materials evaluated with TEG....186
7.2 Summary of quantitative clot kinetic measurements....192

8.1 Wettability data for plasma-modified PCL:PLA constructs....214
8.2 Surface chemical composition of PCL:PLA materials....217
8.3 WCA as a function of *P*, position in reactor, and treatment time for OD films....222
8.4 RMS roughness values for OD treated Si wafers as a function of treatment time....228

PART II

2.1 Summary of course characteristics....258
2.2 Performance and calibration statistics for Fall and Spring semesters....266
2.3 Exam scores of students who were well calibrated and those who were not....270
2.4 Effect sizes – exam score category (r_{exam}) and |calibration| ($r_{|calibration|}$)....273

3.1 Volunteer attendance throughout the intervention pilot study in Fall 2014....294
3.2 Pre- and post- measures from the MAI....297

AI.1 Comparing male vs. female students: calibration statistics, Mann-Whitney U test results, and postdiction accuracies....303
AI.2 Comparing male vs. female students: exam performance data....304
AI.3 Sample sizes for students who were well calibrated and those who were not....305
AI.4 Comparing high vs. low performers: performance and calibration statistics....306
AI.5 Comparing high vs. low performers: Mann-Whitney U test results comparing exam scores and |calibration|....308
AI.6 Comparing high vs. low performers: Effect sizes – exam score category (r_{exam}) and calibration| ($r_{|calibration|}$)....309

AI.7 Spring only: Performance and calibration statistics.....310
AI.8 Spring only: Effect sizes – exam score category (r_{exam}) and |calibration| ($r_{|calibration|}$) 311
AI.9 Students who took both courses: performance and calibration statistics.....312
AI.10 Students who took both courses: Effect sizes – exam score category (r_{exam}) and |calibration| ($r_{|calibration|}$) 313

LIST OF FIGURES

PART I

2.1 Inductively-coupled plasma reactor schematic 16
2.2 Overview of in-house substrate polymeric fabrication methodologies 22
2.3 Representative high-resolution C_{1s} XPS spectra of a native PCL scaffold 29
2.4 Overview of interfacing 3D printed consumables with the TEG instrument 36

3.1 SEM images of 3D polymer constructs 44
3.2 Schematic representations of static and dynamic CA measurements 48
3.3 Image of a water drops on plasma treated PLGA fibers and PCL scaffolds 56
3.4 SEM images of untreated and C_3F_8 plasma treated electrospun PCL fibers 66
3.5 WCA as a function of drop age for PCL scaffolds track-etched PET membranes 68
3.6 WCA as a function of drop age for membranes and scaffolds (fresh and aged) 75
3.7 WCA as a function of pH on H_2O plasma treated SiO_xN_y and PCL films 78

4.1 The structure of *S*-nitrosated PLGH-cysteine 93
4.2 O/N, C/N, and C/O as a function of plasma treatment time 95
4.3 High-resolution C_{1s} XPS spectra for *S*-nitrosated PLGH-cysteine films 99
4.4 *S*-nitrosated PLGH-cysteine acid and base catalyzed ester hydrolysis 104
4.5 C_{1s} XPS spectrum for PLGH-cysteine; C/O ratios as a function of treatment time 107
4.6 Treatment time and *P* vs. water droplet spreading time 109
4.7 SEM images of *S*-nitrosated PLGH-cysteine films 111
4.8 GSNO structure; photographs of Tygon® and GSNO20 films 117
4.9 High-resolution C_{1s} XPS spectra, images from WCA analysis, and WCA values 119

5.1 XPS survey spectra untreated and FC plasma treated scaffolds 131
5.2 High-resolution XPS C_{1s} spectra of C_3F_8 films deposited on PCL scaffolds 132
5.3 High-resolution XPS C_{1s} spectra of HFPO films deposited on PCL scaffolds 135
5.4 F/C ratios FC plasma treated PCL scaffold tops and cross sections 136
5.5 SEM images of untreated and FC plasma treated PCL scaffolds 138
5.6 Film thicknesses for FC film depositions on Si wafers measured using VASE 139
5.7 Overlaid fluorescence microscope images of HDF on scaffolds 141

6.1 O/C and N/C ratios for films deposited in allylOH/allylNH plasmas 157
6.2 Representative SEM images of PCL scaffold tops treated with allylOH/NH plasmas 159
6.3 Wettability data on plasma-modified scaffolds 161
6.4 Overlaid fluorescence microscopy images of HDF attachment (films) 163
6.5 Overlaid fluorescence microscopy images of HDF attachment (scaffolds) 164
6.6 CellTiter-Blue® cell viability assay results for HDF 166
6.7 Overlaid fluorescence microscopy images of live/dead stained *E. coli.* 167

7.1 TEG tracings for blood plasma in Cyrolite® cups and 3D printed ABS cup.....188
7.2 TEG tracings with elevated and non-elevated baselines.....190
7.3 TEG tracings and velocity curve for a blank cups and cups with PCL scaffolds.....191
7.4 Figures of merit from TEG velocity curve data.....193

8.1 Conceptual framework for the systematic variation of polymer construct properties.....205
8.2 SEM images of electrospun fiber meshes fabricated using PCL and PCL:PLA 207
8.3 DiameterJ analysis of OD plasma treated PCL fibers 209
8.4 SEM images of constructs fabricated using PCL:PLA.....213
8.5 High-resolution C_{1s} XPS spectra of PCL:PLA scaffolds.....218
8.6 FTIR and VASE results of OD plasma treated substrates 225
8.7 Representative optical profilometry data (OD film growth).....227

9.1 Principal component analysis of ToF-SIMS positive ion data collected on scaffolds 242
9.2 Overlays of the $C_6H_{11}O_2^+$ and CF_2^+ signals measured on scaffolds via ToF-SIMS 243

PART II

2.1 Sample questions from first- and second-semester general chemistry exams.....260
2.2 Bubble plots of exam postdictions versus exam scores (fall semester).....264
2.3 Bubble plots of exam postdictions versus exam scores (fall semester).....265

3.1 Gantt chart: planned workshop timeline.....286
3.2 Workshop outline for test taking and exam preparation strategy groups 288
3.3 Sample student responses from the workshop #1 writing activity 296

PART I: DEVELOPMENT OF PLASMA SURFACE MODIFICATION AND CHARACTERIZATION STRATEGIES FOR THREE-DIMENSIONAL POLYMER CONSTRUCTS USED IN BIOLOGICAL APPLICATIONS

CHAPTER 1

MATERIALS CHEMISTRY-FOCUSED RESEARCH: AN INTRODUCTION

Millions of synthetic biomaterial devices are deployed in medical settings annually,[1] and a recent review claims the global biomaterials market will reach a value of approximately $84 billion by 2017.[2] Synthetic biomaterial devices have enormous potential to improve quality of life for patients worldwide, which has created a critical need for the biomaterials industry to produce and deploy next-generation devices. Addressing the needs of this quickly expanding market requires targeted research and development efforts, including the design of customizable and multifunctional device platforms. Devices (often designed using polymeric and multi-dimensional materials) can serve a range of crucial functions, including regenerative tissue engineering,[3-5] wound healing,[6] and controlled-release drug delivery.[7] Deployment in these applications requires a comprehensive knowledge of interactions between biological species and the material of interest, where interactions are dictated by material properties. Although these properties (e.g., surface chemistry, wettability, porosity, and architecture) have the potential to control biological response, the inherent properties of synthetic devices can limit their translation across a broad range of applications. To overcome intrinsic properties associated with a specific device material, it is necessary to develop strategies to create devices with customizable properties and therefore, tunable biological response. This approach will propel efforts forward to meet the growing needs of the synthetic biomaterials market.

Research presented in Part I of this dissertation builds a fundamental understanding of how polymer biomaterial surface and bulk properties affect the interplay at the material-biomolecule interface. This chapter presents background information to frame these research

efforts, including the motivation for employing three-dimensional polymeric constructs in biomedical devices, modifying construct surfaces using low-temperature plasma processing techniques, and assessing interactions with biological species.

1.1 Three-dimensional Polymeric Materials for Biomedical Device Applications

Traditionally, the term biopolymer refers to biodegradable polymers produced by living organisms (e.g., cellulose, muscle tissues, and DNA). During the last few decades, however, researchers have developed synthetic biodegradable and bioresorbable polymers that mimic natural materials.[8-9] The term "biopolymer" has thus grown to include natural and synthetic polymer constructs that elicit specific biological responses.[10-11] Synthetic biopolymeric materials can be fabricated into an essentially unlimited number of architectures using a multitude of polymers, making them desirable for a variety of biological applications. Common polymeric materials for biomedical devices include those fabricated using polyesters such as polycaprolactone (PCL), polylactic acid (PLA), polyglycolic acid, poly(lactic acid-co-glycolic acid), and polyhydroxybutyrate, all of which are typically hydrophobic and, thus, often require surface modification to improve compatibility in biological (i.e., aqueous) environments.

Three-dimensional biopolymeric scaffolds that comprise an interconnected porous network are of particular interest because they can be fabricated to mimic the extracellular matrix, both with respect to geometry and to mechanical properties.[12-13] The morphology of these scaffolds is advantageous for mammalian cell, antibacterial agent, or pharmaceutical loading for applications including regenerative tissue engineering,[3-5] chronic wound treatment,[6] and controlled drug delivery.[7] Despite the multitude of available 3D biopolymeric scaffold materials with desirable mechanical, morphological, and biocompatible/bioresorbable bulk properties, the

ability to customize surface properties remains an elusive key to tuning these 3D materials for specific biomedical device applications.

Synthetic biomaterial surface properties control mammalian and bacterial cell attachment and proliferation – critical factors for improving the biocompatibility of a plethora of medical devices.[14] Properties that directly influence biological species-surface interactions include surface chemical composition, surface free energy, surface topography, and surface wettability.[15] Although microorganism surface hydrophobicity, charge, and electronegativity also contribute to its interactions with material surfaces,[16-17] manipulation of surface properties of synthetic materials is the most accessible path for controlling biological species-surface interactions and enhancing biocompatibility. Therefore, the ability to tune material surface properties while retaining the desirable bulk properties can allow for customizable interactions between synthetic biomaterials and biological environments.

In particular, surface chemical composition and wettability greatly influence interfacial interactions between surfaces and biological components. For example, Arima and Iwata highlighted the effect of terminal functional groups for self-assembled monolayers on protein adsorption and cell adhesion.[14] Increased protein adsorption was observed for surfaces with increasing hydrophilicity for many functional groups (e.g. OH, CH_3/COOH). Additionally, endothelial and epithelial cells attached and spread significantly on surfaces with increased hydrophilicity (i.e. increase in surface COOH or NH_2), which promotes wound healing and synthetic biomaterial device integration into a given biological environment. Parreira et al. reported a correlation between the presence of different functional groups on a surface (i.e., CH_3 and OH) and wettability with the increase or reduction of *Helicobacter pylori (H. pylori)* attachment.[18] Although the 17875/Leb strain showed a distinctive preference for hydrophilic

surfaces, the remainder of the *H. pylori* strains exhibited the opposite behavior. This result indicated that bacterial attachment to surfaces is both surface- and strain-dependent. Collectively, observations that mammalian and bacteria cells demonstrate surface property-dependent behavior emphasizes the need to develop materials with tunable surface chemical composition and wettability to meet application needs. One such methodology for tuning construct properties is via plasma processing, discussed in Sections 1.2 and 1.3.

1.2 Fundamentals of Plasma Modification

A common approach for modifying polymer materials utilizes plasmas to etch, implant functional groups, or deposit conformal films, thereby providing a facile route to customize material surface properties. The objective of this discussion is to provide a broad overview of plasma processing fundamentals, with a more detailed account of plasma treatment of synthetic polymeric biomaterials included below (Section 1.3).

Plasma, the fourth state of matter, is a partially ionized gaseous mixture containing neutral and excited state molecules, ions, electrons, photons, and radicals. Work in this dissertation utilizes low-pressure, low-temperature plasma (LTP) processing. By definition, the majority of species in LTPs are neutral precursor molecules (density ~10^{15} cm^{-3}) such that the gas temperature is approximately room temperature (~300 K).[19] The population of ions and electrons in LTPs is significantly lower than that of neutral species, ranging from 10^{8} – 10^{12} cm^{-3}. An additional hallmark of LTPs is that the average electron energy is greater than the average ion energy, typically ranging from 1–10 eV depending on plasma parameters.[19] Because of disparate electron and ion energies, LTPs are also referred to as non-equilibrium plasmas.

A wealth of excitation, dissociation, and ionization reactions occur in LTPs, which depend on reactive species populations and energetics. These reactions are largely controlled by

the wide parameter space available in LTP modification, including precursor identity (i.e., the gaseous or low-vapor pressure liquid precursor(s) present in the plasma feed gas), applied power (P), system pressure (p), precursor flow rate (F), and plasma treatment time. Notably, all plasma processing reported in this dissertation utilizes radio frequency (rf) applied power, although microwave LTPs are also used in research and industrial applications.[20-23] LTP complexity further increases upon addition of a substrate to the plasma, wherein reactions occurring at the plasma-surface interface dictate the type of processing that occurs. As mentioned above, plasma surface modification systems can be broadly classified as resulting in etching, implanting functional groups, or depositing thin films via plasma-enhanced chemical vapor deposition (PECVD). These processes are often competing within LTP systems, and the predominance of one over the other depends largely on the energetics of plasma species and on the substrate material properties. Another factor influencing inductively coupled LTP surface modification is the substrate position relative to the region of most intense plasma emission. For example, placing substrates downstream of this region typically reduces plasma etching. This type of downstream processing allows plasma etchant species to recombine before reaching the substrate, while deposition precursors (typically having longer lifetimes) can reach the surface. The identity of etching and depositing species depends on the LTP precursor(s) and parameter space. A detailed account of reactive species in each LTP system reported in this dissertation precedes the chapter introducing the system.

Industrial and commercial applications of LTPs are ubiquitous owing to precise control of material surface properties achieved through the wide range of available processing capabilities. Although the most common industrial LTP-modified material systems are those involved in semiconductor processing (in the microelectronics field),[24-25] substantial efforts have

focused on expanding LTP technologies to include modification of polymer constructs.[26-31] Plasmas can be used to create customizable polymer surfaces without disrupting construct bulk properties, which is especially advantageous for polymers as their surface properties limit translation across a broad range of applications. For example, polymers typically have low surface energies and may have poor durability which presents challenges for applications relying on polymer adhesion, wetting properties, and wear resistance. Multiple approaches to improve polymer surface properties using plasmas have been examined, including plasma-polymerized coatings (i.e., coatings fabricated using PECVD) for improving adhesion and wear-resistance.[32-33] Additionally, LTPs can be utilized for surface cleaning and heat-sealing, both of which have applications in packaging.[33] Another major area of active research is the LTP modification of polymers designed to interface with biological systems (Section 1.3), which is the focus of the present work.

1.3 Plasma Processing of Polymeric Materials for Biologically-relevant Applications

As discussed in Section 1.2, plasmas afford the ability to tune surface chemical composition and wettability by deposition of thin films or via implantation of desirable functional groups (typically nitrogen or oxygen-containing groups are incorporated when the goal is to enhance mammalian cell attachment and growth).[34] In these approaches, several process variables introduced in Section 1.2, including precursor, P, p, F, treatment time can be adjusted to impact the efficacy of the plasma treatment.

The type of polymer construct plasma modification can be broadly classified as resulting in either a *bioreactive* or *non-bioreactive* surface. Notably, these classifications are highly dependent on the desired surface-biological species interaction(s) for a specific application and are therefore presented here as a generalized set of guidelines rather than definitive rules. A

bioreactive modification is advantageous when the goal is to promote interactions between a synthetic biomedical construct and specific biomolecules at the construct surface (e.g., proteins, DNA, mammalian cells, and bacterial cells); these plasma modifications generally result in hydrophilic surfaces.[35] Surface modifications that enhance material bioreactivity are more commonly reported than those that are non-bioreactive. This is primarily because aliphatic polymer materials commonly used when fabricating biomedical devices, including the polyesters highlighted in Section 1.1, are nominally hydrophobic.[36-37] Although these materials present desirable bulk properties regarding biocompatibility, bioresorption, and mechanical strength, hydrophilic surfaces are generally preferred in applications requiring cell adhesion to biopolymeric constructs (e.g., tissue engineering). Thus, the ability to render the hydrophobic surfaces of these polyesters hydrophilic greatly expands their utility in many biomedical applications. For example, plasma treatments of hydrophobic biopolymeric materials using precursors such as allylamine (allylNH),[38-41] O_2,[42-43] and NH_3[44] have resulted in hydrophilic surfaces, demonstrating an increase in cell adhesion relative to untreated materials.

A non-bioreactive surface modification is necessary for applications wherein non-specific protein and bacteria attachment can lead to undesirable effects (e.g., loss of material properties and/or negative response from biological media).[35] Non-bioreactive plasma surface modifications typically result in hydrophobic, low-fouling surfaces that minimize bacterial attachment and subsequent biofilm formation. Furthermore, such non-bioreactive materials could also be used in applications wherein cell attachment and proliferation are undesirable. Biomaterial modifications resulting in a hydrophobic surface, although less frequently reported than those resulting in hydrophilic surfaces, are important for applications requiring low-fouling or those that resist bacteria or mammalian cell attachment. In this arena, diethyl glycol dimethyl

ether has been used as a precursor to deposit polyethyleneoxide-like films, and fluorocarbon (FC) precursors (e.g., C_xF_y and hexafluoropropylene oxide (HFPO)) have been used to deposit Teflon^{TM}-like films on biomedical materials, via PECVD.[45] Studies on FC plasma deposition, however, have largely focused on coating stainless steel substrates used for stents,[46] and thin metal wires[47] rather than biopolymeric substrates. Indeed, there are relatively few reports on the deposition of hydrophobic films on biopolymeric substrates. One study involved PECVD of hexane on the exterior of PLA scaffolds that were previously modified via allylNH plasma polymerization,[40] whereas another study utilized N_2 plasma modification of PCL scaffolds followed by PECVD of ethylene.[4] In these reports, the intended purpose of the deposited hydrophobic plasma polymerized films was to create a chemical gradient that discouraged cell adhesion solely on the exterior of the scaffold, and that encouraged cell migration into the polymer scaffold core.

Regardless of whether bioreactive or non-bioreactive surfaces are desired, the breadth of available plasma precursors makes LTP processing an excellent candidate for modification of polymeric materials for biological applications. Specifically, polymer surfaces can be plasma treated to customize response between the material and the surrounding biological environment. Controlling response at the biomaterial-biomolecule interface provides a route to either promote or prevent attachment of biological species depending on the targeted application.

1.4 Overview of Research

Overall, this research is focused on creating model polymeric constructs that allow for control of interactions with biological species. Several themes connect the chapters herein, including material properties considerations for biomedical applications, fabrication of polymer constructs with complex 3D architectures, surface modification using plasma processing, and

analysis strategies for both material properties assessments and performance evaluation in model biological systems.

Part I of this dissertation begins by presenting a detailed explanation of experimental methodologies used to conduct work presented in subsequent chapters, including characterization and biological assessment techniques (Chapter 2). A critical review of techniques used to evaluate surface wettability is presented in Chapter 3. As discussed in Section 1.3, synthetic biomaterial wetting properties are of central importance for understanding interfacial interactions of such materials upon interfacing with aqueous environments. Wetting behavior evaluation of plasma-modified polymer materials having complex geometries, however, is not straightforward; this motivates the overview of state-of-the-art techniques discussed in Chapter 3.

Chapters 4–8 focus on plasma modification, characterization, and biological assessment of different polymer constructs. The goal of the work described in these chapters is to customize polymer surface properties via plasma modification while maintaining bulk construct properties. Chapter 4 presents work from collaborative projects with Dr. Melissa Reynolds' group, wherein the effects of water vapor plasma modification on two different nitric oxide-releasing polymer films are evaluated. The objective of this work is to create drug-releasing films with enhanced surface properties (e.g., wettability, surface chemistry) for interfacing with biological systems (initially targeting their efficacy as antimicrobial constructs). Specifically, this chapter presents contributions to the work focusing on characterizing construct surface properties before and after plasma treatment.

Chapters 5–8 contain studies on plasma-modified polyester constructs, including porogen-leached scaffolds and electrospun fibers. Chapter 5 presents work on plasma modifying

PCL scaffolds using two different fluorocarbon precursors, octofluoropropane and HFPO to evaluate their potential to fabricate non-bioreactive 3D constructs. Chapter 6 details the use of an allyl alcohol and allylNH plasma copolymerization system for tuning nitrogen content and wettability of PCL scaffolds, with a focus on subsequent assessment of scaffold interactions with mammalian and bacterial cells. Chapter 7 discusses the analysis of blood coagulation activity upon interfacing human blood plasma with allyl alcohol, water vapor, and octofluoropropane plasma-modified PCL scaffolds. Chapter 8 includes initial fabrication and characterization efforts that are part of a larger research effort to develop a library of polymer constructs, systematically modifying surface and bulk material properties by varying the base polymer, construct geometry, and plasma modification parameter space.

Chapter 9 includes a summary of plasma modification of polymer constructs and provides possible avenues for future directions of this research, namely plasma modification to customize properties of complex polymeric materials and subsequent construct assessment in biological systems. Materials having complex geometries are emphasized because of their relevance for biomedical device use (e.g., mimicking the extracellular matrix), such as for tissue engineering and wound healing applications. Collectively, this research enhances our fundamental understanding of how construct surface properties control interactions with biological species through providing a comprehensive evaluation, both in terms of materials characterization and performance evaluation in biological environments.

REFERENCES

1. Ratner, B. D., The Catastrophe Revisited: Blood Compatibility in the 21st Century. *Biomaterials* **2007,** *28* (34), 5144-5147.
2. John, A.; Subramanian, A.; Vellayappan, M.; Balaji, A.; Jaganathan, S.; Mohandas, H.; Paramalinggam, T.; Supriyanto, E.; Yusof, M., Review: Physico-chemical Modification as a Versatile Strategy for the Biocompatibility Enhancement of Biomaterials. *RSC Adv.* **2015,** *5* (49), 39232-39244.
3. Agrawal, C.; Ray, R. B., Biodegradable Polymeric Scaffolds for Musculoskeletal Tissue Engineering. *J. Biomed. Mater. Res.* **2001,** *55* (2), 141-150.
4. Intranuovo, F.; Gristina, R.; Brun, F.; Mohammadi, S.; Ceccone, G.; Sardella, E.; Rossi, F.; Tromba, G.; Favia, P., Plasma Modification of PCL Porous Scaffolds Fabricated by Solvent-Casting/Particulate-Leaching for Tissue Engineering. *Plasma Process. Polym.* **2014**.
5. Khang, G.; Lee, S. J.; Kim, M. S.; Lee, H. B., Biomaterials: Tissue Engineering and Scaffolds. *Encyclopedia Med. Devices Instrumen.* **2006**.
6. Madhumathi, K.; Kumar, P. S.; Abhilash, S.; Sreeja, V.; Tamura, H.; Manzoor, K.; Nair, S.; Jayakumar, R., Development of Novel Chitin/Nanosilver Composite Scaffolds for Wound Dressing Applications. *J. Mater. Sci.: Mater. Med.* **2010,** *21* (2), 807-813.
7. Kim, K.; Luu, Y. K.; Chang, C.; Fang, D.; Hsiao, B. S.; Chu, B.; Hadjiargyrou, M., Incorporation and Controlled Release of a Hydrophilic Antibiotic Using Poly(lactide-co-glycolide)-based Electrospun Nanofibrous Scaffolds. *J. Controlled Release* **2004,** *98* (1), 47-56.
8. Ratner, B. D.; Hoffman, A. S.; Schoen, F.; Lemons, J. E., Biomaterials Science: an Introduction to Materials in Medicine. *San Diego, California* **2004**, 162-164.
9. Vert, M.; Hellwich, K.-H.; Hess, M.; Hodge, P.; Kubisa, P.; Rinaudo, M.; Schué, F., Terminology for Biorelated Polymers and Applications (IUPAC Recommendations 2012). *Pure Appl. Chem.* **2012,** *84* (2).
10. Ong, J.; Appleford, M. R.; Mani, G., *Introduction to Biomaterials: Basic Theory with Engineering Applications*. Cambridge University Press: 2013.
11. Ratner, B. D.; Bryant, S. J., Biomaterials: Where We Have Been and Where We Are Going. *Annu. Rev. Biomed. Eng.* **2004,** *6*, 41-75.
12. Rosso, F.; Marino, G.; Giordano, A.; Barbarisi, M.; Parmeggiani, D.; Barbarisi, A., Smart Materials as Scaffolds for Tissue Engineering. *J. Cell. Phys.* **2005,** *203* (3), 465-470.
13. Seal, B.; Otero, T.; Panitch, A., Polymeric Biomaterials for Tissue and Organ Regeneration. *Mater. Sci. Eng. R: Reports* **2001,** *34* (4), 147-230.
14. Arima, Y.; Iwata, H., Effect of Wettability and Surface Functional Groups on Protein Adsorption and Cell Adhesion Using Well-defined Mixed Self-assembled Monolayers. *Biomaterials* **2007,** *28* (20), 3074-3082.
15. Castner, D. G.; Ratner, B. D., Biomedical Surface Science: Foundations to Frontiers. *Surf. Sci.* **2002,** *500* (1), 28-60.
16. Van Loosdrecht, M. C.; Lyklema, J.; Norde, W.; Schraa, G.; Zehnder, A., The Role of Bacterial Cell Wall Hydrophobicity in Adhesion. *Appl. Environ. Microbiol.* **1987,** *53* (8), 1893-1897.
17. Bruinsma, G. M.; van der Mei, H. C.; Busscher, H. J., Bacterial Adhesion to Surface Hydrophilic and Hydrophobic Contact Lenses. *Biomaterials* **2001,** *22* (24), 3217-3224.

18. Parreira, P.; Magalhães, A.; Gonçalves, I. C.; Gomes, J.; Vidal, R.; Reis, C. A.; Leckband, D. E.; Martins, M. C. L., Effect of Surface Chemistry on Bacterial Adhesion, Viability, and Morphology. *J. Biomed. Mater. Res. Part A* **2011,** *99* (3), 344-353.
19. Grill, A., *Cold Plasma in Materials Fabrication*. IEEE Press, New York: 1994; Vol. 151.
20. Ivković, M.; Jovićević, S.; Konjević, N., Low Electron Density Diagnostics: Development of Optical Emission Spectroscopic Techniques and Some Applications to Microwave Induced Plasmas. *Spectrochim. Acta, Part B* **2004,** *59* (5), 591-605.
21. Jin, Q.; Duan, Y.; Olivares, J. A., Development and Investigation of Microwave Plasma Techniques in Analytical Atomic Spectrometry. *Spectrochim. Acta, Part B* **1997,** *52* (2), 131-161.
22. Tsugawa, K.; Ishihara, M.; Kim, J.; Hasegawa, M.; Koga, Y., Large-area and Low-temperature Nanodiamond Coating by Microwave Plasma Chemical Vapor Deposition. *New Diamond Front. Carbon Technol* **2006,** *16* (6), 337.
23. Yamada, T.; Kim, J.; Ishihara, M.; Hasegawa, M., Low-temperature Graphene Synthesis Using Microwave Plasma CVD. *J. Phys. D: Appl. Phys.* **2013,** *46* (6), 063001.
24. Poulsen, R., Plasma Etching in Integrated Circuit Manufacture—A Review. *J. Vac. Sci. Technol.* **1977,** *14* (1), 266-274.
25. Pelletier, J.; Anders, A., Plasma-based Ion Implantation and Deposition: A Review of Physics, Technology, and Applications. *IEEE Trans. Plasma Sci.* **2005,** *33* (6), 1944-1959.
26. Förch, R.; Zhang, Z.; Knoll, W., Soft Plasma Treated Surfaces: Tailoring of Structure and Properties for Biomaterial Applications. *Plasma Process. Polym.* **2005,** *2* (5), 351-372.
27. Meyer-Plath, A.; Schröder, K.; Finke, B.; Ohl, A., Current Trends in Biomaterial Surface Functionalization—Nitrogen-containing Plasma Assisted Processes with Enhanced Selectivity. *Vacuum* **2003,** *71* (3), 391-406.
28. Chan, C.-M.; Ko, T.-M.; Hiraoka, H., Polymer Surface Modification by Plasmas and Photons. *Surf. Sci. Rep.* **1996,** *24* (1), 1-54.
29. Desmet, T.; Morent, R.; Geyter, N. D.; Leys, C.; Schacht, E.; Dubruel, P., Nonthermal Plasma Technology as a Versatile Strategy for Polymeric Biomaterials Surface Modification: A Review. *Biomacromolecules* **2009,** *10* (9), 2351-2378.
30. Morent, R.; De Geyter, N.; Desmet, T.; Dubruel, P.; Leys, C., Plasma Surface Modification of Biodegradable Polymers: A Review. *Plasma Process. Polym.* **2011,** *8* (3), 171-190.
31. Jacobs, T.; Morent, R.; De Geyter, N.; Dubruel, P.; Leys, C., Plasma Surface Modification of Biomedical Polymers: Influence on Cell-material Interaction. *Plasma Chem. Plasma Process.* **2012,** *32* (5), 1039-1073.
32. Tran, N. D.; Dutta, N.; Choudhury, N. R., Weatherability and Wear Resistance Characteristics of Plasma Fluoropolymer Coatings Deposited on an Elastomer Substrate. *Polym. Degrad. Stab.* **2006,** *91* (5), 1052-1063.
33. Dowling, D. P.; Stallard, C. P., Achieving Enhanced Material Finishing Using Cold Plasma Treatments. *Trans. Inst. Met. Finish.* **2015,** *93* (3), 119-125.
34. Griesser, H. J.; Hodgkin, J. H.; Schmidt, R., *Progress in Biomedical Applications*. Plenum Press: New York, 1990; p 205-215.
35. Förch, R.; Chifen, A. N.; Bousquet, A.; Khor, H. L.; Jungblut, M.; Chu, L. Q.; Zhang, Z.; Osey-Mensah, I.; Sinner, E. K.; Knoll, W., Recent and Expected Roles of Plasma-Polymerized Films for Biomedical Applications. *Chem. Vapor Dep.* **2007,** *13* (6 – 7), 280-294.

36. Hutmacher, D. W., Scaffolds in Tissue Engineering Bone and Cartilage. *Biomaterials* **2000,** *21* (24), 2529-2543.
37. Ikada, Y.; Tsuji, H., Biodegradable Polyesters for Medical and Ecological Applications. *Macromolecular Rap. Commun.* **2000,** *21* (3), 117-132.
38. Barry, J. J.; Silva, M. M.; Shakesheff, K. M.; Howdle, S. M.; Alexander, M. R., Using Plasma Deposits to Promote Cell Population of the Porous Interior of Three-Dimensional Poly (D, L-Lactic Acid) Tissue-Engineering Scaffolds. *Adv. Func. Mater.* **2005,** *15* (7), 1134-1140.
39. Guerrouani, N.; Baldo, A.; Bouffin, A.; Drakides, C.; Guimon, M. F.; Mas, A., Allylamine Plasma-polymerization on PLLA Surface Evaluation of the Biodegradation. *J. Appl. Polym. Sci.* **2007,** *105* (4), 1978-1986.
40. Intranuovo, F.; Howard, D.; White, L. J.; Johal, R. K.; Ghaemmaghami, A. M.; Favia, P.; Howdle, S. M.; Shakesheff, K. M.; Alexander, M. R., Uniform Cell Colonization of Porous 3-D Scaffolds Achieved Using Radial Control of Surface Chemistry. *Acta Biomater.* **2011,** *7* (9), 3336-3344.
41. Intranuovo, F.; Sardella, E.; Gristina, R.; Nardulli, M.; White, L.; Howard, D.; Shakesheff, K. M.; Alexander, M. R.; Favia, P., PE-CVD Processes Improve Cell Affinity of Polymer Scaffolds for Tissue Engineering. *Surf. Coatings Technol.* **2011,** *205*, S548-S551.
42. Hasirci, N.; Endogan, T.; Vardar, E.; Kiziltay, A.; Hasirci, V., Effect of Oxygen Plasma on Surface Properties and Biocompatibility of PLGA Films. *Surf. Interface Anal.* **2010,** *42* (6‐7), 486-491.
43. Wan, Y.; Qu, X.; Lu, J.; Zhu, C.; Wan, L.; Yang, J.; Bei, J.; Wang, S., Characterization of Surface Property of Poly (lactide-co-glycolide) After Oxygen Plasma Treatment. *Biomaterials* **2004,** *25* (19), 4777-4783.
44. Yang, J.; Bei, J.; Wang, S., Improving Cell Affinity of Poly(D, L-lactide) Film Modified by Anhydrous Ammonia Plasma Treatment. *Polym. Adv. Technol.* **2002,** *13* (3‐4), 220-226.
45. Favia, P., Plasma Deposited Coatings for Biomedical Materials and Devices: Fluorocarbon and PEO-like Coatings. *Surf. Coatings Technol.* **2012,** *211*, 50-56.
46. Haïdopoulos, M.; Turgeon, S.; Laroche, G.; Mantovani, D., Chemical and Morphological Characterization of Ultra-Thin Fluorocarbon Plasma-Polymer Deposition on 316 Stainless Steel Substrates: A First Step Toward the Improvement of the Long-Term Safety of Coated-Stents. *Plasma Process. Polym.* **2005,** *2* (5), 424-440.
47. Limb, S. J.; Gleason, K. K.; Edell, D. J.; Gleason, E. F., Flexible Fluorocarbon Wire Coatings by Pulsed Plasma Enhanced Chemical Vapor Deposition. *J. Vac. Sci. Technol. A* **1997,** *15* (4), 1814-1818.

CHAPTER 2

EXPERIMENTAL METHODS

This chapter describes model synthetic biomaterial systems presented throughout this dissertation, including plasma modification strategies, fabrication methods, materials characterization techniques, and protocols for investigating material interactions in biological systems. These methodologies are also presented in publications that are the basis for Chapters 3-7.[1-6] This chapter includes four main sections: plasma reactor set-up and treatment conditions (2.1), substrate preparation and fabrication (2.2), material characterization techniques (2.3), and biological assessment strategies (2.4).

2.1 Plasma Reactor Set-up and Treatment Conditions

2.1.1 Plasma reactor set-up. All plasma treatments were performed using a home-built glass tubular reactor, inductively coupled to precursor gases via an 8-turn Ni-plated copper coil (schematic in Figure 2.1).[7-10] Radio frequency (rf, at 13.56 MHz) power (*P*) was applied through a matching network using either an RFX 600 or RFPP power supply (Advanced Energy Industries Inc., Fort Collins, CO). Vacuum was maintained using a rotary vane pump, and reactor pressure (*p*) was monitored using a Baratron® capacitance manometer (MKS Instruments Inc., Andover, MA). The reactor was allowed to stabilize at the base pressure (<10 mTorr) before introduction of plasma precursors. After the introduction of gaseous or high vapor pressure liquid precursor(s), the pressure was allowed to stabilize at pressures indicated for at least 5 min before plasma ignition.

2.1.2 Plasma treatments. Purity and manufacturer information for precursors used in plasma treatments are summarized in Table 2.1. Relevant plasma treatment conditions for these

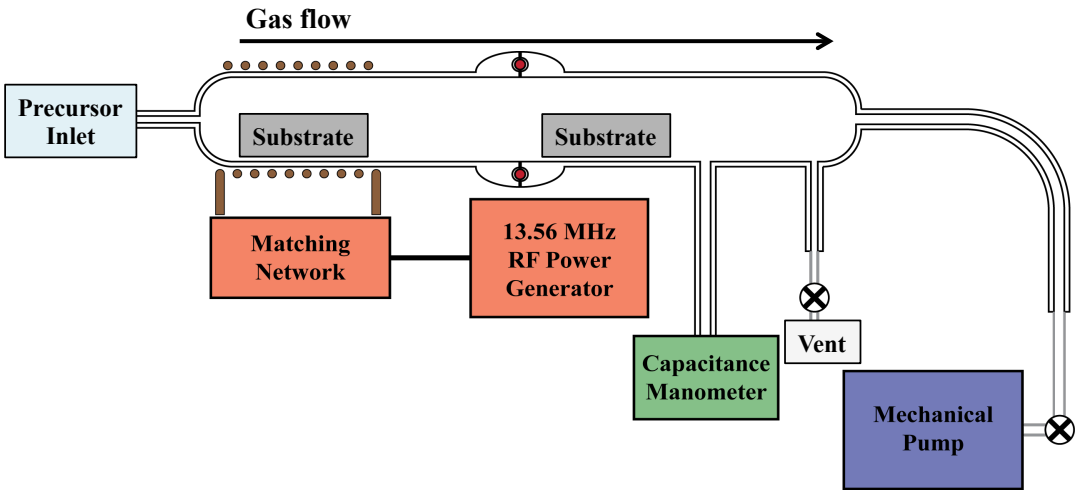

Figure 2.1. Inductively-coupled plasma reactor schematic. Here, the substrate is depicted both in the coil region and 19 cm downstream of the coil region, illustrating the range of substrate positions in the reactor.

Table 2.1. Summary of plasma precursors used for work presented in this dissertation.

Precursor	Precursor chemical formula or abbreviation	Purity	Manufacturer
1,7-octadiene [a]	OD	98%	Sigma-Aldrich
Ultrapure deionized water [a]	H_2O	-----	Millipore
Octofluoropropane	C_3F_8	99.96%	Airgas
Hexafluoropropylene oxide	HFPO	98%	Sigma-Aldrich
Allylamine [a, b]	AllylNH	≥99%	Sigma-Aldrich
Allyl alcohol [a, b]	AllylOH	98%	Sigma-Aldrich

[a] Liquid precursors
[b] AllylNH and allylOH were used both independently and as co-precursors

Table 2.2. Summary of plasma treatment conditions used for work presented in this dissertation.

Precursor	*P* (W)	Duty cycle (%)	Treatment time (min)	*p* (mTorr)	Flow rate (sccm)	Substrate placement	Chapter(s)
OD	4	100 [a]	5	100	0.35	In coil	3
	4, 25, 50		1, 5, 8, 10, 20			In coil, 10 cm, 19 cm	8
H_2O	20, 30, 50	100 [a]	1, 3, 5	200	0.70	15 cm	4
	20		4	150	0.53		7
C_3F_8	50	100 [a]	1, 5, 20, 60, 90	50	5.00	15 cm	3, 5, 7
		5	1				3
HFPO	300	10	5, 20, 60, 90	85	10.0	15 cm	5
AllylNH	50	5	15	100	0.35	15 cm	3, 6
AllylOH	50	5	15	100	0.35	15 cm	6, 7, 8

[a] 100% duty cycle is equivalent to a CW plasma.

precursors are summarized in Table 2.2, many of which were chosen based on previous optimization studies reported elsewhere.[8, 11-13] Parameters include the nature of the applied power, which was either continuous wave (CW) or pulsed. Pulsed power is reported in the form of duty cycle (d.c.), which is the ratio of pulse on time to total cycle time (e.g., a 5% d.c. represents 10 ms of on time in every 200 ms cycle). A d.c. of 100% is equivalent to CW plasma conditions. In Table 2.2, the power listed for each pulsed plasma condition is the peak power (i.e., the power applied during the on time), which can be converted into the equivalent CW power by multiplying the by the duty cycle (i.e., a pulsed plasma with a 5% duty cycle and 50 W peak power is equivalent to a 2.5 W CW plasma).

Gaseous precursors were used as-received and introduced into the reactor with flow rate regulated through mass flow controllers (MKS Instruments Inc., Andover, MA). Liquid precursors (identified in Table 2.1) were subjected to a minimum of three freeze-pump-thaw cycles to remove trapped atmospheric gases prior to use, and introduced into the reactor from a 50 mL Pyrex sidearm vacuum flask with a Teflon stopcock. Flow rates for liquid precursors were estimated following the methodology reported by Griesser and Gengenbach.[14] Substrates (described in Section 2.2) were placed on glass slides 15 cm from the center of the induction coil (except for select OD treatments where substrates were placed in the center of the coil) and up to nine substrates were treated simultaneously. Plasma treatments were performed using a single precursor except in the case of treatments with the mixed feed gas system containing allylNH and allylOH. Here, feedgas compositions were 20, 40, 60, and 80% allylNH by pressure for Si wafer treatments and 25, 50, and 75% allylNH by pressure for scaffold treatments. The remainder of the feedgas was allylOH.

2.2 Substrate Preparation and Fabrication

Three broad types of polymer constructs were fabricated in-house: porogen-leached scaffolds, electrospun fibers, and spin-coated films (Figure 2.2). In addition, silicon wafers (University Wafer, N-type 100) and glass slides (VWR micro slides, plain, 1 in × 3 in, 1.2 mm thickness) were used for select analysis, cut to approximately 1 cm × 3 cm rectangles and otherwise used as received. For work presented in Chapter 4, round glass slides were utilized as received (VWR micro cover glass, 12 mm diameter, 113 mm^2 area). For cell culture experiments presented in Chapter 6, non-tissue culture (NTC) polystyrene disks (diameter = 13.5 mm) were cut from polystyrene petri dishes (Fisher Scientific). NTC disks also served as the underlying substrate for spin-coated polymer films (Section 2.2.3).

2.2.1 Polymer scaffold fabrication. Polymer scaffolds were fabricated using the porogen leaching method (Figure 2.2a). Fabrication began by dissolving either PCL pellets (Sigma Aldrich, average M_n = 80,000), PLA pellets (NatureWorks IngeoTM Biopolymer grade 6202D), or a 50:50 mixture of PCL:PLA (by mass) in chloroform ($CHCl_3$, Fisher Scientific, ≥ 99.8%) in a sealed Pyrex media storage bottle. The solution was held at room temperature until the polymer was fully dissolved (~2 h for PCL only, ~6 h for PLA-containing solutions). As received sodium chloride (NaCl, Sigma Aldrich) was sieved (particle size 150–300 μm), and used as the porogen material. The porogen was added to the dissolved polymer/$CHCl_3$ mixture (5:95 w/w polymer:NaCl) and cast into Teflon molds that were machined in-house. Three different types of molds were used depending on the study: those with 18 10 mm x 3 mm wells (illustrated in the Figure 2.2a schematic), those with 16 20 mm x 3 mm wells, and those with 18 10 mm x 6 mm wells. After casting, scaffolds dried in the molds for 1 h under ambient conditions followed by submersion in absolute ethanol (Pharmco-AAPER®, ACS/USP) for 3 h, allowing for $CHCl_3$

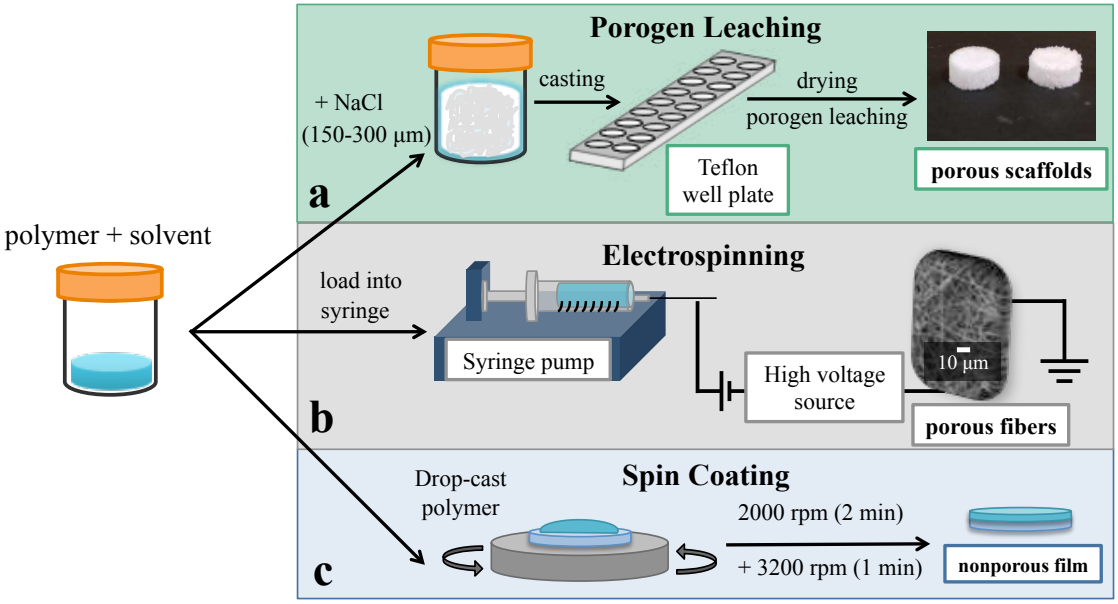

Figure 2.2. Overview of in-house substrate polymeric fabrication methodologies including (a) porogen leaching to create scaffolds, (b) electrospinning to make fiber mats, and (c) spin coating to produce polymer films. All materials began with a polymer solution containing either polycaprolactone, polylactic acid, or a combination of the two polyesters.

removal via phase separation and evaporation. Scaffolds were then placed in deionized water to allow for porogen leaching, where the water was changed three times a day for four days to ensure complete leaching (scaffolds were removed from the mold approximately halfway through the leaching process). Scaffolds were removed from the water and placed in a petri dish to fully dry under ambient laboratory conditions before use. Untreated and plasma-modified scaffolds were freeze-fractured by placing in liquid nitrogen for 4–6 s and slicing vertically using a scalpel for cross-sectional X-ray photoelectron spectroscopy and scanning electron microscopy analyses (outlined in more detail in Section 2.3).

2.2.2 Polymer electrospun fiber fabrication. Electrospun fibers were fabricated using PCL, PLA/PCL, and PLA. Specific parameters for each polymer system studied are summarized in Table 2.3, and an overview of the electrospinning process is displayed in Figure 2.2b.

PCL and PCL/PLA solutions were prepared by fully dissolving the polymer (either PCL or a 1:1 mixture of PCL:PLA) at room temperature. The PLA solution was prepared by dissolving the polymer in the solvent by heating in a vented scintillation vial placed in a water bath held at ~80 ºC for 4 h. This solution was cooled for 30 min before electrospinning. Polymer solutions were loaded into a 5 mL syringe (BD, Luer-Lok™ tip) equipped with a needle (Hamilton 90520). The syringe was placed in a syringe pump (Kent Scientific Corporation, Genie Touch) with a constant dispensing rate, and the pump was oriented such that the tip of the needle was 15 cm away from a conductive disk wrapped in heavy-duty Al foil (the collector). Positive and negative electrodes were attached to the collector and the needle, respectively, and a constant voltage was applied for the entirety of the electrospinning process using a high voltage power supply (Gamma High Voltage Research, Ormond Beach, FL).

Table 2.3. Summary of electrospinning parameters used to fabricate electrospun mats presented in this dissertation.

Polymer	Co-solvent ratio [a]	Solution concentration (w/v%)	Applied voltage (kV)	Flow rate (mL/h)	Fiber spinning time (h)
PCL	7:3 dichloromethane:methanol	8	16	5	1
PCL/PLA	3:1 $CHCl_3$:methanol	10	20	1	2
PLA	3:1 $CHCl_3$:dimethylformamide	12	20	0.5	1

[a] Solvent manufacturers and grades are as follows: dichloromethane: EMD, HPLC grade; methanol: EMD, ACS grade, $CHCl_3$: Fisher Scientific, HPLC grade; dimethylformamide: Fisher Scientific, ACS grade.

2.2.3 Polymer film fabrication. Polymer films were fabricated using a spin coater (Laurell Technologies, WS-650-23NPP/LITE), as shown in Figure 2.2c. Polymer solutions (17% w/v) were prepared by dissolving either PCL, PLA, or 1:1 PCL:PLA in $CHCl_3$ using identical methodologies described in Section 2.2.1. To fabricate a spin-coated film, an NTC disk was loaded on the spin coater and the polymer solution was dispensed onto the center of the disk using a transfer pipette (solutions were too viscous for automatic pipette use). The spin coater program was set such that films spun in two steps: the first at 2000 rpm for 2 min and directly followed by the second at 3200 rpm for 1 min. After spinning, films were immersed in absolute ethanol for 1 h and fully dried under ambient laboratory conditions before further use.

2.2.4 Nitric oxide releasing film fabrication. The full methodologies for preparation of nitrosated-PLGH cysteine and nitrosated Tygon® films are described elsewhere,[5-6, 15-16] but a brief overview is included here to provide context for data presented in Chapter 4.

For nitrosated-PLGH cysteine, a carboxyl-functionalized polymer was prepared from L-lactide, glycolide and 2,2-bis(hydroxymethyl propionic acid) (PLGH). The carboxyl group of the polymer segment was further functionalized with cysteine. To facilitate nitrosation, the *t*-butyl nitrite (8.4 mg in 1 mL of 2 MeOH: 1 DCM) was added to the polymer solution, which was stirred and protected from light for 4 h followed by a 2 h vacuum step to remove the excess solvent. The final product was a pink-colored powder which is a visual confirmation of the success of the nitrosation process (nitrosation efficiency was ~35%, as quantified via modified Ellman's assay).[16] Films of the *S*-nitrosated PLGH-cysteine were prepared by re-dissolving the polymer in 2 MeOH: 1 DCM (50 mg mL^{-1}). Aliquots of the polymer solution (100 µL) were dispensed on round glass slides (VWR micro cover glass, 12 mm diameter, 113 mm^2 area) and dried overnight protected from light.

The base of the other NO-releasing film discussed in Chapter 4 is Tygon® (Formula R-3603, Saint-Gobain Performance Plastics, Akron, OH, USA). The NO donor used in Tygon® films is *S*-nitrosoglutathione (GSNO). GSNO was synthesized following the protocol published by Hart.[17] Tygon® was dissolved in THF at a concentration of 0.075 g mL^{-1}. Tygon® only films were used as controls, and were prepared by delivering 750 µL of the Tygon®/THF solution to the bottom of a 20 mL glass beaker. GSNO-incorporated films were prepared by incorporating either 5% or 20% w/w GSNO in Tygon® solution (denoted as GSNO5 and GSNO20, respectively) before casting into the beaker. Films were dried overnight at room temperature and protected from light. The resulting Tygon® films were transparent whereas GSNO5 and GSNO20 films are pink in color because of the GSNO donor.

2.3 Material Characterization Techniques

A multitude of surface and bulk characterization techniques were used to evaluate material properties both before and after substrate modification. The values reported throughout this dissertation represent a minimum of three replicate measurements made on each sample with a minimum of three different samples ($N \geq 9$), regardless of the analysis unless otherwise noted. All analyses were conducted immediately (<2 h) after plasma treatment with the exception of X-ray photoelectron spectroscopy on porogen-leached scaffolds and NO-releasing polymer constructs. Here, outgassing required samples to remain in the pre-evacuation chamber for approximately 8 h before introduction into the main chamber.

2.3.1 Wettability analysis. Water contact angle (WCA) experiments were performed using a Krüss DSA30 goniometer. Substrates (described in Section 2.2) did not require further sample preparation for WCA analysis with the exception of electrospun fibers and NO-releasing Tygon® films, which were fixed to glass slides using a piece of double stick tape at each end.

Static and dynamic WCA data were collected depending on the nature of the substrate. Regardless of the type of data, deionized water (Millipore, 18 mΩ cm) was used, and ambient laboratory conditions were 23 ± 1 °C and ~25% relative humidity for all data collection. The probe liquid parameters (density = 0.9970 g/mL, viscosity = 0.0010 cP, and surface tension = 72.16 mN/m) were programmed into the onboard software and utilized when performing all WCA fitting. For non-sorbing materials, static WCA values were collected using drop volumes between 2 and 8 μL, depending on the substrate, where drops stabilized in <1 s. When WCA values were < 20º and >20º, the circle and tangent methods contained within the onboard software were utilized to fit static data, respectively (algorithms assumes circular and elliptical drop profiles, respectively).

Different types of dynamic data were collected depending on the sample, all using the high-speed video recording capabilities of the goniometer. Regardless of the type of dynamic data, a program for video recording and drop dispensing was created using the onboard software, and the tangent method was used for fitting. Advancing and receding CA values on plasma-treated substrates (Chapter 3) were collected by using a drop volume loop running from 0 to 2 to 10 to 2 μL, where the first step occurred at a dispensing rate of 500 μL/s and subsequent steps occurred at a dispensing rate of 300 μL/s. Video data were collected over the duration of these dynamic experiments (typically 15 s) at 25 frames/s. CA values were plotted as a function of time to obtain advancing and receding angles, and hysteresis was calculated by subtracting the receding angle value from the advancing angle value. Different types of dynamic wettability data were reported in cases where measuring a static WCA was not possible (i.e., when the equilibrium CA was equal to 0º because of sorption or spreading phenomena). In these cases, time = 0 s is defined as the time the water drop first comes into contact with the construct

surface. In some cases, water absorption data reported in Chapters 3 and 6 were used to calculate average absorption rate by dividing drop volume by the time it took for the drop to be fully absorbed (determined from video analysis). Video data taken at 25 frames/s over 10 s were used to measure water sorption behavior for relevant constructs in Chapters 3 and 6. Wettability data for H_2O plasma-treated PLGH constructs (Chapter 4) were collected at 64 frames/s for 10 s and are reported in terms of water spreading time (for PLGH films) or stabilized WCA values (Tygon® films). The tangent fitting method contained within the onboard software was utilized to fit all dynamic data, where CA values were plotted as a function of time.

Contact angle titration experiments were performed for results reported in Chapter 3. Three different aqueous solutions (pH ~1, 7, 13) were prepared using Millipore water, hydrochloric acid (0.6 M, EMD, ACS grade) and sodium hydroxide (0.1 M, Mallinckrodt Chemicals, ACS grade), where pH was determined using a pH probe (Mettler Toledo, SevenEasy pH Meter S20). To avoid contamination between solutions, drops were delivered using an external syringe pump (New Era Pump Systems, Inc., Model NE-1000) equipped with a separate set of hardware (i.e., tubing, syringe, etc.) for each solution. A minimum of three different replicate measurements on two different samples were collected to determine the wetting characteristics of each plasma-treated substrate.

2.3.2 Composition analysis. X-ray photoelectron spectroscopy (XPS) performed on a Physical Electronics PE5800 ESCA/AES system with a monochromatic Al K_α X-ray source (1486.6 eV), hemispherical analyzer, and multichannel detector provided information on surface composition and binding environments. All substrates with the exception of Si wafers were mounted on the sample holder using carbon tape. For porogen-leached scaffolds, both the argon ion and electron (~5 eV) neutralizers were used to minimize sample charging. For other

constructs, only the electron neutralizer was used. Survey spectra were collected for 2–5 min from 10 to 1100 eV (pass energy = 187.9 eV, resolution = 0.80 eV). High-resolution spectra were typically collected over 15 min for all elements with compositions >1% from survey spectra (pass energy = 23.5 eV, resolution = 0.10 eV), and high-resolution spectra were used for all quantification, including atomic composition ratios (i.e., F/C, N/C, O/C) reported in Chapters 3, 5, 6, and 8.

Charge correction and fitting of high-resolution C_{1s} were performed using either XPSPEAK 4.1 software (Raymund Kwok, UK Surface Analysis Forum) or CasaXPS (Neil Fairley, Casa Software Ltd., Cheshire, UK). Spectra were charge-corrected using different peaks in the C_{1s} high-resolution spectra depending on the sample. For fluorocarbon plasma treated materials, the CF_2 component was used to index at 292.0 eV (Chapter 5). For all other constructs, the C-C/C-H component was used. Although reported binding energy values used to index the aliphatic environment cover the 285.0 ± 0.4 eV range,[18] we opted to use 285.0 eV to index spectra. High-resolution C_{1s} spectra were fit using multiple Gaussian fits corresponding to different carbon binding environments, where the FWHM value for each environment was constrained to be ≤ 2.0 eV (chi-squared values <1.5). More detail on specific binding environments included in C_{1s} spectra can be found accompanying XPS data in each chapter. For comparison with plasma-modified materials throughout this dissertation, a deconvoluted high-resolution C_{1s} spectrum for untreated PCL scaffolds are shown in Figure 2.3. Also pictured in Figure 2.3 are the polymer structures of polyesters used for construct fabrication (PCL and PLA).

2.3.3 Morphological analysis. Scanning electron microscopy (SEM) was performed using a JEOL JSM-6500F microscope to qualitatively evaluate substrate architecture. Samples were grounded with carbon tape. For scaffolds, an accelerating voltage of 1.0 kV and a working

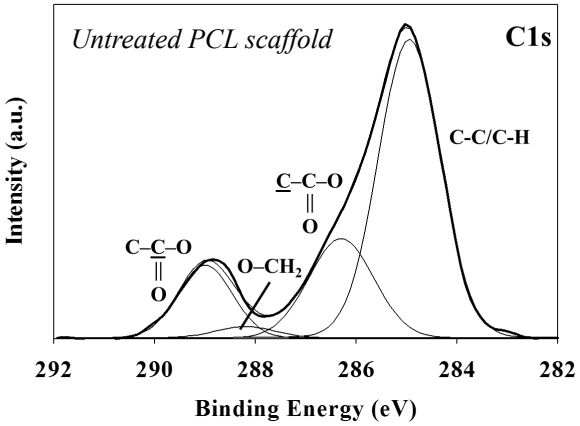

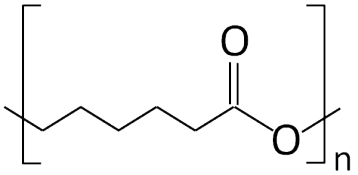

poly(ε-caprolactone) (PCL) **poly(lactic acid) (PLA)**

Figure 2.3. Representative high-resolution C_{1s} XPS spectra of a native PCL scaffold; chemical structures of polyesters used to fabricate polymer constructs for work presented throughout this dissertation (bottom).

distance of ~10.0 mm were typically used (Chapters 3, 5, and 6). For scaffolds, images were collected at 30, 100, and 270× magnification. PCL electrospun fibers were coated with ~5 nm Au prior to SEM analysis, accelerating voltage of 5.0 kV, and a working distance of ~10.0 mm were used (Chapters 3 and 8). For SEM evaluation of asymmetric polysulfone ultrafiltration membranes (US Filter Inc.) presented in Chapter 3, materials were coated with ~10 nm Au prior to analysis (accelerating voltage of 5.0 kV and working distance of ~4.0 mm). For PLGH constructs (Chapter 4), images were collected at 100, 250, and 500× magnification. Three to five images were taken of each sample with an accelerating voltage of 1 kV and a working distance of approximately 10.0 mm.

Collecting quantitative morphological data on porogen-leached scaffolds is challenging because of their complex morphology. A quantitative assessment of polymer film roughness, however, was attainable using a Zemetrics ZeScope optical profilometer (Chapters 3, 4 and 8). For unmodified and plasma-modified glass slides (Chapter 3), scans were collected of $2220 \times 2200\ \mu m^2$ areas using a 20× magnification objective with a scan length of 150 μm in the z-axis and a signal threshold of 1.0%. Two scans were collected on two independent samples for a total of n = 4. For NO-releasing polymer films (Chapter 4), a single scan was collected for a $250 \times 350\ \mu m^2$ area using the same magnification objective, scan length, and signal threshold described above. Two to three scans were collected on each of 3 samples, for a total of n = 6 (PLGH films) or n = 9 (Tygon® films) for each treatment. Both R_a and R_q values were determined from an average of the 6-9 scans using the ZeMaps measurement and analysis software (Fourier filter fit used), where R_a and R_q represent the arithmetic mean and root mean square roughness across a sample scan, respectively. For polymer films discussed in Chapter 8, three scans were collected on each type of film (unmodified, OD plasma treated, allylOH plasma

treated) for a 1280 × 960 μm^2 area with the same objective, scan length, and threshold listed above. For OD films deposited on Si wafers (Chapter 8), a minimum of three scans were collected on each sample (scan length of 30 μm in the z-axis, signal threshold of 2.0%). Here, most data were collected using the 20× magnification objective (375 × 280 μm^2 scan area), but the 100× magnification objective was used in the case of wafers placed 19 cm downstream and treated using 25 W OD plasmas for 20 min (47 × 35 μm^2 scan area).

2.3.4 Additional surface analysis. One important film characteristic presented in this dissertation is film thickness. Specifically, fluorocarbon and hydrocarbon film thicknesses were determined using a VB-400 VASE Ellipsometer (J.A. Woollam Co., Lincoln, NE). VASE spectra collected over a 300–1100 nm range in 20 nm increments at incident angles of 55º, 65º, and 75º. Isotropic scans (with depolarization) were collected for all VASE measurements. VASE spectra were fit with a four-layer model (bulk Si, amorphous Si, SiO_2, and a Cauchy layer) using the WVASE modeling software.

Initially, concurrently fitting all four components of the model (including thickness and optical constants) did not accurately reproduce experimental VASE data. This was likely because of wafer contamination. Thus, Si wafers were first pre-treated using an oxygen plasma (typical conditions: P = 100 W, p = 100 mTorr, treatment time = 5 min), which resulted in oxide layer growth. The oxygen plasma-treated wafer was then analyzed immediately using VASE, and the first three layers of the model (bulk Si, amorphous Si, and SiO_2) were fit with regards to both thickness and optical constants. The same wafer was then treated using plasma deposition conditions of interest, and the fourth layer of the model (Cauchy layer) was fit separately.

Systems evaluated following this methodology included films deposited from C_3F_8 and HFPO plasmas under identical processing conditions as PCL scaffolds (Chapter 5), as well as

films from OD plasmas were deposited on Si wafers under identical processing conditions as polymer constructs (Chapter 8). Notably, data collected on OD plasma deposited films were fit over restricted wavelength ranges (400–1100 nm for films deposited at P = 4W in the coil and 800–1100 nm for films deposited at P = 25 W 19 cm downstream) because films absorbed at lower wavelengths.

An additional methodology for assessing substrates treated with OD plasmas was Fourier transform infrared spectroscopy (FTIR). Specifically, FTIR was used to assess bulk chemical functionality after plasma treatment. FTIR spectra were collected in transmission mode using a Nicolet 6700 FTIR (Thermo Fisher Scientific, Madison, WI). Spectra were compiled from 120 scans with a 4 cm^{-1} resolution. Baseline correction and atmospheric signal suppression were performed on each spectrum using Omnic 8.2.

2.4 Biological Assessment Strategies

2.4.1 Cell attachment and growth on fluorocarbon plasma-modified constructs. Interactions between fluorocarbon-modified materials and mammalian cells (presented in Chapter 5) were assessed using human dermal fibroblasts (HDF, ZenBio, Inc.). HDF were grown in media (Media 106 supplemented with 2% v/v fetal bovine serum, 1 μg/ml hydrocortisone, 10 ng/ml human epidermal growth factor, 3 ng/ml basic fibroblast growth factor, 10 μg/ml heparin, 125 μg⁄ml amphotericin B, 5 mg⁄ml gentamicin from Gibco®) on a tissue culture (TC) plate (VWR), and were collected from a 25T flask by adding 1 mL of a trypsin-EDTA (0.25%) solution and re-suspended at 50,000 cells/mL. Untreated scaffolds, C_3F_8 and HFPO plasma treated scaffolds were used in cell experiments. Representative FC plasma treated scaffolds (20 min C_3F_8 and 60 min HFPO) were used as the F/C ratios on the scaffold tops and cross-sections reached a maximum value at these treatment times, and did not change (within error) upon

longer treatment times. All scaffolds were fixed at the base of a TC plate using a minimal amount of double-sided carbon tape to ensure complete immersion of the scaffold in cell culture; a 1 mL aliquot of cells was added to each well. Several wells of HDF cells only were used as positive controls and cells were also exposed to the double-sided carbon tape as a control experiment. All control sample wells were seeded with 50,000 cells/well. Samples were incubated for 72 h (37 °C, 5% CO_2) and cell culture medium was replaced with fresh medium after 24 and 48 h. Samples were rinsed twice with 150 mM phosphate buffered saline (PBS), and fixed with 3.7% methanol-free formaldehyde in PBS for 10 min at room temperature. After rinsing samples twice with PBS and exposing to acetone cooled to 0 °C for 4 min, samples were rinsed twice again with PBS and stained using 0.5 mL of staining solution for 20 min at room temperature. Staining solution comprised DAPI and Alexa Fluor® 568 Phalloidin (Life Technologies) at concentrations of 7.60 μM and 6.60 μM, respectively, in PBS. Samples were finally rinsed three times with PBS, and scaffolds were placed in dry wells for >24 h before imaging.

Fluorescence microscopy images were taken using an Olympus IX73 fluorescence microscope. An excitation wavelength of 358 nm was used for DAPI (461 nm emission observed), and a wavelength of 578 nm was used for Alexa Fluor® 568 Phalloidin (600 nm emission observed). Images of cells on scaffolds are composed of three overlayed images (transmitted, DAPI, and Alexa), combined using the Olympus CellSens software, whereas images of cells on control wells comprise two overlayed images (DAPI and Alexa).

2.4.2 Cell attachment, growth, and viability on allylNH and allylOH plasma-modified substrates. HDF were grown and collected as described in Section 2.4.1. Plasma polymer films (allylNH, allylOH, and copolymerized allylNH/OH) on scaffolds and NTC disks, as well as

untreated scaffolds and NTC disks, were used in cell experiments. Experiments were performed using 24 well plates wherein a 1 mL aliquot of cell solution (~50,000 cells) was added to each well. Several wells were used as positive controls, which were also seeded with 50,000 cells/well. Samples were incubated for 48 h (37 °C, 5% CO_2) and cell culture medium was replaced with fresh medium after 24 h. Samples were fixed, stained, and imaged following protocols described in Section 2.4.1.

Viability assays were performed on allylNH/OH plasma treated materials. For each replicate, three wells (TC plate, positive control), three untreated substrates (either scaffolds or NTC disks), and three plasma-modified substrates were used for each plasma treatment studied. Media was removed from all samples and plasma modified substrates were moved to a clean plate. A CellTiter-Blue® solution was prepared by adding 20 µL aliquot of as-received CellTiter-Blue® reagent (Promega) for every 100 µl of warm cell media, and a 400 µl aliquot of this solution was added to each well. After 3 h incubation at 37 °C in a humid atmosphere (i.e., a pan of water was placed at the bottom of the incubator) with 5% CO_2, absorbance readings were measured with a plate reader (BioTek Synergy 2) at 570 nm and 600 nm.

2.4.3 Bacteria attachment and growth on allylNH and allylOH plasma-modified substrates. To further assess bioreactivity of the copolymerized materials, bacterial attachment on plasma polymer films deposited on glass slides was evaluated using *Escherichia coli* (*E. coli)*. Lyophilized bacteria were reconstituted in warm nutrient broth media (NBM) and grown overnight at 37 °C and 150 rpm. The overnight culture was diluted 1:1 using a glycerol solution (30% v/v) and stored at −80 °C. Prior to each assay, a tube of bacterial culture was thawed and centrifuged at 4700 rpm for 10 min to collect a pellet. The pellet was re-suspended in warm NBM and incubated overnight at 37 °C and 150 rpm. The overnight culture was diluted with

fresh warm NBM to an optical density at 600 nm ($O.D._{600nm}$) of ~0.1 and incubated (37 ºC at 100 rpm) until it reached the logarithmic growth phase ($O.D._{600nm}$ ~0.3) prior to exposing the substrates to the bacteria solution.

Substrates were placed in individual wells of a 6 well TC plate and covered with 4 mL of bacterial solution in the logarithmic growth phase. Samples used for attachment and growth assessment were incubated at 37 °C for 18 h in static condition and triple rinsed with sterile NaCl solution (0.85 % w/v). The viability of the bacteria cells was assessed by performing a live/dead assay where rinsed samples were exposed to propidium iodide (PI) and SYTO9 solution (3 µL PI, 0.5 µL SYTO9 in 0.85% w/v $NaCl_{(aq)}$) and incubated at room temperature for 30 min, protected from light. Substrates were rinsed with copious amounts of ultrapure water and stored protected from light in clean 6-well TC plates until further analysis. The above procedure was repeated for control substrates, including a hydrophilic control (glass slide, WCA = 20.3 ± 1.4°) and a hydrophobic control (plasma polymerized C_3F_8 film, WCA = 110.3 ± 0.3°).

Fluorescence microscopy images were acquired using an Olympus IX73 fluorescence microscope. An excitation wavelength of 543 nm was used for PI (617 nm emission observed), and a wavelength of 488 nm was used for SYTO9 (500 nm emission observed). All fluorescence images shown here are composites of PI and SYTO9 image combined using the Olympus CellSens software.

2.4.4 Thromboelastography (TEG) analyses. Experimental methods presented in this Section correspond to experiments presented in Chapter 7, wherein a commercial thromboelastography instrument was modified to accommodate unmodified and plasma-modified 3D PCL scaffolds.

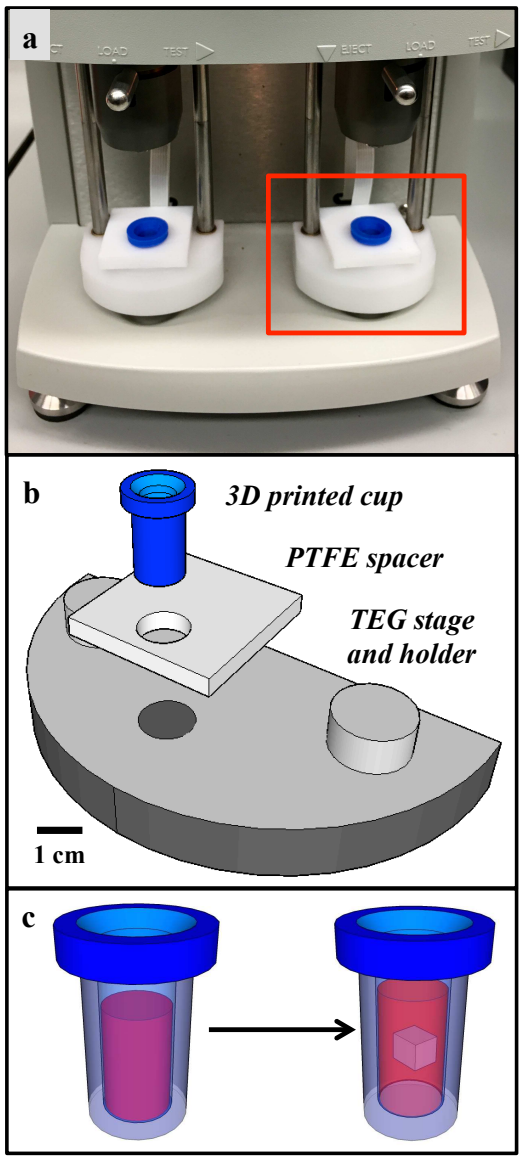

Figure 2.4. Overview of interfacing 3D printed consumables with the TEG instrument. (a) photograph of the 3D printed cups loaded into the TEG instrument. The red box in (a) shows the region of the TEG instrument illustrated in panel (b). (b) Expanded view CAD model of the 3D printed cup, PTFE spacer, and TEG stage (posts connecting the stage to load cell are cut off for clarity). (c) CAD model of 3D printed cup after the addition of the blood plasma solution (left) and after addition of the solid polymer scaffold (right).

CAD models of TEG cups were created using Google SketchUp Make 2015. Cups were designed such that all dimensions were identical to standard Cyrolite® plastic TEG consumables (Haemonetics Corporation) with the exception of the cup height. This resulted in a cylindrical cup with a sloped lip (Figure 2.4a) with the following dimensions: outer base radius = 5.44 mm, outer lip radius (i.e., closest to the top of the cup) = 7.5 mm, total height = 18.30 mm. SketchUp files were converted to .gcode files for 3D printing, and were printed with a LulzBot AO-100 3D printer (Aleph Objects Inc., Loveland Colorado) using a blue 2.85 mm acrylonitrile butadiene styrene (ABS) filament (ABS films have a water contact angle of ~80º [19]). 3D printed cups had a volume of ~520 μL – approximately 50% larger than standard consumables. A white Teflon PTFE sheet (height = 0.188", McMaster Carr) was machined to accommodate the 3D printed TEG cup (Figure 2.4), effectively serving as a spacer between the TEG stage and load cell.

Porogen-leached scaffolds (section 2.2.1) were cut into quarters by slicing vertically using a scalpel such that they could be placed easily into the TEG cups (the volume of each sample was ~75 μL). Typically, two scaffolds (8 scaffold quarters) were plasma-modified simultaneously. Different low-temperature plasma precursors and treatment conditions were selected based on previous studies to create scaffolds with a variety of surface functionality (fluorocarbon,[2] nitrogen-containing,[4] alcohol-containing[4, 20]). In other words, bulk properties (porosity, geometry) were maintained and surface properties (chemistry, wettability) were varied. See Tables 2.1 and 2.2 for plasma parameters used.

For the proof-of-concept experiments presented in Chapter 7, blood was collected from a single healthy, non-smoking volunteer individual on no medications with normal complete blood count, serum diagnostic panel, no evidence of inflammation, and a normal physical examination. The Colorado State University Institutional Review Board (IRB) deemed that IRB approval was

not required. Blood was collected in tubes containing buffered sodium citrate (BD Vacutainer), and plasma was harvested from citrated human whole blood collected after centrifugation at 4500 × g for 10 minutes. After processing, blood plasma aliquots (700 μL) were added to 2 mL cryogenic vials (Fisher Scientific) and stored in a −80º C freezer until use (less than two weeks).

Before each run, one vial of plasma was removed from the freezer and rapidly thawed with shaking for approximately 1 min in a 37º C water bath. After thawing, the vial was kept on ice until use (<25 min). A TEG® 5000 Thromboelastograph® Hemostasis System (Haemonetics Corporation) was used for all TEG experiments. For each experiment, the disposable TEG pin was loaded in the instrument using standard TEG consumables (Haemonetics Corporation). The 3D printed cup was loaded into the instrument over the machined Teflon®, assuring that the cup fit snugly into the instrument. 10 μL of freshly prepared tissue factor solution [TriniCLOT PT Excel Reagent (TCoag) and distilled water] were added, resulting in a 1% w/v final concentration in the cup. 330 μL of thawed plasma were then added to the cup. For experiments wherein a scaffold was added to the TEG cup, the solid scaffold was immediately placed directly into the plasma mixture (i.e., the scaffold was free floating in solution, Fig. 2.4c). After the solution was left to warm up to the temperature of the TEG (37^{o}C, ~2 min), 20 μL of a calcium chloride solution (0.2 M, Haemonetics Corporation) were added to recalcify the mixture and initiate coagulation. After mixing several times via pipette, the TEG run was started and left to run for either 25 min or until maximum amplitude was reached. TEG experiments were performed within 24 h of scaffold LTP modification. TEG data were collected in triplicate for each type of sample (e.g., blank, untreated scaffold) to gauge reproducibility.

Both standard thromboelastograph tracings and velocity curves were analyzed in this work, where velocity curves are the first derivatives of the thromboelastograph tracings. In

addition to the standard TEG parameters obtained from thromboelastograph tracings [reaction time (R), maximum amplitude (MA), and time to maximum amplitude (TMA)], clot lifespan parameters were collected:[21] maximum rate of thrombus generation (TMRTG, the time interval observed prior to maximum speed of clot growth), maximum rate of thrombus generation (MRTG, the maximum velocity of clot growth observed), and total thrombus generation (TTG, the total area under the velocity curve during clot growth and a measure of overall clot growth). A detailed explanation of these parameters can be found elsewhere.[22-23] Although there is controversy in the literature regarding the relative utility of the thromboelastograph tracings and the velocity curves,[21, 24] these data collectively provide a reasonably comprehensive coagulation assessment.

A one-way ANOVA was conducted to explore differences in the mean TEG measurement values (velocity curve data) of different materials. Significant differences were observed between materials for both the maximum rate of thrombus generation, MRTG [$F(4, 10) = 37.3$, $p < 0.0001$] and total thrombus generation, TTG [$F(4, 10) = 25.8$, $p < 0.0001$]. Effect sizes (η^2) were >0.9. Post-hoc comparisons (Tukey HSD) were used to evaluate differences in MRTG and TTG, and significant differences from these comparisons are denoted in Figure 7.4 ($p < 0.05$ level).

REFERENCES

1. Hawker, M. J.; Olver, C. S.; Fisher, E. R., Modification of a Commercial Thromboelastography Instrument to Measure Coagulation Dynamics with Three-dimensional Biomaterials. *Biointerphases* **2016,** *11* (2), 029602.
2. Hawker, M. J.; Pegalajar-Jurado, A.; Fisher, E. R., Conformal Encapsulation of Three-Dimensional, Bioresorbable Polymeric Scaffolds Using Plasma-Enhanced Chemical Vapor Deposition. *Langmuir* **2014,** *30* (41), 12328-12336.
3. Hawker, M. J.; Pegalajar-Jurado, A.; Fisher, E. R., Innovative Applications of Surface Wettability Measurements for Plasma-Modified Three-Dimensional Porous Polymeric Materials: A Review. *Plasma Process. Polym.* **2015,** *12* (9), 846-863.
4. Hawker, M. J.; Pegalajar-Jurado, A.; Hicks, K. I.; Shearer, J. C.; Fisher, E. R., Allylamine and Allyl Alcohol Plasma Copolymerization: Synthesis of Customizable Biologically-Reactive Three-Dimensional Scaffolds. *Plasma Process. Polym.* **2015,** *12* (12), 1435-1450.
5. Joslin, J. M.; Lantvit, S. M.; Reynolds, M. M., Nitric Oxide Releasing Tygon Materials: Studies in Donor Leaching and Localized Nitric Oxide Release at a Polymer-Buffer Interface. *ACS Appl. Mater. Interfaces* **2013,** *5* (19), 9285-9294.
6. Mann, M. N.; Neufeld, B. H.; Hawker, M. J.; Pegalajar-Jurado, A.; Paricio, L. N.; Reynolds, M. M.; Fisher, E. R., Plasma-modified Nitric Oxide-releasing Polymer Films Exhibit Time-delayed 8-log Reduction in Growth of Bacteria. *Biointerphases* **2016,** *11*, 031005.
7. Bogart, K.; Dalleska, N.; Bogart, G.; Fisher, E. R., Plasma Enhanced Chemical Vapor Deposition of SiO_2 Using Novel Alkoxysilane Precursors. *J. Vac. Sci. Technol., A* **1995,** *13* (2), 476-480.
8. Butoi, C. I.; Mackie, N. M.; Gamble, L. J.; Castner, D. G.; Barnd, J.; Miller, A. M.; Fisher, E. R., Deposition of Highly Ordered CF_2-rich Films Using Continuous Wave and Pulsed Hexafluoropropylene Oxide Plasmas. *Chem. Mater.* **2000,** *12* (7), 2014-2024.
9. Mackie, N. M.; Dalleska, N.; Castner, D. G.; Fisher, E. R., Comparison of Pulsed and Continuous-wave Deposition of Thin Films from Saturated Fluorocarbon/H_2 Inductively Coupled rf Plasmas. *Chem. Mater.* **1997,** *9* (1), 349-362.
10. Mackie, N. M.; Castner, D. G.; Fisher, E. R., Characterization of Pulsed-plasma-polymerized Aromatic Films. *Langmuir* **1998,** *14* (5), 1227-1235.
11. Cuddy, M. F.; Fisher, E. R., Contributions of CF and CF_2 Species to Fluorocarbon Film Composition and Properties for C_xF_y Plasma-Enhanced Chemical Vapor Deposition. *ACS Appl. Mater. Interfaces* **2012,** *4* (3), 1733-1741.
12. Martin, I. T.; Malkov, G. S.; Butoi, C. I.; Fisher, E. R., Comparison of Pulsed and Downstream Deposition of Fluorocarbon Materials from C_3F_8 and c-C_4F_8 Plasmas. *J. Vac. Sci. Technol., A* **2004,** *22* (2), 227-235.
13. Tompkins, B. D.; Dennison, J. M.; Fisher, E. R., H_2O Plasma Modification of Track-etched Polymer Membranes for Increased Wettability and Improved Performance. *J. Membr. Sci.* **2013,** *428*, 576-588.
14. Gengenbach, T. R.; Griesser, H. J., Deposition Conditions Influence the Postdeposition Oxidation of Methyl Methacrylate Plasma Polymer Films. *J. Polym. Sci., Part A: Polym. Chem.* **1998,** *36* (6), 985-1000.

15. Damodaran, V. B.; Reynolds, M. M., Biodegradable S-nitrosothiol Tethered Multiblock Polymer for Nitric Oxide Delivery. *J. Mater. Chem.* **2011,** *21* (16), 5870-5872.
16. Pegalajar-Jurado, A.; Joslin, J. M.; Hawker, M. J.; Reynolds, M. M.; Fisher, E. R., Creation of Hydrophilic Nitric Oxide Releasing Polymers via Plasma Surface Modification. *ACS Appl. Mater. Interfaces* **2014,** *6* (15), 12307-12320.
17. Hart, T. W., Some Observations Concerning the S-nitroso and S-phenylsulphonyl Derivatives of L-cysteine and Glutathione. *Tetrahedron Lett.* **1985,** *26* (16), 2013-2016.
18. Swift, P., Adventitious Carbon—the Panacea for Energy Referencing? *Surf. Interface Anal.* **1982,** *4* (2), 47-51.
19. Desrousseaux, C.; Cueff, R.; Aumeran, C.; Garrait, G.; Mailhot-Jensen, B.; Traoré, O.; Sautou, V., Fabrication of Acrylonitrile-Butadiene-Styrene Nanostructures with Anodic Alumina Oxide Templates, Characterization and Biofilm Development Test for Staphylococcus epidermidis. *PLoS One* **2015,** *10* (8), e0135632.
20. Shearer, J. C. Enhanced Surface Functionality via Plasma Modification and Plasma Deposition Techniques to Create More Biologically Relevant Materials. Ph.D. Dissertation, Colorado State University, Fort Collins, CO, 2013.
21. Nielsen, V. G., Beyond Cell Based Models of Coagulation: Analyses of Coagulation with Clot "Lifespan" Resistance-time Relationships. *Thromb. Res.* **2008,** *122* (2), 145-152.
22. TEG® 5000 Thrombelastograph® Hemostasis System User Manual. *Haemoscope Corporation, Niles, IL, USA.* **2004**, 1-11.
23. Peng, H. T., Thromboelastographic Study of Biomaterials. *J. Biomed. Mater. Res. Part B Appl. Biomater.* **2010,** *94* (2), 469-485.
24. Ellis, T. C.; Nielsen, V. G.; Marques, M. B.; Kirklin, J. K., Thrombelastographic Measures of Clot Propagation: A Comparison of Alpha with the Maximum Rate of Thrombus Generation. *Blood Coagul. Fibrinolysis* **2007,** *18* (1), 45-48.

CHAPTER 3

INNOVATIVE APPLICATIONS OF SURFACE WETTABILITY MEASUREMENTS FOR PLASMA MODIFIED THREE-DIMENSIONAL POROUS POLYMERIC MATERIALS

This chapter addresses the current state-of-the-art of wettability measurements for plasma-modified, three-dimensional, porous, polymeric materials, providing an in-depth exploration of one characterization technique that we have used in the Fisher group. Specifically, inherent challenges associated with evaluating the wettability of complex constructs are evaluated. Issues associated with expanding contact angle goniometry-based techniques from two-dimensional to three-dimensional substrates, including the collection of both static and dynamic contact angle data, are discussed. Dynamic data refer to advancing and receding contact angle measurements, as well as measuring changes in static contact angle as a function of time, with a focus on complications that arise from the intricate architectures of these polymeric materials. Limitations in analysis and interpretation of wettability data are highlighted to explore how best to represent the wetting characteristics of plasma-treated porous constructs. Additional emphasis is given to the importance of placing wettability data in context by simultaneously assessing surface chemistry and architecture, providing a holistic approach to evaluating the wettability behavior of three-dimensional materials. A list of recommendations for best practices is provided.

This chapter is based on work published in an invited review for *Plasma Processes and Polymers* by Morgan J. Hawker, Adoracion Pegalajar-Jurado, and Ellen R. Fisher, and is reproduced with permission, Wiley 2013.[1] This work was supported by the National Science Foundation (CHE-1152963) and the Colorado Office of Economic Development via the

Biosciences Discovery Evaluation Grant Program. I would like to thank Dori Pegalajar for her contributions to this work, specifically in researching the debate outlined in Section 3.2.2 and many rounds of edits. I also want to thank Mr. John Wydallis for assistance with optical profilometry and Dr. Patrick McCurdy for assistance with SEM and XPS analyses.

3.1 Introduction

Three-dimensional (3D) porous polymeric materials have enormous potential for applications including, but not limited to, water filtration, tissue engineering, and wound healing. Their native surface properties, however, must often be specifically tailored to enhance performance for a given application. Over the past 15 years, there has been a significant increase in the number of reports of solvent-free, plasma-based techniques to modify 3D porous polymeric materials, with the overall goals of uniform surface modification, minimal environmental impact, and preservation of the bulk material properties desirable for the intended application. One property of plasma-treated materials most critical for a diverse set of applications, including water filtration, biomedical, and coating technologies, is material wettability.[2-9] Characterization methods and data interpretation targeting accurate and reliable wettability measurements for plasma-modified 3D materials, however, represent significant challenges for the scientific community and remain disparate throughout the literature.

Developing sound experimental methodologies is key to accurately assessing the wettability of plasma-modified porous 3D polymer materials. Thus, this chapter will focus on several polymeric materials and explore wettability measurements on different porous architectures fabricated out of those polymers, including scaffolds, membranes, and electrospun fibers. As shown in Figure 3.1, these architectures span a wide range of morphologies that can introduce specific challenges or concerns with respect to accurately collecting and analyzing

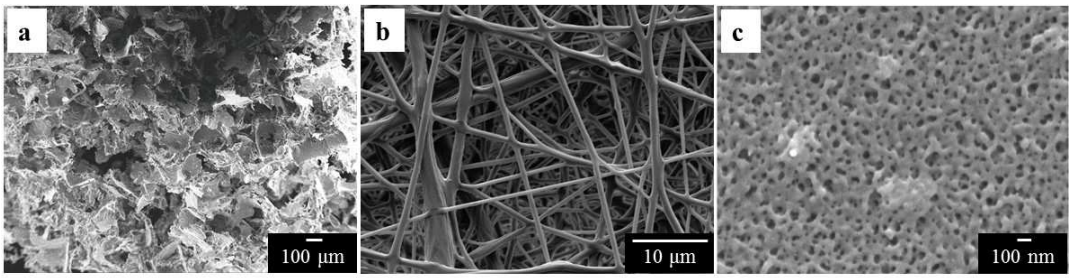

Figure 3.1. SEM images of (a) a water vapor plasma treated PCL scaffold (55X); (b) untreated PCL/PLA composite electrospun fibers (coated with 5 nm Au, 1500X); and (c) a water vapor plasma treated asymmetric PSF ultrafiltration membrane (coated with 10 nm Au, 100X). Note that the scale for the SEM image shown in (a) is 100 µm, (b) is 10 µm, and (c) is 100 nm.

wettability data. Adding an additional level of complexity, we focus on plasma-modified materials and categorize plasma treatments by separating those that result in materials exhibiting absorption behavior from those that do not. Furthermore, we will specifically focus on porous materials' interactions with water [via water contact angle (WCA) measurements] as these constructs are typically fabricated with the goal of being used in aqueous-based devices or applications. Although this work does not exhaustively cover every possible combination of polymers, architectures, and plasma treatments, we will present wettability measurements on a variety of different systems with the intention of offering a critical analysis of the state-of-the-field, and providing approaches to overcome characterization challenges when working with porous 3D materials.

This work focuses on a variety of common polymer systems, including bioresorbable polyester scaffolds for biomedical applications [polycaprolactone (PCL), polylactic acid (PLA), polyglycolic acid (PGA) and polylactic-co-glycolic acid (PLGA)], as well as polymers typically applied in membrane technologies because of their flexibility and durability [polysulfone (PSF), polyethersulfone (PES), polycarbonate (PC), polyethylene (PE) and polyethylene terephthalate (PET)]. Regardless of material or architecture, attaining a complete understanding of the wettability of plasma-modified 3D substrates presents numerous challenges not observed with 2D materials (e.g., thin films).

This chapter highlights issues associated with wettability measurements on 3D porous polymeric materials and provides recommendations for addressing these concerns. Initially, we discuss controversies pertaining to wettability measurements on plasma-treated 2D materials, specifically concentrating on the debate previously published in *Plasma Processes and Polymers*

(PPP),[10-14] and then link this discussion to wettability measurements on plasma-treated porous 3D constructs. Previously reported methods for determining wettability of this class of materials, as well as alternative methods and corresponding data from our work, including new data specifically collected for the purposes of this chapter, will be outlined, and merits will be assessed using two guiding questions: *What do we hope to attain when measuring the wettability of plasma-treated 3D materials?*; and *How should wettability measurements be used and interpreted?*

3.2 Background

As discussed in Chapter 1, many traditional surface modification techniques are often performed at elevated temperatures and/or are solvent-based, thereby resulting in compatibility issues for delicate polymer structures that cannot withstand the required modification conditions. Additionally, these methods can produce residues that are incompatible with or harmful to the environment. Plasma-based techniques offer several advantages for the surface modification of intricate 3D polymeric materials, including that they typically take place at room temperature, allowing for preservation of 3D structures; can employ a multitude of gaseous and liquid precursors providing excellent tunability of resulting surface functionality; and offer a sterile environment for processing, which is ideal for biomedical applications. As plasma modification specifically targets the surface (i.e., the outermost portion of a material that acts as the interface between the surrounding environment and the bulk material), a variety of surface characterization techniques are required to gain a comprehensive understanding of plasma-modified material surfaces. Notably, the collection of properties of interest may differ depending on the intended application. For example, composition can be assessed using Fourier transform infrared spectroscopy (FTIR), X-ray photoelectron spectroscopy (XPS), time-of-flight secondary

ion mass spectrometry (ToF-SIMS), and near-edge X-ray absorption fine structure spectroscopy (NEXAFS); topographical features and architecture can be evaluated using scanning electron microscopy (SEM); surface charge can be assessed using zeta potential measurements; and surface roughness can be measured using atomic force microscopy (AFM) and profilometry. Data from these techniques can be coupled with surface tension and contact angle (CA) data to further inform our understanding of surface wettability. Although CA goniometry has proven a valuable technique in determining surface wettability on 2D substrates, we argue that the collection, interpretation, and analysis of CA data on plasma-modified 3D materials pose unique challenges that must be considered to fully understand a material's interfacial behavior.

3.2.1 Contact angle goniometry to measure wettability. One of the most prevalent techniques currently used to measure wettability is CA goniometry, wherein the static CA (typically using water as a probe liquid), serves as the "gold standard" for wettability measurements. Young's equation (Equation 3.1), describes the relationship between surface tension and CA on an ideal smooth, planar surface:

$$\gamma_{LV} cos\theta = \gamma_{SV} - \gamma_{SL} \quad (3.1)$$

Here, γ_{ij} represents the surface tension between the two indicated phases, phases included are solid, liquid and vapor; and θ represents the static CA, describing the edge of the two-phase boundary where it ends at a third phase, a 2D graphical representation of which is depicted in Figure 3.2a. A more detailed explanation of Young's equation and its application is outlined elsewhere.[15-16] In general, the more wettable a solid material is by a specific liquid, the lower the observed contact angle will be.

Specifically pertaining to WCA measurements, materials having WCA values < 90º are traditionally defined as hydrophilic, whereas materials with WCA values ≥ 90º are traditionally

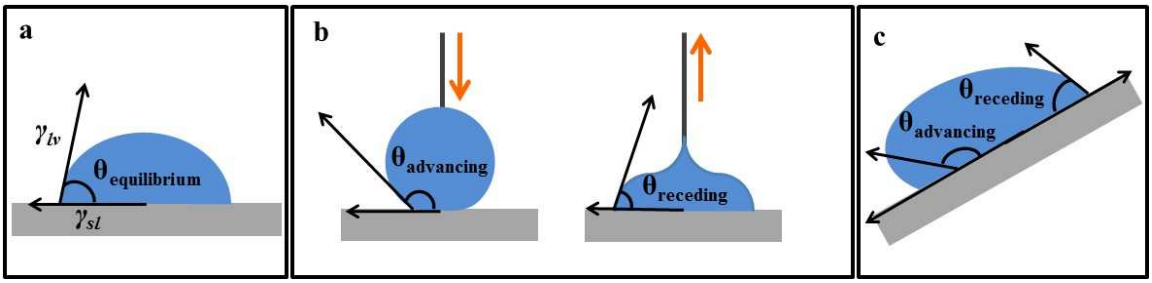

Figure 3.2. Schematic representations of (a) a static CA measurement between the liquid-vapor interface (γ_{lv}) and the solid-liquid interface (γ_{sl}), and dynamic measurements of the advancing and receding CAs via either (b) increasing and decreasing the drop volume or (c) using a tilting table.

defined as hydrophobic. There is, however, significant discrepancy regarding the quantitative values applied to distinguish between "hydrophilic" and "hydrophobic" as these terms are inherently ambiguous, and some authors recommend the use of these words only as qualitative adjectives.[17] Moreover, the extent to which these definitions are used to appropriately describe the result of a surface modification process can become muddled depending on the starting material and the intended outcome or application. For example, when starting with a polymeric material possessing a WCA of ~85º, arguably relatively "hydrophobic" even though WCA < 90º, the goal might be to render the material less hydrophobic via plasma treatment. Thus, if the treatment produces a modified polymer surface with a contact angle of 75º, one might claim this was a success in the sense that the treatment did create a *more* wettable surface. Whether or not this could be considered truly "hydrophilic", however, is a debatable question. Furthermore, the extent to which a material's hydrophilicity can vary after modification (e.g., aging effects such as hydrophobic recovery,[18-21] etc.) makes it difficult to claim that all materials below a specific CA value (e.g., 90º) should be broadly categorized as "hydrophilic". Thus, we support the approach of using this terminology as qualitative descriptors.

Goniometry techniques rely on geometric measurements to yield CA values. Modern goniometers come standard with onboard software for drop analysis, wherein the researcher can subjectively set a baseline at the solid-liquid interface (or, in the case of certain software, the software can automatically determine a baseline using image contrast algorithms). After the baseline is determined, different geometric fitting methods can be used to determine the CA. We use the Krüss DSA30 contact angle goniometer with the DSA4 onboard software in our laboratories, and this software allows us to fit drop shape with different methods depending on the CA range of the surface and the need to make dynamic (advancing and receding CAs or CAs

as a function of time) or static measurements.[22] For example, our goniometer allows us to make static measurements on samples with symmetric drops having CAs < 20º either assuming circular arc contour shape or assuming a flattened curve with different curvature at every level due to the drop weight. Furthermore, we can perform "dynamic" measurements either assuming an elliptical arc drop shape or having no prior assumption about the drop shape (i.e., fitting the drop shape with a polynomial fit). These fitting methods are recommended for surfaces with CA values > 20º. Note that the term "dynamic" can refer to measuring the advancing and receding contact angles on a surface, but can also refer to measurement of the CA as a function of time (e.g., with porous substrates that adsorb the probe liquid). This will be elaborated on further below. CA data are fit by first defining the solid-liquid interface (i.e., the drop baseline), and then using the on-board software to fit the drop shape based on the selected fitting method. When performing CA measurements, it is critical that a consistent method is used and that the fitting technique(s) employed are reported.

In addition to static CA measurements, dynamic CA measurements are a valuable tool for assessing surface wettability. Multiple methods can be used to make these measurements, including increasing and decreasing the drop volume (Figure 3.2b) or utilizing a tilting table (Figure 3.2c), each of which involves measuring the maximum and minimum observed CA values (termed the advancing and receding CA values). As surface roughness can profoundly affect CA values,[23-25] roughness should be accounted for using such dynamic CA measurements. Indeed, rough materials can be considered as having a surface containing two distinct components, where the advancing CA represents the CA measured on a smooth, homogenous surface of the low energy component and the receding CA represents the CA measured on a smooth, homogenous surface of the higher energy component.[26] CA hysteresis is thus defined by

the difference of the advancing and receding CAs. By definition, ideal flat surfaces have CA hysteresis values of 0º; in contrast, hysteresis values on rough surfaces can reach values as large as the advancing CA on those surfaces.[24] CA goniometry can be utilized as a surface-sensitive analysis technique to measure wettability of plasma-modified substrates, even in the case of materials with considerable surface roughness. Expanding goniometric techniques from 2D to 3D systems, presents several challenges for both dynamic and static CA measurements; in the next section we will outline and discuss these challenges, and their implications for data collection and interpretation.

3.2.2 Challenges of measuring wettability on 2D and 3D substrates. Although static CA values are most commonly reported to assess the wettability of a material, they are not without controversy. Indeed, the dearth of experimental detail included in manuscripts reporting such measurements and the gross misinterpretation of wettability data obtained from these methods opened the door to significant debate within the plasma community. In 2010, Strobel and Lyons presented a debate-essay in *PPP* that addressed the misuse and misinterpretation of contact angle measurements on plasma-modified polymer surfaces.[13] The authors highlighted the need to include CA data in any future *PPP* publications, calling for at least inclusion of advancing and receding CAs that are properly measured, reported, and analyzed, recognizing that plasma-modified polymers can clearly represent non-ideal surfaces. In this debate-essay, Strobel and Lyons overviewed several techniques including the sessile-drop approach, the tilting plate method, and the Wilhelmy plate technique. The authors openly support the use of the Wilhelmy plate method for assessing the wettability properties of a plasma-modified material.

Similarly, in continuing the debate, Di Mundo and Palumbo agreed with Strobel and Lyons that dynamic CA measurements are indispensable.[10] They, however, strongly emphasized

the importance of contributions made by roughness and chemical heterogeneity to CA measurements, especially with hydrophobic, superhydrophobic surfaces (generally defined as having WCA > ~130º), and aged samples. Although Di Mundo and Palumbo likewise recognized the advantages of using the Wilhelmy plate technique, they also stressed the limitations of this technique when samples are inhomogeneous and detailed how the sessile drop method, when performed systematically (i.e., using identical methodological conditions), can provide more specific details about inhomogeneous surfaces. Müller and Oehr subsequently published a third debate-discussion paper in *PPP*.[12] These authors argued that comparing contact angles is a more appropriate approach than trying to compare surface energies deduced from CA data. They also commented on the importance of using a standardized methodology when meaningful comparisons are intended. Müller and Oehr further observed that accurate measurements validated with quality statistical analysis are sufficient to corroborate deposition of films or other results of plasma treatments.

In 2011, two other papers followed the initial debate by Strobel and Lyons.[13] González-Elipe et al. followed Di Mundo and Palombo's comments about the importance of surface roughness on wetting behavior, focusing their discussion on how to accurately measure roughness parameters on non-ideal materials.[14] For example, a minimum area of 5 μm x 5 μm was recommended for systems wherein surface roughness is expected to make significant contributions. The last of the debate-discussion papers, prepared by Kietzig,[11] again addressed challenges related to measuring CAs on non-wetting surfaces. Kietzig highlighted the trend of researchers looking for inspiration from nature to understand the different wetting effects observed on modified materials, and how surface roughness and methodology used for measuring CAs affect the wetting behavior observed. Emphasis was placed on the need to

describe every experimental detail when performing CA measurements, including environmental factors, drop volume, dispensing rate and pressure applied to the droplet, among others.

Overall, we agree with many of the points made by debate contributors. In particular, statistical analysis of the wettability data obtained on any substrate is an absolute requirement and when discussing wettability data, authors should take a more qualitative, comparison-based approach, rather than placing emphasis on the absolute quantitative values measured. Unsurprisingly, the remaining debate points regarding the best practices for measuring wettability on plasma-treated 2D substrates do not necessarily translate directly to morphologically diverse materials, which suffer from CA hysteresis effects arising from both functionality and roughness. Substantially developed models on rough substrates exist, including those of Wenzel and Cassie-Baxter, and have been thoroughly outlined in the issue of *PPP* where this debate was originally published[25] and elsewhere.[24] Although these models provide some insight regarding measurements on non-ideal substrates, they do not necessarily expand to describe the wettability of plasma-treated 3D substrates, specifically those that are porous. Indeed, 3D porous materials introduce additional complications when measuring wettability, most notably absorption behavior, whereby the drop of probe liquid is absorbed by the material during the measurement.

Difficulties in measuring wettability in terms of absorption behavior have led multiple researchers to use non-goniometry based techniques. For example, Jansen et al. measured the capillary rise behavior of untreated and argon plasma treated PCL electrospun fibers upon immersion in deionized water.[27] From the data presented, the measurement of the height of the water front on their samples reveals that Ar plasma treatment results in an increase in wettability relative to the untreated fibers. This technique, however, raises serious concerns about

reproducibility in distinguishing the liquid front on the material, as well as meaningful quantification of the results. Kang and Lee use a similar technique to explore the extent of blue dye absorption throughout the 3D network of PLGA scaffolds, both before and after air plasma treatment.[28] By examining photographs of the cross sections of control (untreated) and plasma-treated scaffolds soaked in a dye solution, the authors claim that they can distinguish differences in "wettability" based on the extent of penetration into the porous network. Similar to the water front data presented by Jansen et al., this methodology does not provide even semi-quantitative data, and is inherently highly subjective. Likewise, Dolci et al. took a gravimetric approach and reported "water uptake percentage" for control and oxygen plasma-treated electrospun PLA fiber samples. In this work, untreated samples displayed relatively low water uptake percentage of <10%. In contrast, all plasma treated fiber samples soaked for 3 to 24 hours exhibited water uptake of ~300%.[29] Although this technique does provide comparative values, it is difficult to understand how the data relate to surface wettability or how it is affected by the amount of material being used in each experiment. Arguably, these descriptions move a step closer toward placing the wettability of a plasma-treated 3D material in context of more global material properties and capabilities. None of these approaches, however, provide a complete explanation of a specific material's absorption behavior, nor do they deliver a satisfactory methodology for comparison between samples. Thus, the experimental methods used in these non-goniometry based techniques present serious reproducibility and repeatability issues, as well as limitations associated with using qualitative techniques to report quantitative or semi-quantitative comparisons.

The combination of 3D architecture (including roughness and porosity) and surface chemistry of plasma-modified substrates is a major challenge when measuring wettability. A

multitude of materials with varying degrees of porosity have been explored for applications where understanding wettability is critical to predict function (Figure 3.1). Distinguishing between different porous structures (overall porosity and geometry) is an important aspect of measuring wettability as this can strongly influence absorption behavior. Furthermore, plasma modification can render a material more or less wettable than its untreated counterpart. More importantly, because of the variable architecture in 3D structures, areas of the surface may be unevenly treated such that the underlying material can still influence wetting behavior after plasma treatment.

Measuring the wettability of some plasma-modified materials appears more clear-cut than others. For example, measuring the static WCA on a hydrophobic porous material with a smaller scale roughness (i.e., has a distinguishable baseline) is more straightforward than on materials with localized macroscopic roughness in the vicinity of the CA measurement. This is clearly demonstrated by two examples shown in Figure 3.3, O_2 plasma-treated electrospun PLGA fibers (Figure 3.3a)[30] and octafluoropropane (C_3F_8) plasma-treated PCL scaffolds (Figure 3.3b). In Figure 3.3a, the water drop has a distinctive baseline at the solid-liquid interface. In contrast, the solid-liquid interface shown in Figure 3.3b is more challenging to distinguish because of the larger scale roughness of the substrate. The relative roughness of the two samples can be elucidated from the SEM images shown as insets, where the scale bars differ by an order of magnitude. As alluded to above, baseline determination can have a major influence on the measured CA value. This is depicted in Figure 3.3c where the same image of a water drop on a C_3F_8 plasma treated PCL scaffold was fit with two different potential baselines, resulting in two different WCA values.

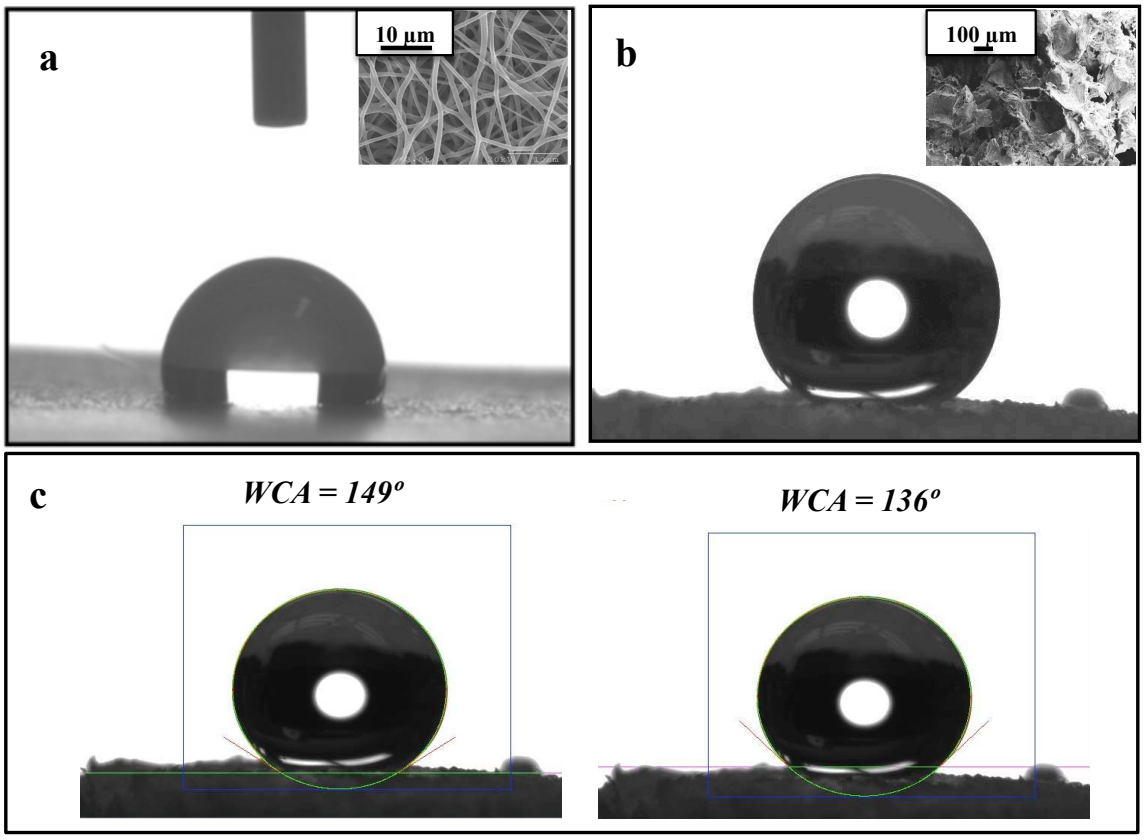

Figure 3.3. Image of a water drop on (a) oxygen plasma-treated PLGA fibers; [30] and (b) C_3F_8 plasma-treated PCL scaffold (this work). Insets in each figure contain SEM images that reveal the micro-scale architecture of the substrates. Note that the scale for the SEM image shown in (a) is 10 µm and that (b) is 100 µm. Panel (c) contains two identical images of water drops on a C_3F_8 plasma-treated PCL scaffold, along with two different baseline fits to the same image.
(a) Reproduced with permission.[30] 2007, Springer.

Regardless of fitting methodology, CA hysteresis must still be taken into account as the roughness and chemistry both influence drop hysteresis. For hydrophilic 3D materials, measuring static WCA values is often not viable due to drop absorption. Indeed, irrespective of the specific liquid or surface involved, wettability measurements become more complicated as the interactions of a particular probe liquid with the surface functional groups and the porous structure are intertwined and simultaneously affecting the measured CA value.

The challenges of making wettability measurements on 3D porous materials, as well as the difficulty with interpreting these data, leads to the fundamental question of whether there is any value in making CA measurements on these types of substrates. We argue that establishing the relative wettability of a plasma-treated 3D porous material is more meaningful (and more realistic, given the aforementioned challenges) than measuring absolute wettability. In the following sections, we will substantiate this argument with findings from the literature, as well as recent work from our group, not published elsewhere, with the goal of developing a comprehensive picture of innovative wettability measurements on 3D porous materials.

3.2.3 Simulations of drop dynamics on porous and rough substrates. As we alluded to above, numerous studies have reported experimental data pertaining to the wettability of porous constructs. Arguably, it is critical to develop the ability to predict wetting behavior on porous materials so as to provide further mechanistic and quantitative insight regarding experimental results on these complex substrates. A substantial body of literature aims to characterize the dynamics of liquid drops on porous surfaces via molecular dynamics modeling. Although this aspect of wettability on porous 3D substrates is not a primary emphasis of this chapter, we provide some illustrative examples of this work. For example, Sevano and coworkers proposed simple models of the wetting of a porous surface (composed of a series of isolated cylindrical

capillaries) with sessile drops of non-volatile liquids, and validated these models using molecular dynamics simulations. [31-32] This work demonstrated that developed models can accurately reproduce the wetting dynamics of simple porous surfaces, specifically pertaining to measuring CA, drop volume, drop base radius, and liquid height in the pore as a function of time.[31-32]

Although models proposed and validated by Sevano, et al. provide insight regarding the wettability of porous materials, the authors acknowledge they do not account for any hysteresis effects in their models. More recent numerical modeling by Nosonovsky and coworkers has, however, considered the effects of hierarchical roughness on material wetting behavior, specifically aimed at developing a more comprehensive understanding of CA hysteresis phenomena.[33-34] Work by Nosonovsky et al. differentiates between 1) surface roughness that results in the pinning of the solid-liquid-vapor triple line and 2) the influence of adhesion hysteresis in the solid-liquid contact area, and demonstrates the importance of both of these factors on the observed hysteresis via modeling.[33] Furthermore, Nosonovsky, et al. expanded on the traditionally considered roughness factor (i.e., the ratio between the actual and projected surface area, appearing in the Wenzel model[24]) by defining the *effective* roughness factor. Here, the authors refer to the roughness factor corresponding to asperities that have the potential to trap air pockets, eliciting Cassie-Baxter behavior.[34] Notably, the authors discuss limitations in measuring the effective roughness factor on rough surfaces, illustrating challenges in investigating the wettability of such materials. Overall, these examples demonstrate the multifaceted nature of the wetting behavior of rough, porous surfaces and simultaneously suggest modeling efforts can be combined with experimental data to provide a more comprehensive picture of wetting of complex 3D constructs.

3.3 Plasma-treated 3D Material Wettability Measurements

Before discussing wettability measurements of plasma treated 3D materials, it is important to note that the native polymer materials listed in Section 3.1 are all nominally hydrophobic, especially in porous morphologies (i.e., WCAs > 90º). From this standpoint, researchers are typically interested in exploring how the wettability of a plasma treated material differs from that of the base material. At each extreme, there is interest in using plasma processing to both fabricate materials that are "superhydrophobic" and low-fouling (generally of interest when water penetration into the material is undesirable) and to fabricate materials that are hydrophilic to varying degrees. Again, the use of hydrophilic and hydrophobic (as well as all of their derivatives such as "superhydrophobic") should be used as qualitative adjectives and specifically defined in the context of the work.[17] In the context of plasma-treated, porous, polymeric, 3D materials, we differentiate between hydrophilic or hydrophobic materials by illustrating cases where plasma treatment results in 3D porous polymer constructs that do or do not completely absorb water on a time scale relevant to goniometry-based techniques. Although we categorize materials in this way, we are aware that the absolute study of absorption behavior requires different considerations regarding data collection and analysis.

Regardless of the type of plasma treatment, one common criticism of wettability measurements is that results are often reported without considering changes in surface chemistry and/or material architecture, both of which influence wettability. Furthermore, these measurements are often discussed either without evaluating their meaning, or are incorrectly interpreted, in terms of the intended application for the plasma-treated material. We argue that assessing changes in wettability, as well as changes in surface chemistry and topography of a material, both before and after plasma treatment are absolutely essential to attain a

comprehensive understanding of the system of interest. Thus, our focus will be on placing wettability measurements in the context of potential changes in these other material properties.

3.3.1 Plasma treated 3D materials that do not exhibit absorption behavior. When a water drop can stabilize on the surface of a porous 3D material, its interactions with water may be similar to that observed with non-porous materials. Thus, the measurement techniques used to evaluate the wettability of 2D materials can be extended to these 3D systems. The noted shortcomings associated with these techniques on 2D materials also extend to 3D materials. As discussed above, additional challenges arise from macroscopic roughness causing ambiguities in determination of the baseline necessary to perform geometric static or dynamic CA measurements. Returning to the examples shown in Figure 3.3, we can further explore the relationship between WCA measurements and other changes to a material upon plasma treatment. In the case of the PLGA fibers in Figure 3.3a, Park et al. state that the material likely becomes more hydrophilic upon oxygen treatment because of "the introduction of new polar groups…on the surface".[30] In this study, the authors collected XPS survey spectra and used these data to calculate changes in the composition of O-C functionality. Unfortunately, it is unclear how the percentage of O-C functional groups was calculated, as the fitting parameters of high-resolution spectra were not included. In our work on fluorocarbon plasma modified PCL scaffolds, we observed an increase in WCA after plasma treatment, and attributed it to an increase in carbon/fluorine functionality as measured by elemental analysis obtained from high-resolution XPS spectra (a more detailed discussion is included in Chapter 5).[35] In both studies, the material architectures remain largely unchanged, as evidenced by SEM analysis. Thus, differences in wettability are attributed solely to changes in surface chemistry. Nonetheless, these two examples illustrate the importance of measuring CA, surface architecture and surface

composition so as to understand the mechanisms by which wettability changes upon plasma treatment.

The two reports noted above focus exclusively on static WCA measurements, which are typically adequate for comparing relative changes in wettability before and after plasma treatment for hydrophobic 3D materials. Although static WCA values may be sufficient under some circumstances, assuming that replicate measurements are performed, more detailed information can be gained by also measuring advancing and receding WCAs, and therefore CA hysteresis. Kim and coworkers measured advancing CAs for O_2 plasma-treated PSF ultrafiltration membranes, demonstrating that the advancing WCA decreases with increasing plasma treatment time.[36] The authors did not, however, report the receding CA and any accompanying hysteresis that may have influenced the interpretation of the results. Without including hysteresis data, the measurements are virtually useless and do not add much to our understanding of how the plasma has modified the surface. In contrast, Intranuovo et al. measured both advancing and receding WCA values for PCL scaffolds treated with C_2H_4/N_2 mixed plasmas directly followed by either a short H_2 or C_2H_4 plasma treatment. In this study, the plasma-treated scaffolds exhibited a larger hysteresis value than untreated scaffolds, indicating that the plasma treatment induced changes to either the surface chemistry and/or surface topography. The authors attributed larger hysteresis values to increased chemical inhomogeneity in their surfaces introduced by the second plasma treatment.[37] No specific data are presented, however, that directly support this claim. Nevertheless, the measurement of CA hysteresis allows more insight into each of the plasma treatments than would have been possible without such information. We acknowledge it is extremely difficult to distinguish between contributions to

CA hysteresis from surface roughness versus those from surface chemistry within systems that contain inhomogeneities in both parameters (e.g., plasma modified scaffolds).

To further explore this concept, we have plasma treated a variety of material architectures under identical conditions and examined them using XPS, SEM and WCA measurements. Table 3.1 contains both static and dynamic wettability data as well as XPS compositional data acquired in our laboratories on three different substrates (glass slides, electrospun PCL fibers, and PCL scaffolds). Glass slides were used as a model flat substrate to allow us to decouple surface chemistry from substrate architecture. Using two different plasma treatments, a CW 1,7-octadiene system (discussed in more detail in Chapter 8) and a pulsed C_3F_8 system, we have created surfaces that are nominally more hydrophobic than the untreated materials, where C_3F_8 plasma treatment creates the most hydrophobic surfaces. For 1,7-octadiene treatments, plasma modification occurs via hydrocarbon-rich film deposition,[38] whereas C_3F_8 plasma treatment deposits a fluorocarbon film (a more detailed discussion of fluorocarbon film deposition with C_3F_8 can be found in Chapter 5).[35] Regardless of substrate identity, advancing CA values are greater than receding CAs as expected. On glass slides, both plasma treatments result in a significant increase in static and dynamic CAs, as well as a substantial increase in hysteresis values. These results can be attributed to differences in surface chemistry (i.e., changes in O/C and F/C ratios), as the surface roughness of the plasma treated glass substrates is within experimental error of the untreated glass (~3 nm, as measured by optical profilometry).

Static and dynamic WCA data on the 3D PCL constructs are more difficult to interpret, because they are strongly influenced by both surface chemistry and surface roughness, leading to much higher experimental errors relative to flat surfaces. All plasma treated 3D porous substrates have significantly higher static, advancing, and receding CA values than on glass slides, Table

3.1. This is expected as the roughness of the 3D materials is considerably greater than that of the glass slides. Both types of native PCL constructs have static WCAs ≥100°, indicative of the inherent roughness of these materials as flat PCL films have WCAs of 55 ± 5°.[39] Notably, 1,7-octadiene plasma treatment does not appreciably alter the WCAs of either 3D construct, whereas the C_3F_8 treatment results in a significant increase in both static and dynamic WCA values. Highlighting results from the scaffold substrates, we see that the chemistry of the treated scaffolds has changed dramatically after plasma treatment. For 1,7-octadiene treatment, the O/C ratio is significantly lower than that for the untreated material, clear evidence that a hydrocarbon-rich film has been deposited. Given that the WCAs do not change appreciably upon 1,7-octadiene plasma treatment but the surface chemistry is clearly altered, the porous architecture of the substrate must be the dominant factor that influences WCA measurement. Note, however, that the errors associated with these measurements decrease our ability to distinguish between the two contributing factors (chemistry and architecture). For C_3F_8 plasma treatment, significant amounts of fluorine are incorporated into both PCL constructs, Table 3.1, clearly indicative of fluorocarbon film deposition (similar fluorocarbon film deposition to that observed for different plasma treatment conditions, Chapter 5). This result, combined with the substantial change in WCAs, suggests that the change in surface chemistry is the primary cause of the WCA increase in this system. This is further substantiated by the observation that neither plasma treatment results in a detectable change in 3D material architecture (as measured with SEM). Finally, comparison of CA hysteresis (Table 3.1) provides further insight into the effects of plasma treatment. For flat substrates, we note that hysteresis increases significantly upon plasma treatment, regardless of precursor. As the surface roughness is not changing appreciably, this is fully attributable to changes in surface chemistry. For the 3D constructs, however, it is much less

Table 3.1. WCA and XPS elemental data for untreated and plasma-treated materials.[a]

Substrate	Static and Dynamic WCA Data[b]				XPS Elemental Composition Data	
	θ_{static} (°)	$\theta_{advancing}$ (°)	$\theta_{receding}$ (°)	Hysteresis (°)	O/C	F/C[c]
Glass slides						
Untreated	20.3 ± 1.4	26.0 ± 3.0	7.3 ± 2.1	18.7 ± 3.2	0.56 ± 0.04	--
1,7-octadiene	98.3 ± 0.6	102.3 ± 2.5	77.3 ± 3.1	25.0 ± 2.7	0.03 ± 0.01	--
C_3F_8	110.4 ± 0.9	114.0 ± 1.6	80.0 ± 1.4	34.0 ± 2.4	0.13 ± 0.04	1.29 ± 0.08
Electrospun PCL fibers						
Untreated	129.1 ± 4.2	131.4 ± 6.4	112.0 ± 7.7	19.4 ± 4.9	0.18 ± 0.02	--
1,7-octadiene	138.5 ± 3.9	130.3 ± 8.4	119.0 ± 6.1	11.3 ± 3.9	0.16 ± 0.01	--
C_3F_8	140.1 ± 2.0	143.0 ± 2.7	127.7 ± 3.5	15.3 ±4.2	0.07 ± 0.01	1.02 ± 0.07
PCL scaffolds						
Untreated	119.5 ± 1.6	125.6 ± 0.5	99.5 ± 10.5	25.8 ± 10.6	0.34 ± 0.01	--
1,7-octadiene	121.3 ± 5.3	127.0 ± 15.2	96.8 ± 15.2	30.2 ± 4.0	0.11 ± 0.02	--
C_3F_8	138.6 ± 3.0	135.8 ± 5.0	121.8 ± 7.3	14.0 ± 4.1	0.12 ± 0.01	1.00 ± 0.07

[a]For each plasma treatment, the substrates were treated under identical rf plasma conditions (for 1,7-octadiene plasma treatments, p = 100 mTorr, P = 4 W, 5 min treatment time; for C_3F_8 plasma treatments, p = 50 mTorr, pulsed plasma was used with 5% d.c. and peak P = 50 W, 1 min treatment time). [b]Values represent the mean and standard deviation of three measurements made on three different samples ($N \geq 9$). [c]F/C values represent the mean and standard deviation of three measurements made on a single sample made to verify previously found[35] F/C ratio

straightforward to interpret. Indeed, with a specific substrate, the differences in CA hysteresis can be as much as a factor of two (i.e., for the scaffolds), illustrating the difficulty in performing and interpreting dynamic measurements on plasma treated 3D surfaces, especially those that are porous.

One of the important challenges with plasma treatment of relatively delicate 3D polymer materials is the potential for the plasma to induce significant damage.[40] We have explored this issue with electrospun PCL fibers using our C_3F_8 plasma treatment. Figure 3.4 contains an SEM image of untreated fibers, Figure 3.4a, and two images of these fibers treated in pulsed and CW C_3F_8 plasmas, Figure 3.4b and c, respectively. The image in Figure 3.4b shows no apparent change in overall substrate architecture; in contrast, the image in Figure 3.4c shows CW plasma treatment considerably fragments the fibers. Interestingly, the O/C and F/C ratios of PCL fibers treated under the two different plasma conditions are the same within experimental error. Thus, if surface chemistry was measured in the absence of topographical information, one might conclude that these were identical surfaces. The static CA of the pulsed plasma treated fibers is, however, significantly lower than that of the CW plasma treated fibers (130.3 ± 6.3° and 140.1 ± 2.0°, respectively). Not only does this example illustrate the effect of roughness on apparent WCA, but it also highlights the importance of exploring changes in surface roughness and surface chemistry in conjunction with CA measurements.

An additional challenge with dynamic measurements on porous materials arises from measuring advancing and receding CAs if any absorption of the water drop is occurring, even if the material does not completely absorb the water drop. Clearly, this becomes a more critical issue with more hydrophilic materials, which is discussed in some detail in Section 3.3.2. Nevertheless, if measurements are being performed on porous substrates, the effect of probe

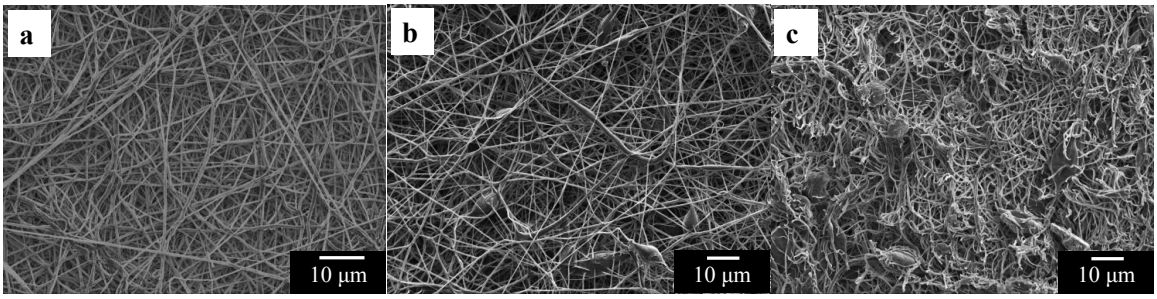

Figure 3.4. SEM images of (a) untreated (1400X) and (b) pulsed C_3F_8 plasma treated (1000X) and (c) CW C_3F_8 plasma treated electrospun PCL fibers (1000X). The applied rf power conditions for the pulsed C_3F_8 plasma treatment were 5% d.c., peak P = 50 W (b) and those for the CW C_3F_8 plasma treatment were P = 50 W. In each plasma treatment, the sample was treated for 1 min with p = 50 mTorr.

liquid absorption into the material should be taken into consideration in evaluating resulting CA values. In some instances, measuring the CA as a function of drop age using a goniometer equipped with a high-speed camera can more thoroughly elucidate wettability behavior.

To further explore this approach, we present data from two plasma treatments of two different 3D porous polymer constructs: PCL scaffolds and PET membranes (0.2 μm and 3.0 μm pore diameters). First, Formosa et al. examined Ar/O_2 plasma treatment of PCL scaffolds and reported WCA as a function of drop age, Figure 3.5a.[41] These data demonstrate a case wherein the plasma treatment renders the surface more hydrophilic but the water drop is not fully absorbed by the substrate and therefore stabilizes over time. In comparing the data for the untreated and treated materials, we note that collecting WCA data over the course of three minutes with relatively long (10-30 s) intervals between data points (also reported by Wang and coworkers[42]) is inappropriate, as the WCA does not continually decrease or change over the entire time period. Moreover, when data are collected with long intervals between points, researchers may fail to capture changes in WCA that occur initially after the water drop contacts the surface. In addition, reporting data over a relatively long time period may introduce artifacts resulting from drop evaporation or other destabilizing events, potentially interfering with interpretation. The second treatment entails H_2O plasma treatment of track-etched PET membranes (Figure 3.5b) with two pore diameters.[20] Here, the plasma treatment results in much more hydrophilic surfaces than the untreated materials, but the water droplet stabilizes on the porous substrate, and thus the WCA can be measured reliably as a function of drop age.

These two examples also provide us with the opportunity to comment on the importance of understanding CA, architecture and compositional changes upon plasma modification. In addition to collecting WCA data on plasma-modified PCL scaffolds, Formosa et al. explored

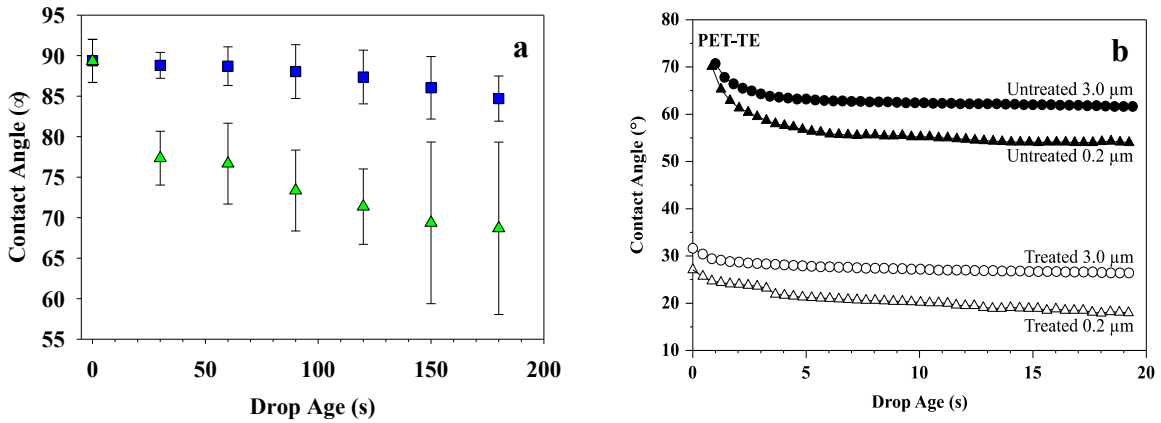

Figure 3.5. WCA as a function of drop age for (a) untreated (squares) and Ar/O_2 plasma treated honeycomb PCL scaffolds (triangles) [41] and (b) untreated and water plasma treated track-etched PET membranes with two different pore diameters.[20]
(b) Reproduced with permission. [20] 2013, Elsevier.

concomitant changes in architecture and surface chemistry using SEM and FTIR.[41] The SEM images showed the Ar/O_2 plasma treatment resulted in observable etching of the scaffold structure. Similarly, FTIR data on flat PCL films treated in the same plasma system showed exposure to the plasma eliminated the characteristic vibrational bands of PCL. Notably, the authors did not analyze changes in surface chemistry using the 3D construct, thus it is difficult to know precisely how the plasma affected scaffold surface chemistry. Given that there are both changes in surface topography and chemistry, assuming the FTIR results from the flat substrate translate directly to the scaffolds, it is difficult to discern the contributions of each to the overall change in surface wettability. In contrast, Tompkins et al. further characterized their untreated and H_2O plasma treated PET membranes using SEM and XPS. For short treatment times (i.e., 2 min), there was no discernable change in pore diameter or overall morphology, whereas that same plasma treatment nearly doubled the O/C ratio. Thus, it is clear that the observed increase in wettability (>30º change in WCA) is a result of changes in surface chemistry and not topography. These studies demonstrate nicely that simply reporting the stabilized WCA does not fully describe the wetting behavior of the material, and that plotting CA data as a function of time is far more informative. Perhaps more importantly, combining such dynamic CA data with both morphological and compositional data is vital. We will revisit and expand upon dynamic CA data collection in the next section.

3.3.2 Plasma treated 3D materials that exhibit absorption behavior. The polymer materials listed in Section 3.1 are usually chosen for deployment in specific applications because of their desirable bulk properties, such as biodegradability, system compatibility, and/or mechanical stability. Plasma modification can, however, be used to selectively modify the polymer material's surface properties, further enhancing the ability to tailor a material for a

given application. For the majority of biomedical and environmental applications, the most desirable outcome of the plasma modification of 3D porous polymeric materials is to permanently increase their hydrophilicity. As such, the majority of literature on plasma treating these constructs centers on plasma systems that either deposit thin films or implant functional groups that produce a more hydrophilic surface than that of the untreated material. As noted above, inherent challenges exist in accurately measuring the wettability of 3D hydrophilic materials, especially when the substrate fully absorbs the probe liquid. As such, the static WCA cannot be measured and alternative methods must be used to measure and report wettability behavior.

In one often used approach, polymer film analogs of porous materials are employed to elicit wettability behavior without the complications of a porous architecture. In these studies, many authors have argued that this approach primarily reveals differences in wettability attributable to changes in surface chemistry. For example, studies conducted by Park et al. (PLA, PGA, and PLGA films treated in oxygen/acrylic acid mixed plasmas),[43] Khang and Lee (air plasma treated PLGA films),[28] and Ma et al. (PCL films treated in air plasmas) all discuss wettability data on polymer films either exclusively or in conjunction with 3D porous materials fabricated out of the same polymers.[44] Park et al. used polymer films exclusively for WCA measurements and although they found an increase in film wettability after plasma treatment and acrylic acid grafting, it is unclear how plasma modification altered the wettability of 3D constructs. Presenting wettability data for a 2D material and combining that directly with morphology and composition data acquired using the 3D architecture paints an inadequate picture of plasma surface modification effects.

An alternate approach employed by Intranuovo et al. entailed fabricating a model pore system to optimize plasma parameters and thereby maximize the extent of plasma penetration into the model pore. In this model system, which is arguably closer to a 3D construct, a mask with a 0.7 μm diameter hole is used to track film deposition, which is then likened to deposition within a pore of a 3D porous PLA scaffold.[45] In this study, a WCA gradient was created by measuring WCA spatially across the model pore. These data provide valuable insight into deposition uniformity within a single model pore, but do not address issues associated with making WCA measurements on a polymer network containing a plethora of interconnected pores. Although we agree that important information can be gleaned from evaluating the wettability of a flat polymer film or a simplified pore model, we concur with Safinia and coworkers in that flat surfaces are not ideal for modeling and predicting the wettability of more complex 3D structures.[46] Indeed, results on flat films cannot and should not be directly extrapolated to describe the wettability of 3D materials, especially when differences in surface roughness and porosity are considered. Furthermore, authors should provide a clear rationale for utilizing polymer film analogs for wettability measurements and avoid drawing unsupported conclusions related to 3D polymer substrates. If both flat and 3D substrates are used, we recommend that wettability, architectural and compositional information be presented for all substrates.

An additional area of concern with respect to how wettability measurements on plasma modified 3D materials are reported arises from terminology. Because of the lack of uniformity in methodology (Section 3.3.2), as well as the challenges associated with wettability measurements, data on plasma-treated porous 3D materials are often discussed in vague terms that do not allow for even semi-quantitative comparison. For example, in the nanofiber literature, the following

phrases were used to describe air plasma-treated PCL nanofiber scaffolds: "…absorb water *immediately*";[47] "…showed *rapid* penetration of water drops into the scaffolds";[48] and "…water drop was *suddenly sucked* into the nanofiber mat, giving a contact angle of 0º" [44] [italics added for emphasis]. In other studies, water drops on Ar plasma treated PCL nanofibers "…*absorbed suddenly and thoroughly* when they contacted with the fibers" [49] or "…*sunk into the material*"[27] [italics added for emphasis]. These phrases may be descriptive, but they are highly subjective and simply do not provide a rational platform for comparison between treatments. Even when authors do attempt to report numerical values associated with WCA measurements on absorbing materials, the results are equally unsatisfactory. For example, the WCA was reported to be "0 ± 0º" on air plasma treated PLA/PCL nanofibrous meshes, [50] or simply reported as 0º with no further explanation for oxygen plasma treated PES nanofiber membranes.[51] Reporting a static WCA of 0º is misleading as it represents a perfectly wetting, ideal surface, and does not accurately convey the absorption that is undoubtedly occurring in each of these cases. Clearly, these data indicate that plasma treatment resulted in a more hydrophilic material from a qualitative perspective. This approach becomes unsatisfactory, however, when the goal is to compare how different plasma treatment conditions influence wettability and how surface wettability is affected by changes in surface roughness and chemical composition.

Some researchers have attempted to more specifically evaluate changes in wettability after plasma treatment by providing some semi-quantitative measure of the absorption behavior of plasma-treated 3D constructs. For example, in 2001 Steen et al., categorized PSF membranes treated under different water plasma conditions as either "wettable" or as wettable in under a specified time (such as 60 s or 90 s). [52] Likewise, Dolci et al. described the spreading of a water drop on an oxygen plasma treated PLA nanofiber by reporting that the WCA went from 120º to

20º within 60 s.[29] In another study, despite using a high speed camera (running at 25 frames/s), Baker and coworkers were unable to measure a reliable WCA value for Ar plasma-treated electrospun PS fibers. They did note, however, that the water absorption rate "significantly increased" for plasma-treated materials.[53] In some of these studies, instrument capabilities were not sufficient to provide useful wettability data. Fortunately, these have improved significantly in the past decade such that exploring water (or alternative probe liquid) absorption phenomena of porous materials through dynamic data collection is a more widely available technology. Nevertheless, these examples highlight the extreme ambiguity associated with the terminology used to describe dynamic WCA results on 3D materials.

We argue that evaluating the wettability of plasma modified 3D materials via dynamic techniques (e.g., measuring WCA as a function of time along with absorption rate analyses) has multiple advantages. This approach can offer comparative metrics (e.g., time for drop to completely absorb, initial water absorption rate) by which to assess the wettability of different materials. It can also specifically capture the overall absorption behavior and function as a benchmark to assess changes in relative wettability. Here, we do not distinguish between different wetting phenomena, including 1) wetting attributed to the modified material itself disregarding contributions of porous structure, 2) wetting attributed to the 3D material explicitly accounting for the porous structure, and 3) the water uptake by the interior of the 3D material absorbing water (i.e., polymer swelling). Although the overall observed wetting phenomenon likely encompasses some combination of these three mechanisms, polymer swelling is likely a minor contributing factor as the swelling kinetics of 3D polymeric materials is on the order of months, and CA experiments take place on the order of seconds.[54]

Figure 3.6 shows WCA data for 3D materials treated with plasmas designed to create hydrophilic surfaces.[40, 55-56] Figure 3.6a includes dynamic WCA data for untreated and H_2O plasma-treated PE membranes. In these studies, the membranes are placed in a holder perpendicular to gas flow. As one measure of treatment efficacy, the WCAs of both the upstream (side 1) and downstream (side 2) sides of the membrane are evaluated to determine the completeness and uniformity of the treatment. These data clearly show that the treated membrane is "wettable" (drop absorbs in < 30 s) and that both sides have nearly equal wetting behavior. These measurements can also be used to evaluate the effects of sample aging, as illustrated in Figure 3.6b. Here, NH_3/O_2 plasma-treated PSF membranes were allowed to age for 12 months; prior to treatment, these materials exhibited a WCA of ~96º, whereas treated membranes absorbed a water drop in < 1 s. Dynamic WCA data taken at the end of this aging period clearly show the membranes are still extremely wettable (drop absorbs in < 1.5 s), but also reveal differences in the upstream and downstream sides of the membrane not discernable via other characterization methods. Similarly, such techniques can be used for comparison between different sets of treatment conditions.[41, 52, 55-56] This allows for rapid optimization across a plasma system parameter space, especially when a fabricating materials with a certain wetting behavior is desired for a specific application.

Additionally, analyzing this type of dynamic CA data allows for comparison of both WCA and absorption behavior including water absorption rate, which can also be collected as a function of aging time in systems where understanding changes in wetting is critical for applications requiring long-term shelf-stability. For example, dynamic WCA data captured over a mere 180 ms in Figure 3.6c (materials treated with H_2O/N_2 plasmas) demonstrate that both freshly treated PCL scaffolds and those aged for 1 week are hydrophilic, absorbing materials,

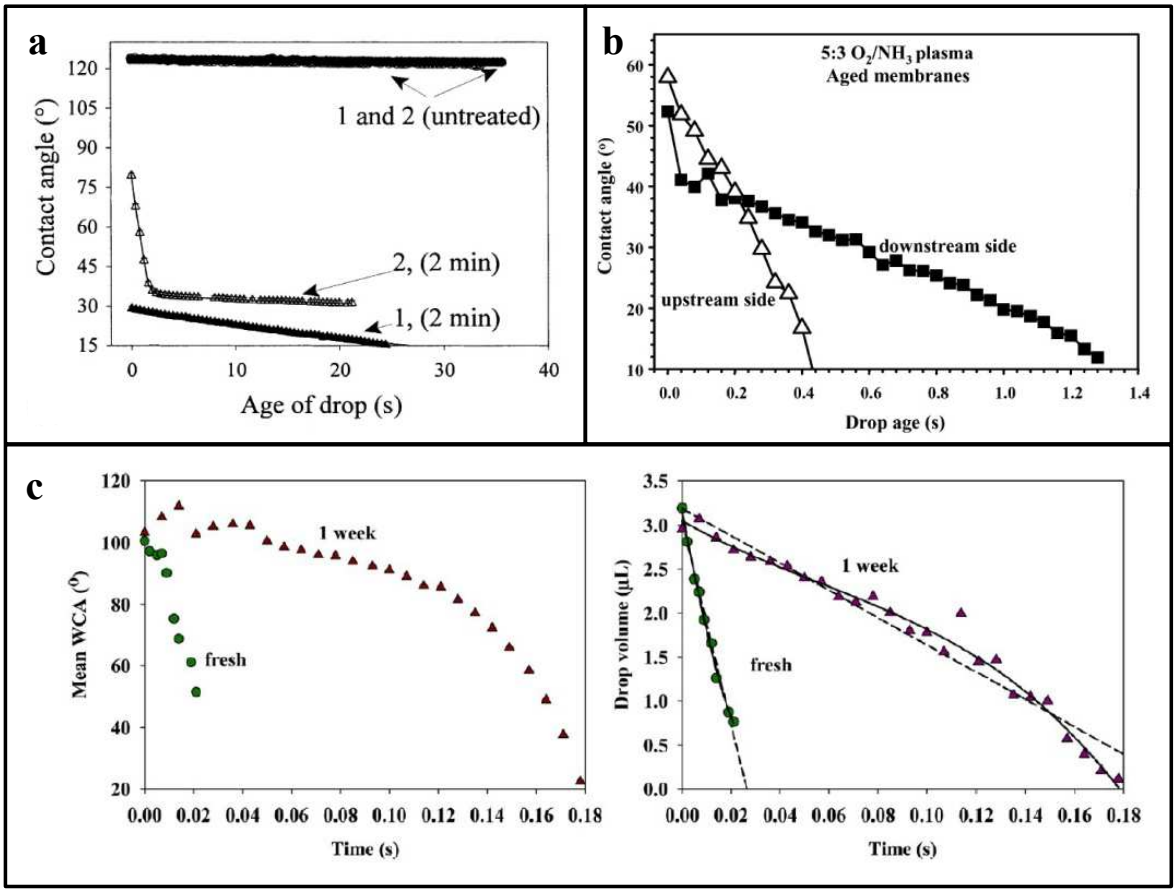

Figure 3.6. WCA as a function of drop age on (a) untreated and 2 min H_2O plasma treated PE membranes on both the side of the membrane directly contacting the plasma (upstream, side 1) and the downstream side (side 2);[55] (b) the upstream and downstream sides of a 5:3 O_2/NH_3 PES membrane aged for 12 months;[56] (c, left) a 1:1 H_2O/N_2 plasma treated PCL scaffold freshly treated and aged for 1 month.[40] Panel (c) also depicts drop volume as a function of drop time for a 1:1 H_2O/N_2 plasma treated PCL scaffold, both freshly treated and aged for 1 week (right).
(a) Reproduced with permission.[55] 2002, Elsevier.
(b) Reproduced with permission.[56] 2005, Elsevier.
(c) Reproduced with permission.[40] 2013, American Chemical Society.

with initial WCAs of ~100º. The freshly treated material, however, shows a more rapid decrease in WCA, with the water drop fully absorbing in < 30 ms. After 1 week, the water drop takes ~200 ms to fully absorb. Along with WCA data, drop volume is shown as a function of drop age on the surface. Here, fitting of the data yields initial water absorption rates, providing a more quantitative comparison of the two materials (fresh and aged).

Other examples of dynamic CA measurements illustrating the value of this technique include studies of NH_3-based plasma treatment of PES membranes,[56] O_2/acrylic acid plasma treated PLGA fibers,[30] and O_2 plasma-treated PLA fibers.[29] In the case of O_2 plasma treated PLA fibers, Dolci et al. reported WCA as a function of time on both treated and untreated PLA fibers, but did not use these data as a means of quantitative assessment. Similarly, Park et al. did not analyze dynamic CA data for plasma-treated PLGA fibers, despite there being a very clear time dependence to the measurements. Clearly, current instrumentation allows researchers to collect valuable dynamic wettability data for porous materials; the next step must be to appropriately analyze these data. By doing so, we can start to establish rules and best practices for applying techniques utilized in 2D material wettability analysis to 3D porous substrates. This will allow us to exploit these best practices to enhance our understanding of the wetting characteristics of porous plasma treated materials.

3.3.3 Adapting alternate CA techniques to 3D substrates. Techniques that use probe liquids other than water are commonly utilized on 2D substrates,[57-59] and can provide a wealth of additional information than what can be gleaned from WCA measurements alone. Simply changing out the probe liquid for any CA measurement allows exploration of effects such as oleophobicity (e.g., exchanging water with a nonpolar probe liquid).[60-62] Another technique entails CA titrations, whereby static CAs are determined using several aqueous-based probe

liquids that exhibit a wide range of pH values. The dependence of static CA on pH is fit most commonly to a 2nd-order polynomial, which allows for determination of the surface isoelectric point (IEP). The IEP, a measure of surface charge, is a critical property of plasma treated materials as it can dictate the pH-dependent interfacial interactions that control material degradation, corrosion, adhesion, and catalysis.[63-64] As with other methods that utilize CA measurements, adapting CA titrations to 3D materials may prove problematic.

CA titrations have been successfully utilized to explore IEP values for 2D metal oxide substrates,[65] including evaluating effects of plasma surface modification.[66-67] For example, a CA titration curve of H_2O plasma treated silicon oxynitride (SiO_xN_y) is shown in Figure 3.7a,[66] with CA values ranging from ~8 to 35° over the reported pH range. A 2nd order polynomial fit to the data yielded an IEP value of 6.0 ± 0.1, suggesting a surface with a slightly acidic nature. For comparison, the untreated SiO_xN_y substrate was amphoteric, with no dependence on pH, indicating an uncharged surface. Similarly, Sardella et al. used CA titrations to measure IEPs for plasma treated 2D polymer substrates.[39] Figure 3.7b illustrates that untreated polymer substrates (flat PCL films) can also display amphoteric behavior, with an average CA of ~60°.[39] Upon N_2 plasma treatment, however, the CA values ranged from 35-70º, suggesting the substrate is no longer amphoteric, and the surface IEP = 9, Figure 3.7c. This indicates a basic surface is created via plasma modification, which is somewhat expected, given the accompanying compositional data which revealed implantation of nitrogen functionality.[39] Clearly, the obvious differences in pH dependence and therefore IEPs of different plasma-treated 2D materials helps elucidate potential acid/base character of these surfaces, vital information for a range of applications that utilize plasma treated materials.

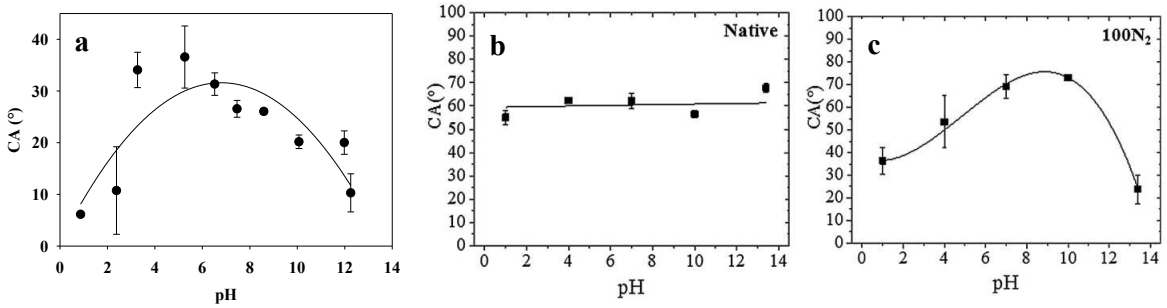

Figure 3.7. WCA as a function of pH on (a) a H_2O plasma treated SiO_xN_y;[66] (b) an untreated PCL film;[39] and (c) a N_2 plasma treated PCL film.[39] A 2nd-order polynomial was used to fit data in (a), a linear fit was used to fit data in (b), and a 3rd-order polynomial was used to fit data in (c).
(a) Reproduced with permission.[66] 2010, Wiley.
(b, c) Reproduced with permission.[39] 2015, Wiley.

The ability to utilize CA titrations with 3D porous materials could be even more important for these complex substrates, especially in biological applications as biomolecules are often charged, and these charges are highly pH-dependent. Thus, the ability to tailor a 3D substrate to obtain a specific IEP could revolutionize biomolecule-surface interactions in applications such as tissue engineering or biofouling. Although the literature is extremely sparse in this area, examples of CA titrations on 3D porous materials, including work by Hurwitz et al. (polyamide reverse osmosis membranes),[68] Molina et al. (human hair),[69] and Wagner et al. (*in vitro* and *in vivo* and stratum corneum substrates)[70] have been reported. Although none of these reports are on plasma-modified materials, they provide us with insight regarding the interaction between 3D substrates and solutions with different pH values. For example, Molina et al.,[69] showed that various solution-based surface modifications changed the CA of the surface of hair, but overall the surface remained amphoteric. CA titration data of Wagner et al.,[70] showed a bimodal function with respect to pH, indicative of a polyprotic surface. Interestingly, the values (nominally pK_a values) derived from these data align with expected pH values for fatty acid functional groups present on their surfaces. Many of the challenges in applying CA titrations to porous materials, however, echo those noted with static WCA measurements (Section 3.2.2), as the titration technique relies on collecting static CA data as a function of pH (i.e., the probe liquid drop must stabilize on the material surface). This point is well illustrated by the work of Hurwitz et al.,[68] who performed CA titrations on nanofiltration membranes and found that their probe liquids equilibrated on the surface over a relatively long period of time (30-120 s). As these materials are porous, undoubtedly some of the probe liquid was absorbed by the membrane, and the absorption is likely pH dependent.

To further explore changes in wettability as a function of pH for 3D constructs, we performed proof-of-concept CA titration experiments on allylamine plasma-treated substrates using three different probe liquids (pH ~1, 7, and 13). Allylamine was chosen as a precursor because 2D films deposited on glass substrates showed pH-dependent wetting behavior (CAs ranged from 12–40º). Likewise, differences in wetting behavior were also observed for allylamine plasma treated 3D PCL scaffolds. Specifically, scaffolds absorbed the pH~1 and pH~7 probe liquids where absorption rates = 56.6 ± 15.7 μL/s and 0.92 ± 0.33 μL/s, respectively. Conversely, the pH~13 probe liquid was not fully absorbed by the treated scaffold, exhibiting static CA values of 53.2 ± 4.0º. Given that two of the probe liquids were fully absorbed by the porous substrate, it becomes impossible to create a "titration curve" similar to those shown in Figure 3.7. Thus the challenge comes in the interpretation of these data to provide a meaningful measure of surface charge for these constructs. This example nicely illustrates the difficulty in applying alternate CA measurement techniques to 3D substrates, especially when complicated by absorption behavior.

3.4 Recommendations for Best Practices and Future Vision

This chapter presents challenges and opportunities associated with evaluating the wetting capabilities of plasma-modified, 3D porous polymeric materials, including limitations associated with data analysis and interpretation. In Section 3.3.1, we presented a variety of wettability measurements on different architectures and demonstrated the importance of combining surface chemistry and morphological characterization with wettability assessments to fully understand the effects of plasma modification on a given 3D substrate. In addition, we described the detailed methodology followed in our experiments in Chapter 2, aiming to provide a baseline to design future wettability studies within the plasma community.

Here, we present a list of five recommendations for best practices in the assessment of surface wettability of unmodified and plasma-modified 3D porous constructs. (1) Our first recommendation aligns with the endorsements presented in the *PPP* debate: to ensure that CA results on plasma-treated 3D materials are both reproducible and meaningful, researchers must utilize identical experimental and data analysis conditions, including consistently placing the baseline directly above the point of the highest macroscale roughness feature(s). Along with this we recommend that emphasis be placed on comparative data (e.g., with static WCAs) rather than absolute measurements, especially when evaluating the efficacy of different plasma treatments. (2) Evaluating changes in surface chemistry and architecture in parallel with wettability analyses is critical to better comprehend any reported changes in material wetting behavior. (3) Performing replicate measurements on independent samples and including experimental error when reporting CA data (whether static or dynamic) ensures values can be evaluated by the community on the basis of statistical representation of experimental variability. This is critical for quantitative comparison between measurements and is a clear necessity when working with morphologically diverse substrates. (4) For plasma-treated 3D materials that do not exhibit absorption behavior, experimental details should be reported, including the time period used for the stabilization of the probe liquid drop, drop volume, and fitting parameters. This recommendation applies to both static and dynamic CA measurements. (5) For plasma-treated 3D materials that exhibit absorption behavior, the evaluation of dynamic data, including absorption rate and potential hydrophobic recovery, is vital to provide a semi-quantitative overview of the material wetting behavior. This must be accompanied by precise definitions of terminology that would mitigate the use of highly ambiguous, qualitative descriptions of wettability data. Overall, we believe there is much promise for the future development of robust

CA measurement techniques that can be easily applied to 3D porous polymer substrates. Furthermore, we welcome the opportunity for further discussion of establishing a well-defined approach across the community to evaluating CA measurements for these complex materials.

REFERENCES

1. Hawker, M. J.; Pegalajar-Jurado, A.; Fisher, E. R., Innovative Applications of Surface Wettability Measurements for Plasma-modified Three-dimensional Porous Polymeric Materials: A Review. *Plasma Processes Polym.* **2015,** *12* (9), 846-863.
2. Xu, J.; Liu, W.; Du, J.; Tang, Z.; Xu, L.; Li, N., Fabrication of Superhydrophobic Surface with Controlled Wetting Property by Hierarchical Particles. *J. Nanosci. Nanotechnol.* **2015,** *15* (4), 2870-2876.
3. Ghochaghi, N.; Taiwo, A.; Winkel, M.; Dodd, B.; Mossi, K.; Tepper, G., Electrospun Polystyrene Coatings with Tunable Wettability. *J. Appl. Polym. Sci.* **2015,** *132* (10).
4. Liu, Y.; Liu, J.; Li, S.; Wang, Y.; Han, Z.; Ren, L., One-step Method for Fabrication of Biomimetic Superhydrophobic Surface on Aluminum Alloy. *Colloids Surf., A* **2015,** *466*, 125-131.
5. Huang, Y.; Li, H.; Wang, L.; Qiao, Y.; Tang, C.; Jung, C.; Yoon, Y.; Li, S.; Yu, M., Ultrafiltration Membranes with Structure-optimized Graphene-oxide Coatings for Antifouling Oil/Water Separation. *Adv. Mater. Interface* **2014,** *2* (2), 1400433.
6. Shayan, M.; Jung, Y.; Huang, P.-S.; Moradi, M.; Plakseychuk, A. Y.; Lee, J.-K.; Shankar, R.; Chun, Y., Improved Osteoblast Response to UV-irradiated PMMA/TiO_2 Nanocomposites with Controllable Wettability. *J. Mater. Sci. Mater. Med.* **2014,** *25* (12), 2721-2730.
7. Teng, S.-H.; Wang, P.; Dong, J.-Q., Bioactive Hybrid Coatings of Poly(ε -caprolactone)-Silica Xerogel on Titanium for Biomedical Applications. *Mater. Lett.* **2014,** *129*, 209-212.
8. Song, J.; Huang, S.; Lu, Y.; Bu, X.; Mates, J. E.; Ghosh, A.; Ganguly, R.; Carmalt, C. J.; Parkin, I. P.; Xu, W., Self-driven One-step Oil Removal from Oil Spill on Water via Selective-wettability Steel Mesh. *ACS Appl. Mater. Interfaces* **2014,** *6* (22), 19858-19865.
9. Wang, N.; Zhu, Z.; Sheng, J.; Al-Deyab, S. S.; Yu, J.; Ding, B., Superamphiphobic Nanofibrous Membranes for Effective Filtration of Fine Particles. *J. Colloid Interface Sci.* **2014,** *428*, 41-48.
10. Di Mundo, R.; Palumbo, F., Comments Regarding 'An Essay on Contact Angle Measurements'. *Plasma Process. Polym.* **2011,** *8* (1), 14-18.
11. Kietzig, A. M., Comments on "An Essay on Contact Angle Measurements"–An Illustration of the Respective Influence of Droplet Deposition and Measurement Parameters. *Plasma Processes Polym.* **2011,** *8* (11), 1003-1009.
12. Müller, M.; Oehr, C., Comments on "An Essay on Contact Angle Measurements" by Strobel and Lyons. *Plasma Processes Polym.* **2011,** *8* (1), 19-24.
13. Strobel, M.; Lyons, C. S., An Essay on Contact Angle Measurements. *Plasma Processes Polym.* **2011,** *8* (1), 8-13.
14. Terriza, A.; Alvarez, R.; Yubero, F.; Borras, A.; González-Elipe, A. R., Comments on "An Essay on Contact Angle Measurements": Determination of Surface Roughness and Modeling of the Wetting Behavior. *Plasma Processes Polym.* **2011,** *8* (11), 998-1002.
15. Young, T., An Essay on the Cohesion of Fluids. *Phil. Trans. R. Soc. Lond.* **1805**, 65-87.
16. Kwok, D.; Neumann, A., Contact Angle Measurement and Contact Angle Interpretation. *Adv. Colloid Interface Sci.* **1999,** *81* (3), 167-249.

17. Gao, L.; McCarthy, T. J., Teflon is Hydrophilic. Comments on Definitions of Hydrophobic, Shear versus Tensile Hydrophobicity, and Wettability Characterization. *Langmuir* **2008,** *24* (17), 9183-9188.
18. Xie, X.; Gengenbach, T. R.; Griesser, H. J., Changes in Wettability with Time of Plasma-modified Perfluorinated Polymers. *J. Adhes. Sci. Technol.* **1992,** *6* (12), 1411-1431.
19. Wavhal, D. S.; Fisher, E. R., Membrane Surface Modification by Plasma-induced Polymerization of Acrylamide for Improved Surface Properties and Reduced Protein Fouling. *Langmuir* **2003,** *19* (1), 79-85.
20. Tompkins, B. D.; Dennison, J. M.; Fisher, E. R., H_2O Plasma Modification of Track-etched Polymer Membranes for Increased Wettability and Improved Performance. *J. Membr. Sci.* **2013,** *428*, 576-588.
21. Tompkins, B. D.; Dennison, J. M.; Fisher, E. R., Etching and Post-Treatment Surface Stability of Track-Etched Polycarbonate Membranes by Plasma Processing Using Various Related Oxidizing Plasma Systems. *Plasma Processes Polym.* **2014,** *11* (9), 850-863.
22. *DSA4 Software for Drop Shape Analysis*. Krüss GmbH: Hamburg, 2004-2012; Vol. V1.0-03.
23. Öner, D.; McCarthy, T. J., Ultrahydrophobic Surfaces. Effects of Topography Length Scales on Wettability. *Langmuir* **2000,** *16* (20), 7777-7782.
24. Quéré, D., Wetting and Roughness. *Annu. Rev. Mater. Res.* **2008,** *38*, 71-99.
25. Palumbo, F., Wettability Characterization of Plasma Texturing of Polymers. *Plasma Processes Polym.* **2015**.
26. Hiemenz, P. C.; Rajagopalan, R., *Principles of Colloid and Surface Chemistry, Revised and Expanded*. CRC press: Boca Raton, FL, 1997; Vol. 14, p 248-292.
27. Yang, F.; Wolke, J.; Jansen, J., Biomimetic Calcium Phosphate Coating on Electrospun Poly(ε-caprolactone) Scaffolds for Bone Tissue Engineering. *Chem. Eng. J.* **2008,** *137* (1), 154-161.
28. Khang, G.; Lee, H., *Methods of Tissue Engineering*. Elsevier Academic Press: San Diego, CA, 2001.
29. Dolci, L. S.; Quiroga, S. D.; Gherardi, M.; Laurita, R.; Liguori, A.; Sanibondi, P.; Fiorani, A.; Calzà, L.; Colombo, V.; Focarete, M. L., Carboxyl Surface Functionalization of Poly(L-lactic acid) Electrospun Nanofibers through Atmospheric Non-Thermal Plasma Affects Fibroblast Morphology. *Plasma Processes Polym.* **2014,** *11* (3), 203-213.
30. Park, H.; Lee, K. Y.; Lee, S. J.; Park, K. E.; Park, W. H., Plasma-treated Poly(lactic-co-glycolic acid) Nanofibers for Tissue Engineering. *Macromol. Res.* **2007,** *15* (3), 238-243.
31. Seveno, D.; Ledauphin, V.; Martic, G.; Voué, M.; De Coninck, J., Spreading Drop Dynamics on Porous Surfaces. *Langmuir* **2002,** *18* (20), 7496-7502.
32. Martic, G.; Gentner, F.; Seveno, D.; De Coninck, J.; Blake, T., The Possibility of Different Time Scales in the Dynamics of Pore Imbibition. *J. Colloid Interface Sci.* **2004,** *270* (1), 171-179.
33. Hejazi, V.; Nosonovsky, M., Contact Angle Hysteresis in Multiphase Systems. *Colloid Polym. Sci.* **2013,** *291* (2), 329-338.
34. Hejazi, V.; Moghadam, A. D.; Rohatgi, P.; Nosonovsky, M., Beyond Wenzel and Cassie–Baxter: Second-Order Effects on the Wetting of Rough Surfaces. *Langmuir* **2014,** *30* (31), 9423-9429.

35. Hawker, M. J.; Pegalajar-Jurado, A.; Fisher, E. R., Conformal Encapsulation of Three-dimensional, Bioresorbable Polymeric Scaffolds Using Plasma-enhanced Chemical Vapor Deposition. *Langmuir* **2014,** *30* (41), 12328-12336.
36. Kim, K.; Lee, K.; Cho, K.; Park, C., Surface Modification of Polysulfone Ultrafiltration Membrane by Oxygen Plasma Treatment. *J. Membr. Sci.* **2002,** *199* (1), 135-145.
37. Intranuovo, F.; Gristina, R.; Brun, F.; Mohammadi, S.; Ceccone, G.; Sardella, E.; Rossi, F.; Tromba, G.; Favia, P., Plasma Modification of PCL Porous Scaffolds Fabricated by Solvent-Casting/Particulate-Leaching for Tissue Engineering. *Plasma Process. Polym.* **2014,** *11* (2), 184-195.
38. Akhavan, B.; Jarvis, K.; Majewski, P., Evolution of Hydrophobicity in Plasma Polymerised 1, 7-Octadiene Films. *Plasma Process. Polym.* **2013,** *10* (11), 1018-1029.
39. Sardella, E.; Fisher, E. R.; Shearer, J. C.; Garzia Trulli, M.; Gristina, R.; Favia, P., N_2/H_2O Plasma Assisted Functionalization of Poly(ε -caprolactone) Porous Scaffolds: Acidic/Basic Character versus Cell Behavior. *Plasma Processes Polym.* **2015**.
40. Fisher, E. R., Challenges in the Characterization of Plasma-processed Three-dimensional Polymeric Scaffolds for Biomedical Applications. *ACS Appl. Mater. Interfaces* **2013,** *5* (19), 9312-9321.
41. Formosa, F.; Sánchez-Vaquero, V.; Rodríguez-Navas, C.; Muñoz-Noval, Á.; Tejera-Sanchez, N.; Silván, M. M.; García-Ruiz, J. P.; Marletta, G., Evaluation of Plasma Modified Polycaprolactone Honeycomb Scaffolds by Human Mesenchymal Stem Cells Cultured in Vitamin D Differentiation Medium. *Plasma Processes Polym.* **2010,** *7* (9-10), 794-801.
42. Wang, X.; Zhang, J.; Wang, Q., Surface Modification of GTA Crosslinked Collagen-based Composite Scaffolds with Low Temperature Plasma Technology. *J. Macromol. Sci. A* **2008,** *45* (7), 585-589.
43. Park, K.; Ju, Y. M.; Son, J. S.; Ahn, K.-D.; Han, D. K., Surface Modification of Biodegradable Electrospun Nanofiber Scaffolds and their Interaction with Fibroblasts. *J. Biomater. Sci., Polym. Ed.* **2007,** *18* (4), 369-382.
44. Ma, Z.; He, W.; Yong, T.; Ramakrishna, S., Grafting of Gelatin on Electrospun Poly(caprolactone) Nanofibers to Improve Endothelial Cell Spreading and Proliferation and to Control Cell Orientation. *Tissue Eng.* **2005,** *11* (7-8), 1149-1158.
45. Intranuovo, F.; Howard, D.; White, L. J.; Johal, R. K.; Ghaemmaghami, A. M.; Favia, P.; Howdle, S. M.; Shakesheff, K. M.; Alexander, M. R., Uniform Cell Colonization of Porous 3-D Scaffolds Achieved Using Radial Control of Surface Chemistry. *Acta Biomater.* **2011,** *7* (9), 3336-3344.
46. Safinia, L.; Blaker, J. J.; Maquet, V.; Boccaccini, A. R.; Mantalaris, A.; Bismarck, A., Characterisation of 'Wet' Polymer Surfaces for Tissue Engineering Applications: Are Flat Surfaces a Suitable Model for Complex Structures? *E polymers* **2005,** *5* (1), 92-109.
47. Venugopal, J.; Low, S.; Choon, A. T.; Kumar, A. B.; Ramakrishna, S., Electrospun-modified Nanofibrous Scaffolds for the Mineralization of Osteoblast Cells. *J. Biomed. Mater. Res. A* **2008,** *85* (2), 408-417.
48. Prabhakaran, M. P.; Venugopal, J.; Chan, C. K.; Ramakrishna, S., Surface Modified Electrospun Nanofibrous Scaffolds for Nerve Tissue Engineering. *Nanotechnology* **2008,** *19* (45), 455102.
49. Jia, J.; Duan, Y. Y.; Yu, J.; Lu, J. W., Preparation and Immobilization of Soluble Eggshell Membrane Protein on the Electrospun Nanofibers to Enhance Cell Adhesion and Growth. *J. Biomed. Mater. Res. A* **2008,** *86* (2), 364-373.

50. He, W.; Ma, Z.; Yong, T.; Teo, W. E.; Ramakrishna, S., Fabrication of Collagen-coated Biodegradable Polymer Nanofiber Mesh and its Potential for Endothelial Cells Growth. *Biomaterials* **2005,** *26* (36), 7606-7615.
51. Shabani, I.; Haddadi-Asl, V.; Soleimani, M.; Seyedjafari, E.; Babaeijandaghi, F.; Ahmadbeigi, N., Enhanced Infiltration and Biomineralization of Stem Cells on Collagen-grafted Three-dimensional Nanofibers. *Tissue Eng. Part A* **2011,** *17* (9-10), 1209-1218.
52. Steen, M. L.; Hymas, L.; Havey, E. D.; Capps, N. E.; Castner, D. G.; Fisher, E. R., Low Temperature Pasma Treatment of Asymmetric Polysulfone Membranes for Permanent Hydrophilic Surface Modification. *J. Membr. Sci.* **2001,** *188* (1), 97-114.
53. Baker, S. C.; Atkin, N.; Gunning, P. A.; Granville, N.; Wilson, K.; Wilson, D.; Southgate, J., Characterisation of Electrospun Polystyrene Scaffolds for Three-dimensional *in vitro* Biological Studies. *Biomaterials* **2006,** *27* (16), 3136-3146.
54. Hutmacher, D. W., Scaffold Design and Fabrication Technologies for Engineering Tissues—State of the Art and Future Perspectives. *J. Biomater. Sci., Polym. Ed.* **2001,** *12* (1), 107-124.
55. Steen, M. L.; Jordan, A. C.; Fisher, E. R., Hydrophilic Modification of Polymeric Membranes by Low Temperature H_2O Plasma Treatment. *J. Membr. Sci.* **2002,** *204* (1), 341-357.
56. Kull, K. R.; Steen, M. L.; Fisher, E. R., Surface Modification with Nitrogen-Containing Plasmas to Produce Hydrophilic, Low-fouling Membranes. *J. Membr. Sci.* **2005,** *246* (2), 203-215.
57. Chhatre, S. S.; Guardado, J. O.; Moore, B. M.; Haddad, T. S.; Mabry, J. M.; McKinley, G. H.; Cohen, R. E., Fluoroalkylated Silicon-Containing Surfaces− Estimation of Solid-Surface Energy. *ACS Appl. Mater. Interfaces* **2010,** *2* (12), 3544-3554.
58. Li, H.; Sedev, R.; Ralston, J., Dynamic Wetting of a Fluoropolymer Surface by Ionic Liquids. *Phys. Chem. Chem. Phys.* **2011,** *13* (9), 3952-3959.
59. Chibowski, E.; Jurak, M., Comparison of Contact Angle Hysteresis of Different Probe Liquids on the Same Solid Surface. *Colloid Polym. Sci.* **2013,** *291* (2), 391-399.
60. Yu, Q.; Tao, Y.; Huang, Y.; Lin, Z.; Zhuang, Y.; Ge, L.; Shen, Y.; Hong, M.; Xie, A., Preparation of Porous Polysulfone Microspheres and their Application in Removal of Oil from Water. *Ind. Eng. Chem. Res.* **2012,** *51* (23), 8117-8122.
61. Wang, C.-F.; Tzeng, F.-S.; Chen, H.-G.; Chang, C.-J., Ultraviolet-durable Superhydrophobic Zinc Oxide-coated Mesh Films for Surface and Underwater-oil Capture and Transportation. *Langmuir* **2012,** *28* (26), 10015-10019.
62. Calcagnile, P.; Fragouli, D.; Bayer, I. S.; Anyfantis, G. C.; Martiradonna, L.; Cozzoli, P. D.; Cingolani, R.; Athanassiou, A., Magnetically Driven Floating Foams for the Removal of Oil Contaminants from Water. *ACS Nano* **2012,** *6* (6), 5413-5419.
63. Dumitrascu, N.; Borcia, G.; Apetroaei, N.; Popa, G., Immobilization of Biologically Active Species on PA-6 Foils Treated by a Dielectric Barrier Discharge. *J. Appl. Polym. Sci.* **2003,** *90* (7), 1985-1990.
64. McCafferty, E.; Wightman, J., Determination of the Surface Isoelectric Point of Oxide Films on Metals by Contact Angle Titration. *J. Colloid Interface Sci.* **1997,** *194* (2), 344-355.
65. Cuddy, M. F.; Poda, A. R.; Brantley, L. N., Determination of Isoelectric Points and the Role of pH for Common Quartz Crystal Microbalance Sensors. *ACS Appl. Mater. Interfaces* **2013,** *5* (9), 3514-3518.

66. Trevino, K. J.; Shearer, J. C.; McCurdy, P. R.; Pease-Dodson, S. E.; Okegbe, C. C.; Fisher, E. R., Isoelectric Points of Plasma-modified and Aged Silicon Oxynitride Surfaces Measured Using Contact Angle Titrations. *Surf. Interface Anal.* **2011,** *43* (9), 1257-1270.
67. Trevino, K. J.; Shearer, J. C.; Tompkins, B. D.; Fisher, E. R., Compaing Isoelelctric Point and Surface Composition of Plasma Modified Native and Deposited SiO_2 Films Using Contact Angle Titrations and X-ray Photoelectron Spectroscopy. *Plasma Processes Polym.* **2011,** *8*, 951-964.
68. Hurwitz, G.; Guillen, G. R.; Hoek, E. M., Probing Polyamide Membrane Surface Charge, Zeta Potential, Wettability, and Hydrophilicity with Contact Angle Measurements. *J. Membr. Sci.* **2010,** *349* (1), 349-357.
69. Molina, R.; Comelles, F.; Juliá, M. R.; Erra, P., Chemical Modifications on Human Hair Studied by Means of Contact Angle Determination. *J. Colloid Interface Sci.* **2001,** *237* (1), 40-46.
70. Wagner, M.; Mavon, A.; Haidara, H.; Vallat, M. F.; Duplan, H.; Roucoules, V., From Contact Angle Titration to Chemical Force Microscopy: a New Route to Assess the pH-dependent Character of the Stratum Corneum. *Int. J. Cosmetic Sci.* **2012,** *34* (1), 55-63.

CHAPTER 4

CHARACTERIZATION OF H_2O PLASMA-MODIFIED NITRIC OXIDE-RELEASING POLYMERIC MATERIALS

This chapter describes results from H_2O plasma modification of two unique polymeric materials: a nitrosated poly(lactic-*co*-glycolic acid)-based hydrophobic polymer (herein referred to as PLGH-cysteine) and a poly(vinyl chloride) (PVC)-based polymer blended with a nitric oxide (NO) donor. These two systems were selected for their capabilities of releasing the therapeutic agent NO. Although much effort has gone into a comprehensive characterization of these systems in terms of surface analysis, NO release, and biological compatibility,[1-3] this chapter focuses on a subsection of these analyses, including changes in material properties of each polymer system upon plasma modification. The ability to tune NO-releasing polymer film surface properties is demonstrated in each system, echoing work presented on plasma-modified polymeric scaffolds in Chapters 3 and 5–8. Additionally, outcomes of H_2O plasma treatment of the two different systems under identical conditions will be compared. Collectively, this body of work establishes our ability to customize surface properties of two unique NO-releasing polymeric constructs using a non-depositing plasma system.

This chapter is reproduced in part with permission from two articles: (1) published in *ACS Applied Materials & Interfaces* by Adoracion Pegalajar-Jurado, Jessica M. Joslin, Morgan J. Hawker, Melissa M. Reynolds, and Ellen R. Fisher [*6* (15), pp 12307–12320, Copyright 2014 American Chemical Society],[3] and (2) published *Biointerphases* by Michelle N. Mann, Bella H. Neufeld, Morgan J. Hawker, Adoracion Pegalajar-Jurado, Melissa M. Reynolds, and Ellen R. Fisher [*11*, pp 031005, Copyright American Vacuum Society, 2016].[2] Note that the entirety of the study on PLGH materials (i.e., NO release data and all other aspects of the work)

was previously presented in Dr. Jessica Joslin's dissertation; the surface analysis and its interpretation have been excerpted and adapted for this dissertation as these components collectively represent my direct contribution to this work. The entirety of the study on Tygon® materials (Section 4.3), including evaluating film antibacterial activity, will be included in Michelle Mann's dissertation. Collectively, work included in this chapter was supported by the National Science Foundation (CHE-1152963 and DMR-0847641), the Camille and Henry Dreyfus Foundation Postdoctoral Program in Environmental Chemistry, Department of Defense Congressionally Directed Medical Research Program (DOD-CDMRP), the Vice President for Research at Colorado State University (Catalyst for Innovative Partnerships), the state of Colorado Bioscience Discovery Evaluation Grant Program, and the Boettcher Foundation's Webb-Waring Biomedical Research Program.

I want to thank Jess Joslin and Dori Pegalajar for establishing the collaboration that led to work presented in this chapter, as well as Michelle Mann and Bella Neufeld for sustaining the collaboration through experiments with Tygon® films. I performed the surface analysis and interpretation presented in this chapter, with the exception of surface roughness measurements (Jess Joslin and Bella Neufeld). Dori Pegalajar assisted with water spreading analysis on PLGH films.

4.1 Introduction

As discussed in Chapter 1, one route to advanced biomedical material development is the modification of constructs with desirable bulk properties to enhance surface properties, thus customizing interactions at the material/biological species interface. This type of modification represents a passive approach to control such interactions, whereas therapeutic release approaches aim to actively eradicate bacteria and enhance cellular proliferation.[4-6] Thus, a

material that combines these tactics would represent a functional material that targets different biological species, thereby offering precise control over physiological responses at the biomaterial surface. Notably, such ability to control multiple facets of biocompatibility is key for developing advanced multifunctional materials for applications such as tissue engineering, wound dressing fabrication and antimicrobial materials development.

We utilized this dual approach by selecting model polymeric materials that are well-established as polymeric biomaterials [poly(lactic-*co*-glycolic acid)[7-9] and PVC[10-12]] and integrating NO into each polymer (see Section 2.2.4 for fabrication methodology). NO, a therapeutic agent produced by endothelial cells that line blood vessels to control coagulation and platelet adhesion, plays an important role in the immune response to inflammation.[13] The use of NO as the agent of choice for drug-eluting polymer systems is distinctive because NO can target multiple physiological actions, compared to agents that target only a single function (e.g., heparin or antibiotics). An inherent challenge associated with NO integration, however, is that the molecule cannot be retained in polymers because it is highly reactive and short-lived.[14] Thus, to integrate NO into polymer materials, a variety of NO donors [molecules that release NO upon stimulation (e.g., by light, heat, Cu^{2+})], such as metal nitrosyls, *N*-diazeniumdiolates, and *S*-nitrosothiols, can be employed.[15]

An ideal NO-releasing material would exhibit (a) bulk mechanical and chemical properties that ensure stability over the device lifetime (from hours to years, depending on the device) when exposed to biological systems; (b) controllable NO release directed at the microorganism-material interface; and (c) tunable surface properties to control interactions with targeted biological species. Although plasma treatments have been used to modify the surface properties of drug-releasing polymers,[16-18] to date, no attempts to modify the surface properties

of an NO releasing polymer while maintaining the material's bulk properties have been reported. Therefore, the combined ability to tune the NO delivery and surface properties represents a unique approach to potentially creating NO releasing biopolymers that can modulate biological interactions while controllably releasing a therapeutic agent.

Although some NO-releasing materials such as hydrogels are hydrophilic,[19] unfortunately, many that have high antimicrobial activity are also hydrophobic,[20-24] thereby limiting the number of applications in which these materials would be useful.[25] Thus, H_2O plasma systems were selected for modification because of their well-established ability to increase surface wettability of different materials by incorporation of alcohol functionality.[26-29] For example, we previously demonstrated the H_2O plasma modification of hydrophobic polysulfone membranes resulted in a permanent improvement in wettability throughout the membrane cross-section, lasting for >2 years.[27] Moreover, Lee et. al. highlighted an increase in cell adhesion, spreading, and growth for H_2O plasma treated polymers.[26] Thus, H_2O plasma treatment is a highly suitable methodology for tuning wettability toward enhancing cell-surface compatibility. Unfavorable effects can be promoted by improved wettability, however, including biofilm formation and thrombosis. Thus, we have adopted the dual approach of incorporation of a therapeutic agent and surface property enhancement via plasma modification to develop a targeted biocompatible material.

This work explores the use of well-established H_2O plasma treatments to increase the hydrophilicity of two different NO-releasing polymer systems, with the overarching goal of tuning surface properties without measurable morphological damage, while maintaining the bulk properties (e.g., NO-release capabilities) and ultimately creating materials with enhanced biological performance. The following sections detail material analysis results related to each

polymer system, as well as a comparison of plasma modification outcomes between the two materials.

4.2 Results and Discussion: NO-releasing PLGH

Because the PLGH system represents the first H_2O plasma modification of an NO-releasing polymer material, it was of interest to evaluate changes in bulk composition, surface composition, surface wettability, and morphology (for both untreated and plasma-modified samples). The following sections include results from this comprehensive materials characterization. For reference throughout, the chemical structure of the starting material (nitrosated PLGH) is depicted in Figure 4.1.

4.2.1 Effect of plasma treatment on composition of S-nitrosated PLGH-cysteine films. To determine the effects of plasma treatments on polymer composition, X-ray photoelectron spectroscopy (XPS) analyses were performed, providing information about the surface chemical composition as XPS sampling depth is only 5-10 nm.[30] XPS atomic composition ratios derived from C_{1s}, O_{1s}, and N_{1s} high resolution spectra of treated and untreated *S*-nitrosated PLGH-cysteine films are summarized in Table 4.1. High-resolution S_{2p} spectra were also collected, although no appreciable change in S content was observed. Figure 4.2a highlights that the C/N ratio decreases with increasing treatment time at $P = 20$ W, indicating an increase in the surface nitrogen. No leaks were detected in the plasma system during treatment; thus, it is unlikely that the additional nitrogen was present during the plasma treatment. There are, however, two other possible sources of this surface nitrogen: (1) plasma treatment can create long-lived reactive radical sites at the surface of the polymer, which then react with atmospheric nitrogen upon exposure to air, or (2) the polymer can reorganize as a result of plasma treatment. Although the former has been observed previously,[31-33] the small changes observed in surface composition

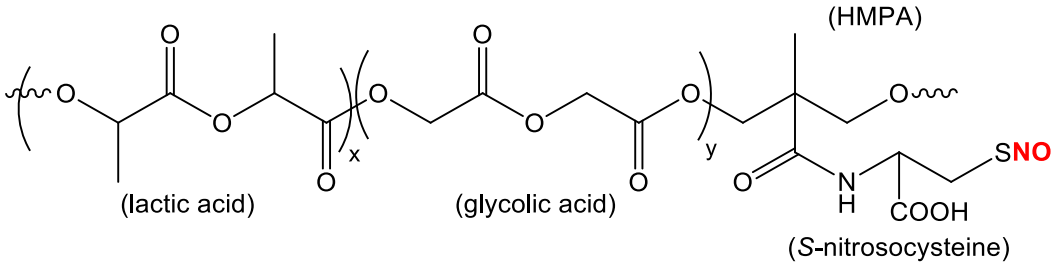

Figure 4.1. The structure of *S*-nitrosated poly(lactic-co-glycolic acid)-cysteine (PLGH-cysteine).

Table 4.1. XPS atomic composition ratios of untreated and plasma treated *S*-nitrosated PLGH-cysteine films.[a]

Plasma treatment		C/O	O/N	C/N
***P* (W)**	**Treatment Time (min)**			
Untreated	---	1.67 ± 0.08	18.4 ± 2.5	30.6 ± 3.8
20	1	1.60 ± 0.05	16.4 ± 1.8	26.3 ± 2.7
20	3	1.48 ± 0.05	14.7 ± 1.5	21.7 ± 2.0
20	5	1.43 ± 0.05	12.0 ± 1.1	17.1 ± 2.0
30	5	1.51 ± 0.03	11.6 ± 1.3	17.6 ± 1.8
50	5	1.58 ± 0.03	13.6 ± 1.1	21.5 ± 1.5
20	5 (10 days aged)	1.54 ± 0.02	17.8 ± 1.4	27.5 ± 2.3

[a]All analyses were performed for an n = 6; the mean ± standard deviation are reported.

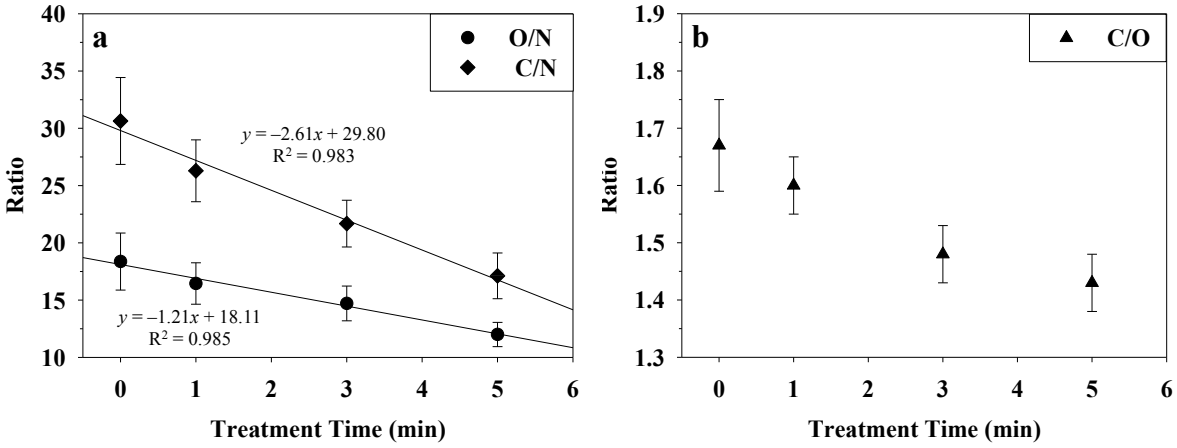

Figure 4.2. (a) O/N, C/N, and (b) C/O as a function of plasma treatment time (P = 20 W) on *S*-nitrosated PLGH-cysteine substrates. Values are calculated from XPS elemental composition data (error bars represent ± 1 standard deviation, n = 6). Additionally, linear regression fits with corresponding equations are shown for O/N and C/N in (a).

ratios upon sample aging (see Section 4.2.5) suggests the latter explanation may be contributing to the observed nitrogen incorporation, as discussed below. The shallow reorganization of polymer chains when exposed to H_2O plasma treatments has been previously reported in the literature.[34] Here, the *S*-nitrosated PLGH-cysteine comprises a large hydrophobic backbone with hydrophilic pendant groups of the cysteine residue (Figure 4.1). Consequently, we hypothesize that in the H_2O plasma environment, the *S*-nitrosocysteine pendant groups on the polymer reorient toward the plasma, thereby exposing more of these hydrophilic microdomains at the surface.

For a fixed 5 min treatment time, an increase from $P = 20$ W to $P = 30$ W does not result in a statistically significant difference in the C/N ratio, whereas an additional increase in P to 50 W results in a small increase over the lower power treatments, Table 4.1. Compared to the untreated films (C/N = 30.6 ± 3.8), however, the C/N ratio for the 50 W treatment (21.5 ± 1.5) is not as low as those measured for the 20 W (17.1 ± 2.0) and 30 W (17.6 ± 1.8) treatments, which could indicate film etching is occurring in the higher P plasma.[35]

Although our XPS data support the possibility that reorientation of hydrophilic microdomains to the film surface may be occurring, implantation of hydrophilic functional groups that would improve the surface wettability is also an important surface modification to consider. Several reports demonstrate the use of H_2O plasma treatments to implant moieties with a variety of chemical environments (i.e., C=O, C-O, O-C=O) into polymer surfaces.[27, 29, 35] In this work, implantation of O-containing functional groups into the *S*-nitrosated PLGH-cysteine film surface via plasma modification was monitored via XPS C/O ratio as a function of plasma treatment conditions, Figure 4.2b. These data show a general trend of decreasing C/O with increasing treatment time for $P = 20$ W, suggesting a relative increase in surface oxygen species

with increasing plasma exposure. Although the C/O ratio declines slightly from untreated materials to films treated in P = 30 and 50 W systems, Table 4.1, this decrease is not very pronounced, possibly as a result of competitive etching under relatively harsher plasma conditions.

To further consider O-containing functional group implantation, the O/N and C/N ratios can be compared as a function of treatment time. In Figure 4.2a, the slope of the regression line for C/N is steeper than that for O/N. This further suggests O-containing functional group incorporation is occurring, along with polymer rearrangement, to enhance the N signal at the surface of the films. Despite the elemental ratios suggesting oxygen incorporation, these data do not provide information regarding changes in the oxygen binding environments after plasma treatment. To understand changes in surface chemical functionality as a function of plasma treatment time, high-resolution C_{1s} XPS spectra were deconstructed for untreated and plasma treated samples (1 and 5 min treatment times, P = 20 W). This process involved fitting each C_{1s} spectrum with four unique binding environments, Figure 4.3a-c, corresponding to C-C/C-H (285.0 eV), O-C-C=O (~287 eV), and C=O (~289 eV) of the polymer backbone, and HN-C=O (~288 eV) corresponding to the amide linkage of the *S*-nitrosocysteine residue. For the untreated polymer sample, the C=O binding environment comprises multiple functionalities, namely the carboxylic acid moiety on the cysteine residues, as well as the multiple ester linkages in the lactic acid and glycolic acid portions of the polymer backbone, which results in a broadened peak relative to all other binding environments. The C_{1s} binding environments corresponding to the polymer backbone exhibit comparable intensities relative to each other, whereas the HN-C=O of the cysteine residue yields a smaller intensity. These proportions are consistent with the polymer structure (Figure 4.1).

The ratios between the C-C/C-H binding environment and the other C_{1s} binding environments were calculated, revealing a significant decrease in the C-C/C-H to HN-C=O ratio with increasing treatment time (Table 4.2). More specifically, the C-C/C-H to HN-C=O ratio is 10.12 ± 2.03 for the untreated sample, which decreases to 7.10 ± 0.71 for a 1 min treatment, and 4.55 ± 0.83 for a 5 min treatment. The increase in the relative intensity of the HN-C=O binding environment further supports the hypothesis that some rearrangement of the hydrophilic cysteine residues is occurring during plasma treatment. The other significant change in binding environments as a function of treatment time is the ratio of the sum of C=O-containing binding environments (C=O + HN-C=O) relative to the C-C/C-H binding environment (Figure 4.3d). Although these ratios are within experimental error for the untreated and 1 min plasma treated PLGH-cysteine films, that for the 5 min treated film is significantly lower. This implies contributions from C=O environments increase with treatment time, suggesting extended plasma treatment promotes incorporation of carbonyl-containing functionalities such as aldehyde, ketone, and/or carboxylic acid groups.

Previous studies of H_2O plasma treatment of polysulfone and polyetherimide membranes demonstrated implantation of O-containing groups at high *P* (20-200 W) arises from increased concentrations of OH and H radicals in the plasma.[35] Using optical emission spectroscopy (OES), a direct correlation was established between the intensity of emission lines attributable to OH• and the concentration of oxygen in the material surface, as measured by XPS. This relationship further translated to improved wettability for the samples with increased surface oxygen. Notably, the deconstructed C_{1s} XPS spectrum for the untreated sample indicated two binding environments corresponding to C-C/C-H and C-O. After H_2O plasma treatment, the C-O contribution increased and C=O and O-C=O binding environments appeared.[35] These data

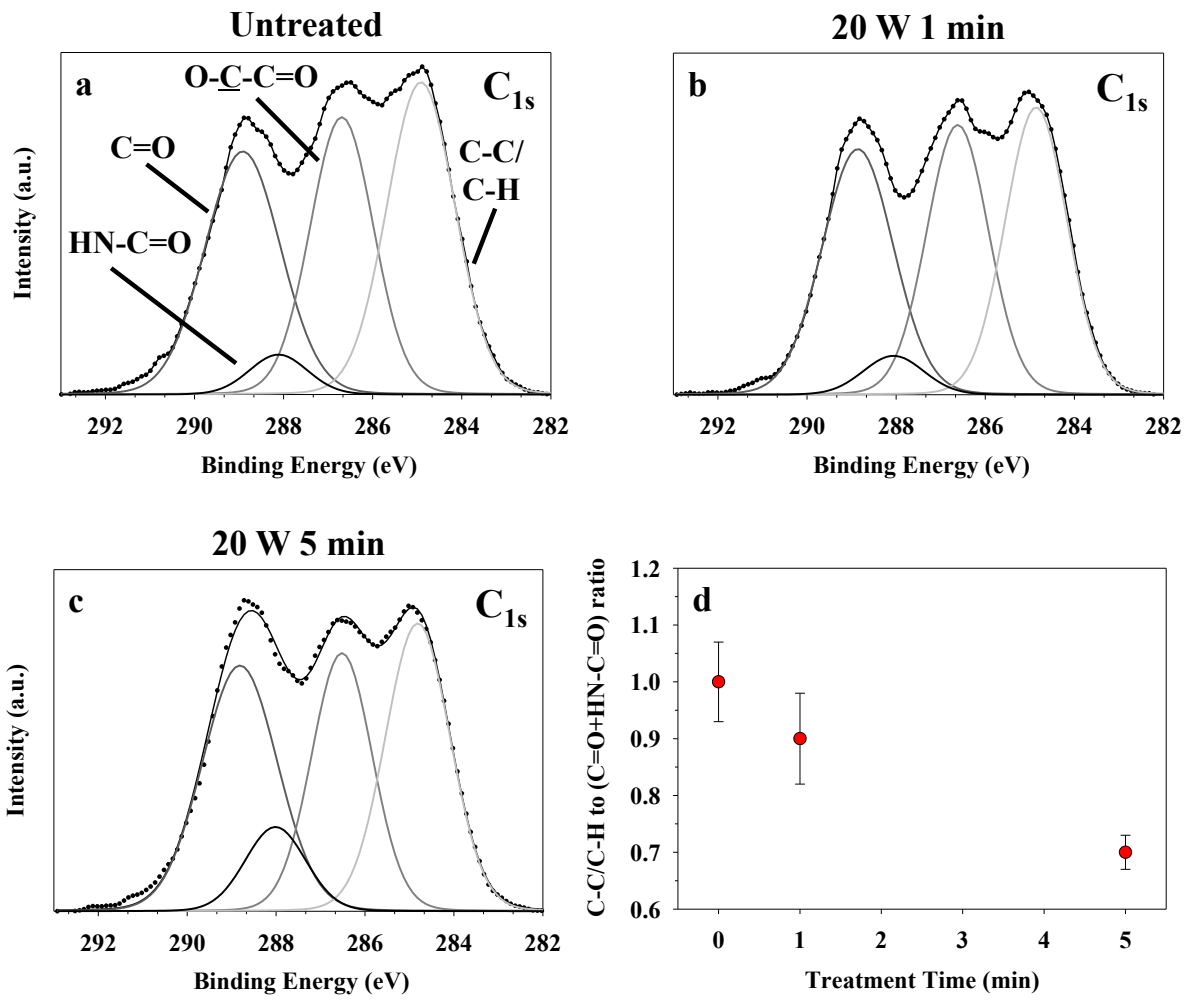

Figure 4.3. High-resolution C_{1s} XPS spectra and fits for (a) untreated, (b) 20 W 1 min treated, and (c) 20 W 5 min treated *S*-nitrosated PLGH-cysteine films. (d) C-C/C-H to (C=O + HN-C=O) binding environment ratios as a function of treatment time (P = 20 W). Error bars represent ± 1 standard deviation (n = 6).

Table 4.2. Binding environment ratios for untreated films and films treated for different times (P = 20 W) as determined from deconstructed C_{1s} XPS spectra.[a]

Treatment Time (min)	C-C/C-H to C=O	C-C/C-H to O-C-C=O	C-C/C-H to HN-C=O
0	1.13 ± 0.08	1.14 ± 0.06	10.12 ± 2.03
1	1.06 ± 0.12	1.12 ± 0.12	7.10 ± 0.71
5	0.90 ± 0.06	1.15 ± 0.08	4.55 ± 0.83

[a] All analyses were performed for an n = 6; the mean ± standard deviation are reported.

suggested that polymer treatment via H_2O plasma treatments resulted in the formation of alcohol, aldehyde/ketone and carboxylic acid/ester functionalities at the material surface, which increased the surface wettability of the samples. Translating these findings to our *S*-nitrosated PLGH-cysteine system, we can infer a direct correlation likely exists between the increase in the surface oxygen content and surface wettability. This is discussed further in Section 4.2.3. Notably, XPS data cannot be used to distinguish between alcohol and other C-O binding environments, as hydrogen cannot be detected using XPS because of its low ionization cross-section. Here, as with work presented in Chapter 6, Fourier transform infrared spectroscopy (FTIR) spectra were collected, demonstrating increased alcohol functionality in H_2O plasma treated films when compared to untreated films (data and associated discussion can be found in the full article this chapter is based on).[3]

The notable increase in the C=O environment relative to the C-C/C-H binding environment after a 20 W, 5 min plasma treatment observed here can be understood by considering possible oxidation sites on the polymer. Previous work in the Fisher group demonstrated smaller changes in the C-O binding environment for H_2O plasma treated polysulfone materials, with a more significant impact on the C=O/O-C=O groups, such as the aldehyde/ketone and carboxylic acid/ester functional groups.[27] These data suggested the possible oxidation of alcohol groups formed during the treatment, or the oxidation of other sites within the polymer backbone, such as methyl groups and quaternary carbon sites, to yield aldehydes and ketones, respectively. Further oxidation of aldehydes could result in carboxylic acid groups. Other studies demonstrated surface functionalization using H_2O plasma treatments for polymers with rigid, aromatic backbones versus linear, hydrocarbon backbones.[28] In all cases, binding environments and relative elemental compositions obtained were similar to those measured in

this work. Formation of highly oxidized species is supported by the data presented here, where we saw a notable decrease in the C-C/C-H to C=O ratio, with no distinguishable difference in the C-C/C-H to O-C-C=O ratio when comparing an untreated and 20 W, 5 min treated sample. This suggests the oxidation sites associated with the *S*-nitrosated PLGH-cysteine are likely the methyl groups of the lactic acid portion, the secondary carbon sites of the glycolic acid and HMPA portions, and the quaternary carbon site in the HMPA portion to form ketone and aldehyde functional groups (Figure 4.1).

Another study demonstrated that, at lower *P* (e.g., 25 W), the OES spectrum as a function of plasma treatment time showed the O• signal dropped by ~80% when the sample was introduced, which is more significant than the drop in OH•, indicating that the key player at lower applied powers is O•.[28] Additionally, there were notable differences in the resulting functionalities after plasma treatment depending on the specific material being treated. Differences in the % O incorporated and the corresponding extent of oxidation were attributed to the initial polymer structure and the number of oxidizable sites, in addition to the ability of certain polymers to undergo hydrolysis in aqueous environments. The possibility of polymer chain scission at ester sites was also acknowledged. As *S*-nitrosated PLGH-cysteine is composed of several ester linkages, it could easily undergo acid or base catalyzed hydrolysis to form carboxylic acid groups (Figure 4.4) and ultimately result in chain scission.[36]

Overall, the XPS data suggest combined pathways that could lead to increased hydrophilicity and thereby greater cell affinity for the *S*-nitrosated PLGH-cysteine films surfaces after plasma treatment. An increase in N content relative to both O and C content, combined with a decrease in the ratio of C-C/C-H to HN-C=O with increasing treatment time, suggests polymer rearrangement to reorient the amide linked, hydrophilic *S*-nitrosocysteine pendant groups to the

surface. Additionally, an increase in the surface O, specifically the ratio of C-C/C-H to C=O, suggests implantation of OH groups at the alkyl sites along the polymer backbone, which subsequently oxidize to carbonyl sites, including ketone/aldehyde and carboxylic groups. Additionally, chain scission via ester hydrolysis is a possibility due to the large number of ester sites on the backbone.

4.2.2 Effect of prolonged treatment time on surface composition. As we found greater changes occurred in film chemistry with prolonged plasma exposure, we increased treatment time to 60 min to explore parameter extremes. PLGH-cysteine films were prepared and treated for 5 or 60 min at 20 W. Because the NO donating moiety (S-nitrosothiol, RSNO) does not contribute significantly to any of the binding environments under analysis, the thiol does not need to be nitrosated to probe functionality differences before and after treatment. Thus, non-nitrosated PLGH-cysteine films were prepared to simplify these experiments.

A representative high resolution C_{1s} spectrum for a PLGH-cysteine film treated at P = 20 W for 60 min along with the C/O ratios for both the *S*-nitrosated and non-nitrosated PLGH-cysteine films as a function of treatment time are shown in Figure 4.5, which clearly indicate that the C/O ratio decreases with increasing treatment time out to 60 min for non-nitrosated PLGH-cysteine films.

There is, however, no statistical change in the C-C/C-H to HN-C=O ratio for the 5 and 60 min treated samples. This suggests no further rearrangement or functionalization occurs at prolonged treatment times, but that surface etching may be occurring. Additionally, we collected IR data on 60 min treated films (not shown). These data suggest that H_2O plasma treatment results in the incorporation of OH into the PLGH polymer structure, likely because of the

(a)

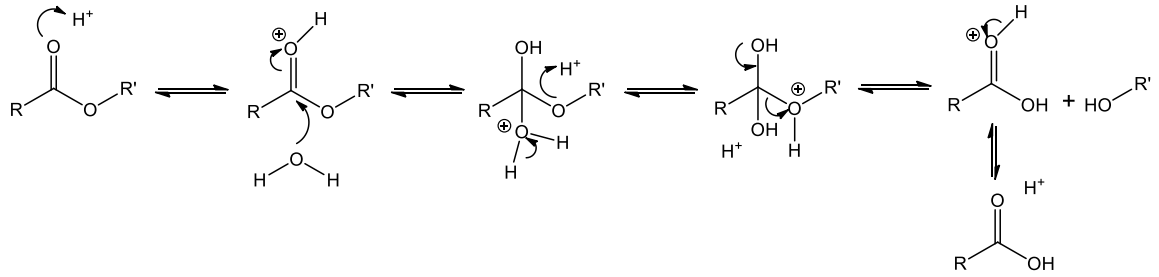

(b)

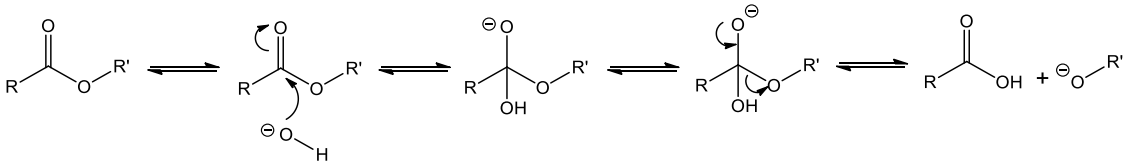

Figure 4.4. (a) Acid catalyzed ester hydrolysis occurs due to reaction with H^+ and H_2O species and yields carboxylic acid and alcohol products. (b) Base catalyzed ester hydrolysis occurs due to reaction with OH^- and yields carboxylic acid and alkoxide products.

formation of carboxylic acid groups, similar to what has been observed previously with other polymers.[28]

4.2.3 Effect of plasma treatment on surface wettability. To assess the effect of H_2O plasma treatments on the surface wettability of the *S*-nitrosated polymer films, static WCA measurements were performed. Untreated samples exhibited a relatively high WCA of 116.6 ± 3.4°, indicating the hydrophobicity of these polymers. After plasma treatment, the surfaces became hydrophilic, with the water droplet spreading completely in <100 ms (i.e., equilibrium contact angle = 0º). To distinguish between different treatments in a semi-quantitative manner, we report water droplet spreading times for plasma treated surfaces in Table 4.3 and in Figure 4.6a. Figure 4.6a highlights that increasing the treatment time from 1 to 5 min resulted in faster water spreading, as indicated by a lower spreading time (all with P = 20 W). Water droplet spreading time for the 5 min treatment was just 43 ± 7 ms, compared to 87 ± 16 ms for the 1 min treatment. Although we consider both of these surfaces to be hydrophilic, the spreading time values do suggest longer treatment time results in a more hydrophilic surface.

The increase in hydrophilicity upon plasma treatment can be attributed to multiple factors. Namely, H_2O plasma treatment implants hydroxyl and carbonyl groups which can serve to increase surface hydrophilicity.[26] Additionally, plasma treatments can initiate shallow reorientation of polymer microdomains,[34] wherein the more hydrophilic regions are brought to the surface of the film. For a fixed treatment time of 5 min, changing P (20, 30 or 50 W) reveals a slight increase in water spreading time with increasing power (Figure 4.6b), although there is no significant change in water spreading time between the 20 W and 30 W treatments. When P is increased to 50 W, however, the water spreading time increases significantly. This effect at the

highest *P* could result from a competition between implantation of OH functional groups and some etching of the polymer surface, which has been previously demonstrated.[28]

4.2.4 Effect of plasma treatment on surface morphology. Often, plasma treatment of polymers can result in extensive changes to surface morphology, including increased surface roughness, pitting, and formation of protrusions.[28] These changes can affect both surface wettability and interactions of biological components with a material surface.[37-40] Thus, evaluating surface morphology and topography is critical not only from the viewpoint of biological applications, but also to ensure that observed changes in surface properties are not solely attributable to changes in surface morphology as a result of plasma treatment. Surface roughness exists perpendicular to the surface (described as height deviation), and in the plane of the surface (described by spatial parameters and identified as texture).[41] Amplitude parameters are critical to characterize surface topography for biological application, and they include the arithmetic average roughness (R_a) and root mean square roughness (R_q).[42-43] Table 4.4 summarizes the roughness parameters (R_a and R_q) of the *S*-nitrosated PLGH-cysteine films prior to and after treatment. No significant changes in the roughness were measured, regardless of plasma parameters used to treat the polymers. Likewise, there are no discernable differences (e.g., pitting) in the SEM images of the film surfaces, Figure 4.7. These observations and the insignificant changes in roughness parameters (R_a and R_q) after plasma treatment demonstrate that the observed changes in surface wettability cannot be attributed to morphological changes. This also illustrates that any etching of the surface that occurs during the 50 W treatment does not significantly alter the overall topography of the films. It is, however, well-established that surface microtopography can either promote or inhibit cell/surface interactions, depending on the

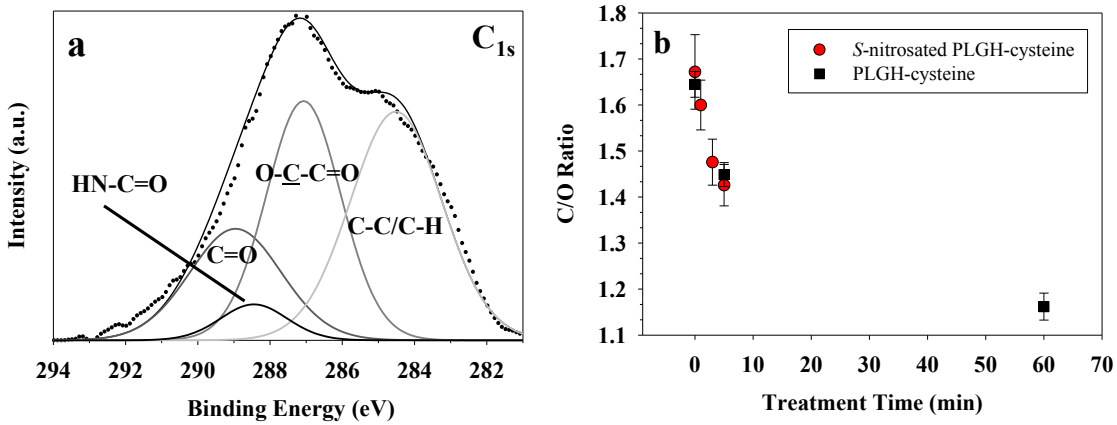

Figure 4.5. (a) A representative high-resolution C_{1s} XPS spectrum with deconstructed fits for a PLGH-cysteine film (60 min treatment time, P = 20 W). (b) C/O ratios as a function of treatment time (P = 20 W) for films of *S*-nitrosated and non-nitrosated PLGH-cysteine films (error bars represent ± 1 standard deviation, n = 6).

Table 4.3. Water droplet spreading times associated with plasma treated samples.[a]

Plasma treatment		Spreading Time (ms)
P **(W)**	**Treatment Time (min)**	
20	1	87 ± 16
20	3	65 ± 13
20	5	43 ± 7
30	5	49 ± 13
50	5	70 ± 8

[a] All analyses were performed for an n = 3, where the mean ± standard deviation are reported.

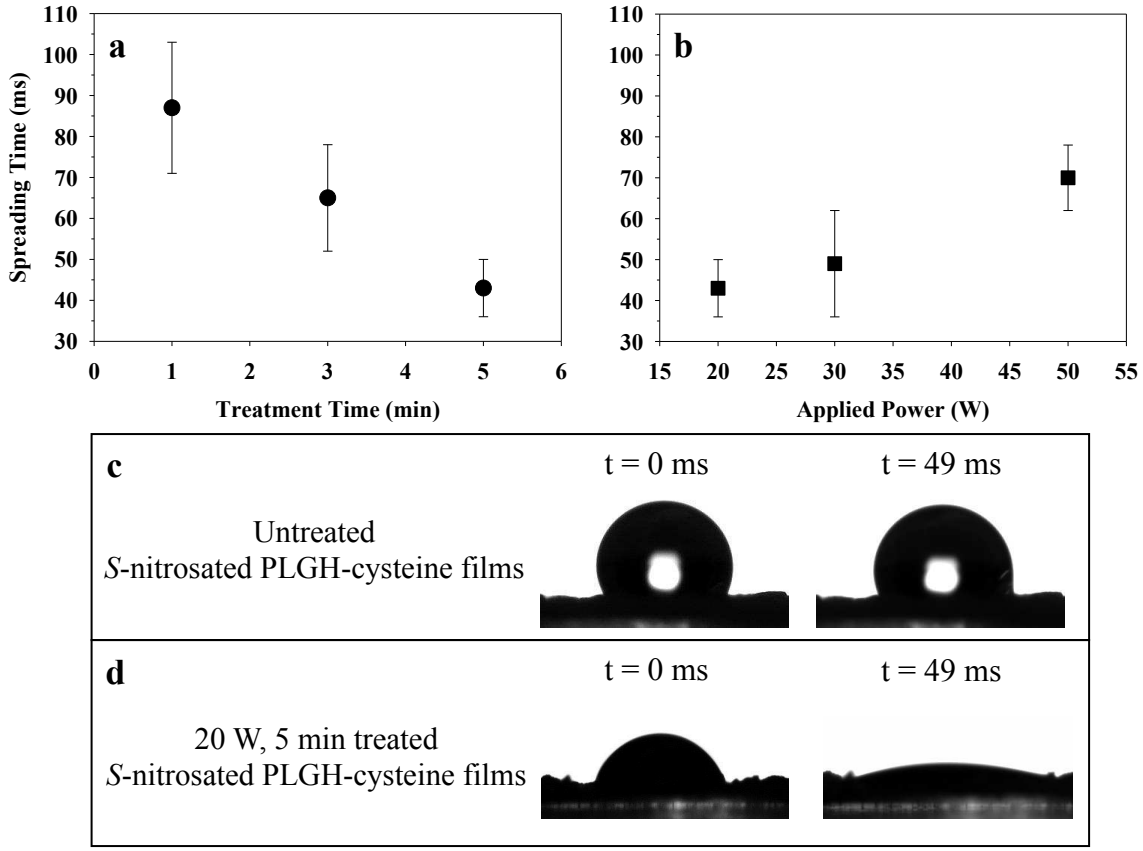

Figure 4.6. (a) Treatment time (P = 20 W) vs. water droplet spreading time, and (b) applied power (treatment time = 5 min) vs. water droplet spreading time for *S*-nitrosated PLGH-cysteine films. Additionally, representative images of water droplets on (c) untreated and (d) plasma treated *S*-nitrosated PLGH-cysteine films 0 and 49 ms after a 6 µL drop has been placed on the surface. Error bars in (a) and (b) represent ± 1 standard deviation (n = 3).

Table 4.4. Surface roughness of untreated and plasma treated *S*-nitrosated PLGH-cysteine films.[a]

Plasma treatment		R_q (µm)	R_a (µm)
P **(W)**	**Treatment Time (min)**		
-	-	18.02 ± 6.92	14.26 ± 6.76
20	1	17.89 ± 4.56	13.73 ± 3.68
20	3	20.45 ± 3.49	16.45 ± 3.08
20	5	15.01 ± 4.84	10.96 ± 3.51
30	5	17.85 ± 3.91	13.63 ± 3.49
50	5	18.57 ± 6.12	13.82 ± 4.48

[a] All analyses were performed for an n = 3, where the mean ± standard deviation are reported

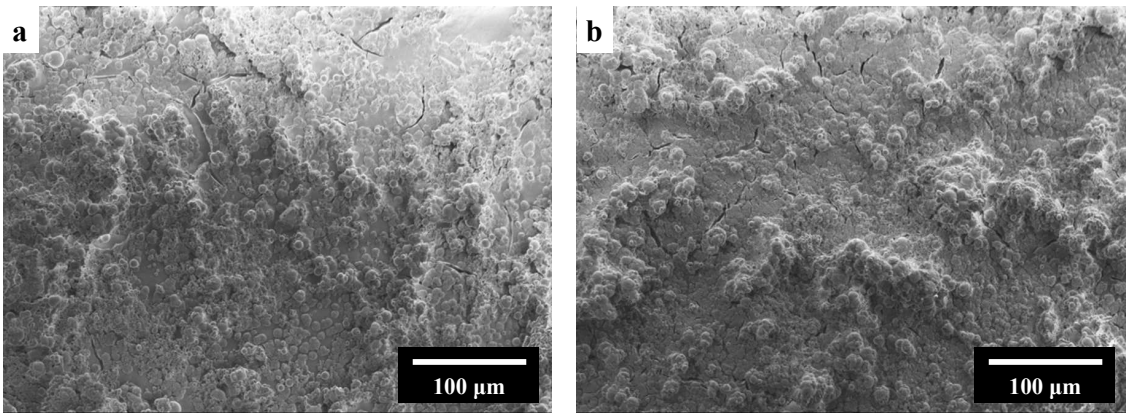

Figure 4.7. Representative SEM images of (a) untreated and (b) 20 W, 5 min treated *S*-nitrosated PLGH-cysteine films (both at 250× magnification).

specific material (i.e., surface chemistry) and the cell type.[44-46] Thus, surface roughness of these films is a parameter that must be considered and tuned to each intended application.

4.2.5 Stability of the plasma treatment. Plasma-modified surfaces can undergo what is generally referred to as hydrophobic recovery, wherein surfaces that are rendered hydrophilic ultimately revert to their original hydrophobic nature shortly after the treatment.[32-34] This aging effect is generally thought to occur via polymer rearrangement, chain migration or diffusion, or burial of hydrophilic groups (e.g., O and N-containing) within the bulk of the polymer. To examine aging effects with our materials, *S*-nitrosated PLGH-cysteine films were plasma treated (P = 20 W, 5 min) and then placed into a freezer at −18 °C under ambient conditions for a 10 day aging period. These conditions were chosen to minimize the decomposition of the RSNO during storage, while still effectively assessing the treatment stability. Hydrophobic recovery of stored samples was evaluated by WCA and XPS measurements, and results were compared to untreated and freshly treated samples. Water spreading time on the plasma treated material after the 10 day storage period was 249 ± 33 ms, significantly longer than that on freshly treated films (43 ± 7 ms). Despite this increase in the water spreading time, these surfaces are considered very hydrophilic as the water droplet still spreads extremely rapidly on the surface.

XPS analysis reveals the 10 day storage resulted in a significant increase in the O/N (17.8 ± 1.4), C/N (27.5 ± 2.3), and C/O (1.54 ± 0.02) ratios compared with those of freshly treated samples, Table 4.1. These differences in the elemental ratios between freshly treated and aged samples were normalized by the elemental ratio for the untreated samples to yield 32, 34 and 7% changes for the O/N, C/N and C/O ratios, respectively. This suggests slight hydrophobic recovery may be the result of burial of the N-containing hydrophilic cysteine microdomains, accompanied by some burial of surface O-containing moieties. Furthermore, the C/O ratio is

larger for the untreated sample than the 10 day aged sample, which suggests that oxygen-containing functional groups implanted via plasma treatment are maintained even after the 10 day storage period.

We have previously demonstrated that H_2O plasma treated polymeric materials can exhibit either minor changes in hydrophilicity over extended periods of time or complete hydrophobic recovery over time as a result of polymer rearrangement, depending on the material. For example, H_2O plasma treatments have resulted in permanent hydrophilic modifications (lasting months to years) for polymers with more rigid, aromatic backbones, such as polysulfone, polycarbonate, and polyethylene terephthalate.[27-29] The less rigid polyethylene materials, however, experienced significant hydrophobic recovery after only 48 h to 1 week as the migration of polymer chains effectively buried the polar surface groups incorporated during H_2O plasma treatment. Comparatively, although plasma treated *S*-nitrosated polymer films exhibit a small amount of hydrophobic recovery, they still maintain their overall hydrophilic nature. These aging studies clearly indicate that our materials are relatively stable in terms of wettability and surface functionality. This result is significant in that other non-aromatic backbone polymers exposed to H_2O plasma treatment exhibited nearly complete immediate hydrophobic recovery in terms of the WCA.[28]

Overall, we report the ability to tailor the surface properties of a model NO-releasing polymer. H_2O plasma treatments effectively modified the surface wettability of *S*-nitrosated PLGH-cysteine films, creating much more hydrophilic surfaces. XPS analysis revealed an increase in N signal relative to O and C, which indicates the rearrangement of the polymer exposing hydrophilic cysteine residues on the film surface. The observed decreasing trend in the C/O ratio as a plasma treatment time increases likely results from conversion of pre-existing

carbonyl groups to hydroxyl groups. Surface roughness analysis indicated no significant changes in the surface morphology after plasma treatment, supporting that the changes in surface wettability primarily result from changes in chemical functionality. Notably, plasma treated surfaces remain hydrophilic after a 10 day storage period in the freezer (−18 °C), which suggests that the films do not experience short-term hydrophobic recovery. The ability to tune the surface wettability of a polymer film while maintaining the bulk properties, as well as the stability of the treatment over time, is critical towards creating multi-functional biomaterial systems.

4.3 Results and Discussion: NO-releasing Tygon®

After proof-of-concept experiments with PLGH films demonstrated our ability to modify NO releasing polymers via plasma processing (Section 4.2), we expanded this modification to a more mechanically robust polymer system with the goal of designing even more stable materials for biological applications. Here, we chose to utilize Tygon® as the base polymer, and an NO donor (*S*-nitrosoglutathione, GSNO) was manually blended into Tygon® solutions for film fabrication (Section 2.2.4). Two different concentrations of donor were incorporated into Tygon® films (5 and 20%), referred to as GSNO5 and GSNO20, respectively. For reference throughout, the chemical structure of GSNO and photographs of fabricated films are depicted in Figure 4.8. Notably, an extensive assessment of Tygon® film antibacterial efficacy against *Escherichia coli* and *Staphyloccocus aureus* was performed (demonstrating water plasma treatment resulted in a delay in antibacterial activity) is reported elsewhere.[2] Work presented in the following sections highlights our ability to translate water plasma modification to an additional NO-releasing polymer system.

4.3.1 Effect of plasma treatment on composition of Tygon® and NO-releasing films. The chemical composition of the topmost surface (5-10 nm) of each film was quantified using XPS.[30]

Atomic compositions and C/O ratios obtained from high-resolution XPS spectra of Tygon® as well as untreated and treated GSNO20 and GSNO5 films are presented in Table 4.5. In addition to the reported elements, we observed the presence of small amounts of Si on all samples (<4%), likely arising from polydimethylsiloxane contamination from the polymeric film production and molding processes.[47-48]

The C/O ratios for untreated GSNO5 and GSNO20 fall within the range of that for Tygon® without donor, 3.32 ± 0.17 (Table 4.5). Experimental error associated with the elemental composition (e.g., %C, %O) for GSNO5 and GSNO20 films is greater than that of the Tygon® by an order of magnitude, illustrating the heterogeneity of these materials on the scale of the XPS spot size (~1 mm). This is unsurprising given the fabrication process of these films (described in Section 2.2.4). Interestingly, no nitrogen is detected on Tygon®, GSNO5, or GSNO20 films, suggesting the donor is not present on the outermost surface of NO-releasing films.

Deconstructed fits of the C_{1s} spectra revealing functionalities present at the film surface are presented in Figure 4.9. Tygon® films (Fig. 4.9a) have three C_{1s} binding environments: (1) a peak at 285.0 eV representing aliphatic carbon (C-C/C-H); (2) a peak at ~286.4 eV representing C-O/C-Cl functionality; and (3) a peak at ~289.2 eV indicative of carboxylic acid groups (O-C=O).[49] A slight increase in the area of the C-O/C-Cl peak at ~286.4 eV is the only apparent change in the C_{1s} spectrum upon GSNO incorporation (Fig. 4.9b). Plasma treatment decreases the C/O ratios for both GSNO5 and GSNO20 films. For GSNO20, the C/O ratio is 1.05 ± 0.04, less than one third of that of Tygon® only films (Table 4.5). Furthermore, a significant change occurs in the C_{1s} envelope caused by the appearance of peak (4) at ~287.6 eV, suggestive of

carbonyl groups as well as an increase in the relative contributions from the carboxylic acid binding environment (Fig. 4.9d).[49]

Upon plasma treatment, ~1% nitrogen is detected on the surface of the films, likely attributable to amine and amide functionalities (as predicted from the GSNO structure, Fig. 4.8a), which ultimately contribute to C_{1s} binding environments 2 and 3. The presence of nitrogen on plasma-treated film surfaces likely results from rearrangement of the polymer during plasma treatment (exposing amide and amine functionalities in the donor molecule). Polymer rearrangement during H_2O plasma treatment is thought to occur in other materials, including our plasma treated PLGH films (Section 4.2).[3, 34] Effectively, polymer chains reorganize such that hydrophilic domains are preferentially oriented towards the H_2O plasma (i.e., hydrophilic domains are present at the plasma-polymer interface). Collectively, this work demonstrates we can effectively modify surface properties of NO-releasing Tygon® films via plasma processing.

Another observation from XPS data of treated GSNO20 films is the dramatic decrease in chlorine content. Tygon® films have ~19% Cl, and upon incorporation of 20% GSNO, this increases to ~22% Cl (note that these compositions are within experimental error). After plasma treatment, however, chlorine content declines considerably to 3.5 ± 1.2%, indicating that the GSNO20 surface is almost entirely dechlorinated after the 5 min treatment time. A similar decrease in chlorine content is observed with plasma treatment of GSNO5, suggesting the amount of NO donor incorporated does not alter the plasma interaction with the material surface. Plasma dechlorination of polymers has been previously reported,[50-53] and likely arises from the relatively weak C-Cl bonds (bond energy ~81 kcal mol^{-1}) in the polymer backbone. When compared to C-C and C-H bonds (~83 and 99 kcal mol^{-1}, respectively),[54] the C-Cl bond is more

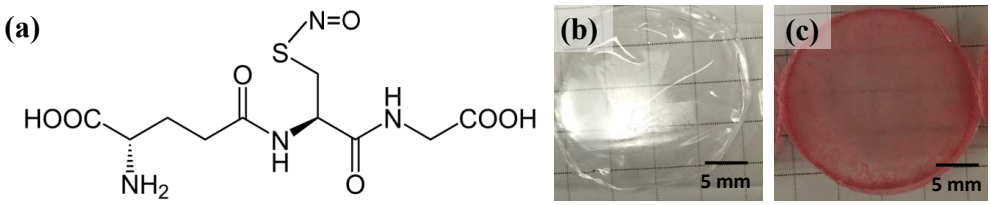

Figure 4.8. (a) *S*-nitrosoglutathione (GSNO) structure; (b) Tygon® and (c) GSNO20 films immediately after fabrication.

Table 4.5. Elemental Composition and WCA Values for Tygon® Films [a]

Film	%C	%O	%Cl	%N	C/O	WCA (º)
Tygon ®	61.9 ± 0.6	18.7 ± 0.8	19.4 ± 0.2	---	3.32 ± 0.17	87.1 ± 6.8
Untreated GSNO20	54.1 ± 1.0	21.0 ± 6.0	21.9 ± 6.9	---	2.70 ± 0.47	87.7 ± 3.7
Treated GSNO20	47.5 ± 1.1	45.0 ± 0.7	3.5 ± 1.2	1.2 ± 0.3	1.05 ± 0.04	49.8 ± 3.5
Untreated GSNO5	59.9 ± 7.3	21.3 ± 7.6	19.7 ± 2.4	---	2.93 ± 0.52	88.9 ± 4.6
Treated GSNO5	55.2 ± 2.5	41.2 ± 2.5	1.0 ± 0.2	1.0 ± 0.4	1.35 ± 0.14	52.1 ± 5.2

[a] Elemental composition data from high resolution XPS spectra. All values reported as the mean ± one standard deviation (n = 3 for Tygon® only, n = 9 for all other films). Trace amounts (<4%) of Si were detected on all samples (see text for discussion).

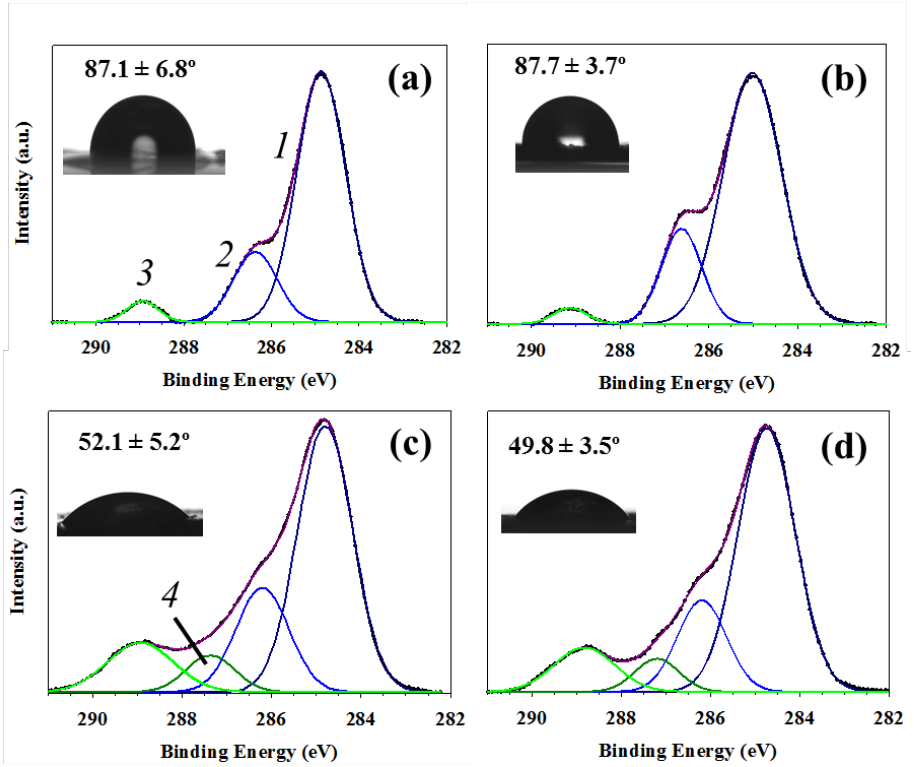

Figure 4.9. Representative high-resolution C_{1s} XPS spectra with accompanying images from WCA analysis, and WCA values (n = 9), inset. Films included are (a) untreated Tygon®, (b) untreated GSNO20, (c) treated GSNO5 and (d) treated GSNO20. C_{1s} binding environments include 1) C-C/C-H [285.0 eV], 2) C-O/C-Cl/C-N [~286.4 eV], 3) O-C=O/N-C=O [~289.2 eV], and 4) C=O [~287.6 eV].

likely to be cleaved during plasma treatment, leading to elimination of Cl from the material and simultaneously creating implantation sites ripe for incorporation of oxygen functionalities.

4.3.2 Effect of plasma treatment on NO-releasing Tygon® film wettability and roughness. WCA values and accompanying images are presented in Table 4.5 and Figure 4.9. Tygon® films without NO donor have static WCA values of 87.1 ± 6.8°, and incorporation of the NO donor does not significantly change the contact angle of films, with GSNO5 and GSNO20 displaying WCAs of 88.9 ± 4.6° and 87.7 ± 3.7°, respectively. WCA values for treated GSNO-incorporated films are significantly lower: GSNO5 films reach a static WCA of 52.1 ± 5.2°, and GSNO20 films have a similar value of 49.8 ± 3.5° after plasma treatment, again indicating the level of NO donor incorporation does not impact the plasma-surface interactions. Prior work demonstrated that H_2O plasma treatment of polymer surfaces results in increased alcohol functionality. The increase in functional groups capable of hydrogen bonding after plasma modification explains differences in wettability of untreated versus plasma treated films.

To investigate the effect of plasma treatment on both Tygon® and GSNO20 films, surface roughness (R_a and R_q) was measured by optical profilometry. Tygon® films without NO donor have R_a and R_q < 0.1 μm, and roughness parameter values are unchanged after treatment. Roughness of GSNO5 changes only slightly, resulting in R_a = 0.1 ± 0.1 μm and R_q = 0.4 ± 0.2 μm. After incorporation of 20% GSNO, surface roughness is increased to R_a = 0.6 ± 0.2 μm and R_q = 1.2 ± 0.4 μm. No significant change in roughness is observed for treated GSNO5 films with R_a = 0.1 ± 0.1 μm and R_q = 0.5 ± 0.3 μm. Likewise, treated GSNO20 films have R_a = 0.7 ± 0.2 μm and R_q = 1.5 ± 0.4 μm, comparable to the untreated materials, indicating extent of GSNO loading does not impact roughness imparted during plasma treatment.

GSNO5 and GSNO20 films as fabricated are nominally hydrophobic by conventional definitions, and become hydrophilic after plasma treatment. Roughness is minimally affected by plasma modification; therefore, the increased wettability can be primarily attributed to the change in surface oxygen content and functionality. The more wettable surface of plasma treated films renders them more suitable for interfacing with aqueous environments (e.g., in biological applications) than unmodified films.[55]

4.4 Summary: Comparison of Plasma-modified NO-releasing PLGH and Tygon® Films

Collectively, this body of work demonstrates that plasma treatment is a facile technique to significantly increase the oxygen content and wettability of NO-releasing polymer films while maintaining material topography. Although identical plasma parameters were employed for both polymer film modifications (20 W, 5 min), substantial differences in surface properties between the two types of polymer films were observed. This section includes a brief discussion highlighting notable differences, namely comparing all films treated with 20 W H_2O plasmas for 5 min.

The Tygon® films here experience a more substantial compositional change (e.g., change in C/O ratio) than PLGH films under identical plasma modification conditions. Specifically, the C/O ratio values of plasma treated Tygon® films are less than half that of unmodified films, whereas plasma treated PLGH film C/O is ~0.8 that of unmodified films. This dissimilar behavior likely arises from differences in polymer composition, namely the presence of C-Cl bonds in Tygon®. Another notable compositional difference between the two polymers is the detection of nitrogen via XPS in unmodified PLGH films, whereas nitrogen was not observed on the surface of unmodified Tygon® films. This is somewhat surprising as there was a higher theoretical amount of donor incorporated in the Tygon® system (0.496 mmol/g for GSNO20

films) than in the PLGH system (0.155 mmol/g). The disparity in nitrogen content likely arises from differences in NO donor incorporation methodology between the polymers: PLGH films were fabricated by dissolving a nitrosated polymer powder, whereas Tygon® films were fabricated by manually blending the NO donor (GSNO) into dissolved Tygon®. Thus, it is likely that the NO donor is encased in the Tygon® matrix and is therefore not detectable on the outermost film surface via XPS. Moreover, the surface roughness, and thus the surface area, is significantly greater for PLGH films. This finding suggests that more NO donor may be exposed at the surface of PLGH films, providing a possible explanation for differences in nitrogen content between the two polymer systems.

Although plasma modification enhances the wettability of both polymer films, the stability of water drops dictated the adoption of different methodologies for characterizing wetting behavior. Water drops spread on plasma-modified PLGH films in <50 ms (equilibrium WCA = 0º), whereas drops completely stabilized on Tygon® films. This difference likely arises from the robustness of fabricated films, specifically PLGH films comprised a powder on an underlying support (glass coverslip), whereas Tygon® films were mechanically stable (no support required). With this in mind, water drops interacting with PLGH films likely also interact with the underlying glass (a well-known hydrophilic surface).

Overall, the work presented in this chapter demonstrates our ability to utilize plasma processing to enhance the surface properties, including functionality and wettability, of two unique NO-releasing polymer film systems. These plasma-modified drug-releasing constructs represent a promising pathway for advanced biomaterial development using both passive and active polymer modification techniques. Furthermore, NO-releasing biomaterials have immense potential for targeted therapeutic delivery in biological systems. Collectively, this work holds

promise as a generalizable method for modifying drug-releasing polymer devices that could be extended to a multitude of additional drug delivery systems.

REFERENCES

1. Joslin, J. M. Combining Fundamental Studies with Advanced Characterization for Analyzing Nitric Oxide Polymer Systems. Ph.D. Dissertation, Colorado State University, Fort Collins, CO, 2014.
2. Mann, M. N.; Neufeld, B. H.; Hawker, M. J.; Pegalajar-Jurado, A.; Paricio, L. N.; Reynolds, M. M.; Fisher, E. R., Plasma-modified Nitric Oxide-releasing Polymer Films Exhibit Time-delayed 8-log Reduction in Growth of Bacteria. *Biointerphases* **2016,** *11*, 031005.
3. Pegalajar-Jurado, A.; Joslin, J. M.; Hawker, M. J.; Reynolds, M. M.; Fisher, E. R., Creation of Hydrophilic Nitric Oxide Releasing Polymers via Plasma Surface Modification. *ACS Appl. Mater. Interfaces* **2014,** *6* (15), 12307-12320.
4. Boateng, J. S.; Matthews, K. H.; Stevens, H. N.; Eccleston, G. M., Wound Healing Dressings and Drug Delivery Systems: A Review. *J. Pharm. Sci.* **2008,** *97* (8), 2892-2923.
5. Hubbell, J. A., Bioactive Biomaterials. *Curr. Opin. Biotechnol.* **1999,** *10* (2), 123-129.
6. Pillai, O.; Panchagnula, R., Polymers in Drug Delivery. *Curr. Opin. Chem. Biol.* **2001,** *5* (4), 447-451.
7. Danhier, F.; Ansorena, E.; Silva, J. M.; Coco, R.; Le Breton, A.; Préat, V., PLGA-based Nanoparticles: An Overview of Biomedical Applications. *J. Controlled Release* **2012,** *161* (2), 505-522.
8. Gentile, P.; Chiono, V.; Carmagnola, I.; Hatton, P. V., An Overview of Poly(lactic-co-glycolic) acid (PLGA)-based Biomaterials for Bone Tissue Engineering. *Int. J. Mol. Sci.* **2014,** *15* (3), 3640-3659.
9. Pan, Z.; Ding, J., Poly(lactide-co-glycolide) Porous Scaffolds for Tissue Engineering and Regenerative Medicine. *Interface Focus* **2012,** *2* (3), 366-377.
10. Moreira, P. d. L.; Marreco, P. R.; Moraes, A. M.; Wada, M. L. F.; Genari, S. C., Analysis of Cellular Morphology, Adhesion, and Proliferation on Uncoated and Differently Coated PVC Tubes Used in Extracorporeal Circulation (ECC). *J. Biomed. Mater. Res. Part B Appl. Biomater.* **2004,** *69* (1), 38-45.
11. Prowse, C.; Korte, D.; Hess, J.; Meer, P., Commercially Available Blood Storage Containers. *Vox Sang.* **2014,** *106* (1), 1-13.
12. Sampson, J.; De Korte, D., DEHP-plasticised PVC: Relevance to Blood Services. *Transfus. Med.* **2011,** *21* (2), 73-83.
13. Feng, Y.; Zhao, H.; Lu, J.; Guo, J., Nitric Oxide Release from Polycarbonate-urethane Films Containing Copper(II) Complexes. *J. Controlled Release* **2011,** *152, Supplement 1* (0), e202-e204.
14. Thomas, D. D.; Liu, Z. P.; Kantrow, S. P.; Lancaster, J. R., The Biological Lifetime of Nitric Oxide: Implications for the Oerivascular Dynamics of NO and O_2. *Proc. Natl. Acad. Sci. U.S.A.* **2001,** *98* (1), 355-360.
15. Heilman, B. J.; St John, J.; Oliver, S. R.; Mascharak, P. K., Light-triggered Eradication of Acinetobacter Baumannii by Means of NO Delivery from a Porous Material with an Entrapped Metal Nitrosyl. *J. Am. Chem. Soc.* **2012,** *134* (28), 11573-82.
16. Osaki, S. G.; Chen, M.; Zamora, P. O., Controlled Drug Release thorough a Plasma Polymerized Tetramethylcyclo-tetrasiloxane Coating Barrier. *J. Biomater. Sci., Polym. Ed.* **2012,** *23* (1-4), 483-496.

17. Yasuda, H.; Gazicki, M., Biomedical Applications of Plasma Polymerization and Plasma Treatment of Polymer Surfaces. *Biomaterials* **1982,** *3*, 68-77.
18. Yoo, H. S.; Kim, T. G.; Partk, T. G., Surface-functionalized Electrospun Nanofibers for Tissue Engineering and Drug Delivery. *Adv. Drug Deliv. Rev.* **2009,** *61*, 1033-1042.
19. VanWagner, M.; Rhadigan, J.; Lancina, M.; Lebovsky, A.; Romanowicz, G.; Holmes, H.; Brunette, M. A.; Snyder, K. L.; Bostwick, M.; Lee, B. P.; Frost, M. C., S-Nitroso-N-acetylpenicillamine (SNAP) Derivatizaton of Peptide Primary Amines to Create Inducible Nitric Oxide Donor Biomaterials. *ACS Appl. Mater. Interfaces* **2013,** *5*, 8430-8439.
20. Reynolds, M. M.; Frost, M. C.; Meyerhoff, M. E., Nitric Oxide-Releasing Hydrophobic Polymers: Preparation, Characterization, and Potential Biomedical Applications. *Free Radical Biol. Med.* **2004,** *37*, 926-936.
21. Joslin, J. M.; Lantvit, S. M.; Reynolds, M. M., Nitric Oxide Releasing Tygon Materials: Studies in Donor Leaching and Localized Nitric Oxide Release at a Polymer-Buffer Interface. *ACS Appl. Mater. Interfaces* **2013,** *5* (19), 9285-9294.
22. Frost, M. C.; Reynolds, M. M.; Meyerhoff, M. E., Polymers Incorporating Nitric Oxide Releasing/Generating Substances for Improved Biocompatibility of Blood-contacting Medical Devices. *Biomaterials* **2005,** *26* (14), 1685-1693.
23. Jen, M. C.; Serrano, M. C.; van Lith, R.; Ameer, G. A., Polymer-Based Nitric Oxide Therapies: Recent Insights for Biomedical Applications. *Adv. Funct. Mater.* **2012,** *22* (2), 239-260.
24. Varu, V. N.; Tsihlis, N. D.; Kibbe, M. R., Nitric Oxide-releasing Prosthetic Materials. *Vasc. Endovascular Surg.* **2009,** *43* (2), 121-131.
25. Kingshott, P.; Andersson, G.; McArthur, S. L.; Griesser, H. J., Surface Modification and Chemical Surface Analysis of Biomaterials. *Curr. Opin. Chem. Biol.* **2011,** *15* (5), 667-676.
26. Lee, J. H.; Park, J. W.; Lee, H. B., Cell-Adhesion and Growth on Polymer Surfaces with Hydroxyl Groups Prepared by Water-Vappor Plasma Treatment *Biomaterials* **1991,** *12* (5), 443-448.
27. Steen, M. L.; Hymas, L.; Havey, E. D.; Capps, N. E.; Castner, D. G.; Fisher, E. R., Low Temperature Plasma Treatment of Asymmetric Polysulfone Membranes for Permanent Hydrophilic Surface Modification. *J. Membr. Sci.* **2001,** *188* (1), 97-114.
28. Steen, M. L.; Jordan, A. C.; Fisher, E. R., Hydrophilic Modification of Polymeric Membranes by Low Temperature H_2O Plasma Treatment. *J. Membr. Sci.* **2002,** *204* (1), 341-357.
29. Tompkins, B. D.; Dennison, J. M.; Fisher, E. R., H_2O Plasma Modification of Track-etched Polymer Membranes for Increased Wettability and Improved Performance. *J. Membr. Sci.* **2013,** *428*, 576-588.
30. McArthur, S. L., Applications of XPS in Bioengineering. *Surf. Interface Anal.* **2006,** *38* (11), 1380-1385.
31. Ershov, S.; Khelifa, F.; Dubois, P.; Snyders, R., Derivatization of Free Radicals in an Isopropanol Plasma Polymer Film: The First Step toward Polymer Grafting. *ACS Appl. Mater. Interfaces* **2013,** *5*, 4216-4223.
32. Gengenbach, T.; Chatelier, R. C.; Griesser, H. J., Characterization of the Ageing of Plasma-Deposited Polymer Films: Global Analysis of X-ray Photoelectron Spectroscopy Data. *Surf. Interface Anal.* **1996,** *24*, 271-281.
33. Tarasova, A.; Hamilton-Brown, P.; Gengengach, T.; Griesser, H. J.; Meagher, L., Colloid Probe AFM and XPS Study of Time-Dependent Aging of Amine Plasma Polymer Coatings in Aqueous Media. *Plasma Process. Polym.* **2008,** *5*, 175-185.

34. Griesser, H. J.; Da, Y.; Hughes, A. E.; Gengenbach, T. R.; Mau, A. W. H., Shallow Reorientation in the Surface Dynamics of Plasma-treated Fluorinated Ethylene-propylene Polymer. *Langmuir* **1991,** *7* (11), 2484-2491.
35. Asfardjani, K.; Segui, Y.; Aurelle, Y.; Abidine, N., Effect of Plasma Treatments on Wettability of Polysulfone and Polyetherimide. *J. Appl. Polym. Sci.* **1991,** *43*, 271-281.
36. Croll, T. I.; O'Connor, A. J.; Stevens, G. W.; Cooper-White, J. J., Controllable Surface Modification of Poly(lactic-co-glycolic acid) (PLGA) by Hydrolysis or Aminolysis I: Physical, Chemical, and Theoretical Aspects. *Biomacromolecules* **2004,** *5*, 463-473.
37. Parreira, P.; Magalhães, A.; Gonçalves, I. C.; Gomes, J.; Vidal, R.; Reis, C. A.; Leckband, D. E.; Martins, M. C. L., Effect of Surface Chemistry on Bacterial Adhesion, Viability, and Morphology. *J. Biomed. Mater. Res. Part A* **2011,** *99* (3), 344-353.
38. Thissen, H.; Johnson, G.; McFarland, G.; Verbiest, B. C. H.; Gengenbach, T.; Voelckera, N. H., Microarrays for the Evaluation of Cell-biomaterial Surface Interactions In *Smart Materials IV*, Voelcker, N. H., Ed. Spie-Int Soc Optical Engineering: Bellingham, 2007; Vol. 6413, pp B4130-B4130.
39. Deligianni, D. D.; Katsala, N. D.; Koutsoukos, P. G.; Missirlis, Y. F., Effect of Surface Roughness of Hydroxyapatite on Human Bone Marrow Cell Adhesion, Proliferation, Differentiation and Detachment Strength. *Biomaterials* **2000,** *22* (1), 87-96.
40. Quere, D., Wetting and Roughness. *Annu. Rev. Mater. Res.* **2008,** *38*, 71-99.
41. Thomas, T., *Rough Surfaces*. London, UK, 1999.
42. Carneiro, K.; Jensen, C. P.; Jørgensen, J. F.; Garnoes, J.; McKeown, P. A., Roughness Parameters of Surfaces by Atomic Force Microscopy. *CIRP Ann. Manuf. Technol.* **1995,** *44* (1), 517-522.
43. Peltonen, J.; Jarn, M.; Areva, S.; Linden, M.; Rosenholm, J. B., Topographical Parameters for Specifying a Three-dimensional Surface. *Langmuir* **2004,** *20* (22), 9428-9431.
44. Wang, Y. X.; Robertson, J. L.; Spillman, W. B.; Claus, R. O., Effects of the Chemical Structure and the Surface Properties of Polymeric Biomaterials on their Biocompatibility. *Pharmaceut. Res.* **2004,** *21* (8), 1362-1373.
45. Ranucci, C. S.; Prabhas, V. M., Substrate Microtopography Can Enhance Cell Adhesive and Migratory Responsiveness to Matrix Ligand Density. *J. Biomed. Mater. Res.* **2001,** *54* (2), 149-161.
46. Deligianni, D. D.; Katsala, N. D.; Koutsoukos, P. G.; Missirlis, Y. F., Effect of Surface Roughness of Hydroxyapatite on Human Bone Marrow Cell Adhesion, Proliferation, Differentiation and Detachment Strength *Biomaterials* **2000,** *22* (1), 87-96.
47. Asadinezhad, A.; Novák, I.; Lehocký, M.; Sedlařík, V.; Vesel, A.; Junkar, I.; Sáha, P.; Chodák, I., An in vitro Bacterial Adhesion Assessment of Surface-modified Medical-grade PVC. *Colloids Surf., B* **2010,** *77* (2), 246-256.
48. Oran, U.; Ünveren, E.; Wirth, T.; Unger, W., Poly-dimethyl-siloxane (PDMS) Contamination of Polystyrene (PS) Oligomers Samples: A Comparison of Time-of-flight Static Secondary Ion Mass Spectrometry (TOF-SSIMS) and X-ray Photoelectron Spectroscopy (XPS) Results. *Appl. Surf. Sci.* **2004,** *227* (1), 318-324.
49. Babai-Cline, M.; Wightman, J., Surface Analysis and Peel Strength of Aged, Oxygen-plasma-modified Unplasticized Poly(vinyl chloride) Films. *Int. J. Adhes. Adhes.* **1995,** *15* (3), 185-190.
50. Balazs, D. J.; Triandafillu, K.; Wood, P.; Chevolot, Y.; van Delden, C.; Harms, H.; Hollenstein, C.; Mathieu, H. J., Inhibition of Bacterial Adhesion on PVC Endotracheal Tubes by

RF-oxygen Glow Discharge, Sodium Hydroxide and Silver Nitrate Treatments. *Biomaterials* **2004,** *25* (11), 2139-2151.
51. Ru, L.; Jie-rong, C., Studies on Wettability of Medical Poly(vinyl chloride) by Remote Argon Plasma. *Appl. Surf. Sci.* **2006,** *252* (14), 5076-5082.
52. Zhang, W.; Chu, P. K.; Ji, J.; Zhang, Y.; Liu, X.; Fu, R. K. Y.; Ha, P. C. T.; Yan, Q., Plasma Surface Modification of Poly Vinyl Chloride for Improvement of Antibacterial Properties. *Biomaterials* **2006,** *27* (1), 44-51.
53. Kumagai, H.; Tashiro, T.; Kobayashi, T., Formation of Conjugated Carbon Bonds on Poly(vinyl chloride) Films by Microwave-discharge Oxygen-plasma Treatments. *J. Appl. Polym. Sci.* **2005,** *96* (2), 589-594.
54. Stans, M. H., Bond Dissociation Energies in Simple Molecules. *NSRDS-NBS NO. 31, U. S. Dept. Commerce, Washington, D. C.* **1970,** *31*, 1-48.
55. Babaei, S.; Girard-Lauriault, P. L., Tuning the Surface Properties of Oxygen-Rich and Nitrogen-Rich Plasma Polymers: Functional Groups and Surface Charge. *Plasma Chem. Plasma Process.* **2016,** *36* (2), 651-666.

CHAPTER 5

CONFORMAL ENCAPSULATION OF THREE-DIMENSIONAL, BIORESORBABLE POLYMERIC SCAFFOLDS USING PLASMA-ENHANCED CHEMICAL VAPOR DEPOSITION

This chapter reports the modification of PCL scaffolds via PECVD of two different fluorocarbon (FC) precursors: octofluoropropane (C_3F_8) and hexafluoropropylene oxide (HFPO). These plasma modification systems were chosen with the intent of modifying the scaffold surfaces to be non-bioreactive by the deposition of FC films while maintaining desirable bulk properties of the scaffold. X-ray photoelectron spectroscopy showed high-CF_2 content films were deposited on both the exterior and interior of PCL scaffolds, and that deposition behavior is PECVD system-specific. Scanning electron microscopy data confirmed that FC film deposition yielded conformal rather than blanket coatings as the porous scaffold structure was maintained after plasma treatment. Treated scaffolds seeded with human dermal fibroblasts (HDF) demonstrate that mammalian cells do not attach after 72 h, and that the scaffolds are non-cytotoxic to HDF. This work demonstrates conformal FC coatings can be deposited on 3D polymeric scaffolds using PECVD to fabricate 3D non-bioreactive materials.

This chapter is reproduced with permission from an article published in *Langmuir* by Morgan J. Hawker, Adoracion Pegalajar-Jurado, and Ellen R. Fisher [*30* (41), pp 12328–12336, Copyright 2014 American Chemical Society].[1] This work is supported by the National Science Foundation (CHE-1152963), the Camille and Henry Dreyfus Foundation Postdoctoral Program in Environmental Chemistry. I would like to thank Dori Pegalajar for her contributions to this work, including growing human dermal fibroblasts for cell analyses, and providing training on

staining and imaging protocols. I would also like to thank Dr. Patrick McCurdy and Dr. Jeffrey Shearer for assistance with SEM and XPS analyses, and some preliminary deposition studies.

5.1 Introduction

The development of low-fouling biopolymer constructs with complex geometries is critical for applications requiring materials that bacterial or mammalian cell attachment (e.g., wound dressings). FC plasma modification is one particularly advantageous route toward development both because of the precedence of using such systems to tune stent and wire interactions in biological systems,[2-3] as well as the potential for translation to a wide range of additional construct geometries. As discussed in Section 1.3, there are a few reports of FC plasma modification of 3D polymeric constructs as a means of tuning performance in biological systems. For example, low-fouling, non-bioreactive coatings have been deposited on the exterior of 3D polymer constructs using PECVD.[4-5] Deposition of such a film throughout the entire cross section of a 3D biopolymeric scaffold, however, has yet to be reported.

Here, we utilized PECVD with two different FC precursors, octafluoropropane (C_3F_8) and HFPO, to deposit FC films on 3D PCL scaffolds. These precursors were chosen as model PECVD systems that provide hydrophobic, low-fouling surfaces as robust coatings that have been well characterized on two- dimensional substrates.[6-8] Thus, coatings obtained on 3D scaffolds could easily be compared to previous results. Scanning electron microscopy (SEM), X-ray photoelectron spectroscopy (XPS), water contact angle (WCA), and variable angle spectroscopic ellipsometry (VASE) were used to confirm the success of plasma treatment throughout the 3D structure of the scaffolds. The stability of the coatings in biologically-relevant solvents (e.g., cell media and phosphate buffered saline), the presence of leachables at cytotoxic concentrations, and the degree of cell adhesion were evaluated by seeding human dermal

fibroblasts (HDF) on both untreated and plasma treated scaffolds. Herein, we present an efficient methodology for tailoring the surface properties of 3D architectures for specific non-bioreactive biological applications.

5.2 Results

5.2.1 Surface analysis. The initial aim of this study was to examine the behavior of FC plasma deposition systems with PCL scaffolds as substrates. Based on previous studies utilizing 2D substrates,[6-8] we would expect the C_3F_8 and HFPO PECVD systems to deposit conformal, CF_2-rich FC films that completely encapsulate the underlying substrate. Ideally, FC films would be deposited throughout the 3D scaffold network, not just on the exterior of the scaffold.

Resultant films on scaffolds were characterized by a variety of surface analysis techniques, including XPS, SEM, and WCA. WCA measurements were made immediately (<10 min) following plasma treatment to examine any change in the outermost scaffold surface as a result of the treatment. Untreated scaffolds had a WCA of 120º, whereas FC-treated scaffolds had WCA values of approximately 135º regardless of treatment time or precursor (for a more detailed discussion of WCA analyses on substrates with complex architectures, see Chapter 3). This indicates all of the plasma treatments modified the chemical functionality and/or surface topography of the scaffolds.

To explore changes in surface functionality, XPS analysis was performed. Representative XPS survey spectra on scaffold tops are shown in Figure 5.1. Figure 5.2 shows high-resolution C_{1s} XPS spectra and deconstructed fits of C_3F_8 plasma treated scaffold tops and cross-sections. Spectra for films deposited during 5, 20, and 90 min treatment times are shown, which can be compared to the high-resolution C_{1s} spectrum for an untreated PCL scaffold in Figure 2.3. Spectra for C_3F_8 plasma treated scaffolds contain more C_{1s} binding environments than those

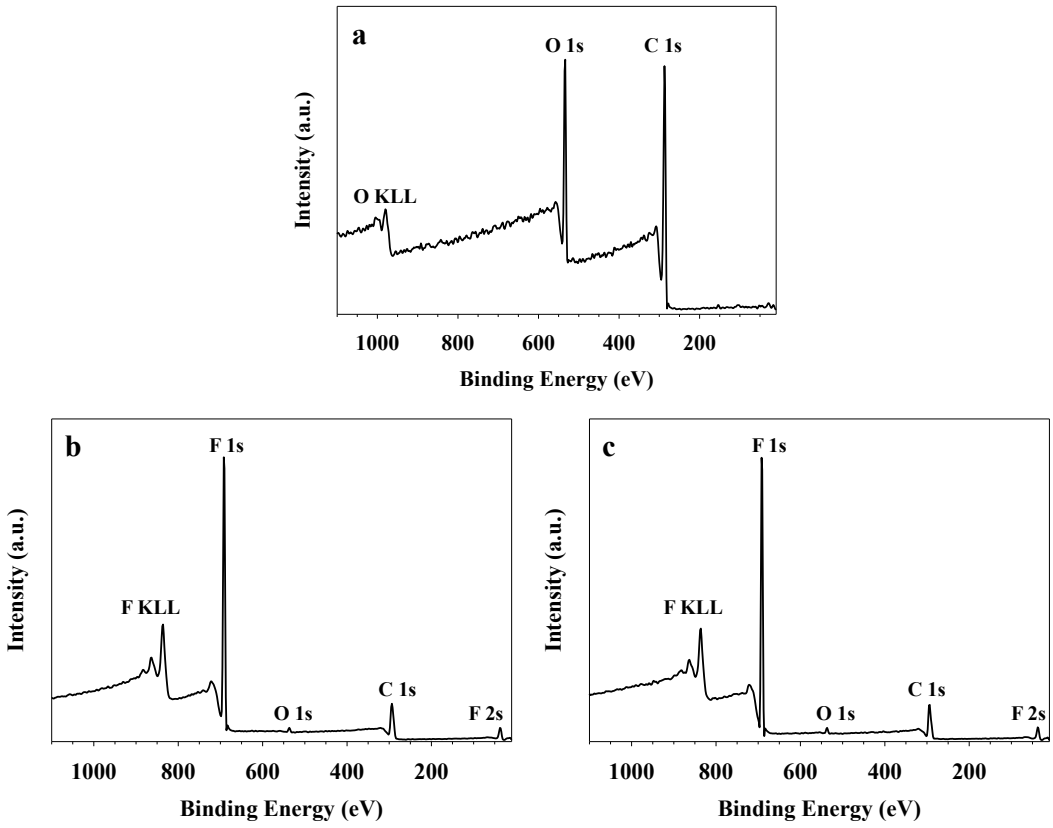

Figure 5.1. Representative XPS survey spectra for a) an untreated scaffold, b) 20 min C_3F_8 treated, and c) 60 min HFPO treated scaffold tops.

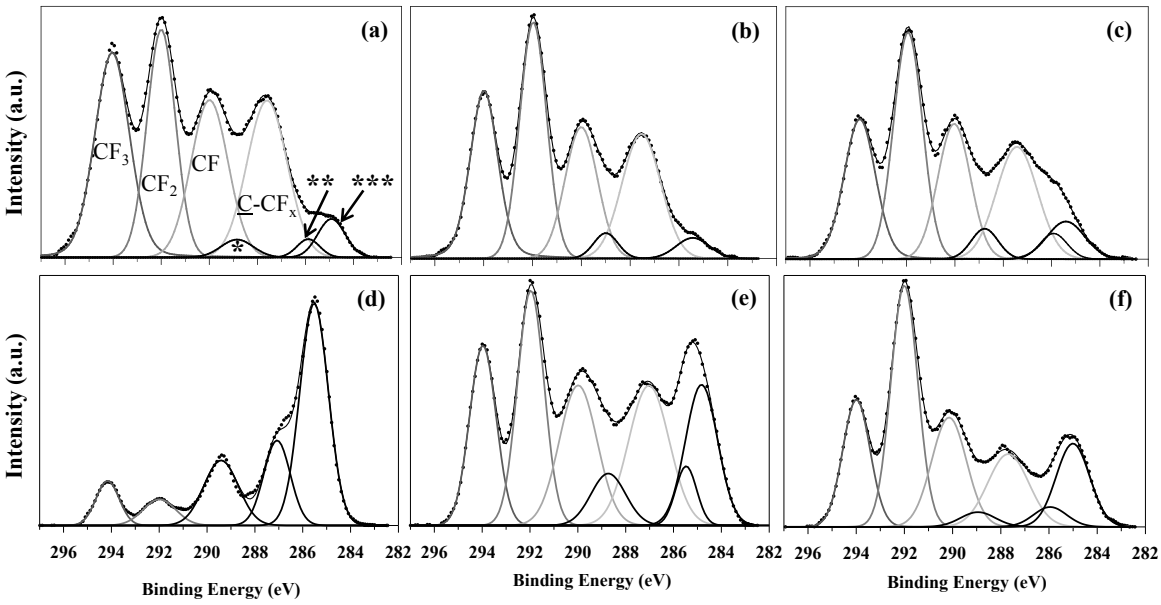

Figure 5.2. High-resolution XPS C_{1s} spectra of C_3F_8 films deposited on PCL scaffolds. Spectra (a), (b), and (c) correspond to scaffold tops treated for 5, 20, and 90 min, respectively; spectra (d), (e), and (f) correspond to scaffold cross-sections treated for 5, 20, and 90 min, respectively. Deconstructed fits are included to show the relative contribution of the various C_{1s} binding environments. Peaks designated with *, **, and *** correspond to underlying PCL material.

found in the spectra of untreated scaffolds, indicative of an array of FC binding environments. Based on previous C_3F_8 PECVD studies, the CF_2 contribution (292.0 eV) should dominate over other FC binding environments,[7-8] which is indeed seen in spectra of the scaffold tops, regardless of treatment time, and on scaffold cross-sections for all but the 5 min C_3F_8 treatment.
In all spectra, additional peaks can be attributed to CF_x moieties such as –CF, -CF_3, and –C-CF_x. Moreover, binding environments corresponding to the underlying PCL substrate are also seen in all spectra. Spectra of scaffold tops contain similar contributions from the underlying substrate regardless of treatment time. Cross-sectional spectra show both a decrease in contributions from the underlying material and an increase in the contributions of CF_x groups with increasing treatment time. The presence of peaks arising from the underlying material in the cross-sectional spectra is not surprising because the fracturing process inherently exposes untreated material. The contribution from the underlying material on the scaffold tops, however, is not necessarily predicted and is further addressed below.

High-resolution C_{1s} XPS spectra and deconstructed fits of HFPO treated scaffold tops and cross-sections are shown in Figure 5.3. These spectra were fit in the same manner as those for C_3F_8 treated scaffolds. CF_2 functionality is dominant in spectra corresponding to scaffold tops regardless of treatment time, similar to the spectra for C_3F_8 plasma treated scaffolds (Figure 5.2). The cross-sectional spectra in Figure 5.3d-f, have a lower relative intensity of FC binding environments compared to the C_3F_8 cross-sectional spectra (Figure 5.2d-f). Notably, the intensity of the FC binding environments for the HFPO plasma-treated scaffolds (relative to those attributable to the PCL) increases with increasing treatment time, suggesting that longer treatment times result in thicker FC coatings. Binding environments corresponding to the underlying PCL are, however, present in all spectra, regardless of treatment time.

Figure 5.4 plots F/C ratios as a function of treatment time for both C_3F_8 and HFPO treatments on both scaffold tops and scaffold cross-sections. The F/C ratio, calculated from elemental compositions obtained from high-resolution C_{1s} XPS data, provides a useful metric by which to compare FC films, independent of precursor. For comparison, the F/C ratio for flat C_3F_8 films (deposited on Si wafers under identical conditions used for plasma treated scaffolds) is 1.61 ± 0.06 and that for a flat HFPO film is very similar at 1.54 ± 0.04. Focusing on C_3F_8 plasma treated scaffolds, the F/C ratios for scaffold tops are within experimental error regardless of treatment time. Furthermore, the cross-sectional F/C ratio is significantly lower than the F/C ratio for 5 min C_3F_8 treated scaffold tops, whereas the F/C ratios for scaffold tops and cross-sections are within experimental error of each other for 20, 60, and 90 min treatments. Similar to the C_3F_8 deposition system, F/C ratios are within experimental error for HFPO plasma treated scaffold tops for all treatment times. Although the HFPO cross sectional F/C ratios increased with increasing treatment time, these values were consistently lower than the F/C ratios for scaffold tops regardless of treatment time.

Comparing SEM images of untreated scaffolds with representative FC plasma treated scaffolds permits examination of changes to the overall architecture of the porous network resulting from plasma treatment. Figure 5.5 displays representative SEM images of an untreated scaffold top and cross-section, as well as a 90 min C_3F_8 plasma treated scaffold top and cross-section. Both images of an untreated scaffold show a random porous network throughout the exterior and interior of the scaffold. SEM images in Figure 5.5c, d clearly demonstrate that the porous structure is maintained, even after 90 min in a 50 W C_3F_8 plasma. Note that SEM images of all other C_3F_8 and HFPO plasma treatments reveal a similar pore structure was conserved, regardless of treatment time and precursor.

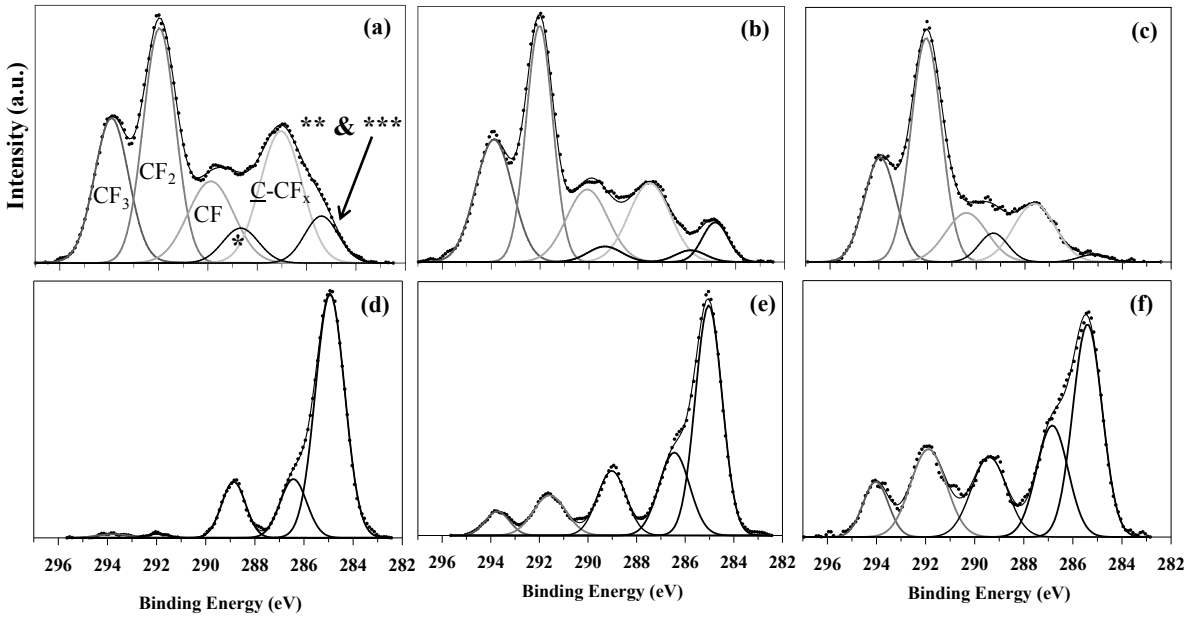

Figure 5.3. High-resolution XPS C_{1s} spectra of HFPO films deposited on PCL scaffolds. Spectra (a), (b), and (c) correspond to scaffold tops treated for 5, 20, and 90 min, respectively; spectra (d), (e), and (f) correspond to scaffold cross-sections treated for 5, 20, and 90 min, respectively. Deconstructed fits are included to show the relative contribution of the various C_{1s} binding environments. Peaks designated with *, **, and *** correspond to underlying PCL material.

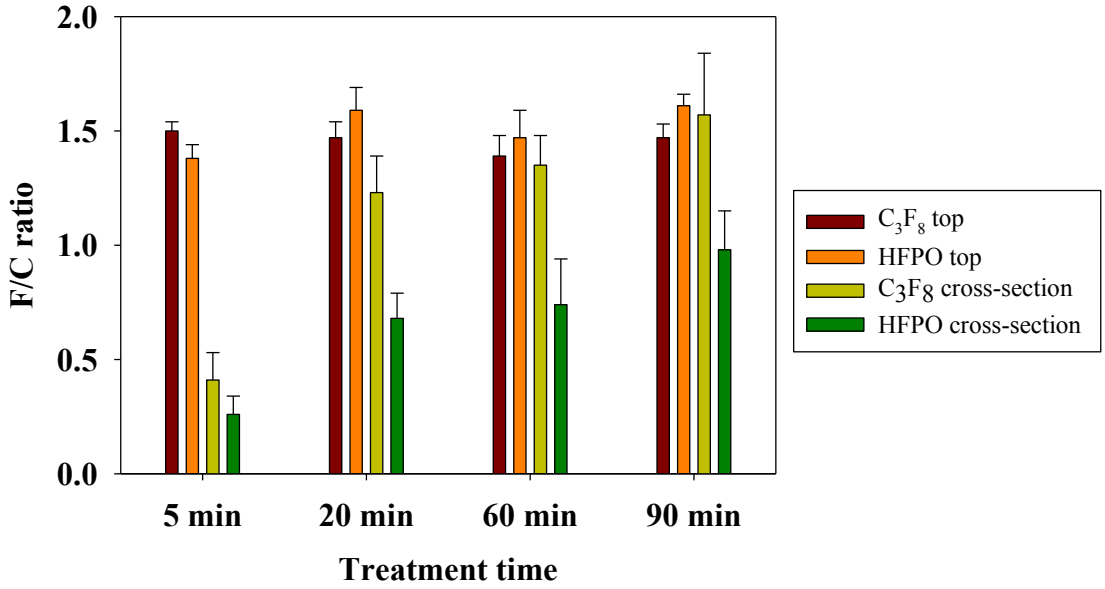

Figure 5.4. F/C ratios (calculated from XPS data) for C_3F_8 and HFPO treated PCL scaffold tops and cross sections for 5, 20, 60, and 90 min treatments.

Film thickness analyses were conducted on flat substrates to further characterize the C_3F_8 and HFPO deposition systems over the treatment time range used here (5-90 min), especially because XPS analyses (Figures 5.2 and 5.3) contained contributions from the underlying PCL material even after a 90 min treatment for both precursors. Flat substrates were used for these measurements as it becomes increasingly difficult to accurately measure film thickness on a 3D substrate such as a PCL scaffold. Figure 5.6 shows plots of film thickness as a function of deposition time for C_3F_8 and HFPO PECVD systems, where film thicknesses were measured using VASE. These data indicate all films deposited from the FC precursors were thicker than 10 nm (the sampling depth of the XPS), except for the 5 min HFPO deposited film. Film thickness measured for the C_3F_8 deposition system increased linearly with increasing treatment time ($R^2 = 0.975$) over the range of treatment times (5–90 min). Film deposition behavior differs for the HFPO deposition system, as film thickness shows an exponential rise to a maximum ($R^2 = 0.999$), ultimately reaching a plateau at the 60 min treatment time. These data suggest that the HFPO deposition system is self-limiting, whereas the C_3F_8 deposition is not.

5.2.2 Cell attachment and growth. Although the primary goal of this work is to demonstrate the ability to conformally encapsulate 3D bioresorbable scaffolds with a non-bioreactive coating using PECVD, the intended application of these materials must also be considered when assessing the overall properties of the resulting scaffolds. For several biomedical applications, a challenging factor is that many biomaterials can simultaneously inhibit bacterial attachment and be cytotoxic for mammalian cells. The former is desirable because it mitigates the risk of bacterial infections, whereas the latter could eliminate a material for consideration depending on the application. Therefore, an initial assessment of the

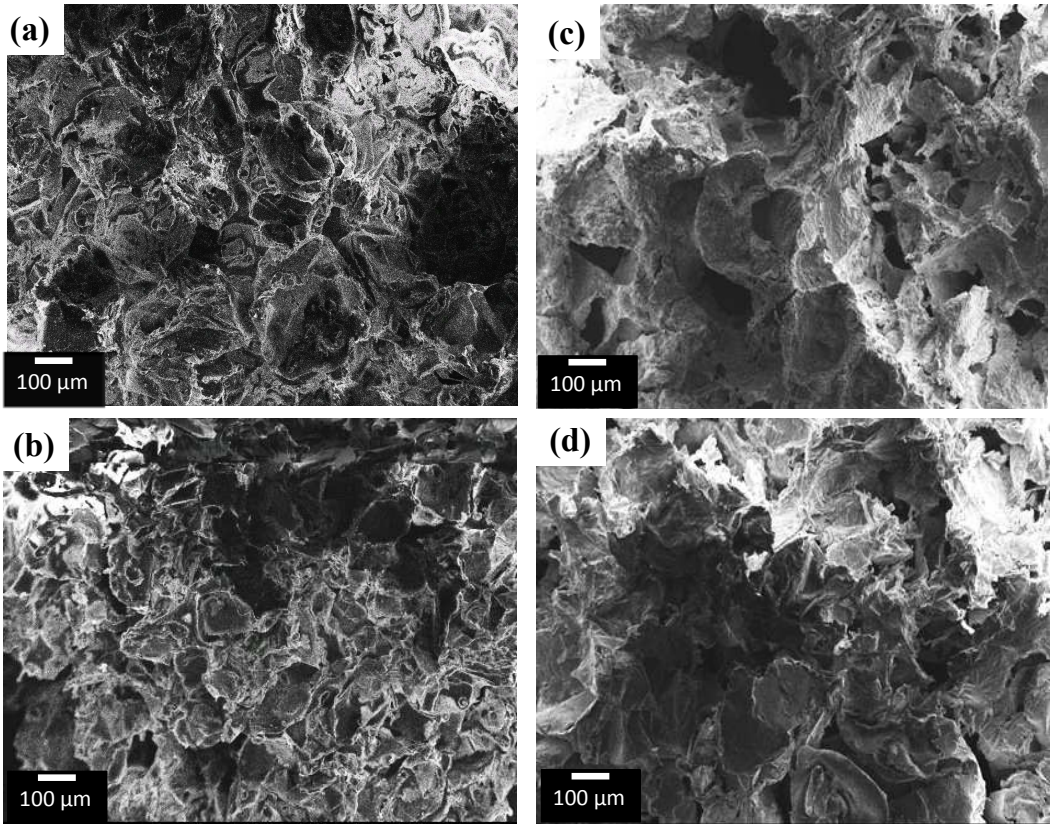

Figure 5.5. Representative SEM images (a) and (b) correspond to untreated PCL scaffolds; (c) and (d) correspond to 90 min C_3F_8 treated scaffolds. Images (a) and (c) are of scaffold tops; images (b) and (d) are of scaffold cross-sections.

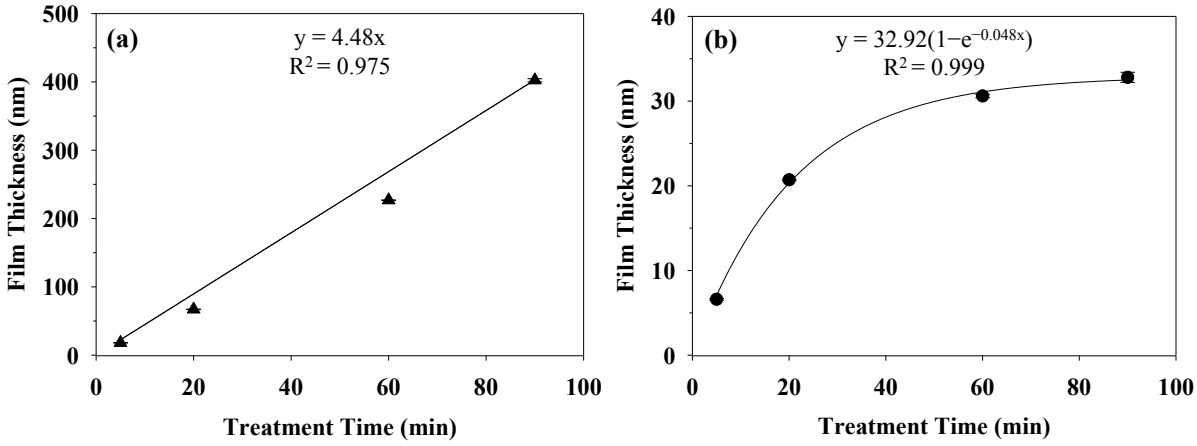

Figure 5.6. Film thicknesses for (a) C_3F_8 and (b) HFPO depositions on Si wafers, measured using VASE. Corresponding fits and equations are shown for each deposition system, where (a) shows a linear fit (constrained by $y_0 = 0$) (a) and (b) shows a two-parameter exponential rise to a maximum fit (b). Error bars representative of standard deviation are $\leq \pm 2.3$ nm.

interaction of FC coated 3D scaffolds with mammalian cells is required to gain a more comprehensive understanding of these 3D materials as functional biomaterials.

Untreated and FC coated 3D scaffolds were seeded with HDF and incubated for 72 h. Figure 5.7 contains a series of overlaid fluorescence microscopy images of HDF seeded on different substrates where the cell actin cytoskeleton is highlighted in red and the nucleus in blue. As a positive control, we seeded a TC plate where the cells attached, spread and proliferated across the entire surface as expected (Figure 5.7a). TC wells with double-sided carbon tape were also used as a control to confirm there was no effect of the double-sided carbon tape on the cells viability (images not shown). Additionally, cell attachment and morphology on the wells that contained untreated and FC plasma treated scaffolds were evaluated to examine the presence of leachable substances at a cytotoxic concentration. This experiment aimed to determine if the cells were viable after 72 h, even if they did not attach and spread on the scaffolds themselves. Figures 5.7b–d show images from three wells that contained an untreated scaffold, a C_3F_8 treated scaffold and an HFPO treated scaffold, respectively. Similar areas covered by HDF were observed in all the wells and cells showed an expected morphology in comparison to TC control samples.

In addition, we imaged tops, Figure 5.7e–g, and interiors (cross sections), Figure 5.7h–i, for untreated, C_3F_8 treated, and HFPO treated scaffolds. Viable HDF were found on the top and interior of untreated scaffolds indicating that after 72 h the cells adhered to the material and migrated to the interior of the 3D architecture. For both types of FC plasma treated scaffolds, we did not find a significant number of cells attached on the top or interior, regardless of treatment type. The faint coloring along the edges of some of the images (e.g., Figure 5.7f) is simply

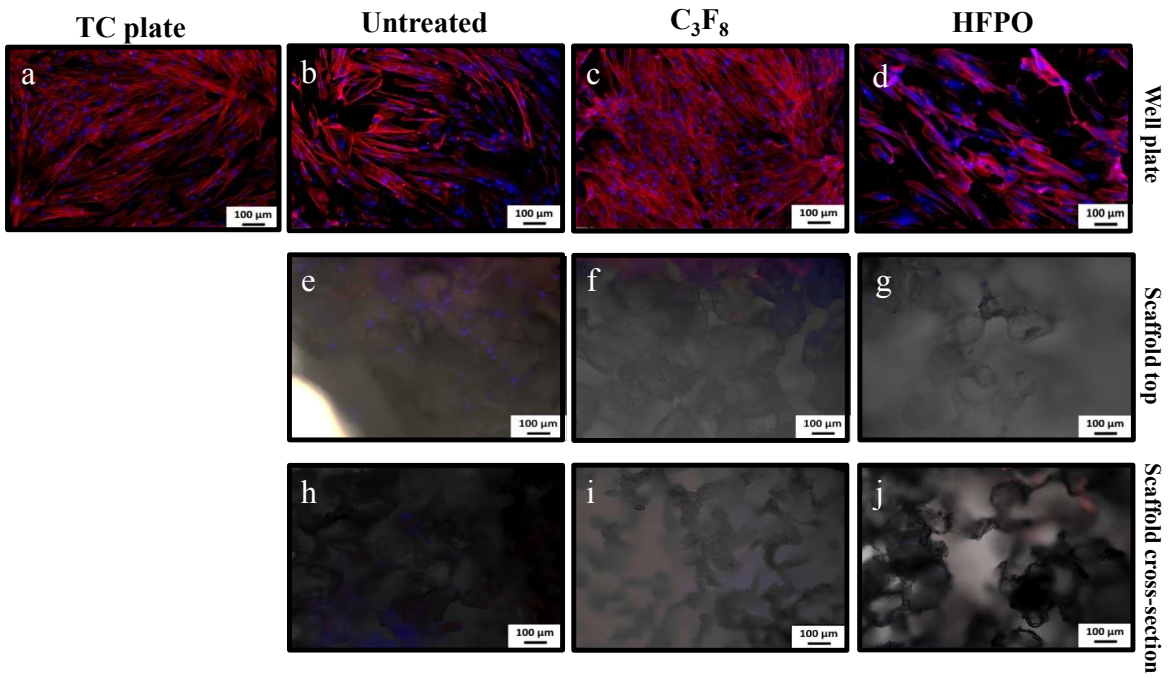

Figure 5.7. Overlaid fluorescence microscope images of human dermal fibroblasts cultured for 72 h on (a) a TC plate; (b)-(d) TC plate wells that contained untreated, C_3F_8 and HFPO treated scaffolds, respectively; (e)-(g) scaffold tops; and (h)-(j) scaffold cross sections. Images (b, e, h) correspond to untreated scaffolds; (c, f, i) correspond to C_3F_8 treated scaffolds; and (d, g, j) correspond to HFPO-treated scaffolds. The cell actin cytoskeleton is shown in red and the blue areas are cell nuclei.

retained stain and is not indicative of adhered HDF. Overall, these images clearly indicate that the FC plasma-modified scaffolds are non-bioreactive toward HDF as they resist cell attachment relative to untreated scaffolds.

5.3 Discussion

As noted Chapter 1 and Section 5.1, non-bioreactive surface modification of polymeric materials is an important aspect of biomaterials research, specifically pertaining to the development and fabrication of low-fouling materials. The overarching goal with the research presented in this chapter was to fabricate 3D polymeric scaffolds with desirable bulk properties, and modify the scaffold surface throughout the 3D structure via PECVD without affecting bulk properties. The data presented here demonstrate the two FC PECVD systems studied act similarly on the 3D substrates, insofar as they deposit conformal, hydrophobic films desirable for low-fouling materials while maintaining the scaffolds' bulk properties. These systems have inherently different deposition behaviors, however, and these differences influence the resultant properties of the FC encapsulated scaffolds.

The deposition behavior of each PECVD system was examined via VASE film thickness data collected on plasma treated Si wafers (Figure 5.6). PCL scaffolds were not used for this analysis because their architecture would further complicate film thickness determination. Although VASE data collected on Si wafers do not allow for direct comparison with the same deposition systems on 3D polymeric materials, we can use these findings as a guide to interpreting deposition behavior on scaffolds. VASE film thickness data demonstrate that deposition behavior is PECVD system dependent. FC film thickness for C_3F_8 plasma deposited films increases linearly with time (Figure 5.6a), suggesting that adsorbing plasma species involved in FC film deposition have a strong affinity toward Si wafers as well as the

subsequently deposited FC film. Alternatively, the HFPO PECVD system could be considered as "self-limiting" (Figure 5.6b) because film thickness does not monotonically increase with increasing treatment time. This observation suggests a strong interaction between plasma species involved in FC film deposition and the Si wafer. The sticking probability of these species to the building HFPO film, however, appears to decrease as the film increases in thickness.[9] Results for the C_3F_8 films are not unexpected, as C_3F_8 plasma systems are ubiquitously fast depositing (deposition rates range from 1-10 nm/min, depending on applied rf power) and previous studies have demonstrated similarly constant deposition rates for C_3F_8 and other C_xF_y species as a function of treatment time.[8, 10]

Although our data support the previous observation that HFPO PECVD systems deposit much more slowly than C_3F_8,[6] the overall behavior we observe here somewhat contradicts previously reported film thickness results for both HFPO and other FC systems. In one report on pulsed HFPO film deposition, Sumitsawan et al. claim that HFPO film thickness varied linearly over treatment times ranging from 5–60 min.[11] Our group has previously reported constant deposition rates for HFPO depositions for treatment times up to 2 h, but most of these depositions were performed much further downstream from the plasma glow than in the present study.[6] The only report of a similar, self-limiting FC PECVD system, to our knowledge, is that of a C_2F_6/CF_4 system, where deposition rate decreased as a function of treatment time.[12] Thus, this is the first report of a self-limiting HFPO PECVD system.

To further explore differences in the deposition behavior of C_3F_8 and HFPO on PCL scaffolds, we turn to F/C ratios. In these experiments, the F/C ratios can represent the extent of film deposition, as it contains contributions from both the deposited FC film and the underlying substrate, as evidenced by the high-resolution XPS data which clearly display PCL binding

environments. On scaffold tops, the maximum F/C ratio is ~1.5 for both FC precursors (Figure 5.4), and accompanying C_{1s} spectra show similar relative FC binding environments (Figures 5.2a–c and 5.3a–c). These data suggest the two deposition systems act similarly on PCL scaffold exteriors as they do on two-dimensional materials. Note that although the rough surface features in these porous materials make XPS interpretation difficult,[13] our data demonstrate that fluorine content increases with increasing treatment time regardless of precursor. Furthermore, these data show a uniform modification in terms of exterior scaffold properties regardless of FC precursor and treatment time. Interestingly, F/C ratios for scaffold cross sections increase with increasing treatment time for both systems (Figure 5.4). As diffusion of reactive deposition precursors (e.g., CF_x radicals in FC plasmas[14]) into porous materials is thought to control film deposition in PECVD systems,[15-16] our finding that film deposition within the interior of the scaffold rises with increasing treatment time can be explained by considering the longer times extend deposition precursor diffusion into the scaffold interior. The extent of cross-sectional deposition was, however, plasma precursor specific. After scaffolds were treated for 90 min in the C_3F_8 PECVD system, the cross-sectional C_{1s} spectrum (Figure 5.2f) shows the same relative contribution of FC binding environments as the scaffold top (Figure 5.2a). Furthermore, F/C ratios for 90 min C_3F_8 treated scaffold tops and cross-sections are the same within error (Figure 5.4). These data suggest the C_3F_8 PECVD system effectively deposited a FC film on both the scaffold interior and exterior at the longest treatment time.

In contrast, the HFPO PECVD system does not display the same cross-sectional deposition properties. Cross-sectional C_{1s} XPS spectra taken on HFPO scaffolds show that the relative FC binding environment contribution increases with increasing treatment time (Figure 5.3d–f), but the FC binding environment contributions are significantly lower for the

scaffold cross sections than scaffold tops (Figure 5.3a–c) regardless of treatment time. Additionally, F/C ratios for HFPO treated scaffolds increase with longer treatment times, Figure 4. These results suggest the HFPO PECVD system is less effective at depositing a FC film throughout the scaffold's 3D structure when compared with the C_3F_8 system. One explanation as to why the HFPO deposition system is significantly slower to deposit in the interior of the scaffold than the C_3F_8 system (based on data presented in Figure 5.6), is that the HFPO plasma system contains only a single predominant deposition precursor (i.e., CF_2) whereas the C_3F_8 plasma contains a multitude of deposition precursors.[14] As indicated above, FC film deposition is likely diffusion-controlled within the scaffold interior. Thus, the various deposition precursors in the C_3F_8 plasma may diffuse more readily into the scaffold interior than the single, predominant deposition precursor in the HFPO plasma. It is, however, possible that if the scaffold treatment time were to be extended to much greater than 90 min, the HFPO scaffolds' interior compositions (i.e., F/C ratio) may eventually match that of the top because sufficient CF_2 radicals could eventually diffuse into the scaffold interior to create a film similar to that on deposited on the exterior surfaces.

Based on the C_{1s} XPS spectra in Figures 5.2 and 5.3, all plasma treated scaffold tops and cross-sections contain contributions from the underlying PCL scaffold regardless of precursor. Thus, this would seem to indicate that FC films on scaffolds for all deposition systems and treatment times are thinner than 10 nm (i.e., the sampling depth of the XPS). Film thickness data (Figure 5.6) do not, however, agree with this prediction, as all FC films deposited on flat substrates are thicker than 10 nm, regardless of treatment conditions (with the exception of the 5 min HFPO treatment). Thus, our results from the encapsulated scaffolds can be partially attributed to substrate differences; the interactions between the plasma and PCL scaffolds likely

lead to a rearrangement or chain scission within the PCL during plasma treatment, which could affect the efficacy of the deposition process, leading to thinner films.

In addition to surface characterization of FC films, we explored interactions between FC treated scaffolds and HDF with the goal of evaluating the capabilities of these scaffolds as non-bioreactive materials. Our aim was to develop a low-fouling, non-reactive material that was not cytotoxic to surrounding cells. To this extent, our experiments demonstrated that cells attached to the TC plate and proliferated in wells where untreated and treated scaffolds were seeded. This observation suggests there were no significant leachables from the encapsulated scaffolds at a cytotoxic concentration, regardless of plasma treatment. In all samples, HDF cell membrane integrity was maintained and cells attached and spread in a similar fashion as seen for TC controls. These results provide further evidence to support that there were no leachables at a cytotoxic concentration (Figure 5.7 a, b, e, h). Note that these results suggest FC films deposited on 3D scaffolds were stable under *in vitro* conditions and did not degrade or delaminate significantly over 72 h. The lack of cell attachment to FC treated scaffolds (Figure 5.7f, i, g, j) is not surprising as a significant reduction or absence of cell adhesion to hydrophobic surfaces is likely to be accentuated with increasing hydrophobicity. It is well established that ECM proteins required for cell attachment and proliferation adsorb in significantly lower quantities on hydrophobic materials, limiting or inhibiting cell adhesion and proliferation,[17-18] although exceptions do exist.[19] Altogether, results from this study demonstrate that FC treated scaffolds are excellent candidates for 3D low-fouling, non-bioreactive materials that are non-cytotoxic.

5.4 Summary

Overall, the data presented demonstrate that FC plasma treatment on PCL scaffolds results in conformal films deposited throughout the 3D structure, regardless of precursor, and

PECVD does not change the interior and exterior porous structure of the scaffolds as observed via SEM analysis. Elemental ratio data from XPS demonstrate that scaffold surface properties can be customized depending on precursor and plasma treatment conditions, in that plasma parameters can be tuned depending on whether an application requires a uniform coating throughout a 3D material, or whether it is more advantageous for the material's exterior to have different properties than its interior. These results confirm PECVD is a viable process for conformally coating 3D substrates in that bulk properties are maintained while surface properties are modified. Cell attachment studies on FC plasma treated scaffolds demonstrate that HDF did not adhere to scaffolds regardless of precursor, and that FC coatings were both non-cytotoxic and stable under *in vitro* conditions, making these excellent candidates for non-bioreactive applications. For surface modification of 3D biopolymeric materials, PECVD is an ideal tool for low-temperature, solvent free, sterile surface modification of biopolymeric materials. The large parameter space (precursor, pressure, and power) afforded by PECVD allows production of customizable, application-specific biomaterials as demonstrated with two different FC precursors.

REFERENCES

1. Hawker, M. J.; Pegalajar-Jurado, A.; Fisher, E. R., Conformal Encapsulation of Three-dimensional, Bioresorbable Polymeric Scaffolds Using Plasma-enhanced Chemical Vapor Deposition. *Langmuir* **2014,** *30* (41), 12328-12336.
2. Haïdopoulos, M.; Turgeon, S.; Laroche, G.; Mantovani, D., Chemical and Morphological Characterization of Ultra-Thin Fluorocarbon Plasma-Polymer Deposition on 316 Stainless Steel Substrates: A First Step Toward the Improvement of the Long-Term Safety of Coated-Stents. *Plasma Process. Polym.* **2005,** *2* (5), 424-440.
3. Limb, S. J.; Gleason, K. K.; Edell, D. J.; Gleason, E. F., Flexible Fluorocarbon Wire Coatings by Pulsed Plasma Enhanced Chemical Vapor Deposition. *J. Vac. Sci. Technol. A* **1997,** *15* (4), 1814-1818.
4. Intranuovo, F.; Gristina, R.; Brun, F.; Mohammadi, S.; Ceccone, G.; Sardella, E.; Rossi, F.; Tromba, G.; Favia, P., Plasma Modification of PCL Porous Scaffolds Fabricated by Solvent-Casting/Particulate-Leaching for Tissue Engineering. *Plasma Process. Polym.* **2014**.
5. Intranuovo, F.; Howard, D.; White, L. J.; Johal, R. K.; Ghaemmaghami, A. M.; Favia, P.; Howdle, S. M.; Shakesheff, K. M.; Alexander, M. R., Uniform Cell Colonization of Porous 3-D Scaffolds Achieved Using Radial Control of Surface Chemistry. *Acta Biomater.* **2011,** *7* (9), 3336-3344.
6. Butoi, C. I.; Mackie, N. M.; Gamble, L. J.; Castner, D. G.; Barnd, J.; Miller, A. M.; Fisher, E. R., Deposition of Highly Ordered CF_2-rich Films Using Continuous Wave and Pulsed Hexafluoropropylene Oxide Plasmas. *Chem. Mater.* **2000,** *12* (7), 2014-2024.
7. Cuddy, M. F.; Fisher, E. R., Contributions of CF and CF_2 Species to Fluorocarbon Film Composition and Properties for C_xF_y Plasma-Enhanced Chemical Vapor Deposition. *ACS Appl. Mater. Interfaces* **2012,** *4* (3), 1733-1741.
8. Martin, I. T.; Malkov, G. S.; Butoi, C. I.; Fisher, E. R., Comparison of Pulsed and Downstream Deposition of Fluorocarbon Materials from C_3F_8 and c-C_4F_8 Plasmas. *J. Vac. Sci. Technol. A* **2004,** *22* (2), 227-235.
9. Masel, R. I., *Principles of Adsorption and Reaction on Solid Surfaces*. John Wiley & Sons, Inc.: New York, 1996.
10. Cicala, G.; Milella, A.; Palumbo, F.; Favia, P.; d'Agostino, R., Morphological and Structural Study of Plasma Deposited Fluorocarbon Films at Different Thicknesses. *Diamond Rel. Mater.* **2003,** *12* (10), 2020-2025.
11. Sumitsawan, S.; Cho, J.; Sattler, M. L.; Timmons, R. B., Plasma Surface Modified TiO_2 Nanoparticles: Improved Photocatalytic Oxidation of Gaseous m-xylene. *Environ. Sci. Technol.* **2011,** *45* (16), 6970-6977.
12. Mackie, N. M.; Dalleska, N.; Castner, D. G.; Fisher, E. R., Comparison of Pulsed and Continuous-wave Deposition of Thin Films from Saturated Fluorocarbon/H_2 Inductively Coupled rf Plasmas. *Chem. Mater.* **1997,** *9* (1), 349-362.
13. Fisher, E. R., Challenges in the Characterization of Plasma-Processed Three-Dimensional Polymeric Scaffolds for Biomedical Applications. *ACS Appl. Mater. Interfaces* **2013,** *5* (19), 9312-9321.

14. d'Agostino, R.; Cramarossa, F.; Fracassi, F.; Illuzzi, F., Plasma Polymerization of Fluorocarbons. *Plasma Deposition, Treatment, and Etching of Polymers. Academic Press, Inc, 1250 Sixth Ave, San Diego, CA 92101, USA, 1990.* **1990**, 95-162.
15. Barry, J. J.; Silva, M. M.; Shakesheff, K. M.; Howdle, S. M.; Alexander, M. R., Using Plasma Deposits to Promote Cell Population of the Porous Interior of Three-Dimensional Poly (D, L-Lactic Acid) Tissue-Engineering Scaffolds. *Adv. Func. Mater.* **2005,** *15* (7), 1134-1140.
16. Intranuovo, F.; Sardella, E.; Gristina, R.; Nardulli, M.; White, L.; Howard, D.; Shakesheff, K. M.; Alexander, M. R.; Favia, P., PE-CVD Processes Improve Cell Affinity of Polymer Scaffolds for Tissue Engineering. *Surf. Coatings Technol.* **2011,** *205*, S548-S551.
17. Daw, R.; Candan, S.; Beck, A.; Devlin, A.; Brook, I.; MacNeil, S.; Dawson, R.; Short, R., Plasma Copolymer Surfaces of Acrylic Acid/1, 7 Octadiene: Surface Characterisation and the Attachment of ROS 17/2.8 Osteoblast-like Cells. *Biomaterials* **1998,** *19* (19), 1717-1725.
18. France, R. M.; Short, R. D.; Duval, E.; Jones, F. R.; Dawson, R. A.; MacNeil, S., Plasma Copolymerization of Allyl Alcohol/1,7-Octadiene: Surface Characterization and Attachment of Human Keratinocytes. *Chem. Mater.* **1998,** *10* (4), 1176-1183.
19. Godek, M. L.; Malkov, G. S.; Fisher, E. R.; Grainger, D. W., Macrophage Serum-Based Adhesion to Plasma-Processed Surface Chemistry is Distinct from That Exhibited by Fibroblasts. *Plasma Process. Polym.* **2006,** *3* (6-7), 485-497.

CHAPTER 6

ALLYLAMINE AND ALLYL ALCOHOL PLASMA COPOLYMERIZATION: FABRICATION OF CUSTOMIZABLE BIOLOGICALLY-REACTIVE 3D SCAFFOLDS

This chapter presents a detailed account of utilizing plasma copolymerization, a powerful PECVD-based technique, to modify the surface of polymer scaffolds. As such, this chapter is an expansion on research presented in Chapter 5 where a single PECVD precursor was used for treating porous scaffolds. Copolymerization offers the distinct advantage over single-precursor PECVD of depositing films with tunable functionality by adjusting the plasma precursor ratio. Here, an allylamine/allyl alcohol plasma copolymerization system was used to modify two- and three-dimensional substrates. Specifically, films with customizable and predictable surface properties (nitrogen/oxygen content and wettability) were deposited on substrates of varying geometries across a range of copolymerization feed gas conditions. Bioreactivity of plasma-modified materials was evaluated using both human dermal fibroblast and *E coli* attachment studies, and bioreactivity results are discussed the context of plasma-modified construct properties.

This chapter is based on work published in *Plasma Processes and Polymers* by Morgan J. Hawker, Adoracion Pegalajar-Jurado, Kiah I. Hicks, Jeffrey C. Shearer, and Ellen R. Fisher, and is reproduced in part with permission from Wiley 2015.[1] Additionally, a fundamental surface analysis relevant to work presented in this chapter is discussed in a previous Fisher Group dissertation (Dr. Jeffrey C. Shearer) and will be included in brief where relevant.[2] This work is supported by the National Science Foundation (CHE-1152963) and the Colorado Office of Economic Development via the Biosciences Discovery Evaluation Grant Program. I would like

to thank Dori Pegalajar for her contributions to this work, including experiments with E. coli, and providing training on viability protocols. I would also like to thank Kiah Hicks for assistance with E. coli experiments, John Wydallis for assistance with optical profilometry, and Jeff Shearer for laying the groundwork for this project.

6.1 Introduction

As discussed extensively in previous chapters, tailoring surface properties is a critical component of fabrication of materials for biomedical applications because of the interplay between material surfaces and biomolecules. Generally, oxygen and nitrogen containing functional groups are commonly sought as they are perceived as imparting improved biocompatibility. Although numerous PECVD studies utilizing a single nitrogen-containing[3-5] or oxygen-containing[6-8] precursor have been performed, plasma copolymerization has been used sparingly to deposit films containing relevant functional groups (e.g., carbon, oxygen and nitrogen-containing functionalities) simultaneously.

Several proof-of-concept studies demonstrated the ability to fabricate and characterize plasma copolymerized films. For example, allylamine (allylNH) has been copolymerized with acrylic acid,[9] ethylene glycol,[10] and octadiene[11-13] to deposit hydrocarbon films with carboxylic acid, alcohol, and amine functionality, respectively. The deposition of films with tunable amine functionality has also been achieved using allylamine and hexane copolymerization precursors.[14] Additionally, Fahmy et al. demonstrated tunability of the carboxylic acid content of plasma copolymerized films by varying concentrations of acrylic acid and styrene precursors in the gas feed.[15] Styrene has also been copolymerized with hydroxyethyl methacrylate, methylmethacrylate, and tetraglyme to fabricate films with variable amounts of unsaturation, aromaticity, and crosslinking.[16] Acrylic acid and hexamethyldisilazane (HMDS) have been

plasma copolymerized to implant carboxylic acid functionality into the Si-C/Si-N network deposited by the HMDS precursor.[17] A few studies have utilized copolymerization to control the material interactions with biological species. For example, Bullett and coworkers demonstrate copolymerization of acrylic acid and 1,7-octadiene to control protein binding,[18] and France and Short used an allyl alcohol (allylOH) and 1,7-octadiene copolymerization process to add alcohol functionality to surfaces to promote human keratinocyte attachment.[19] As all of these studies suggest (and in some cases, demonstrate), producing surfaces with a variety of functional groups is a critical component to further development of many advanced biomedical applications. It is important to note here that all plasma copolymerized films discussed above were deposited on two-dimensional (2D) substrates (i.e., metal foils, glass coverslips, or Si wafers). Substrate geometry is an important factor in many applications, and this is elaborated on below in terms of expanding copolymerization to three-dimensional (3D) substrates.

We can consider a potential application of plasma copolymerization in the context of modifying the surface properties of a particular class of materials, namely polymeric biomaterials. To this extent, there are numerous reports of utilizing plasmas to modify biopolymeric substrates using a single plasma precursor (e.g., non-copolymerization conditions, including those discussed in Chapters 3–5). Additionally, there have been select reports of using plasma copolymerization specifically to control surface functionality of films deposited on polymeric materials, where different plasma precursors (i.e., monomers) have been chosen to impart specific functional groups.[20-21]

In general (and for more specific types of materials including polymers), plasma copolymerization can be used to systematically control surface properties of 2D materials, and thus, to assist in addressing current debates pertaining to controlling biomolecule-surface

interactions. One such ongoing debate centers on which surface properties (i.e., chemistries and wetting behaviors) best promote mammalian cell attachment and growth,[22-27] specifically whether N-content or wettability is the more dominate factor in controlling cell proliferation on a particular surface. Focusing on nitrogen content, a review of modifying polymer surfaces using nitrogen-containing plasmas (e.g., N_2, NH_3) suggested that materials with N/C ratios across a wide range of 0.03–0.39 could facilitate cell attachment.[28] This is confounded, however, by the observation that some of these polymer systems also contain oxygen functionality in some form, which can also affect surface wettability. Indeed, the oxygen content (represented by the XPS O/C ratio) on surfaces considered to be bioreactive surfaces is even more variable, ranging from 0.11-0.80.[18, 20, 29-35] Notably, comparisons between materials, their functional group chemistry, and bioreactivity is challenging because different biomolecules have been targeted in different studies.

Several reports have utilized plasma modification to tune nitrogen and/or oxygen functionality, thereby modifying material wettability and interactions with biological species. Khorasani and coworkers plasma-modified PLA surfaces using CO_2 rf systems, increasing the wettability as well as incorporating a variety of oxygen-containing functional groups into the polymer surface.[22] They showed that these newly functionalized surfaces enhanced the growth and attachment of B65 cells over that on untreated PLA. These enhancements were attributed both to interactions between the cells and implanted O-containing functional groups, as well as to the increased wettability accompanying their implantation. Similarly, Garrido et al. plasma treated 3-hydroxybutyrate-3-hydroxyvalerate (PHBV) with oxygen and nitrogen plasmas and found the hydrophilicity of the surfaces increased after treatment, likely as a result of incorporated C-O and C-N functionality.[27] Although all plasma treated surfaces showed

enhanced cell growth over untreated PHBV, human keratinocytes grew more actively on oxygen plasma-treated PHBV surfaces than on nitrogen plasma-treated surfaces. Similarly, Ion et al. demonstrated enhanced macrophage cytokine secretion for oxygen plasma-modified carbon nanowalls over untreated and nitrogen plasma-modified substrates.[36] In contrast to these reports, Pompe et al. demonstrated that endothelial cells showed enhanced growth on nitrogen-containing surfaces produced by NH_3 plasma treatments relative to that on H_2O plasma treated surfaces.[37] Recently, Jacobs et al. published a comprehensive review listing over 60 methods of enhancing cell growth by imparting oxygen and nitrogen functionality to control wettability and chemical functionality on surfaces.[23] This review noted that the vast array of parameters that exist in cell-surface interaction studies make it difficult to gain a detailed understanding of the specific processes that influence cell growth. It is, however, generally accepted that hydrophilic surfaces containing oxygen and nitrogen functionalities are key to promoting cell attachment and growth mechanisms. In some cases, this hypothesis is further differentiated into the relative merits of specific forms of nitrogen (e.g., primary vs. secondary amines vs. amides) and oxygen (e.g., ether vs. alcohol) functional groups for creating bioactive surfaces. Because it can be difficult to find one material that meets all the requirements for a specific application, the simultaneous implantation of two or more of these functionalities in a single process could efficiently facilitate creation of tailored surfaces for biomedical applications.

The present work focuses on efforts to controllably produce both 2D and 3D materials containing a range of functional groups using plasma copolymerization of allylNH and allylOH (referred to here as the allylNH/OH copolymerization system). Precursor selection was predicated on previous results that indicated a variety of functional groups could be incorporated into deposited films and film functionality could be controlled by deliberately choosing specific

reaction conditions. Specifically, pulsed allylOH plasmas deposit films containing ester and alcohol functional groups, as detailed throughout the literature.[6, 38-40] Likewise, allylNH plasmas can deposit films rich in amine functionality.[41-42] Our group is the first to utilize plasma copolymerization of these two monomers (allylOH and allylNH). Moreover, to our knowledge, this is the first report wherein a plasma copolymerization system is applied to a 3D biopolymeric material for the purpose of tuning chemical functionality and wettability, critical properties that control bioreactivity.

6.2 Results

As noted in Section 6.1, both N and O-containing functional groups are thought to play important roles in interactions between substrates and biological species. Thus, the ability to tune both N and O content and functionality could be key factors for applications where control of the cell/bacteria-surface interactions will determine the ultimate success or failure of a biomedical device. Notably, a comprehensive characterization of polymeric thin films on 2D surfaces (i.e., Si wafers) as well as 3D materials allows a full evaluation of this system for creating a range of biomedically-relevant materials, and has been reported in previous publications upon which this chapter is based.[1-2] As such, characterization results will be summarized to contextualize interactions of materials with biological species (Sections 6.2.3 and 6.3.2).

6.2.1 Plasma copolymerization on Si wafers: surface characterization. Si wafers were plasma-modified using feed gas compositions of 100% allylNH, 100% allylOH, and intermediate compositions (i.e., plasma copolymerization conditions) to explore differences in the retention of precursor functionality in the resultant films. Film chemical composition was analyzed using XPS and wettability was analyzed using contact angle goniometry (Chapter 2). WCA values on films deposited using pulsed conditions increased as a function of allylNH in the gas feed, where

values ranged from ~8–35º. It is important to note that R_q values for plasma-treated substrates were all 2.8 ± 0.6 nm as measured by optical profilometry;[2] thus, differences in WCA values can be attributed primarily to changes in film surface chemistry as feed gas composition varies. By deconstructing high-resolution C_{1s} XPS spectra, we observed that the functionality of films deposited using 100% allyl alcohol includes C-C/C-H, C-OH/C-OR, and C=O/O-C-O, where all of all these binding environments have been previously observed in plasma polymerized allylOH films in different systems.[6, 38-39] Deconstructing spectra of plasma polymerized films from 100% allylNH was less straightforward because of the many oxygen and nitrogen binding environments that can form in the film as well as the overlap in binding energies between these moieties. Thus, several binding environments were grouped together to streamline data analysis, including C-C/C-H, C-N, C-OH/C-OR, and C=O/O-C-O. Although the C=O/O-C-O environment would be indistinguishable from amide binding environments (N-C=O), Massey et al. demonstrated via ToF-SIMS analysis that the presence of amides is negligible in plasma-deposited allylNH films.[43] We can thus ascribe the C=O/O-C-O environment to uptake of oxygen during atmospheric exposure following plasma treatment. Notably, plasma copolymerized films contain all binding environments observed in spectra of films deposited using single-gas systems. We quantitatively assessed changes in functionality using XPS data by calculating O/C and N/C ratios as a function of feedgas composition, where O/C values decrease linearly and N/C ratios increase linearly as a function of allylNH in the gas feed (Figure 6.1a). Because XPS cannot distinguish between ether and alcohol functional groups, FTIR was employed to confirm the presence of alcohol functional groups in films deposited using 100% allyl alcohol and copolymerization conditions. Collectively, these data demonstrate our ability to

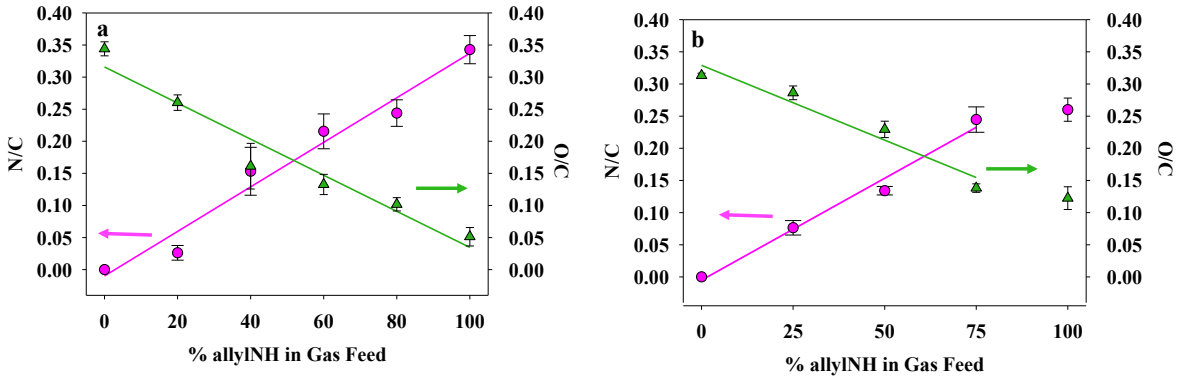

Figure 6.1. O/C ratios (triangle symbols) and N/C ratios (circle symbols) for films deposited in allylOH/allylNH plasmas on (a) Si substrates (b) PCL scaffold tops as a function of feed gas composition. Arrows on each plot indicate which data set corresponds to which *y*-axis. All data sets were fit with a linear least squares analysis; R^2 values ≥ 0.94.

utilize the allylNH/OH plasma copolymerization system to deposit films with tunable nitrogen content and wettability on 2D substrates.

6.2.2 Film deposition on 3D scaffolds. After characterizing films deposited on Si wafers in terms of composition and wettability, we expanded to plasma treating 3D scaffold substrates to address the possibility of tuning surface properties, and thereby tailoring biological response, of biomedical device-relevant constructs. SEM evaluation of the porous structure of 3D PCL scaffolds prior to and after plasma treatment (Figure 6.2) confirms that scaffold morphology was maintained after plasma treatment, as no significant changes to morphology were observed when compared to untreated scaffolds (comparable to results presented in Chapter 5). Similar surface analyses were performed on scaffolds as on 2D substrates. O/C ratios of the deposited films decrease linearly as a function of feed gas composition for films deposited between 0 and 75% allylNH in the gas feed. Above 75% allylNH, the O/C ratio remains approximately the same at ~0.13. In contrast, the N/C ratios of those same films increase linearly as a function of allylNH in the gas feed for ≤ 75% allylNH plasmas, and again stabilizes for films deposited in 100% allylNH systems (Figure 6.1b). Based on these data, a maximum N/C ratio of ~0.25 is achieved on the top of the scaffolds using gas feed compositions of ≥75% allylNH. These data generally confirm that films deposited on the scaffold exterior are similar to those deposited on Si wafers. Important differences, however, exist between the 2D and 3D substrates treated under identical deposition conditions; this is further elaborated in Section 6.3. Plasma-modified scaffolds were further analyzed via high-resolution XPS to explore differences in surface functionality, and identical binding environments were observed on scaffold tops as for plasma-modified Si wafers. Notable differences between spectra on pulsed plasma treated Si wafers and scaffold tops include the addition of environments corresponding to O-C=O and -C-COO, which are attributed to

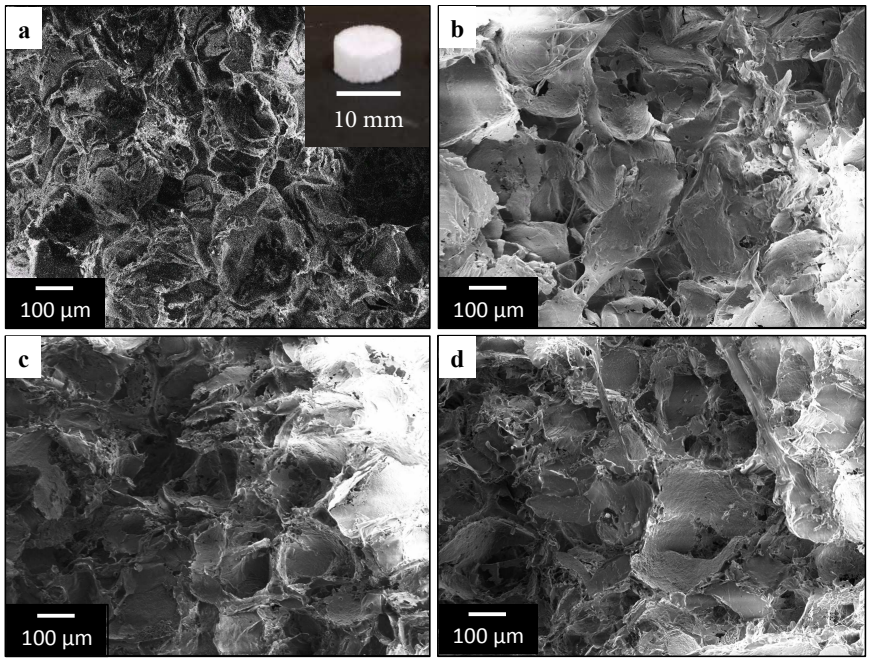

Figure 6.2. Representative SEM images of PCL scaffold tops (100X): a) untreated, and those treated with b) 100% allylNH, c) 50% allylNH, and d) 100% allylOH pulsed plasmas. The inset in (a) is a photograph of an untreated PCL scaffold.

contributions from the underlying PCL substrate. Wettability analysis demonstrates that untreated PCL scaffolds are hydrophobic, with a static WCA of 116 ± 2º (Figure 6.3a). In contrast, the wettability of plasma-modified scaffolds could not be measured using static WCA as the hydrophilic films combined with porous scaffold morphology resulted in sorption of the water drops. Figure 6.3a contains representative frames extracted from dynamic contact angle video data for t = 10 ms (the time that the drop fully separated from the needle) and t = 1 s.

Water sorption behavior was captured from the video by measuring WCA values from each frame and plotting as a function of time (Figure 6.3b; experimental methodology further discussed in Chapter 3). The initial WCA increased as a function of allylNH in the gas feed showing a similar trend to results observed for pulsed plasma-treated Si wafers. Examining the WCA values as a function of time (Figure 6.3b), it is clear that scaffolds treated in 100% allylOH plasmas sorb the water drop the fastest (drop was fully sorbed in ~ 0.5 s). Wettability data collected for a scaffold treated in a 50% allylNH plasma (Figure 6.3b) are representative of scaffolds treated in all copolymerization systems, with a longer water drop absorption time than the 100% allylOH treated scaffold, but still under ~2 s. Scaffolds treated in 100% allylNH plasmas displayed the slowest water absorption behavior, taking longer than 2 s to fully adsorb. Nevertheless, all plasma treated samples are considered to be hydrophilic as the water drops completely absorb.

Surface analysis results summarized in Sections 6.2.1 and 6.2.2 demonstrate our ability to use allylNH/OH plasma copolymerization conditions to deposit films with tunable and predictable surface chemistry and wettability on substrates with varying geometry. We believe this suite of tunable constructs, both in terms of surface and bulk properties, provide us with a platform by which to evaluate how these factors control material cell-surface interactions.

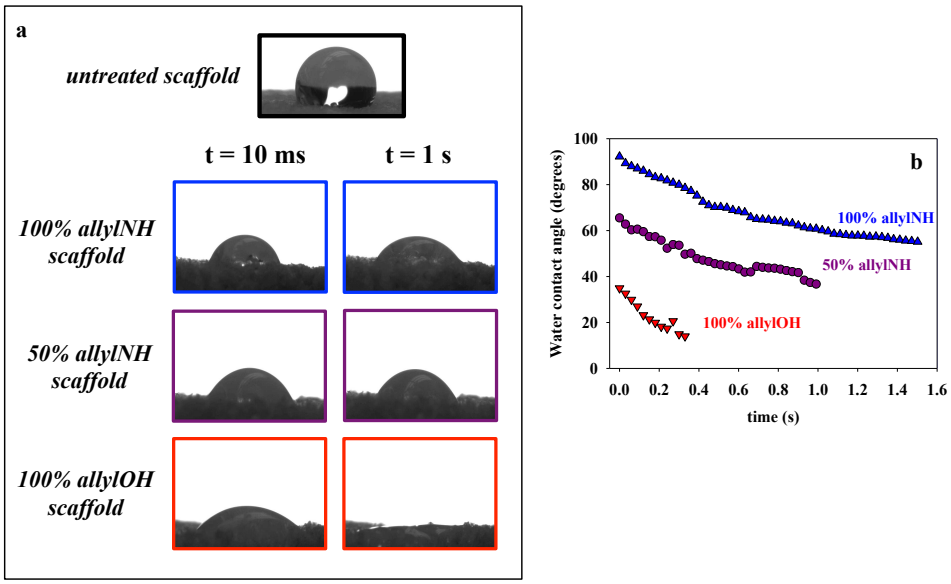

Figure 6.3. Wettability data on plasma-modified scaffolds. (a) Still images extracted from water sorption data plotted in (b) compared to an untreated scaffold, and (b) WCA as a function of drop age for scaffolds treated with 100% allylNH (▲), 50% allylNH (●), and 100% allylOH (▼) plasmas.

Developing such an understanding can contribute more information to the debate presented in Section 6.1. That is, does nitrogen content or wettability play a more important role in regulating substrate bioreactivity?

6.2.3 Cell attachment, growth, and viability. We assessed the biological performance of plasma copolymerized films deposited onto 2D substrates prior to considering interactions of biological species with more complex, 3D materials. To investigate HDF attachment behavior on 2D materials, TC wells (positive control), C_3F_8 plasma treated NTC disks (non-bioreactive, negative control, using treatment conditions reported in Chapter 5),[44] and 100% allylNH, 40% allylNH, and 100% allylOH pulsed plasma treated NTC disks were seeded with HDF. Overlaid fluorescence microscopy images of HDF attachment on the different substrates are displayed in Figure 6.4, where cell actin cytoskeletons are shown in red and cell nuclei are shown in blue. A representative image of HDF attachment and growth on a TC well (Figure 6.4a) illustrates cell proliferation over the entire surface, and the opposite behavior (i.e., lack of HDF attachment) is observed for the FC treated material (Figure 6.4b). The faint red and blue areas in the image in Figure 6.4b are indicative of retained stain on the FC plasma treated substrate. Figure 6.4c, d, and e are representative images of HDF cells attached to 100% allylOH, 40% allylNH, and 100% allylNH pulsed plasma treated NTC disks, respectively. Notably, cell attachment on these plasma treated substrates appears to be less than that observed on the positive control (Fig. 6.4a) but greater than that observed on the negative control (Fig. 6.4b).

Identical cell growth conditions were used to seed scaffolds with HDF, and representative overlaid fluorescence microscopy images are presented in Figure 6.5 for an untreated scaffold (Figure 6.5a), and scaffolds treated with 100% allylOH (Figure 6.5b), 50% allylNH (Figure 6.4c) and 100% allylNH (Figure 6.5d) plasmas. Notably, the cell nuclei (stained blue) are in the same

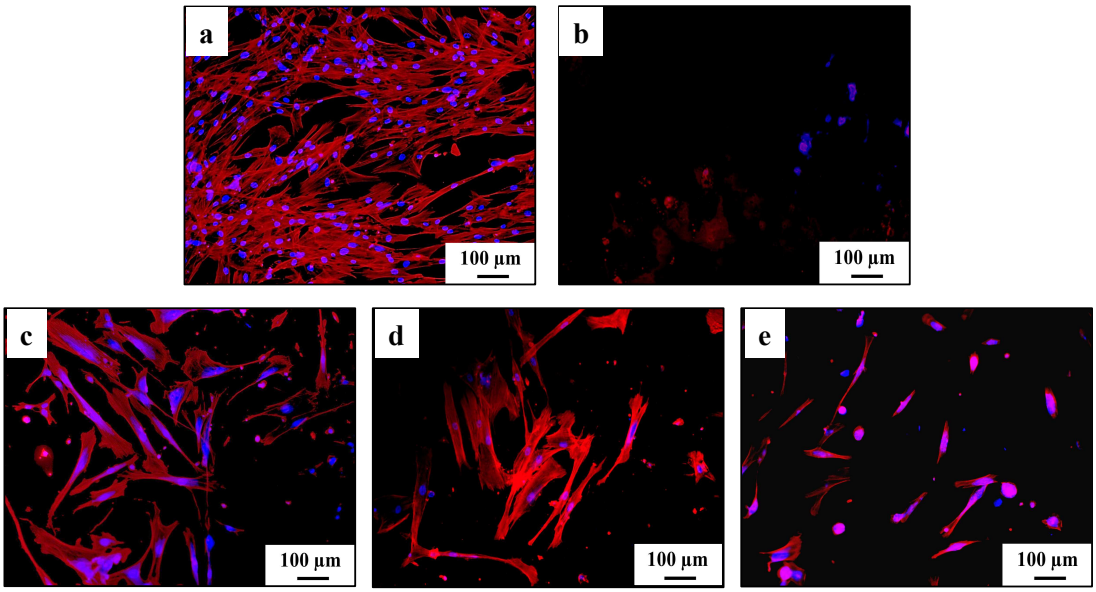

Figure 6.4. Overlaid fluorescence microscopy images of HDF attached to (a) a TC plate, and NTC disks treated with (b) FC (c) 100% allylOH, (d) 40% allylNH and (e) 100% allylNH plasmas. The duration of cell attachment and growth experiments was 48 h for all substrates (n = 9). Red areas indicate cell actin cytoskeletons and blue areas indicate cell nuclei.

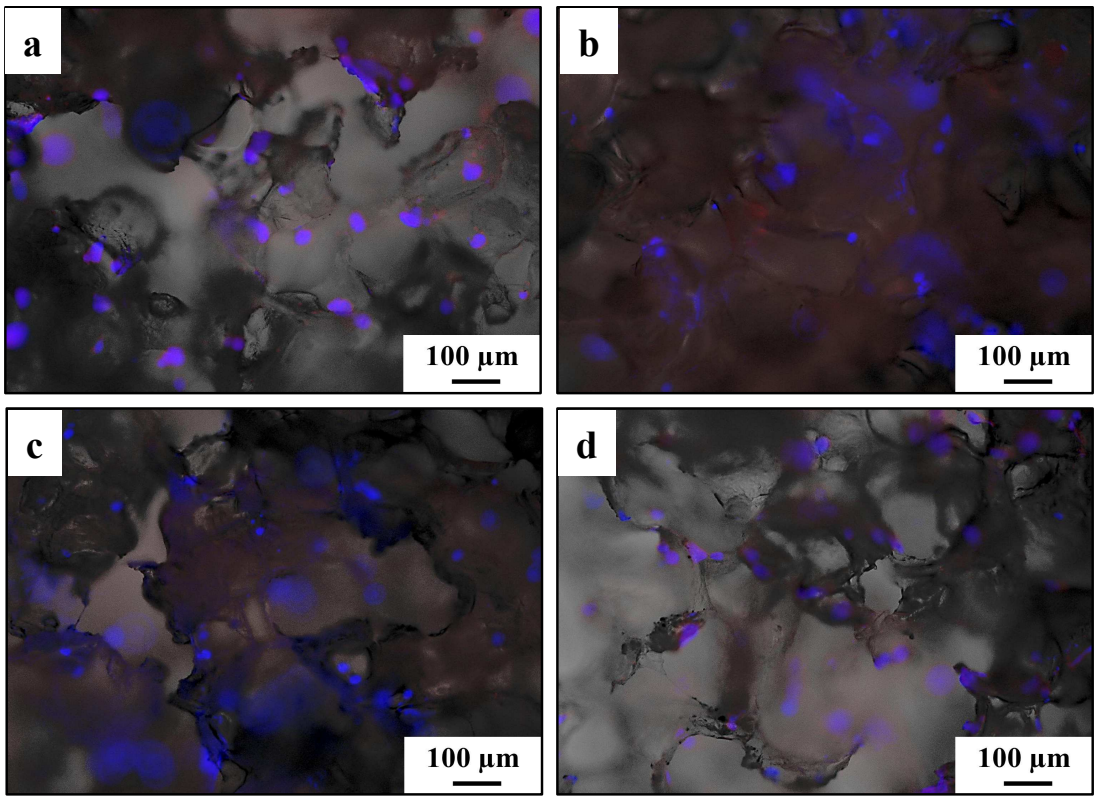

Figure 6.5. Overlaid fluorescence microscopy images of HDF attached to (a) an untreated scaffold, and scaffolds treated with (b) 100% allylOH, (c) 50% allylNH, and (d) 100% allylNH plasmas. The duration of cell attachment and growth experiments was 48 h for all substrates (n = 9). Red areas indicate cell actin cytoskeletons and blue areas indicate cell nuclei.

plane of focus on the untreated scaffold, indicating that cell attachment occurs mainly on the scaffold exterior. Cell nuclei on plasma-treated scaffolds, however, appear to be in different planes of focus, suggesting that HDF penetrate into the 3D scaffold structure such that cell attachment occurs through the porous network.

Although fluorescence microscopy images allow for a qualitative comparison of cell attachment on different 2D and 3D substrates, they do not allow for a quantitative assessment of cell viability on these materials. Therefore, viability assays (CellTiter-Blue®) were performed on HDF attached to plasma treated 2D substrates (Figure 6.6a) and scaffolds (Figure 6.6b), each with corresponding controls. To explore differences in cell viability on flat substrates, NTC disks were used as control substrates as they exhibit a low degree of HDF attachment. NTC disks were plasma treated (with pulsed allylNH/OH as well as FC plasmas) and HDF viability on plasma-treated substrates was normalized to that of untreated NTC disks (Figure 6.6a). These data demonstrate that FC plasma treated substrates (negative controls) have a significantly lower viable HDF content relative to NTC disks, as expected because of the non-bioreactive nature of FC coatings (see Chapter 5).[44] Viable HDF content generally increases for allylNH/OH plasma treated materials relative to the FC coated substrates. These improvements are, however, insignificant compared to the NTC disks. Additionally, the variability associated with these measurements (represented by the standard deviation-based error bars shown in Figure 6.6a) is relatively large, which makes it difficult to elucidate trends in viability assay data on these 2D substrates. Differentiating between the amount of viable HDF attached to untreated and plasma-modified scaffolds is, however, more clear-cut (Figure 6.6b). 100% allylOH and 100% allylNH plasma-treated scaffolds displayed an ~20% improvement in viable cell attachment relative to untreated scaffolds, and scaffolds treated under copolymerization conditions (50% allylNH)

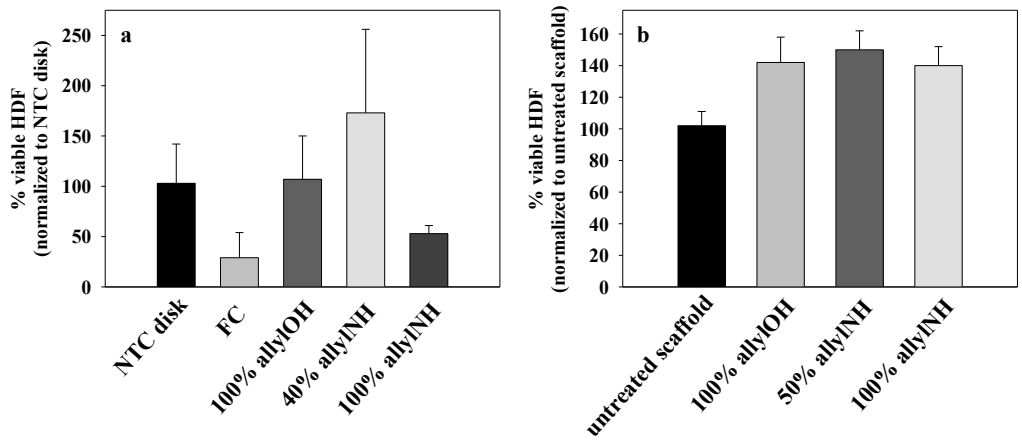

Figure 6.6. CellTiter-Blue® cell viability assay results for HDF attached to untreated and allylNH/OH plasma-treated (a) NTC disks and (b) PCL scaffolds. Results from viability studies on FC plasma treated substrates are included in (a) as a negative control. All plasma treatments occurred using pulsed conditions. For all experiments, n = 9.

showed an even greater enhancement (~30%) in viable HDF content relative to untreated scaffolds.

The bioreactivity of the allylNH/OH pulsed plasma treated materials was further explored by seeding these materials with *E. coli*. It is important to note that imaging challenges prohibited performing bacterial attachment experiments with 3D constructs, but untreated and plasma-modified NTC disks were used as proof-of-concept experiments (and to compare with HDF experiments on 2D substrates). Figure 6.7a illustrates *E. coli* attachment and growth behavior on an untreated glass slide (hydrophilic control) after 20 h, where live/dead staining revealed that a similar number of viable (green) and non-viable (red) bacteria cells were found on the surface. Additionally, there are areas on the hydrophilic control where isolated bacteria cells are not observed, indicative of biofilm formation. Conversely, the majority of the cells attached to FC plasma-treated substrates (hydrophobic controls) were both isolated and non-viable (Figure 6.7b). Similar to the hydrophilic control, *E. coli* attachment and growth on 100% allylOH (Figure 6.7c), 40% allylNH (Figure 6.7d), and 100% allylNH (Figure 6.7e) plasma treated materials reveals biofilm formation. Thus, it is difficult to isolate the number of viable and non-viable bacteria cells. Notably, data on allylNH/OH plasma-treated materials suggest there is a greater amount of viable bacterial cells attached to 100% allylNH substrate than the other two compositions (Figure 6.7e). However, similar overall surface coverage to the hydrophilic control (glass slide) can be estimated for all allylNH/OH plasma-modified materials. Altogether, biological experiments demonstrate that allylNH/OH plasma treatment renders materials bioreactive.

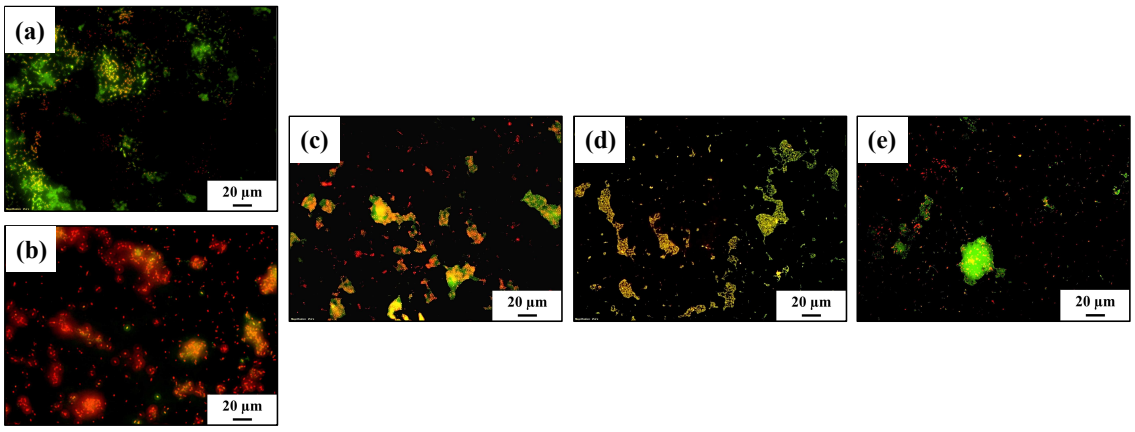

Figure 6.7. Representative overlaid fluorescence microscopy images of live/dead stained *E. coli* after attachment and growth for 20 h on (a) an untreated glass slide (hydrophilic control), and on glass slides modified with b) FC plasmas (hydrophobic control), c) 100% allylOH plasmas, d) 40% allylNH plasmas, and e) 100% allylNH plasmas. For all experiments, n = 9.

6.3 Discussion

From the perspective of both surface modification and biological relevance, the allylNH/allylOH plasma copolymerization system investigated here provides a unique route for tailoring the surface properties of 2D and 3D materials. This copolymerization system allows the customization of chemical composition, functionality, and wettability, thereby facilitating control of the bioreactivity of 2D and 3D constructs. Furthermore, the system is fundamentally interesting both as a general surface modification tool and for biological applications as it provides a specific route to plasma modify both 2D and 3D substrates, resulting in materials with customizable chemical composition, functionality, wettability, and bioreactivity.

6.3.1 Characterization of plasma copolymerized allylNH/OH films: 2D and 3D substrates. The results presented in publications work in this chapter is based on (summarized in Sections 6.2.1 and 6.2.2) demonstrate we can tune material surface properties in a predictable manner by changing the gas feed composition using plasma deposition.[1-2] Previous work on allylNH plasma deposition systems demonstrated the formation of oligomeric allylNH species in the gas phase,[42, 45-46] which can result in the deposition of films with a high concentration of primary amines, as supported by derivatization studies.[41, 45] Our XPS and FTIR spectra of films deposited in allylNH-containing plasmas support these findings and demonstrate that nitrogen in these films primarily resides in the form of amine groups. One additional observation is that in the allylNH/OH copolymerization system, the N content in the resulting films on 2D substrates exhibits a linear response to the feed gas content (Figure 6.1). For 3D substrates, this linearity only exists for plasmas with ≤ 75% allylNH. Nevertheless, to our knowledge, this is the first nitrogen-containing plasma copolymerization system that exhibits a linear response in the N content of plasma-deposited films. Moreover, the predictable nature of the relationship between

feed gas composition and film N content suggests the allylNH/OH copolymerization system is ideal for producing customizable biomaterials.

In addition to characterizing the nitrogen content of deposited films, our surface analysis results provide insight regarding oxygen content and functionality as well. Although high-resolution XPS spectra of films deposited using allylOH-containing plasmas show the presence of C-OH/C-OR functionality, we cannot distinguish between these groups using XPS alone. Pulsed plasma conditions, such as those used in this work, have been previously demonstrated as one route to maintain plasma precursor functionality in deposited films.[47-48] Based on this precedent, we would expect that the alcohol functionality would be maintained in the case of allylOH-containing plasma deposited films. This hypothesis is supported by FTIR data, which indicate films deposited using allylOH-containing plasmas retain alcohol functionality. These findings are further supported by the work of Short and coworkers, who used gas-phase diagnostics of low power allylOH plasmas (P = 1 W) to provide evidence that electron impact in the plasma forms cationic dimer and trimer species and results in the retention of monomer functionality in deposited films.[38-39]

After characterizing the functionality and chemical composition of films deposited with the allylNH/OH copolymerization system on 2D substrates, we expanded pulsed plasma treatments to 3D PCL scaffolds. Based on previous studies of plasma treatment of similar scaffold materials (including those discussed in Chapter 5),[44, 49-50] we anticipated films deposited on the scaffold exterior to be compositionally similar to those deposited on 2D substrates under the same treatment conditions. Our results generally support this hypothesis, specifically with respect to nitrogen and oxygen content on scaffold exterior. Notably, we observe O/C and N/C ratios on the tops of scaffolds treated with 75 and 100% allylNH pulsed plasmas are the same

within experimental error, whereas linear trends across all gas compositions are observed for plasma deposited films on Si wafers (Figure 6.1). Additional differences in O/C and N/C ratios on 2D and 3D substrates treated under identical pulsed plasma conditions can be found when comparing materials treated in 0% allylNH (i.e., 100% allylOH) and 100% allylNH plasmas Specifically, for 0% allylNH plasma treated materials, the O/C ratio on the scaffold exterior is ~10% lower than on the corresponding 2D substrate. For 100% allylNH plasma treated materials, the O/C and N/C ratios of the scaffold exterior are ~100% greater and ~25% lower than those of the corresponding 2D substrate, respectively. The origin of these differences likely lies with the identity of the underlying substrate (i.e., a wafer vs. a porous polymeric material). Indeed, high-resolution spectra on scaffold tops contain contributions from the underlying PCL for all plasma treatments. Although the presence of underlying material functionality could suggest a reorganization of the PCL scaffold upon plasma treatment,[44] it may also simply reflect that film thickness is less than the sampling depth of the XPS. It is difficult, however, to distinguish the underlying scaffold from films deposited from allylOH-containing plasmas as both materials contain similar functionality (i.e., hydrocarbon, ester, and ether functional groups). Underlying substrate contributions are more obvious for films deposited using higher allylNH concentrations, as these films are nitrogen-rich relative to the underlying PCL. Notably, the maximum N/C ratio achieved in these systems on the scaffold exterior (~25%) is well within the reported range of polymeric materials treated with nitrogen-containing plasmas,[28] validating their potential as biomedical materials. Collectively, these findings demonstrate that although differences in elemental composition exist, similar functional groups are present in films deposited on both Si wafers and the exterior of the 3D scaffolds.

We can use surface chemistry data from plasma-copolymerized materials as grounds to explain observed wetting behavior. Materials deposited with higher concentrations of allylOH in the gas feed are less hydrophilic than those deposited in plasmas with lower concentrations of allylNH (Figure 6.3), which can be rationalized by differences in hydrogen bonding capabilities of functional groups present in plasma copolymerized films. All films deposited using allylNH-containing plasmas contain NH_x functional groups. Therefore, the interplay between these NH_x groups with the alcohol functionality of films deposited using allylOH-containing plasmas control wettability of plasma copolymerized films. As anticipated, initial WCA values are higher for scaffolds than for Si wafers treated under the same plasma conditions. These differences are attributable to the higher surface roughness inherent to the porous scaffold architecture. The time it takes for the water drop to absorb into the scaffold decreases with concentration of allylOH in the feed gas, such that scaffolds treated with plasmas containing more allylOH are more hydrophilic (i.e., these materials have faster water absorption rates) than those with higher allylNH concentrations in the gas feed (Figure 6.3). This echoes the trend observed on plasma deposited films on Si wafers, providing support that films deposited on PCL scaffolds are compositionally similar to those deposited on Si wafers and therefore have similar wetting properties. Thus, adjusting the relative amounts of the precursor gas can help regulate the wetting properties of plasma deposited allylNH/OH films. Overall, these studies demonstrate the effectiveness of plasma copolymerization as a versatile surface modification tool for both 2D and 3D substrates.

6.3.2 Bioreactivity assessment of plasma-modified materials using E. coli and HDF. After the comprehensive assessment of both wettability and surface composition on these plasma-modified materials, we explored how these properties control or relate to substrate

bioreactivity. Importantly, directly comparing HDF viability on allylNH/OH plasma-modified 2D materials (Figure 6.6a) to that on 3D scaffolds (Figure 6.6b) is challenging because of the fundamental differences in surface composition and material architecture. As noted above, the O/C and N/C ratios achieved on 2D materials are, in the case of certain gas feed compositions, significantly different than those attained on 3D materials using identical plasma treatments. Differences in surface chemistry may help to elucidate disparities in the cell attachment behavior observed within these systems. Additionally, deposition precursors within allylNH/OH plasmas (i.e., cationic oligomers) may interact differently with NTC disks (i.e., polystyrene) than PCL scaffolds. For example, the behavior of plasma-deposited films on NTC disks may differ from those on PCL scaffolds in aqueous environments because of differences in the underlying polymer chemistry and architecture. Such a detailed exploration of these potential differences is, however, beyond the scope of this study.

Focusing on the bioreactivity of allylNH/OH plasma-modified 2D substrates, morphological studies demonstrate intermediate HDF attachment compared to positive and negative controls. This can be attributed to differences in substrate chemistry and wettability (Figures 6.1 and 6.3, respectively). Despite the presence of HDF cells on allylNH/OH modified 2D materials, viability data demonstrate differences in cell attachment behavior on allylNH/OH plasma polymerized films. Specifically, our findings demonstrate that 2D substrates treated using copolymerization conditions promote cell attachment and growth to a greater extent than the individual precursors, suggesting a synergy between the O and N-containing functional groups and HDF. It is important to note, however, the large experimental error associated with these viability data on 2D substrates, possibly suggesting an instability of plasma polymerized films on NTC disks. One hypothesis is that these films may be swelling, as this behavior has been

previously observed for similar plasma polymerized films.[51-52] Thus, film stability in aqueous environments is an additional consideration that should be accounted for before deploying these plasma-modified materials as biomedical devices.

The main focus of bioreactivity assessments in this work was plasma-modified 3D scaffolds. Our hypothesis was that combining allylNH/OH plasma treatments with scaffolds would enhance cell attachment behavior via customizing scaffold surface chemistry. Specifically, we focused on tuning N and O content and functionality by changing allylNH/OH plasma precursor composition in the gas feed. Viability data presented in Figure 6.6b support this hypothesis, as all plasma treated scaffolds show >20% improvements HDF viability compared to untreated materials. Although changes in wettability and surface chemistry are not mutually exclusive within the allylNH/OH plasma copolymerization system studied here, cell viability data suggest that both properties work in synergy to promote HDF attachment and growth on these scaffold materials. This result clearly suggests additional exploration of plasma copolymerization systems to fabricate biologically-relevant materials holds promise.

6.4 Summary

This chapter details the plasma deposition of functionalized films copolymerized from allylNH and allylOH on 2D and 3D substrates. With this system, the surface properties of the resulting films (i.e., chemical composition and wettability) were customizable by tuning the feed gas composition. Notably, the relatively delicate architecture of the 3D scaffolds was preserved and plasma treatment affected both the interior and exterior of the constructs, highlighting the versatility of this approach. As many of the intended end applications for the 3D scaffolds rely on effective interfaces with biological moieties, we note that our copolymerization process results in enhanced bioreactivity with respect to HDF cell viability. This suggests these materials

could be utilized in a range of biomedical devices. Moreover, the results from this research indicate further exploration of plasma copolymerization systems for the purpose of created tunable biomedical device surfaces could be warranted. In particular, careful selection of alternate precursor pairs could provide different functionality than the nitrogen and oxygen environments created here. Additionally, utilizing substrates formed from different polymers and/or with different architectures would provide further insight into mechanisms for plasma modification of 3D materials to produce biologically relevant constructs.

REFERENCES

1. Hawker, M. J.; Pegalajar‐Jurado, A.; Hicks, K. I.; Shearer, J. C.; Fisher, E. R., Allylamine and Allyl Alcohol Plasma Copolymerization: Synthesis of Customizable Biologically-Reactive Three-Dimensional Scaffolds. *Plasma Process. Polym.* **2015,** *12* (12), 1435-1450.
2. Shearer, J. C. Enhanced Surface Functionality via Plasma Modification and Plasma Deposition Techniques to Create More Biologically Relevant Materials. Ph.D. Dissertation, Colorado State University, Fort Collins, CO, 2013.
3. Truica-Marasescu, F.; Girard-Lauriault, P.-L.; Lippitz, A.; Unger, W. E.; Wertheimer, M. R., Nitrogen-rich Plasma Polymers: Comparison of Films Deposited in Atmospheric-and Low Pressure Plasmas. *Thin Solid Films* **2008,** *516* (21), 7406-7417.
4. Dubreuil, M.; Bongaers, E.; Lens, P., Incorporation of Amino Moieties Through Atmospheric Pressure Plasma: Relationship Between Precursor Structure and Coating Properties. *Surf. Coat. Technol.* **2011,** *206* (6), 1439-1448.
5. Li, L.; Dai, X. J.; Xu, H. S.; Zhao, J. H.; Yang, P.; Maurdev, G.; du Plessis, J.; Lamb, P. R.; Fox, B. L.; Michalski, W. P., Combined Continuous Wave and Pulsed Plasma Modes: For More Stable Interfaces with Higher Functionality on Metal and Semiconductor Surfaces. *Plasma Process. Polym.* **2009,** *6* (10), 615-619.
6. Watkins, L.; Bismarck, A.; Lee, A. F.; Wilson, D.; Wilson, K., An XPS Study of Pulsed Plasma Polymerised Allyl Alcohol Film Growth on Polyurethane. *Appl. Surf. Sci.* **2006,** *252* (23), 8203-8211.
7. Choi, C.; Hwang, I.; Cho, Y.-L.; Han, S. Y.; Jo, D. H.; Jung, D.; Moon, D. W.; Kim, E. J.; Jeon, C. S.; Kim, J. H., Fabrication and Characterization of Plasma-polymerized Poly(ethylene glycol) Film with Superior Biocompatibility. *ACS Appl. Mater. Interfaces* **2013,** *5* (3), 697-702.
8. O'Mahony, C. C.; Gubala, V.; Gandhiraman, R. P.; Daniels, S.; Yuk, J. S.; MacCraith, B. D.; Williams, D. E., Improving the Sensitivity of Immunoassays with PEG-COOH-like Film Prepared by Plasma-based Technique. *J. Biomed. Mater. Res. A* **2012,** *100* (1), 230-235.
9. Beck, A. J.; Whittle, J. D.; Bullett, N. A.; Eves, P.; Mac Neil, S.; McArthur, S. L.; Shard, A. G., Plasma Co‐polymerisation of Two Strongly Interacting Monomers: Acrylic Acid and Allylamine. *Plasma Process. Polym.* **2005,** *2* (8), 641-649.
10. Gomez, L. M.; Morales, P.; Cruz, G. J.; Olayo, M.; Palacios, C.; Morales, J.; Olayo, R., Plasma Copolymerization of Ethylene Glycol and Allylamine. *Macromol. Symp.* **2009,** *283* (1), 7-12.
11. Ruiz, J. C.; Taheri, S.; Michelmore, A.; Robinson, D. E.; Short, R. D.; Vasilev, K.; Förch, R., Approaches to Quantify Amine Groups in the Presence of Hydroxyl Functional Groups in Plasma Polymerized Thin Films. *Plasma Process. Polym.* **2014,** *11* (9), 888-896.
12. Zuber, A. A.; Robinson, D. E.; Short, R. D.; Steele, D. A.; Whittle, J. D., Development of a Surface to Increase Retinal Pigment Epithelial Cell (ARPE-19) Proliferation Under Reduced Serum Conditions. *J. Mater. Sci.: Mater Med.* **2014,** *25* (5), 1367-1373.
13. Coad, B. R.; Bilgic, T.; Klok, H.-A., Polymer Brush Gradients Grafted from Plasma-Polymerized Surfaces. *Langmuir* **2014,** *30* (28), 8357-8365.

14. Beck, A. J.; Jones, F. R.; Short, R. D., Plasma Copolymerization as a Route to the Fabrication of New Surfaces with Controlled Amounts of Specific Chemical Functionality. *Polymer* **1996,** *37* (24), 5537-5539.
15. Fahmy, A.; Mix, R.; Schönhals, A.; Friedrich, J., Structure of Plasma‐Deposited Copolymer Films Prepared from Acrylic Acid and Styrene: Part II Variation of the Comonomer Ratio. *Plasma Process. Polym.* **2013,** *10* (9), 750-760.
16. Li, Z.; Gillon, X.; Diallo, E. M.; Pireaux, J.-J.; Houssiau, L., Synthesis of Copolymer Films by RF Plasma: Correlation Between Plasma Chemistry and Film Characteristics. *IEEE Trans. Plasma Sci.* **2013,** *41* (3), 518-527.
17. Hirotsu, T.; Tagaki, C.; Partridge, A., Plasma Copolymerization of Acrylic Acid with Hexamethyldisilazane. *Plasmas Polym.* **2002,** *7* (4), 353-366.
18. Bullett, N. A.; Whittle, J. D.; Short, R. D.; Douglas, C. I., Adsorption of Immunoglobulin G to Plasma-co-polymer Surfaces of Acrylic Acid and 1, 7-octadiene. *J. Mater. Chem.* **2003,** *13* (7), 1546-1553.
19. France, R. M.; Short, R. D.; Duval, E.; Jones, F. R.; Dawson, R. A.; MacNeil, S., Plasma Copolymerization of Allyl Alcohol/1, 7-octadiene: Surface Characterization and Attachment of Human Keratinocytes. *Chem. Mater.* **1998,** *10* (4), 1176-1183.
20. García, C. G.; Ferrus, L. L.; Moratal, D.; Pradas, M. M.; Sánchez, M. S., Poly (L-lactide) Substrates with Tailored Surface Chemistry by Plasma Copolymerisation of Acrylic Monomers. *Plasma Process. Polym.* **2009,** *6* (3), 190-198.
21. Friedrich, J.; Mix, R.; Kühn, G.; Retzko, I.; Schönhals, A.; Unger, W., Plasma-based Introduction of Monosort Functional Groups of Different Type and Density onto Polymer Surfaces. Part 2: Pulsed Plasma Polymerization. *Compos. Interfaces* **2003,** *10* (2-3), 173-223.
22. Khorasani, M.; Mirzadeh, H.; Irani, S., Comparison of Fibroblast and Nerve Cells Response on Plasma Treated Poly (L-lactide) Surface. *J. Appl. Polym. Sci.* **2009,** *112* (6), 3429-3435.
23. Jacobs, T.; Morent, R.; De Geyter, N.; Dubruel, P.; Leys, C., Plasma Surface Modification of Biomedical Polymers: Influence on Cell-material Interaction. *Plasma Chem. Plasma Process.* **2012,** *32* (5), 1039-1073.
24. Yildirim, E. D.; Besunder, R.; Pappas, D.; Allen, F.; Güçeri, S.; Sun, W., Accelerated Differentiation of Osteoblast Cells on Polycaprolactone Scaffolds Driven by a Combined Effect of Protein Coating and Plasma Modification. *Biofabrication* **2010,** *2* (1), 014109.
25. Yildirim, E. D.; Ayan, H.; Vasilets, V. N.; Fridman, A.; Guceri, S.; Sun, W., Effect of Dielectric Barrier Discharge Plasma on the Attachment and Proliferation of Osteoblasts Cultured over Poly (ε-caprolactone) Scaffolds. *Plasma Process. Polym.* **2008,** *5* (1), 58-66.
26. Park, H.; Lee, J. W.; Park, K. E.; Park, W. H.; Lee, K. Y., Stress Response of Fibroblasts Adherent to the Surface of Plasma-treated Poly (lactic-co-glycolic acid) Nanofiber Matrices. *Colloids Surf., B* **2010,** *77* (1), 90-95.
27. Garrido, L.; Jiménez, I.; Ellis, G.; Cano, P.; García‐Martínez, J. M.; López, L.; de la Pena, E., Characterization of Surface-modified Polyalkanoate Films for Biomedical Applications. *J. Appl. Polym. Sci.* **2011,** *119* (6), 3286-3296.
28. Meyer-Plath, A.; Schröder, K.; Finke, B.; Ohl, A., Current Trends in Biomaterial Surface Functionalization—Nitrogen-containing Plasma Assisted Processes with Enhanced Selectivity. *Vacuum* **2003,** *71* (3), 391-406.

29. Sardella, E.; Fisher, E. R.; Shearer, J. C.; Garzia Trulli, M.; Gristina, R.; Favia, P., N_2/H_2O Plasma Assisted Functionalization of Poly (ε-caprolactone) Porous Scaffolds: Acidic/Basic Character versus Cell Behavior. *Plasma Process. Polym.* **2015,** *12*, 786-798.
30. Bergemann, C.; Quade, A.; Kunz, F.; Ofe, S.; Klinkenberg, E. D.; Laue, M.; Schröder, K.; Weissmann, V.; Hansmann, H.; Weltmann, K. D., Ammonia Plasma Functionalized Polycarbonate Surfaces Improve Cell Migration Inside an Artificial 3D Cell Culture Module. *Plasma Process. Polym.* **2012,** *9* (3), 261-272.
31. Kurniawan, H.; Lai, J.-T.; Wang, M.-J., Biofunctionalized Bacterial Cellulose Membranes by Cold Plasmas. *Cellulose* **2012,** *19* (6), 1975-1988.
32. Sarapirom, S.; Yu, L.; Boonyawan, D.; Chaiwong, C., Effect of Surface Modification of Poly (lactic acid) by Low-Pressure Ammonia Plasma on Adsorption of Human Serum Albumin. *Appl. Surf. Sci.* **2014,** *310*, 42-50.
33. Amornsudthiwat, P.; Mongkolnavin, R.; Kanokpanont, S.; Panpranot, J.; San Wong, C.; Damrongsakkul, S., Improvement of Early Cell Adhesion on Thai Silk Fibroin Surface by Low Energy Plasma. *Colloids Surf., B* **2013,** *111*, 579-586.
34. Silva, S. S.; Luna, S. M.; Gomes, M. E.; Benesch, J.; Pashkuleva, I.; Mano, J. F.; Reis, R. L., Plasma Surface Modification of Chitosan Membranes: Characterization and Preliminary Cell Response Studies. *Macromol. Biosci.* **2008,** *8* (6), 568-576.
35. Lee, H.-U.; Jeong, Y.-S.; Jeong, S.-Y.; Park, S.-Y.; Bae, J.-S.; Kim, H.-G.; Cho, C.-R., Role of Reactive Gas in Atmospheric Plasma for Cell Attachment and Proliferation on Biocompatible Poly ε-caprolactone Film. *Appl. Surf. Sci.* **2008,** *254* (18), 5700-5705.
36. Ion, R.; Vizireanu, S.; Stancu, C. E.; Luculescu, C.; Cimpean, A.; Dinescu, G., Surface Plasma Functionalization Influences Macrophage Behavior on Carbon Nanowalls. *Mater. Sci. Eng., C* **2015,** *48*, 118-125.
37. Pompe, T.; Keller, K.; Mothes, G.; Nitschke, M.; Teese, M.; Zimmermann, R.; Werner, C., Surface Modification of Poly (hydroxybutyrate) Films to Control Cell–matrix Adhesion. *Biomaterials* **2007,** *28* (1), 28-37.
38. O'Toole, L.; Mayhew, C. A.; Short, R. D., On the Plasma Polymerisation of Allyl Alcohol: an Investigation of Ion–molecule Reactions Using a Selected Ion Flow Tube. *J. Chem. Soc., Faraday Trans.* **1997,** *93* (10), 1961-1964.
39. O'Toole, L., Short, R. D., An Investigation of the Mechanisms of Plasma Polymerisation of Allyl Alcohol. *J. Chem. Soc., Faraday Trans.* **1997,** *93* (6), 1141-1145.
40. Fahmy, A.; Mix, R.; Schönhals, A.; Friedrich, J., Structure–Property Relationship of Thin Plasma Deposited Poly (allyl alcohol) Films. *Plasma Chem. Plasma Process.* **2011,** *31* (3), 477-498.
41. Gallino, E.; Massey, S.; Tatoulian, M.; Mantovani, D., Plasma Polymerized Allylamine Films Deposited on 316L Stainless Steel for Cardiovascular Stent Coatings. *Surf. Coat. Technol.* **2010,** *205* (7), 2461-2468.
42. Beck, A. J.; Candan, S.; France, R. M.; Jones, F. R.; Short, R. D., A Mass Spectral Investigation of the RF Plasmas of Small Organic Compounds: An Investigation of the Plasma-phase Reactions in the Plasma Deposition from Allyl Amine. *Plasmas Polym.* **1998,** *3* (2), 97-114.
43. Massey, S.; Gallino, E.; Cloutier, P.; Tatoulian, M.; Sanche, L.; Mantovani, D.; Roy, D., Low-energy Electrons and X-ray Irradiation Effects on Plasma-Polymerized Allylamine Bioactive Coatings for Stents. *Polym. Degrad. Stab.* **2010,** *95* (2), 153-163.

44. Hawker, M. J.; Pegalajar-Jurado, A.; Fisher, E. R., Conformal Encapsulation of Three-Dimensional, Bioresorbable Polymeric Scaffolds Using Plasma-Enhanced Chemical Vapor Deposition. *Langmuir* **2014,** *30* (41), 12328-12336.
45. Denis, L.; Cossement, D.; Godfroid, T.; Renaux, F.; Bittencourt, C.; Snyders, R.; Hecq, M., Synthesis of Allylamine Plasma Polymer Films: Correlation Between Plasma Diagnostic and Film Characteristics. *Plasma Process. Polym.* **2009,** *6* (3), 199-208.
46. Beck, A. J.; Candan, S.; Short, R. D.; Goodyear, A.; Braithwaite, N. S. J., The Role of Ions in the Plasma Polymerization of Allylamine. *J. Phys. Chem. B* **2001,** *105* (24), 5730-5736.
47. Zhang, J.; Feng, X.; Xie, H.; Shi, Y.; Pu, T.; Guo, Y., The Characterization of Structure-tailored Plasma Films Deposited from the Pulsed RF Discharge. *Thin Solid Films* **2003,** *435* (1), 108-115.
48. Rinsch, C. L.; Chen, X.; Panchalingam, V.; Eberhart, R. C.; Wang, J.-H.; Timmons, R. B., Pulsed Radio Frequency Plasma Polymerization of Allyl Alcohol: Controlled Deposition of Surface Hydroxyl Groups. *Langmuir* **1996,** *12* (12), 2995-3002.
49. Fisher, E. R., Challenges in the Characterization of Plasma-Processed Three-dimensional Polymeric Scaffolds for Biomedical Applications. *ACS Appl. Mater. Interfaces* **2013,** *5* (19), 9312-9321.
50. Intranuovo, F.; Gristina, R.; Brun, F.; Mohammadi, S.; Ceccone, G.; Sardella, E.; Rossi, F.; Tromba, G.; Favia, P., Plasma Modification of PCL Porous Scaffolds Fabricated by Solvent-Casting/Particulate-Leaching for Tissue Engineering. *Plasma Process. Polym.* **2014,** *11* (2), 184-195.
51. Igarashi, S.; Itakura, A. N.; Toda, M.; Kitajima, M.; Chu, L.; Chifen, A. N.; Förch, R.; Berger, R., Swelling Signals of Polymer Films Measured by a Combination of Micromechanical Cantilever Sensor and Surface Plasmon Resonance Spectroscopy. *Sens. Actuators, B* **2006,** *117* (1), 43-49.
52. Zhang, Z.; Chen, Q.; Knoll, W.; Förch, R., Effect of Aqueous Solution on Functional Plasma Polymerized Films. *Surf. Coat. Technol.* **2003,** *174*, 588-590.

CHAPTER 7

MODIFCATION OF A COMMERCIAL THROMBOELASTOGRAPHY INSTRUMENT TO MEASURE COAGULATION DYNAMICS WITH THREE-DIMENSIONAL BIOMATERIALS

This chapter expands on research presented in Chapters 3, 5, and 6, specifically regarding response of plasma-modified 3D porous scaffolds in biological systems. In these chapters, scaffolds have been interfaced with simplistic biological systems limited to mammalian cells (human dermal fibroblasts) and gram-negative bacteria cells (*E. Coli*). Although such an exploration has yielded valuable insight regarding cell-surface interactions of plasma-modified 3D polymers, interfacing with more complex biological systems (e.g., blood) is, however, more realistic for construct deployment in biomedical devices. Understanding coagulation phenomena is arguably the most critical aspect for applications involving synthetic biomaterial devices, however, real-time evaluation of the clot formation while interfacing with these materials is difficult to achieve in a reproducible and robust manner. Here, we present work representing first steps toward addressing this deficit, wherein we have fabricated modified consumables for a clinical thromboelastography (TEG) instrument. TEG measures viscoelastic properties throughout clot formation and therefore provides clinically-relevant coagulation measurements in real time (i.e., kinetics and strength of clot formation). Through our modification, TEG consumables can readily accommodate three-dimensional materials (e.g., those for regenerative tissue applications). We performed proof-of-concept experiments using polymer scaffolds with a range of surface properties, and demonstrated that variations in surface properties resulted in differences in blood plasma coagulation dynamics. For example, maximum rate of thrombus

generation ranged from 22.2 ± 2.2 (dyne/cm^2)/s for fluorocarbon coated scaffolds to 8.7 ± 1.0 (dyne/cm^2)/s for nitrogen-containing scaffolds. Through this work, we demonstrate the ability to make real-time coagulation activity measurements during constant coagulation factor interface with biomedically-relevant materials.

This chapter is based on work published in *Biointerphases* by Morgan J. Hawker, Christine S. Olver, and Ellen R. Fisher, and is reproduced with permission, American Vacuum Society, 2016.[1] This work is supported by the National Science Foundation (CHE-1152963), the Colorado Office of Economic Development via the Biosciences Discovery Evaluation Grant (BDEG) Program, and the Vice President for Research at Colorado State University (Compatible Polymer Network Catalyst for Innovative Partnerships funding, CPN CIP). I would like to thank members of the CPN CIP team at Colorado State University for inspiring this project, especially Dr. Matthew J. Kipper. I would also like to thank Christine Olver for her mentorship and insight throughout working on the TEG projects that became this chapter, as well as John Wydallis and Rachel Feeny for assistance with 3D printing and helpful discussions related to consumable design.

7.1 Introduction

Millions of blood-contacting devices (e.g., vascular grafts, stents) are deployed in medical settings annually[2] and a recent review claims the global biomaterials market will grow by 15% per annum, reaching a value of ~$84 billion by 2017.[3] As thrombosis is a primary cause of device failure for such synthetic materials implanted in the body, evaluating coagulation behavior of blood-interfacing materials is critical.[4-6] Although the phrase "blood-interfacing materials" includes many different forms (i.e., suspensions, powders, thin films, hydrogels), delivering a range of functions in blood-contacting applications, we focus here on solid, three-

dimensional, porous constructs designed for wound healing and tissue engineering applications. Despite the importance of assessing coagulation at synthetic biomaterial interfaces, substantial debate revolves around the suitability of existing *in vitro* hemocompatibility tests for such assessment.[7] Thus, creating methodologies that allow translation from the fundamental biomaterials laboratory to clinical setting is imperative. Therefore, developing techniques to provide a more clinically-relevant analysis of coagulation activity at the blood/synthetic biomaterial interface is a critical component of this translational activity.

Thromboelastography (TEG) is a rheometry-based clinical tool used to assess coagulation dynamics of whole blood and blood plasma. A detailed description of standard TEG instrumental operation procedures, as well as the theory and principles governing the TEG technique, can be found elsewhere.[8-12] Briefly, clinical TEG use includes loading a plastic (Cyrolite®) cup into a holder on a stage that slowly rotates (4º45' over 10 s) about a stationary pin attached to a torsion wire. A small volume of whole blood or blood plasma is then added to the cup (typically 330-360 μL), often along with activators (i.e., tissue factor, celite, calcium if blood is citrated), and viscoelasticity measurements of the developing clot are collected in real time. Rapid, point of care measurements of time to clot, clot strength, and rate of clot formation[8] are each used in the clinical setting to guide specific blood component therapy in patients severely at risk for bleeding (e.g., cardiac surgery, acute traumatic coagulopathy, obstetrics), thus reducing total transfusion requirements.[13]

Few studies have reported using TEG instrumentation for the analysis of synthetic blood-interfacing materials. A complete description of TEG analysis of materials can be found elsewhere;[14-15] here we include a (non-exhaustive) summary. Several studies focused on coating the interior of the TEG cup with a thin layer of a blood-insoluble polymer either via dropcasting

techniques[16-18] or using low-temperature plasma polymerization (such as those described in Chapters 3–6 of this dissertation).[19-20] Herein, we will refer to low-temperature plasmas as LTPs to avoid confusion with blood plasma. Whole blood or blood plasma was then added to the modified consumables and coagulation dynamics were measured using TEG. Several alternative approaches to modifying standard TEG consumables have been explored. One alternative involves injecting a small volume of a polymer suspension or slurry into either whole blood or blood plasma in the TEG cup,[21-23] and another includes incubating solid constructs in blood, removing the blood, and pipetting it into the standard TEG consumables for analysis.[14, 24] An additional alternative involves a perfusion-based method where blood is flowed through a material and then used for subsequent TEG analysis.[25-26] To our knowledge, only one study has performed a real-time evaluation of blood interfacing with a solid material within the TEG cup, albeit this study evaluated relatively thin films (area ~0.25 cm^2) with relatively small features (<100 nm).[27]

Although real-time quantitative analysis of coagulation while blood is simultaneously interfacing with a solid construct is perhaps most realistic in terms of the ultimate *in vivo* application of solid implant materials, only one of the studies described above does so. Existing TEG consumables have, however, only <50 μL of accessible volume after the addition of blood, and thus, do not allow for the placement of three-dimensional solid constructs within the TEG cup (at least not those on a scale relevant to tissue engineering or wound healing constructs). Therefore, additional instrumental modification is necessary to realize the enormous potential of TEG for the analysis of the global effects of solid materials on coagulation. This modification includes creating new consumables designed to accommodate the solid construct of interest. Although many next-generation constructs for blood-contacting applications have three-

dimensional architectures,[28-31] the capability to evaluate coagulation behavior of blood interfacing with 3D constructs is an important step in optimizing performance testing. If successful, a clinically-relevant coagulation analysis using TEG would be invaluable for blood-interfacing material screening and eventually in patient-specific, point-of-care applications for personalizing (or, "individual-optimized") blood-interfacing materials. In this work, we report the modification of clinical TEG instrumentation through designing new TEG consumables that can accommodate solid constructs with complex geometries. Through this modification, we demonstrate the ability to evaluate coagulation dynamics while blood plasma is interfacing with model materials having a range of surface properties (LTP-modified three-dimensional polymer scaffolds).

We selected three LTP-modified scaffolds based on previous assessments of construct interactions with biological systems [mammalian cells (human dermal fibroblasts, HDF, and human Saos-2 osteoblasts) and gram-negative bacteria (*E. coli*)]. These constructs included fluorocarbon (FC), allylamine (allylNH) and water vapor LTP-modified scaffolds. As discussed in Chapter 5, the FC surface is low-fouling toward both HDF and *E. coli*, and could be applicable when mitigating attachment of these biological species is of interest.[32] As discussed in Chapter 6, allylNH LTP treated scaffolds show enhanced HDF viability relative to untreated materials and thus have potential in wound healing or other tissue engineering applications.[33] Scaffolds treated with H_2O LTPs had enhanced Saos-2 osteoblast attachment and viability relative to untreated scaffolds, demonstrating their potential for use in bone regeneration.[34]

The present study establishes the ability to measure the effects of fabricated consumables on coagulation by detecting differences in several viscoelastic parameters when

clotting plasma is exposed to a variety of solid constructs. This research thus aids in bridging the gap between fundamental biomaterials and clinical laboratories.

7.2 Results

The overarching goal of this study was to modify a TEG instrument to accommodate 3D solid materials with significant volume such that blood coagulation dynamics in the presence of these materials could be measured. To evaluate the efficacy of our instrumental modification, 3D porous PCL scaffolds were selected as model materials both because of their potential utility in biomedical device applications, and because of previous success in LTP processing these constructs.[32-38] Here, we have chosen to evaluate plasmatic coagulation dynamics of four different constructs: unmodified, C_3F_8, allylNH, and H_2O LTP-modified PCL scaffolds.

7.2.1 PCL scaffold characterization. Surface and bulk properties of scaffolds included in TEG experiments were identical to those reported elsewhere in this dissertation. Nonetheless, data pertaining to scaffold surface chemistry and wettability data are summarized in Table 7.1, demonstrating that comparatively, materials utilized in this study have vastly different surface properties with respect to chemical composition and to wettability. The native scaffold surface contains carbon and oxygen (O/C = 0.34 ± 0.01) in hydrocarbon and ester functionality.[32] Furthermore, these materials are hydrophobic, with a static WCA of 119.5 ± 1.6º. C_3F_8 LTP modification results in conformal fluorocarbon film deposition on the exterior of the scaffold (F/C = 1.50 ± 0.04) with CF, CF_2, and CF_3 functionality - an even more hydrophobic surface (WCA = 134.6 ± 2.2º) than unmodified PCL. AllylNH LTP treated scaffolds have surface nitrogen-containing functionality (N/C = 0.34 ± 0.02), primarily in the form of amine groups. H_2O LTP-modified scaffolds have a similar elemental composition to untreated scaffolds (O/C = 0.45 ± 0.04), but contain alcohol functionality.[34, 38] Both allylNH and H_2O LTP treated

Table 7.1. Elemental composition and wettability of 3D polymeric materials evaluated with TEG.[a] Measurements represent the mean ± standard deviation for n ≥ 9.

Material	O/C	F/C	N/C	Static WCA (º)
Native PCL scaffold	0.34 ± 0.01	--	--	119.5 ± 1.6
C_3F_8 treated PCL scaffold	0.02 ± 0.01	1.50 ± 0.04	--	134.6 ± 2.2
AllylNH treated PCL scaffold	0.05 ± 0.01	--	0.34 ± 0.02	hydrophilic [c]
H_2O treated PCL scaffold	0.45 ± 0.04 [b]	--	--	hydrophilic [c]

[a] Composition data from high-resolution X-ray photoelectron spectroscopy analysis and wettability from water contact angle goniometry.
[b] Data from references 37 and 38.
[c] Because water and allylNH LTP-modified PCL scaffolds absorbed water drops upon WCA measurements, it was not possible to measure a static WCA value.

scaffolds are nominally hydrophilic and fully absorbed water drops used for CA experiments (either 5 or 6 μL) in <10 s. Representative SEM images of untreated and allylNH LTP treated scaffolds (Figure 6.2b) demonstrate the interconnected porous PCL scaffold network is maintained upon LTP treatment, which we have also observed in other LTP modification systems.[32, 36-37] Altogether, the three types of LTP-modified scaffolds presented in this work, C_3F_8, allylNH, and H_2O LTP treated, showcase extremes on both the surface properties and biological interactions spectra (as discussed in Section 7.1): a hydrophobic FC surface (low-fouling) and hydrophilic N- and O- containing surfaces (mammalian cell attachment and enhanced cell viability). With differences in surface characteristics and biological responsiveness in mind, one would expect the LTP-treated materials to have disparate effects on blood coagulation activity.

7.2.2 Design optimization for TEG analysis of solid materials. Initial experiments demonstrated that ABS cups caused blood plasma to be hypercoagulable in comparison to commercial Cyrolite® cups (Figure 7.1). It is important to note that the focus of this study is to systematically compare blood plasma coagulation activity upon interfacing plasma with solid constructs. Thus, all TEG data presented here were collected using our 3D printed ABS cups and Cyrolite® cups were not utilized. CAD models of the experimental set-up used in these TEG experiments can be found in Chapter 2 (Figure 2.4).

Upon first interfacing 3D printed cups with the TEG instrument, the instrument reported an error that consumables were improperly loaded. We eliminated the possibility that the error was arising from friction between the pin and the inside of the 3D printed cup by determining that the interior cup dimensions were identical to the commercial consumables. Rather, we found that the consumable loading error occurred because of instability between the load cell and the

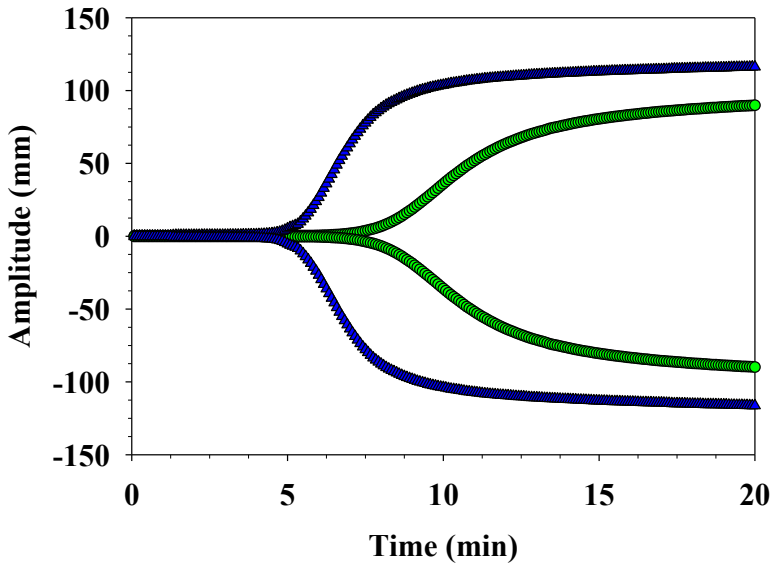

Figure 7.1. Representative TEG tracings for blood plasma in commercially-available Cyrolite® cups (green circles) and 3D printed ABS cups with identical dimensions (blue triangles). Both tracings were collected for blank cups (i.e., without materials loaded) using calf plasma.

stage. To establish this as the cause of error, and to rectify the problem, we added a machined PTFE spacer as part of our modification, effectively mimicking the stage material, which is similar to PTFE. Multiple spacers were fabricated such that two runs could be performed simultaneously as the instrument is equipped with two sample holders, Figure 2.4a. Preliminary experiments showed differences in the signals between the two channels using otherwise identical experimental conditions. In particular, one channel would consistently show an elevated baseline during a set of TEG runs (Figure 7.2). Ultimately, we found that the roughness of the PTFE spacer affected the signal, where rougher surfaces resulted in elevated baselines. With the additional modification of using smoother PTFE spacers, repeatable TEG data could be collected.

7.2.3 TEG analysis of polymer scaffolds with different surface properties. The ability to modify a TEG instrument to accommodate solid constructs was evaluated using untreated and LTP-modified PCL scaffolds as model materials. Figure 7.3 shows representative standard thromboelastograph tracings and corresponding velocity curves. Data obtained from thromboelastographs are listed in Table 7.2, including R, MA, and TMA. Data from the velocity curves are also included in Table 7.2 (MRTG, TTG, and TMRTG. Additionally, the MRTG and TTG are displayed graphically in Figure 7.4.

7.3 Discussion

This study represents one of very few translations between the fundamental biomaterials and clinical settings of TEG, and to our knowledge, the only TEG evaluation of (relatively large) 3D porous constructs. Overall, data presented here provide strong evidence for this proof-of-concept evaluation because they demonstrate the capability to measure clear differences in blood coagulation behavior between the three-dimensional constructs analyzed. It is, however,

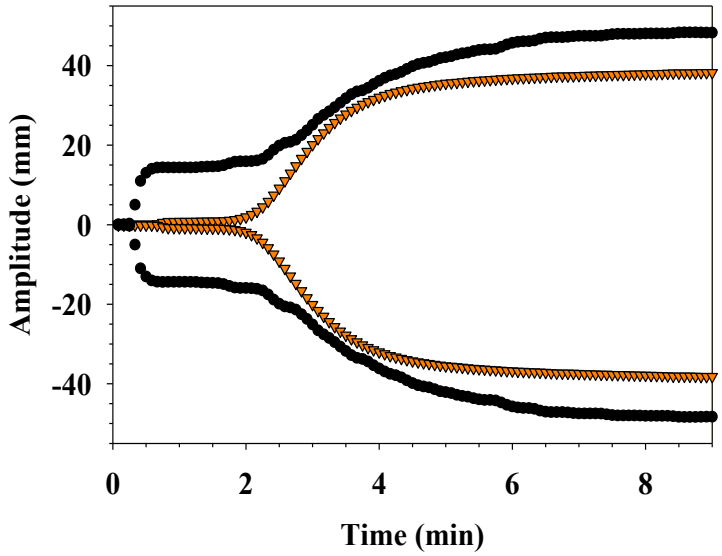

Figure 7.2. Representative TEG tracings with an elevated baseline (black circles) and a non-elevated baseline (orange triangles). Both tracings were collected for cups loaded with untreated PCL scaffolds.

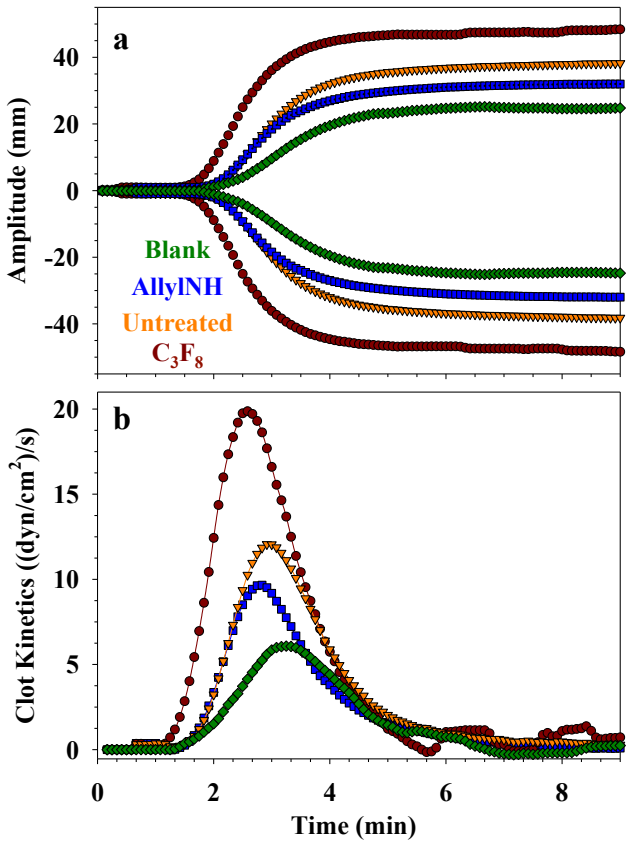

Figure 7.3. Representative examples of (a) the TEG tracings and (b) the velocity curves [the first derivatives of the data in (a)] for a blank cups (no added 3D material) and untreated and plasma treated 3D PCL scaffolds.

Table 7.2. Summary of quantitative clot kinetic measurements upon interfacing each material with human blood plasma Measurements represent the mean ± standard deviation for n = 3.

Scaffold	**Reaction time (min)**	**Maximum amplitude (mm)**	**Time to maximum amplitude (min)**	**Maximum rate of thrombus generation ((dyn/cm^2)/s)**	**Time to maximum rate of thrombus generation (min)**	**Total thrombus generation (dyn/cm^2)**
	R	MA	TMA	MRTG	TMRTG	TTG
None (blank cup)	1.5 ± 1.1	27.0 ± 2.5	8.9 ± 3.1	7.5 ± 1.3	2.9 ± 0.3	185.5 ± 22.4
Untreated	1.3 ± 0.9	40.3 ± 3.5	9.0 ± 3.1	12.0 ± 1.3	2.7 ± 0.3	337.7 ± 40.3
C_3F_8 LTP treated	1.3 ± 0.3	54.1 ± 4.9	8.2 ± 1.0	22.2 ± 2.2	2.6 ± 0.1	549.5 ± 69.2
AllylNH LTP treated	1.9 ± <0.1	32.3 ± 4.6	8.1 ± 2.2	8.7 ± 1.0	3.1 ± 0.4	237.4 ± 46.3

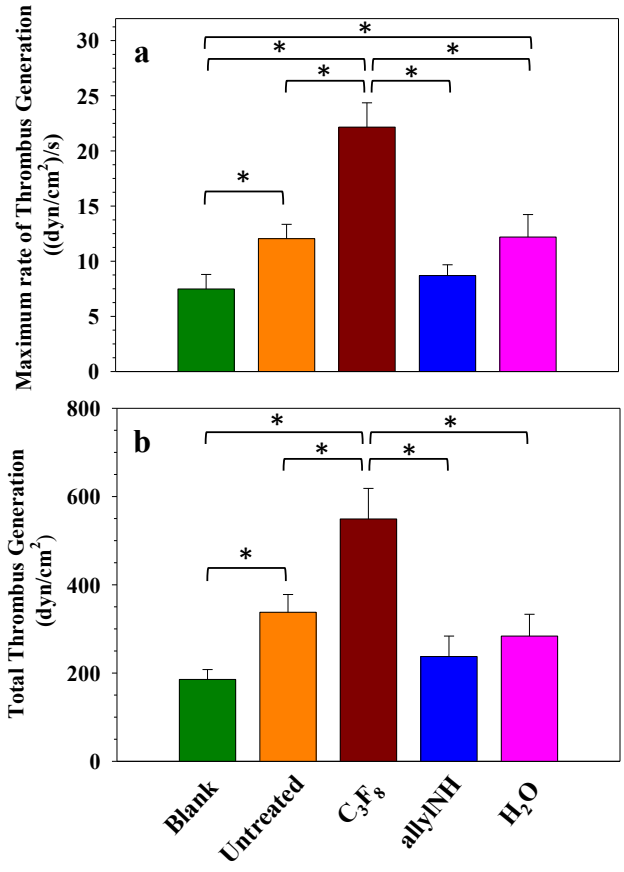

Figure 7.4. Figures of merit from TEG velocity curve data for blank cups with no material (green), cups loaded with untreated (orange), C_3F_8 (red), allylNH (blue), and H_2O plasma-treated (pink) scaffolds. Significant differences ($p < 0.05$) as determined from one-way ANOVA with post-hoc Tukey HSD tests are denoted by asterisks. For each type of sample, n = 3.

important to note that the interpretation of TEG data is challenging in light of complexities present in both the material and the blood plasma matrices, as well as in the coagulation pathways that become activated upon interaction with foreign material. The list of variables that influence coagulation is lengthy (including, but not limited to, substrate geometry, surface roughness, surface area, composition, functionality, charge, wettability, and mechanical properties) and it is often difficult to isolate a single variable. Although the primary goal of this work was to validate the efficacy of our instrumental modification, we would like to devote some discussion of our TEG data qualified by the abovementioned challenge.

One factor that likely influences the coagulation results in this study is the material surface roughness. The impact of roughness on thrombosis has been well established previously (albeit for different material systems than those presented here), and it is typically accepted that roughness is directly correlated with coagulation activation.[39-40] As demonstrated by SEM images of porogen-leached scaffolds (e.g., Fig. 6.2b), scaffold features are on the order of ~100 μm (much greater than the inner surface of the TEG consumables). Thus, an increase in rate of clot formation and clot strength upon the introduction of the untreated scaffold (compared to the blank trials) is rational. If roughness were the dominating factor controlling coagulation, we would expect to see similar responses for all scaffold constructs examined. As this is not the case, it is likely that additional material properties such as surface chemistry (i.e., surface functional groups), wettability, and surface charge are influencing coagulation dynamics. Although the interrelation of these properties makes it challenging to discern the effect of one versus the other on coagulation, the set of materials presented allows for several parallel comparisons.

Two materials with similar elemental composition (e.g., O/C ratios, Table 7.1) are untreated and H_2O LTP treated scaffolds. These materials show nearly identical TEG responses, indicating that the overall elemental composition, rather than specific type of oxygen functionality, may be more predictive of coagulation activity. Additionally, this finding suggests that surface wettability alone may not play a primary role in independently determining TEG/coagulation response. Although there has been substantial discussion in the literature related to influence of wetting behavior on coagulation, a clear correlation between wettability and coagulation does not exist. For example, Hong et al. demonstrated that hydrophilic surface-modified titanium constructs (i.e., completely wetting, WCA = 0º) show increased thrombogenesis over relatively hydrophobic controls (WCA >90º).[41] Others have demonstrated that more hydrophobic constructs (WCAs >100º) show increased platelet adhesion relative to those with WCAs <80º); however, differences in wettability in this study were strongly influenced by differences in roughness.[42] Although we did not measure platelet adhesion in the present study, it is one of many factors that influences coagulation. Another study by Senthilkumar et al. demonstrated that only minor differences in surface wettability (WCA ~50º vs. 60º) showed substantial changes in blood coagulation behavior, with the more hydrophobic surface exhibiting an increase in coagulation (determined by shorter activated partial thromboplastin time and shorter prothrombin time).[43] Again, variations in wetting properties were confounded by differences in material morphology and roughness, making it challenging to establish a direct relationship between wettability and coagulation. Moreover, activated partial thromboplastin time and prothrombin time measurements only represent a small portion of coagulation, whereas TEG measurements capture the entire coagulation cascade. Studies wherein coatings were deposited on the inside of TEG cups reported that minor (<30º)[16, 18] or no[17]

differences in wettability between unmodified and modified materials lead to substantial differences in TEG response, although these studies incorporated either silver nanoparticles,[16] antibodies,[18] or heparin[17] into the polymer coatings. These species may have a more profound influence on coagulation than wettability alone.

Additional evidence that wettability does not primarily control coagulation in the context of materials evaluated here comes when comparing the TEG response of materials with similar wetting behavior, such as untreated and C_3F_8 LTP-modified constructs. These materials are similarly hydrophobic, but have disparate surface chemistries (i.e., elemental composition and functionality). Because they are traditionally considered to be low-fouling, it may seem counterintuitive that FC-coated surfaces promote coagulation when compared with untreated scaffolds.[44] Previous work with microporous PTFE materials, however, demonstrated that unmodified (FC-like) constructs showed enhanced TEG response (i.e., they had lower MA values) when compared with modified (hydrophilic) constructs.[24] This is perhaps a more rational comparison to materials in the present study relative to explorations of coagulation upon interfacing non-porous FC films (e.g., work by Wang et al.),[44] although it is important to note that microporous PTFE constructs were incubated in blood that was used for subsequent TEG analysis. This differs from the present work where TEG was performed with the blood plasma interfacing with solid constructs throughout data collection.

A similar comparison to the untreated/C_3F_8 LTP treated materials can be made when comparing H_2O LTP-modified and allylNH LTP-modified scaffolds. These two materials also have comparable wettability (both are water sorbing and nominally hydrophilic) despite differences in surface chemistry. Although differences in each of the TEG statistics presented here are not statistically significant, we observe an overall reduction in coagulation behavior for

the allylNH LTP treated constructs. Moreover, differences in TEG response are statistically significant when comparing untreated with allylNH LTP treated materials. Previous evidence that nitrogen inclusion reduces coagulation response exists, though many studies assessing nitrogen incorporation utilize nickel-free nitrogen containing stainless steel materials for surgical applications rather than porous polymeric constructs.[45-46]

It is likely that additional material properties are playing a major role in differences in coagulation dynamics observed, especially surface charge. Although a systematic study of the effect of surface charge on coagulation has not been performed to our knowledge, surface charge is known to have an impact on hemostasis as assessed using TEG.[19] We have not, however, performed any direct surface charge measurements (e.g., zeta potential) on the current set of materials. This type of analysis could provide an additional detail influencing mechanisms at play when different scaffold constructs are interfaced with blood plasma. As a final note, we acknowledge that blood interfacing with synthetic biomaterials is an incredibly complicated system. Ideally, we would be able to separate specific contributions of each material property as well as each element in the coagulation cascade process. Thus, the work presented here offers valuable insight and hope for unraveling the details in this complex milieu.

7.4 Summary

Here, we demonstrated the ability to effectively modify TEG consumables to accommodate relatively large 3D constructs. In doing so, we were able to measure dynamic blood coagulation behavior while blood plasma was in contact with polymer scaffolds having significantly different surface properties. This work represents one of the few examples of an explicit attempt to bridge the gap between fundamental biomaterials studies and clinical evaluation of blood coagulation dynamics, critical for rapid advancement of new materials into

clinical settings. The results here clearly reveal coagulation behavior is dependent on surface properties. Nevertheless, the intertwined relationship between factors such as surface wettability and chemical composition make it difficult to deconstruct the impact of any individual material property on coagulation dynamics. Clearly, this represents an opportunity for further exploration.

REFERENCES

1. Hawker, M. J.; Olver, C. S.; Fisher, E. R., Modification of a Commercial Thromboelastography Instrument to Measure Coagulation Dynamics with Three-dimensional Biomaterials. *Biointerphases* **2016,** *11* (2).
2. Ratner, B. D., The Catastrophe Revisited: Blood Compatibility in the 21st Century. *Biomaterials* **2007,** *28* (34), 5144-5147.
3. John, A.; Subramanian, A.; Vellayappan, M.; Balaji, A.; Jaganathan, S.; Mohandas, H.; Paramalinggam, T.; Supriyanto, E.; Yusof, M., Review: Physico-chemical Modification as a Versatile Strategy for the Biocompatibility Enhancement of Biomaterials. *RSC Adv.* **2015,** *5* (49), 39232-39244.
4. Brisbois, E. J.; Handa, H.; Meyerhoff, M. E., Recent Advances in Hemocompatible Polymers for Biomedical Applications. In *Advanced Polymers in Medicine*, Springer: 2015; pp 481-511.
5. Gorbet, M. B.; Sefton, M. V., Biomaterial-associated Thrombosis: Roles of Coagulation Factors, Complement, Platelets and Leukocytes. *Biomaterials* **2004,** *25* (26), 5681-5703.
6. Xu, L.-C.; Bauer, J. W.; Siedlecki, C. A., Proteins, Platelets, and Blood Coagulation at Biomaterial Interfaces. *Colloids Surf., B* **2014,** *124*, 49-68.
7. Braune, S.; Grunze, M.; Straub, A.; Jung, F., Are There Sufficient Standards for the in vitro Hemocompatibility Testing of Biomaterials? *Biointerphases* **2013,** *8* (1), 33.
8. TEG® 5000 Thrombelastograph® Hemostasis System User Manual. *Haemoscope Corporation, Niles, IL, USA.* **2004**, 1-11.
9. Luddington, R., Thrombelastography/Thromboelastometry. *Clin. Lab. Haematol.* **2005,** *27* (2), 81-90.
10. Bolliger, D.; Seeberger, M. D.; Tanaka, K. A., Principles and Practice of Thromboelastography in Clinical Coagulation Management and Transfusion Practice. *Transfus. Med. Rev.* **2012,** *26* (1), 1-13.
11. Ellis, T. C.; Nielsen, V. G.; Marques, M. B.; Kirklin, J. K., Thrombelastographic Measures of Clot Propagation: A Comparison of Alpha with the Maximum Rate of Thrombus Generation. *Blood Coagul. Fibrinolysis* **2007,** *18* (1), 45-48.
12. Nielsen, V. G., Beyond Cell Based Models of Coagulation: Analyses of Coagulation with Clot "Lifespan" Resistance-time Relationships. *Thromb. Res.* **2008,** *122* (2), 145-152.
13. Whiting, D.; DiNardo, J. A., TEG and ROTEM: Technology and Clinical Applications. *Am. J. Hematol.* **2014,** *89* (2), 228-232.
14. Shankarraman, V.; Davis-Gorman, G.; Copeland, J. G.; Caplan, M. R.; McDonagh, P. F., Standardized Methods to Quantify Thrombogenicity of Blood-contacting Materials via Thromboelastography. *J. Biomed. Mater. Res. Part B Appl. Biomater.* **2012,** *100* (1), 230-238.
15. Peng, H. T., Thromboelastographic Study of Biomaterials. *J. Biomed. Mater. Res. Part B Appl. Biomater.* **2010,** *94* (2), 469-485.
16. de Mel, A.; Chaloupka, K.; Malam, Y.; Darbyshire, A.; Cousins, B.; Seifalian, A. M., A Silver Nanocomposite Biomaterial for Blood-contacting Implants. *J. Biomed. Mater. Res. A* **2012,** *100* (9), 2348-2357.

17. Leung, J. M.; Berry, L. R.; Chan, A. K.; Brash, J. L., Surface Modification of Polydimethylsiloxane with a Covalent Antithrombin-heparin Complex to Prevent Thrombosis. *J. Biomater. Sci., Polym. Ed.* **2014,** *25* (8), 786-801.
18. Tan, A.; Goh, D.; Farhatnia, Y.; Natasha, G.; Lim, J.; Teoh, S.-H.; Rajadas, J.; Alavijeh, M. S.; Seifalian, A. M., An Anti-CD34 Antibody-functionalized Clinical-grade POSS-PCU Nanocomposite Polymer for Cardiovascular Stent Coating Applications: A Preliminary Assessment of Endothelial Progenitor Cell Capture and Hemocompatibility. *PLoS One* **2013,** *8* (10), e77112.
19. Contreras-García, A.; Merhi, Y.; Ruiz, J. C.; Wertheimer, M. R.; Hoemann, C. D., Thromboelastography (TEG) Cups and Pins with Different PECVD Coatings: Effect on the Coagulation Cascade in Platelet-poor Blood Plasma. *Plasma Process. Polym.* **2013,** *10* (9), 817-828.
20. Schubert, A.; Wurlitzer, S.; Calatzis, A.; Glauner, M. Surface Treatment of Plastics by Exposing it to Ionized Atoms or Molecules, to Increase the Adhesion Strength of Coagulated Blood on the Surface by Increasing the Surface Interaction of Blood Components like Fibrin, Fibrinogen and Thrombocytes; used in Blood Diagnostics such as Hemostasis Analysis. 7745223 B2, June 29, 2010.
21. Zhang, W.; Zhong, D.; Liu, Q.; Zhang, Y.; Li, N.; Wang, Q.; Liu, Z.; Xue, W., Effect of Chitosan and Carboxymethyl Chitosan on Fibrinogen Structure and Blood Coagulation. *J. Biomater. Sci., Polym. Ed.* **2013,** *24* (13), 1549-1563.
22. Valeri, C. R.; Srey, R.; Tilahun, D.; Ragno, G., In vitro Effects of Poly-N-acetyl Glucosamine on the Activation of Platelets in Platelet-rich Plasma with and without Red Blood Cells. *J. Trauma Acute Care Surg.* **2004,** *57* (1), S22-S25.
23. Lai, B. F.; Creagh, A. L.; Janzen, J.; Haynes, C. A.; Brooks, D. E.; Kizhakkedathu, J. N., The Induction of Thrombus Generation on Nanostructured Neutral Polymer Brush Surfaces. *Biomaterials* **2010,** *31* (26), 6710-6718.
24. Chevallier, P.; Janvier, R.; Mantovani, D.; Laroche, G., In vitro Biological Performances of Phosphorylcholine-grafted ePTFE Prostheses through RFGD Plasma Techniques. *Macromol. Biosci.* **2005,** *5* (9), 829-839.
25. Haraguchi, K.; Takehisa, T.; Mizuno, T.; Kubota, K., Antithrombogenic Properties of Amphiphilic Block Copolymer Coatings: Evaluation of Hemocompatibility Using Whole Blood. *ACS Biomater. Sci. Eng.* **2015,** *1* (6), 352-362.
26. Klöcking, H.-P.; Schunk, W.; Merkmann, G.; Giessmann, C.; Knoll, H.; Borgmann, S., A Natural Rubber Drainage Tube with Antithrombogenic Lumen Surface. *Thromb. Res.* **1993,** *72* (6), 501-507.
27. Murugesan, S.; Mousa, S.; Vijayaraghavan, A.; Ajayan, P. M.; Linhardt, R. J., Ionic Liquid-derived Blood-compatible Composite Nembranes for Kidney Dialysis. *J. Biomed. Mater. Res. Part B Appl. Biomater.* **2006,** *79* (2), 298-304.
28. Rezwan, K.; Chen, Q.; Blaker, J.; Boccaccini, A. R., Biodegradable and Bioactive Porous Polymer/Inorganic Composite Scaffolds for Bone Tissue Engineering. *Biomaterials* **2006,** *27* (18), 3413-3431.
29. Karageorgiou, V.; Kaplan, D., Porosity of 3D Biomaterial Scaffolds and Osteogenesis. *Biomaterials* **2005,** *26* (27), 5474-5491.
30. Lutolf, M.; Hubbell, J., Synthetic Biomaterials as Instructive Extracellular Microenvironments for Morphogenesis in Tissue Engineering. *Nat. Biotechnol.* **2005,** *23* (1), 47-55.

31. Lee, J.; Cuddihy, M. J.; Kotov, N. A., Three-dimensional Cell Culture Matrices: State of the Art. *Tissue Engineering Part B: Reviews* **2008,** *14* (1), 61-86.
32. Hawker, M. J.; Pegalajar-Jurado, A.; Fisher, E. R., Conformal Encapsulation of Three-Dimensional, Bioresorbable Polymeric Scaffolds Using Plasma-Enhanced Chemical Vapor Deposition. *Langmuir* **2014,** *30* (41), 12328-12336.
33. Hawker, M. J.; Pegalajar-Jurado, A.; Hicks, K. I.; Shearer, J. C.; Fisher, E. R., Allylamine and Allyl Alcohol Plasma Copolymerization: Synthesis of Customizable Biologically-Reactive Three-Dimensional Scaffolds. *Plasma Process. Polym.* **2015,** *12* (12), 1435-1450.
34. Sardella, E.; Fisher, E. R.; Shearer, J. C.; Garzia Trulli, M.; Gristina, R.; Favia, P., N_2/H_2O Plasma Assisted Functionalization of Poly(ε-caprolactone) Porous Scaffolds: Acidic/Basic Character versus Cell Behavior. *Plasma Process. Polym.* **2015**.
35. Fisher, E. R., Challenges in the Characterization of Plasma-Processed Three-dimensional Polymeric Scaffolds for Biomedical Applications. *ACS Appl. Mater. Interfaces* **2013,** *5* (19), 9312-9321.
36. Hawker, M. J.; Pegalajar-Jurado, A.; Fisher, E. R., Innovative Applications of Surface Wettability Measurements for Plasma-Modified Three-Dimensional Porous Polymeric Materials: A Review. *Plasma Process. Polym.* **2015,** *12* (9), 846-863.
37. Intranuovo, F.; Gristina, R.; Brun, F.; Mohammadi, S.; Ceccone, G.; Sardella, E.; Rossi, F.; Tromba, G.; Favia, P., Plasma Modification of PCL Porous Scaffolds Fabricated by Solvent-Casting/Particulate-Leaching for Tissue Engineering. *Plasma Process. Polym.* **2014,** *11* (2), 184-195.
38. Shearer, J. C. Enhanced Surface Functionality via Plasma Modification and Plasma Deposition Techniques to Create More Biologically Relevant Materials. Ph.D. Dissertation, Colorado State University, Fort Collins, CO, 2013.
39. Takami, Y.; Nakazawa, T.; Makinouchi, K.; Tayama, E.; Glueck, J.; Benkowski, R.; Nosé, Y., Hemolytic Effect of Surface Roughness of an Impeller in a Centrifugal Blood Pump. *Artif. Organs* **1997,** *21* (7), 686-690.
40. Milleret, V.; Hefti, T.; Hall, H.; Vogel, V.; Eberli, D., Influence of the Fiber Diameter and Surface Roughness of Electrospun Vascular Grafts on Blood Activation. *Acta Biomater.* **2012,** *8* (12), 4349-4356.
41. Hong, J.; Kurt, S.; Thor, A., A Hydrophilic Dental Implant Surface Exhibit Thrombogenic Properties in vitro. *Clin. Implant. Dent. Relat. Res.* **2013,** *15* (1), 105-112.
42. Kim, S. I.; Lee, B. R.; Lim, J. I.; Mun, C. H.; Jung, Y.; Kim, J.-H.; Kim, S. H., Preparation of Topographically Modified Poly (L-lactic acid)-b-Poly (ε-caprolactone)-b-poly (L-lactic acid) Tri-block Copolymer Film Surfaces and its Blood Compatibility. *Macromol. Res.* **2014,** *22* (11), 1229-1237.
43. Senthilkumar, S.; Rajesh, S.; Jayalakshmi, A.; Mohan, D., Biocompatibility and Separation Performance of Carboxylated Poly (ether-imide) Incorporated Polyacrylonitrile Membranes. *Sep. Purif. Technol.* **2013,** *107*, 297-309.
44. Wang, S.; Gupta, A. S.; Sagnella, S.; Barendt, P. M.; Kottke-Marchant, K.; Marchant, R. E., Biomimetic Fluorocarbon Surfactant Polymers Reduce Platelet Adhesion on PTFE/ePTFE Surfaces. *J. Biomater. Sci., Polym. Ed.* **2009,** *20* (5-6), 619-635.
45. Lin, Y.-H.; Lan, W.-C.; Ou, K.-L.; Liu, C.-M.; Peng, P.-W., Hemocompatibility Evaluation of Plasma-nitrided Austenitic Stainless Steels at Low Temperature. *Surf. Coat. Technol.* **2012,** *206* (23), 4785-4790.

46. Wan, P.; Ren, Y.; Zhang, B.; Yang, K., Effect of Nitrogen on Blood Compatibility of Nickel-free High Nitrogen Stainless Steel for Biomaterial. *Mater. Sci. Eng., C* **2010,** *30* (8), 1183-1189.

CHAPTER 8

BUILDING A LIBRARY OF POLYMER CONSTRUCTS FOR EVALUATION AS SYNTHETIC BIOMATERIALS

8.1 Introduction

The majority of work in this dissertation focuses on porogen-leached scaffolds as model 3D polymeric biomaterial constructs. Although these efforts help develop fundamental knowledge in the field of surface modification of complex polymer materials, it is advantageous to evaluate the translation of plasma processing to different polymer morphologies because one class of morphologies may be more appropriate for a given application than another. For example, electrospun fiber meshes could be ideal wound dressing materials because of their porosity whereas a polymer film might be a less appropriate construct because it does not contain an interconnected network to promote air/fluid exchange with the surrounding environment. As another example, a porogen-leached scaffold could be more advantageous for deployment as a tissue engineering construct because it more closely resembles the extracellular matrix geometry of a biological tissue than a construct with a more ordered porous network. Additionally, electrospun fiber meshes offer more precise control of mechanical and structural properties than porogen-leached scaffolds. Thus, fiber mats have the potential to mimic certain types of extracellular matrices more closely than porogen-leached scaffolds. As with previous chapters, the studies reported herein are motivated by the necessity to improve knowledge of fundamental interactions between biological species and synthetic biomaterial devices. Biological environments and biomedical devices are inherently complex systems. Thus, the route to develop an understanding of device performance must consider the multitude of variables that control

interfacial interactions. By creating a library of polymeric materials with systematically varied surface and bulk properties, we can disentangle the role that each of these properties plays in controlling biological species/biomedical material interactions.

The conceptual framework presented in Figure 8.1, including a library comprised of materials that vary in terms of the base polymer, construct morphology, and surface properties, illustrates this approach. Each of the outermost circles in Figure 8.1 serve as representative examples that are explored in this chapter, but could easily be expanded to include any number of polymers, morphologies, and properties of interest. Here, we have focused initial efforts toward spin-coated polymer films and electrospun fibers, in addition to the porogen-leached scaffolds described in Chapters 3 and 5-7. Polymer films can serve as analogs for more complex 3D constructs by providing a platform for de-coupling surface chemistry/wettability and architecture, as well as the relative contributions these properties have in controlling interactions with biological species. The electrospun fiber focus is inspired not only by the growing number of recent literature efforts that focus on interactions between biological species and surface-modified fiber mats,[1-4] but also by the accessibility of a broader range of possible end applications than those provided using only porogen-leached scaffolds.

8.2 Plasma Modification of Electrospun Fibers: Expanding on Work with PCL

Our initial foray into fabrication and plasma modification of electrospun fiber mats is presented in Chapter 3. This investigation included OD and fluorocarbon plasma modification of PCL electrospun fibers and subsequent WCA evaluation of these constructs. Here, we expand upon this work by 1) utilizing a different plasma precursor (allylOH), in addition to OD and 2) fabricating fibers out of a different polymer mixture (PCL/PLA). (Motivation for expanding to PCL/PLA mixtures is further discussed in Section 8.4.) Representative SEM images of

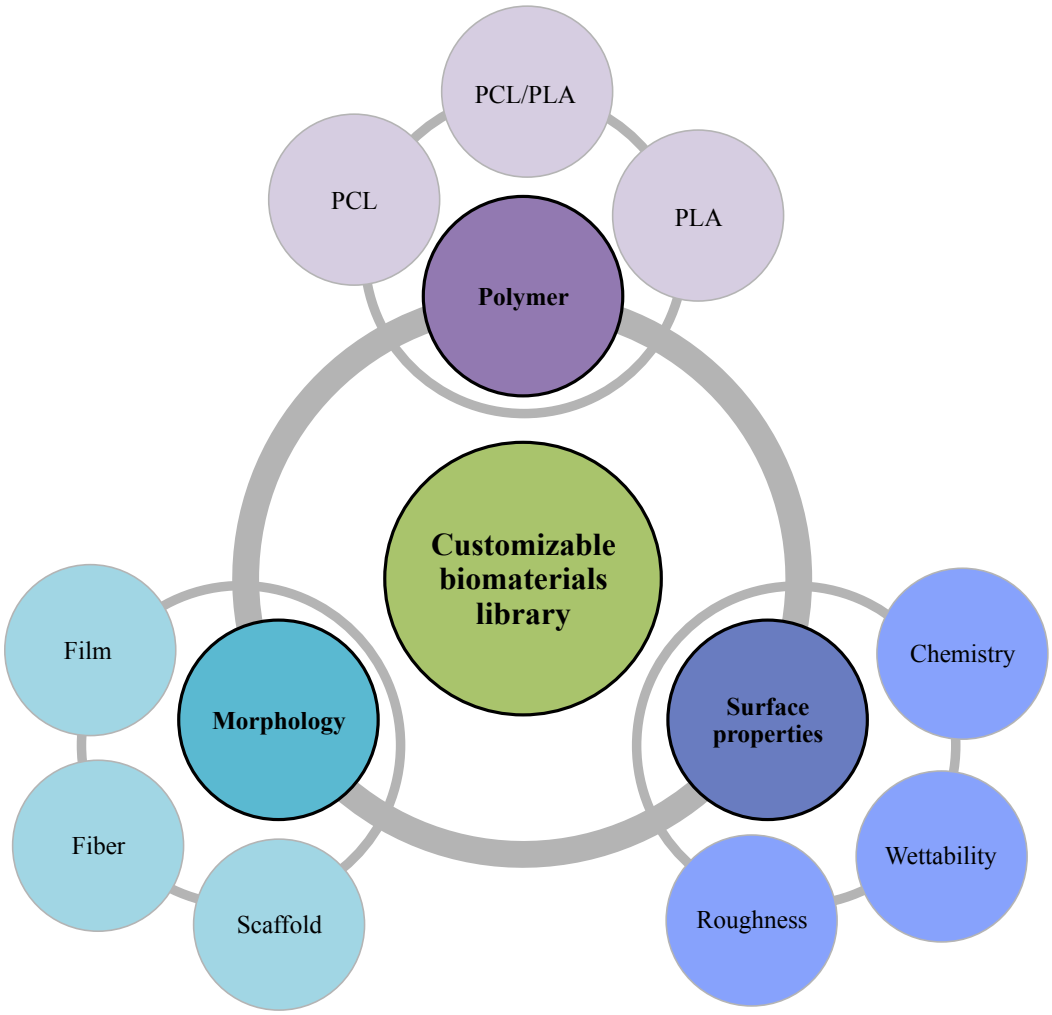

Figure 8.1. Conceptual framework for the systematic variation of polymer construct surface and bulk properties, including the polymer, surface properties, and morphology.

unmodified and plasma-modified PCL fibers (Figure 8.2a-c) demonstrate no appreciable fiber damage upon plasma modification (e.g., when compared to Figure 3.4c), as was also observed with PCL scaffolds in work presented in previous chapters.

Although electrospinning fibers using PCL was relatively straightforward (i.e., required little optimization), translating this technique to different polyester mixtures was a more substantial undertaking. Initial attempts to fabricate fiber mats using PCL/PLA mixtures resulted in the deposition of electrosprayed polymer on to the target where fibers either did not form at all or those that formed were non-uniform. The PLA that was initially used had a much lower average molecular weight (M_n) than that of the PCL (average $M_{n,\,PLA}$ = 10,000 g/mol, average $M_{n,\,PCL}$ = 80,000 g/mol), and was a mixture of D and L isomers. After additional literature consultation, a different PLA formulation was purchased. The average M_n for this formulation was reported to be 140,000 g/mol and contained 98% L-lactide units.[5] Additional optimization was performed with PCL/PLA mixtures made using this PLA formulation, ultimately resulting in fibers pictured in Figure 8.2d. Notably, the PCL/PLA fiber size and morphology is comparable to that of PCL-only fibers (for a quantitative analysis route, see Section 8.3). Additionally, PCL/PLA fiber morphology remains unaltered after modification for both OD and allylOH plasma treatment (Figure 8.2e, f). Altogether, these data support the development of a polymer construct library, both in terms of bulk properties (polymer composition and morphologies) and surface properties (plasma modifications).

8.3 DiameterJ as a Fiber Analysis Tool

In expanding electrospun fiber fabrication strategies to include different polymers and modifications, we wanted to quantitatively assess fiber mat morphology through fiber diameter, porosity, and pore size measurements. Such an evaluation could capture differences in fiber

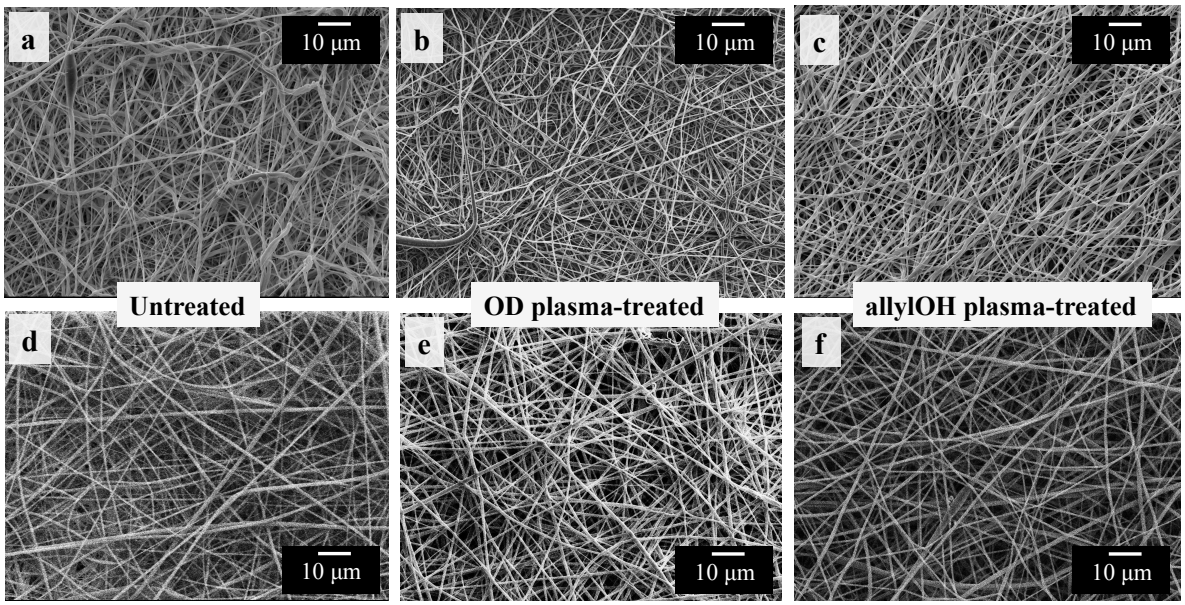

Figure 8.2. Representative SEM images of electrospun fiber meshes fabricated using PCL only (a-c) and PCL:PLA (d–e), all 1000× magnification. Untreated (a, d), OD plasma-treated (b, e), and allylOH plasma-treated (c, f) fiber mats are included.

uniformity (e.g., polydispersity) for different polymer formulations or modifications, and could thus be used to quantify the extent of fiber damage upon modification. For this assessment, we used an ImageJ plugin that was recently developed for quantitative fiber analysis entitled DiameterJ. DiameterJ has been validated for fiber image analysis/measurement and is thoroughly reviewed elsewhere.[6-7] Here, we discuss challenges faced when using DiameterJ and present proof-of-concept DiameterJ data to demonstrate its potential for quantitative analysis of plasma-modified fibers.

8.3.1 Image processing procedure. The first step in performing DiameterJ analysis is converting an SEM image to an 8-bit greyscale image. A representative converted image of OD plasma-modified PCL fibers at 5500× magnification is shown in Figure 8.3a. DiameterJ then segments the 8-bit greyscale images into a black and white image, where white areas represent fibers and black areas represent pores (i.e., the absence of fibers). ImageJ produces 16 potential segmentations from the 8-bit greyscale image and the user must manually select the most accurate segmentation. Although this process is somewhat subjective, it is typically possible to eliminate the majority of segmentations after a careful analysis of each one next to the original SEM image. This is because many segmentation algorithms result in a misidentification of fibers as pores (and vice versa), and thus, produce segmentations with artificially large white or black areas (more information on the segmentation algorithms can be found both in the literature[6] and on the ImageJ webpage[7]). It is also possible to upload an image that is segmented using other means if none of the 16 algorithm options produce reasonable segmentations. The best segmentation produced for OD plasma-treated PCL fibers (Figure 8.3b), shows a reasonable reproduction of the corresponding 8-bit greyscale image, especially when considering the

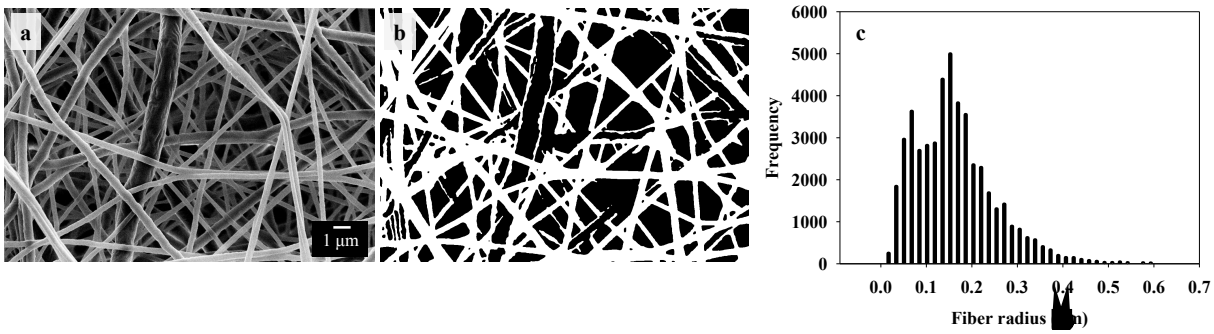

Figure 8.3. DiameterJ analysis of OD plasma treated PCL fibers (5500× magnification). (a) 8-bit greyscale image, (b) segmented black and white image, (c) histogram of fiber radii determined from segmented image (average fiber radius = 0.3 ± 0.1 µm).

foreground of the image. Quantitative data are produced based on the segmentation, where the fibers (white portions of the segmentation) are measured at every pixel along the fiber axis. Data output includes mean fiber radius (as well as the median, mode, and standard deviation of fiber radius), mean pore area (as well as the minimum, maximum, and standard deviation of pore area), percent porosity, and fiber intersection density. An additional output item is a histogram of fiber radii, which is also based on the segmentation (Figure 8.3c). Details on the multiple steps bridging segmentation and quantitative metric output are described elsewhere.[6-7]

8.3.2 Troubleshooting and future work. Our initial work with DiameterJ suggested that images collected at higher magnifications and with higher contrast produced more reliable image segmentations. It is important to note that most SEM images of electrospun fibers were collected to assess overall fiber morphology (not intended for DiameterJ analysis) and were thus captured at relatively low magnifications (≤3500×). The example data set provided here is based on an SEM image collected at 5500×, and images collected at even higher magnifications would likely produce better segmentations and thus, more reliable quantitative results. Furthermore, fiber mats were sufficiently thick as to be peeled from the foil support (>20 μm), which, although beneficial for plasma modification and potential deployment in biomedical settings, may be a disadvantage for DiameterJ analysis. Specifically, the fiber mat thickness is orders of magnitude larger than the thickness of individual polymer fibers, such that SEM images capture fibers in multiple planes of focus and thus, varying levels of brightness (Figure 8.3). Because DiameterJ segmentation algorithms are impacted by the contrast of as-collected SEM images, images of thick mats (i.e., those with significant “backgrounds”), produce less reliable segmentations and therefore, less reliable quantitative metrics.

Future work with DiameterJ should utilize fiber mats produced using identical parameters (e.g., applied voltage, collector distance, and flow rate) employed to produce thicker mats, but spun for a significantly shorter time. This would result in a thin mat that may not be as easily removed from the foil backing without damage, but would contain fibers that are otherwise indistinguishable from those found in thicker mats. Fibers could be imaged directly on the foil backing to mitigate the background issue described above. Overall, this methodology would produce more reliable segmentations and a more realistic assessment of fiber size. Notably, this approach would dictate that fibers be plasma-modified on a foil backing rather than the typical modification strategy reported in this dissertation (where the fiber mat is peeled off of the foil backing, cut, and placed on a glass slide). The introduction of a conductive support into the plasma reactor raises an additional set of challenges that should be addressed if this line of inquiry is pursued in the future.

8.4 Plasma-modified PCL/PLA Construct Surface Properties

An initial step in developing a library of polymeric constructs includes the fabrication of materials from the same base polymer mixture but with different morphologies using methodologies outlined in Figure 2.2. The constructs of interest for the present work include spin-coated polymer films, porogen-leached scaffolds, and electrospun fiber mats. Here, we have expanded upon previously utilized materials through the introduction of films, scaffolds, and fibers using a 1:1 PCL:PLA mixture. This mixture was chosen to evaluate the translation of porogen leaching and electrospinning methodologies to polymer systems other than the PCL used for previous work in this dissertation (Chapters 3, 5-7), as well as a starting place for creating constructs of varied morphology (Figure 8.1). Additionally, the blended PCL/PLA system provides another layer of customizability regarding material mechanical properties,

crystallinity, and bioresorption/degradation. Although these properties are not explicitly evaluated in the present work, such an exploration represents a valuable direction for future research (especially directed toward systematic variations in composition using the two polyesters). As discussed in Chapter 9, controlling material bulk properties represents a pathway to fabricating constructs that mimic specific extracellular matrices (e.g., those present in bone vs. soft tissues).

Representative SEM images demonstrate successful fabrication of this collection of constructs (Figure 8.4), and reveal important differences between them. For example, it is clear that films are effectively non-porous when compared to the 3D constructs (R_q < 8 μm for all films included in this study, as measured via optical profilometry). Another observation is that both of the 3D porous networks (scaffolds and fibers) are random and interconnected, but the network natures differ. Connections between the electrospun fibers (Figure 8.4b) create convex pore walls whereas the porogen-leached scaffold structure (Figure 8.4c) consists of concave pore walls. Additionally, the effective pore size of electrospun fiber mats is much smaller than those in porogen-leached scaffolds. These structural differences may result in distinct biological species attachment and growth behavior and are thus an important consideration for polymer material deployment in biological systems. Wettability of unmodified PCL/PLA constructs was evaluated using contact angle goniometry, specifically by measuring static water contact angles (WCA, Table 8.1). These constructs are all nominally hydrophobic (WCAs < 80º), and although all materials are fabricated from the same base polymer blend (1:1 PCL:PLA), the WCA of polymer films is ~40º lower than that measured on 3D constructs. Differences in wettability are attributed to the introduction of a more complex morphology (related to surface roughness and inhomogeneity), as discussed in detail throughout Chapter 3.[8-10]

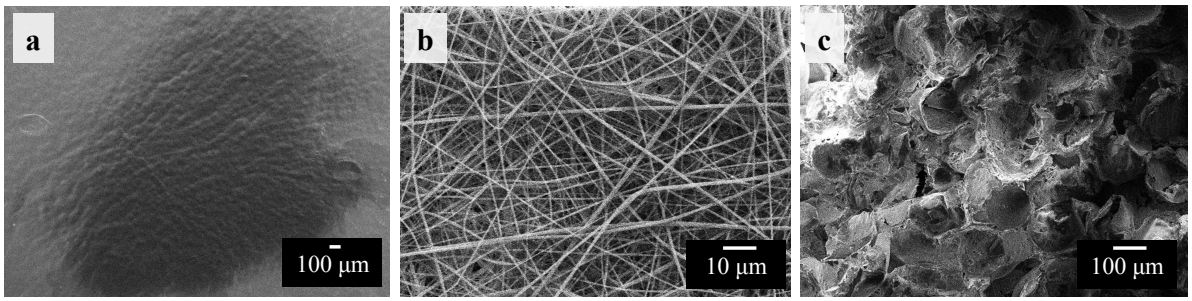

Figure 8.4. Representative SEM images of constructs fabricated using PCL:PLA, including (a) spin-coated film (30× magnification), (b) electrospun fiber mesh (1000× magnification, the same image is included as Figure 8.2d), and (c) porogen-leached scaffold (100× magnification).

Table 8.1. Wettability data, including static WCA values and average water absorption rates, for plasma-modified PCL:PLA constructs. Data are presented as the mean ± standard deviation ($n \geq 3$).

Plasma Modification	PCL:PLA Construct	WCA (º)	Average Water Absorption Rate (µL/s)
Unmodified	Film	81.0 ± 6.0	--
	Fiber	131.0 ± 3.4	--
	Scaffold	123.3 ± 8.1	--
OD	Film	96.4 ± 1.3	--
	Fiber	127.2 ± 4.9	--
	Scaffold	130.3 ± 3.4	--
allylOH	Film	<10	--
	Fiber	--	3.0 ± 1.9
	Scaffold	--	6.6 ± 2.3

PCL/PLA constructs were then plasma treated as a means of modifying construct surface properties while maintaining bulk architecture (Figure 8.1). Here, two different plasma modification precursors were selected: OD and allyl alcohol (allylOH). OD was selected as a hydrophobic film PECVD system, providing a non-fluorinated alternative to the hydrophobic fluorocarbon PECVD systems described in Chapter 5 and building off of work presented in Chapter 3 (OD plasma-modified PCL scaffolds and fibers). AllylOH was chosen to expand on work presented in Chapter 6, which focused on plasma modification of PCL porogen-leached scaffolds. Furthermore, we predicted that films deposited using these precursors would have different surface properties, which provided a rational basis for initial development of a small biomaterial construct library. The allylOH and OD plasma parameters used for PCL/PLA construct modification were chosen for direct comparison to previous work with PCL constructs (Chapters 3 and 6). Notably, this work represents the first use of the OD precursor in our laboratories outside of the proof-of-concept depositions reported in Chapter 3 (Table 3.1). As such, a relatively extensive parameter space exploration using the OD precursor was performed and is discussed in Section 8.5.

The WCAs of OD plasma modified PCL/PLA constructs (Table 8.1) are similar to unmodified materials with the exception of the polymer films, which show a ~15º increase in WCA after plasma modification. AllylOH plasma-modified constructs display the opposite wetting behavior, where all constructs become nominally hydrophilic after plasma treatment. Specifically, the WCA of allylOH plasma-modified polymer films is <10º, exhibiting over a 70º decrease when compared with unmodified films. AllylOH plasma treatment of 3D constructs renders these materials hydrophilic and sorbing (i.e., equilibrium WCA = 0º), as observed for PLA scaffolds treated under identical conditions. Average water absorption rates calculated from

dynamic wettability data (Table 8.1) demonstrate that plasma-modified scaffolds absorb water at approximately double the rate of plasma-modified fibers. Notably, the large experimental error (>30%) associated with water absorption rate data and the multiple variables influencing dynamic goniometry measurements both here and with allylNH/allylOH plasma treated PCL scaffolds (Chapter 6) makes it challenging to elucidate absolute claims. These data, however, allow for a relative comparison between different substrates and/or plasma modification conditions. The water absorption rate of PCL scaffolds treated with identical allylOH plasmas as those utilized here was 6.4 ± 3.8 μL/s (Chapter 6), which was similar to those observed for PCL/PLA scaffolds (6.6 ± 2.3 μL/s). These data suggest that the allylOH plasma is conformally modifying polymer scaffolds in a uniform manner (i.e., regardless of the native polymer surface composition). Another finding from these wettability data is the difference in wetting behavior between plasma-modified scaffold and fibers. One likely explanation is that relative construct feature size controls water sorption. Specifically, the smaller effective "pore size" present in the fiber mat creates a network that may be less permeable to water than that of the scaffolds. An alternative hypothesis is that although the constructs were modified using identical plasma conditions, the modification may not have affected the polymer constructs identically. For example, films deposited on polymer scaffolds versus fibers may differ with regards to conformality (i.e., surface coverage) or uniformity (i.e., regions with different degrees of cross-linking).

To evaluate differences in surface chemistry between unmodified and plasma-treated constructs in terms of both elemental composition and functionality, high-resolution XPS data were collected (Table 8.2, Figure 8.5). The O/C ratio is used as a comparative metric for changes in chemical composition, both between different plasma treatments and different morphologies,

Table 8.2. Surface chemical composition of unmodified and plasma modified PCL:PLA materials from high-resolution XPS data. Binding environment percentages were determined from fitting high-resolution C_{1s} XPS spectra. Data are presented as the mean ± standard deviation ($n \geq 3$).

Plasma Modification	PCL:PLA Construct	O/C	%C-C/C-H	%C-OH/C-OR [a]	%C=O	%O-CH_2 [b]
Unmodified	Film	0.40 ± 0.01	53.0 ± 1.9	16.9 ± 3.5	18.9 ± 4.0	8.7 ± 5.4
	Fiber	0.40 ± 0.01	57.6 ± 3.7	20.5 ± 1.7	17.7 ± 1.5	3.6 ± 0.5
	Scaffold	0.47 ± 0.03	40.4 ± 5.5	31.3 ± 2.9	24.6 ± 5.8	3.7 ± 3.5
OD	Film	0.05 ± 0.02	90.3 ± 4.9	7.0 ± 4.1	2.7 ± 0.8	--
	Fiber	0.10 ± <0.01	88.1 ± 2.6	6.9 ± 2.2	5.1 ± 0.5	--
	Scaffold	0.04 ± <0.01	97.4 ± 0.6	1.4 ± 0.7	1.2 ± 0.2	--
allylOH	Film	0.33 ± <0.01	66.5 ± 3.1	28.0 ± 2.5	5.5 ± 0.6	--
	Fiber	0.34 ± 0.01	66.4 ± 6.6	26.7 ± 6.8	6.9 ± 0.3	--
	Scaffold	0.35 ± 0.01	68.2 ± 3.8	28.6 ± 4.7	3.1 ± 2.9	--

[a] For unmodified constructs, this environment includes the alpha carbon to the carbonyl

[b] This environment refers to the alpha carbon to the ester functionality present in PCL, and was excluded to streamline plasma-treated construct analysis (as described for the XPS data analysis of fluorocarbon-modified materials in Chapter 5).

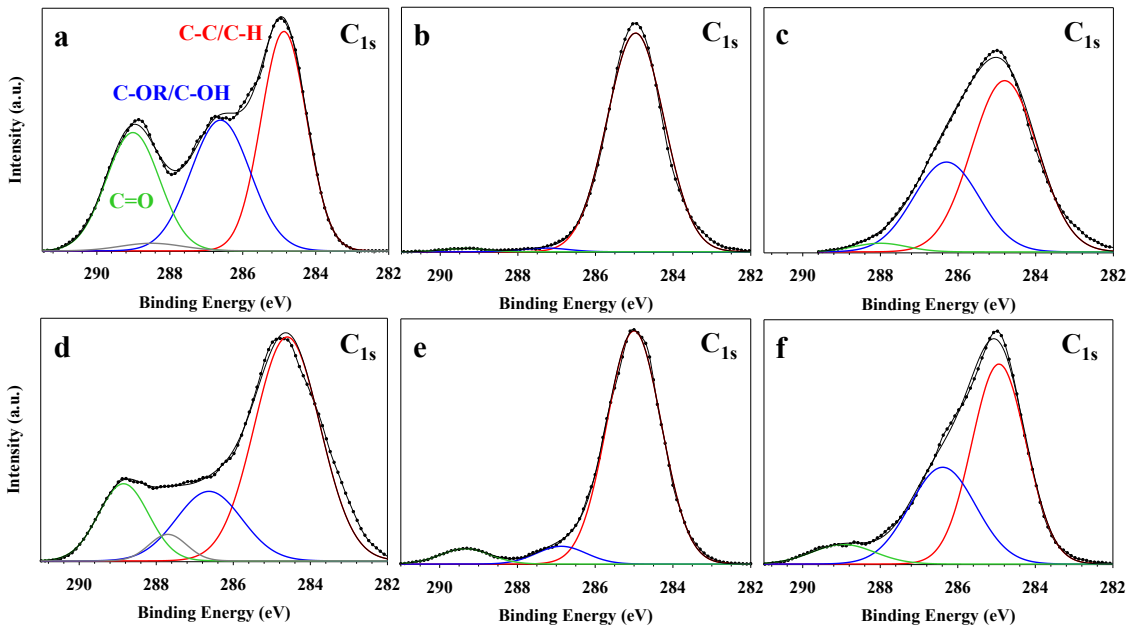

Figure 8.5. Representative high-resolution C_{1s} XPS spectra of PCL:PLA scaffolds (a–c) and fibers (d–f). Untreated (a, d), OD plasma-modified (b, e), and allylOH plasma-modified (c, f) are included. Each spectrum is deconstructed into 3 environments: C-C/C-H (red), C-OH/C-OR (blue) and C=O (green). Unmodified materials include an additional environment (grey) representing the alpha carbon to the ester in the PCL structure (see footnote in Table 8.2).

as the only elements detected on the surface of all constructs were carbon and oxygen. Notably, unmodified PCL/PLA films and fibers have identical O/C ratios within experimental error, which is rational based on polymer composition. The O/C ratio of the unmodified PCL/PLA scaffold is slightly greater (0.47 ± 0.3) than that of films and fibers (0.40 ± 0.01). Within experimental error, however, the unmodified constructs are similar with respect to overall composition. OD plasma treatment results in surfaces with significantly lower O/C ratios than unmodified materials, regardless of morphology. Here, films and scaffolds have similar O/C ratios (i.e., within experimental error), suggesting comparable surface modification with identical plasma treatment conditions. The O/C ratio of fibers treated with OD, however, is double that of the other OD plasma modified constructs. Although all three constructs were treated using identical OD plasmas, these data suggest that the composition of the plasma-treated fiber surface differs from that of plasma-treated films and scaffolds. AllylOH plasma-modified surfaces have the same O/C ratio within experimental error regardless of construct morphology (~0.34), which is slightly lower than that of unmodified constructs.

Representative high-resolution C_{1s} spectra (Figure 8.5) and corresponding quantitative binding environment data (Table 8.2) reveal a more detailed picture of unmodified and plasma-treated construct surface chemistry. OD plasma modification results in a drastic increase in contributions from the hydrocarbon binding environment regardless of construct morphology. Constructs treated with allylOH plasma contain greater relative contributions of the alcohol/ether binding environment than untreated materials. When comparing spectra collected on plasma-modified scaffolds (Figure 8.5b, c) with those collected on plasma-modified fibers (Figure 8.5e, f), clear differences exist regarding contributions from oxygen-containing binding environments (ether, alcohol, and carbonyl). Specifically, more oxygen-containing functionality

is present on fiber surfaces compared to scaffolds modified under identical conditions. This is true of both the OD and allylOH plasma systems. This observation is supported by binding environments in Table 8.2, especially with respect to contributions from the carbonyl environment of the fibers compared with the other two morphologies. Additionally, comparing binding environment contributions between unmodified constructs reveals more oxygen-containing functionality on scaffold surfaces than on films or fibers. This result supports the difference in O/C ratios discussed above, which may arise from different fabrication processes (porogen leaching vs. electrospinning/spin coating). Specifically, the fabrication process may affect the degree of mixing between the polymer components (PCL and PLA), which could alter the uniformity of the surface (i.e., more PCL-rich areas and more PLA-rich areas). Furthermore, non-uniformity may not be accurately captured in the small sample size used for preliminary data collection, as suggested by the larger experimental error accompanying the scaffold O/C ratio measurements (when compared to untreated films and fibers). Films and fibers may be more uniform as their fabrication processes require less viscous polymer solutions, thus resulting in easier manual blending then in the case of porogen leaching. This finding warrants further data collection on a larger sample size, and may also require modifications to the porogen leaching fabrication process.

Altogether, characterization of PCL/PLA constructs represents progress toward developing a library of polymeric biomaterials with systematically varied surface and bulk properties. Broadly, this set of materials comprises three unique morphologies (films, fibers, and scaffolds) and three unique sets of surface properties arising from composition/wettability (e.g., those with oxygen functionality/hydrophobic, carbon functionality/hydrophobic, and oxygen functionality/hydrophilic). Functionality differences on the surface of constructs modified with

identical plasma treatment conditions, however, requires further exploration, which may include tuning plasma parameters to achieve surfaces with identical functionality.

8.5 1,7-octadiene PECVD System: Parameter Space Exploration

As mentioned in Section 8.2, the proof-of-concept experiments using OD plasmas reported in Chapter 3 were the first use of this plasma precursor in our laboratories. As such, it was of interest to evaluate film properties as a function of plasma parameters, including *P*, location in reactor, and treatment time. For this fundamental evaluation, we opted to use glass slides for WCA analysis and Si wafers for FTIR, VASE, and optical profilometry analyses. Data on the plasma modification of these 2D substrates provide a simplified platform for materials characterization. Furthermore, information gained about how OD plasmas interact with this set of substrates can be applied to OD plasma modification of more complex constructs in the future.

Based on previous literature and the limited amount of prior OD plasma modification performed in our laboratories, we expected OD PECVD systems to deposit hydrophobic hydrocarbon films.[11-12] As unmodified glass is hydrophilic (WCA ~ 20º), it was selected as a substrate for WCA analysis because the deposition of a conformal hydrophobic film on glass would be relatively straightforward to detect via an increase in WCA. WCA values of OD plasma-modified glass are presented in Table 8.3 as a function of *P* (4, 25, 50 W), placement in reactor (in coil, 10 cm downstream, 19 cm downstream), and treatment time (1, 5, and 10 min). These parameters were selected both from the OD plasma treatment conditions we had previously employed for polymeric construct plasma modification (4 W, in coil, 5 min) and the literature.[1, 11] From data in Table 8.3, it is evident that the majority of OD plasma treatment conditions result in hydrophobic surfaces with WCAs >95º (and as large as ~110º). This is true of all substrates treated with 25 and 50 W OD plasmas, regardless of treatment time and position

Table 8.3. WCA data collected on glass slides treated with OD plasmas as a function of applied power (4, 25, 50 W), position in reactor (in coil, 10 cm downstream, and 19 cm downstream), and treatment time (1, 5, 10 min). Additional treatment times (8 and 20 min) are included for select treatment conditions (4 W in coil and 25 W 19 cm downstream) to allow direct comparison to profilometry data (Figure 8.6b).

***P* (W) and position in reactor**	**Treatment time (min)**	**WCA (º)**
4 W in coil	1	62.1 ± 4.3
	5	91.2 ± 1.3
	8	92.8 ± 2.2
	10	99.4 ± 1.8
	20	100.4 ± 3.7
4 W 10 cm	1	80.8 ± 1.6
	5	95.2 ± 2.2
	10	104.0 ± 5.1
4 W 19 cm	1	10.9 ± 2.6
	5	22.9 ± 6.9
	10	27.4 ± 2.8
25 W in coil	1	98.3 ± 0.5
	5	100.5 ± 0.1
	10	101.1 ± 0.9
25 W 10 cm	1	97.2 ± 0.1
	5	98.3 ± 1.0
	10	98.7 ± 0.4
25 W 19 cm	1	80.5 ± 0.9
	5	109.8 ± 1.4
	8	92.8 ± 2.2
	10	109.5 ± 3.4
	20	100.4 ± 3.7
50 W in coil	1	97.8 ± 0.6
	5	101.4 ± 0.2
	10	99.3 ± 1.0
50 W 10 cm	1	95.8 ± 0.6
	5	100.6 ± 0.2
	10	97.9 ± 0.6
50 W 19 cm	1	96.3 ± 1.0
	5	97.9 ± 0.4
	10	95.7 ± 0.5

in reactor, with the exception of substrates placed 19 cm downstream treated with a 25 W plasma for 1 min (WCA = 80.5 ± 0.9º). Regardless of substrate position, the WCA values of substrates treated with 25 and 50 W OD plasmas are significantly greater than that of unmodified glass, suggesting film deposition occurs throughout the reactor. More variability in WCA is observed for substrates treated with lower *P* OD plasmas (4 W). Within the 4 W data set, WCA values typically increase with treatment time and decrease with position in reactor. WCAs are lowest for 4 W plasmas on substrates placed 19 cm downstream, where the lowest measured WCA value is 10.9 ± 2.6º (treatment time = 1 min). Indeed, all WCA values for 4 W plasmas on substrates placed 19 cm downstream are equal to or less than that of unmodified glass, suggesting either a lack of film deposition and/or non-conformal film deposition. Low *P* treatment of substrates placed in the coil or closer to the coil (10 cm), however, results in more hydrophobic surfaces. These data suggest these are more conformal films than those deposited on substrates placed downstream, but with the same applied power. Maximum WCA values are ~10º greater than those reported in what is, to our knowledge, the only published comprehensive OD PECVD parameter space evaluation (by Akhavan and coworkers).[11] This discrepancy may be attributed to differences in drop shape fitting parameters (see Section 2.3.1) as Akhavan et al. did not report specific fitting method(s) used.[11] An alternative explanation is that hydrocarbon films deposited in the present study had different surface properties (surface roughness, functionality, and/or conformality) than those evaluated by Akhavan et al. Notably, it is challenging to directly compare results between these studies because the plasma parameter space explored by Akhavan et al. was somewhat different than the space presented here. Specifically, Akhavan and coworkers use a ratio of applied power/precursor flow rate to classify plasma treatment conditions, where their power/flow rate ratios range from 0.024-1.35 kJ/cm^3. In

the present study, power/flow rate ratios cover a much wider range (0.68-8.58 kJ/cm^3), where flow rate is held constant but applied power is varied.

To qualitatively and quantitatively evaluate hydrocarbon film thickness, we elected to utilize two techniques: FTIR and VASE (Figure 8.6). A subset of plasma treatment conditions was selected from the parameter space explored for WCA analysis with the intention of choosing conditions that resulted in differing WCA values. FTIR data (Figure 8.6a, right) demonstrate that the intensity of the signal associated with C-H stretching (3050-2800 cm^{-1}) generally increases with *P* and treatment time. As FTIR is a bulk technique, this increase in C-H stretch intensity is thus a qualitative measure of functionality present in the entire plasma-modified substrate. As no signal is observed in the 3050–2800 cm^{-1} region for unmodified substrates, it can be deduced that signal increase is attributed to depositing progressively thicker films on the substrate surface. These data support WCA results in that treatments that yield hydrophobic surfaces display a prominent FTIR signal for the C-H stretching band, and the intensity of this signal typically increases with increasing WCA. The exception to this observation is for substrates treated in the coil at 4 W, where WCA is ~50º greater than those treated 19 cm downstream at 4 W. This is not evident, however, in the FTIR data (3050–2800 cm^{-1} region) where the signals are virtually indistinguishable from one another. Again, this result can be rationalized by the bulk nature of this technique.

To obtain a quantitative evaluation of film thickness as a function of plasma parameters, VASE was utilized in a similar manner to that used for fluorocarbon films in Chapter 5. VASE analysis (Figure 8.6b) demonstrates that film thickness increases linearly with treatment time for substrates treated with 4 W plasmas in the coil region, as well as for those treated with 25 W plasmas 19 cm downstream. Notably, films deposited on substrates placed 19 cm downstream

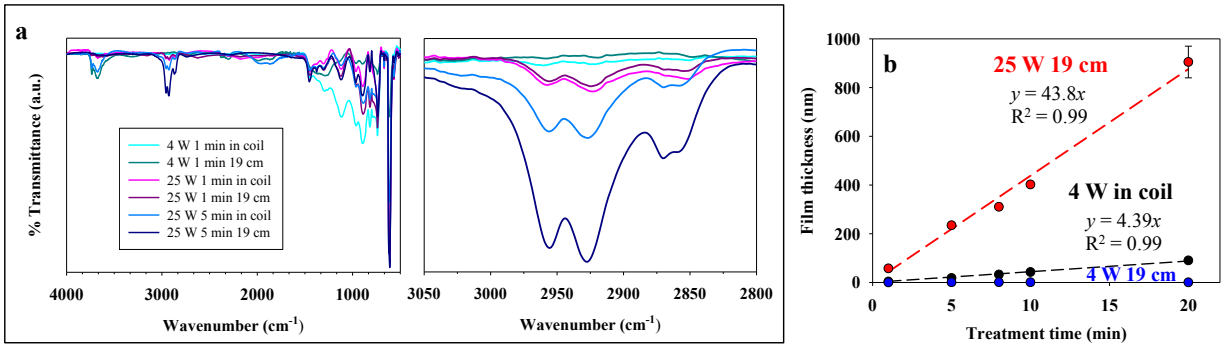

Figure 8.6. A summary of the OD plasma parameter space exploration including (a) FTIR analysis with an expanded region detailing the CH stretch (right), and (b) film thickness as a function of plasma treatment time for three OD plasma treatments conditions as determined using VASE (except for 25 W 19 cm 20 min, which were evaluated using optical profilometry). Linear regression results (constrained by $y_0 = 0$) are included in panel b.

and treated for 20 min with a 25 W OD plasma were so thick that the wafer surface was no longer reflective, and thus, could not be measured using ellipsometry. Thus, optical profilometry was employed to measure film thickness for this sample. Collectively, these data demonstrate the relationship between deposition rate and substrate placement. Essentially no films were deposited on substrates placed 19 cm downstream treated with 4 W OD plasmas, regardless of treatment time, whereas the deposition rate of the same 4 W plasma in the coil region is 4.4 nm/min. Moreover, these data show that deposition rate increases substantially with power: the deposition rate of a 4 W plasma 19 cm downstream is ~0 nm/min, whereas that of a 25 W plasma at the same position in the reactor is ~43.8 nm/min. Akhavan et al. observed that film thickness increased linearly as a function of treatment time (over a 20 s-60 min range), which was also seen in the present study in cases where film deposition occurred. The authors, however, reported deposition rates that were <4 nm/min (lower than those reported here), although it is important to re-emphasize that direct comparisons between the studies should be made with caution because of differences in parameter space.[11] Surprisingly, Akhavan and coworkers found that deposition rate increased with applied power/flow rate ratio to a point, and then decreased as the power/flow rate ratio exceeded 0.75 kJ/cm^3.[11] This trend is not observed in the present study, but too much emphasis should not be placed on this observation as the deposition rate was evaluated for a much smaller set of plasma conditions.

In addition to information gleaned from VASE related to OD film growth behavior, a more detailed analysis of OD film growth and properties (including surface roughness) was obtained using optical profilometry. Here, conditions chosen for VASE analysis that resulted in film deposition (4 W in coil and 25 W downstream) were selected for comparison to other surface analysis results. The first complete set of profilometry data collected on OD plasma

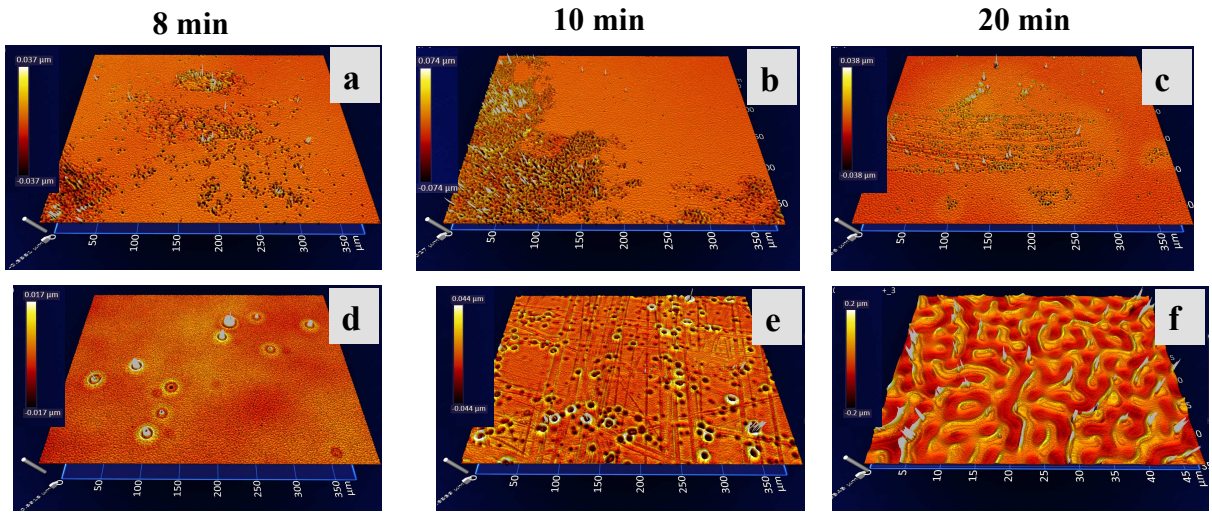

Figure 8.7. Representative optical profilometry heat maps detailing the evolution of OD film growth for 4 W in coil (a-c) and 25 W 19 cm (d-f) conditions. Data of wafers treated for 8, 10, and 20 min are included for each condition. All maps were collected with 20x magnification with the exception of panel f, which was collected using 100x magnification.

Table 8.4. RMS roughness (R_q) values for select OD treatment conditions as a function of treatment time, measured on Si wafers using optical profilometry. Data represent the mean and standard deviation for n = 3.

P **(W) and position in reactor**	**Treatment time (min)**	**R_q (nm)** [b]
4 W in coil	1	2.0 ± <0.1
	5	2.0 ± <0.1
	8	6.5 ± 3.8
	10	10.3 ± 10.9
	20	5.0 ± 4.7
25 W 19 cm	1	3.0 ± <0.1
	5	9.7 ± 3.8
	8	14.3 ± 10.6
	10	56.3 ± 39.1
	20[a]	140.3 ± 64.8

[a] All data were collected at 20x magnification with the exception of that of the 25 W 19 cm 20 min sample (collected 100x magnification).

[b] R_a values were similar to R_q values

treated wafers (e.g., one wafer treated under each set of conditions) is summarized in Figure 8.7 and Table 8.4. Notably, films for all samples shown in Figure 8.7 are <30 nm (as measured using VASE, Figure 8.6b). Therefore, observed topography is on the exterior of each wafer and may not be indicative of the "bulk" film structure. Heat map data in Figure 8.7 show that wafers treated using 4 W plasmas look topographically similar, where portions of each surface appear to have both relatively smooth areas along with patches of roughness (Figure 8.7a-c). Upon further inspection, we observed that these rough areas comprised crater-like features (μm-scale diameter), and each feature had a lip that was taller than the surrounding film. The lip formed a convex pore-like structure in the center of each feature (~100 nm in depth). Similar features were observed for wafers treated with 25 W plasmas for 8 and 20 min, although they were larger (~10 μm in diameter) and covered the surface more uniformly (i.e., not isolated in patches as for wafers treated with 4 W plasmas). Another feature of note for the substrate treated 19 cm downstream using a 25 W plasma for 10 min was the appearance of crosshatches over the entire surface, which was not observed for other treatment conditions. The wafer treated for 20 min, 19 cm downstream using 25 W OD plasmas had a maze-like topography comprising loosely interdigitated features (Figure 8.7f). Although OD film morphology varies over this parameter space, samples, generally speaking, do not display drastically different wetting behaviors (Table 8.3). One explanation for this finding is that OD film features (and corresponding surface roughness values) are not large and/or uniform enough so as to dramatically alter the interaction of water drops with the surface. As with PCL/PLA constructs discussed in Section 8.4, however, a larger sample size is likely required to more accurately capture the extent of surface inhomogeneity and its impact on wettability.

These data suggest film growth may be occurring through the formation of these crater-like features. One explanation for feature formation is that interactions between deposition precursors (proposed to be oligomeric ions[11] and excited-state precursor molecules[13]) are more energetically favorable than those between the deposition precursor and underlying film. Furthermore, feature size appears to be dependent on applied power, suggesting energies of deposition precursors may facilitate feature formation. For wafers treated with longer treatment times and higher applied power, the crater-like features appear to merge together to create the topography shown in Figure 8.7f. All samples evaluated in the present work differ in topography from those observed by Akhavan and coworkers, who observed (using atomic force microscopy) a patch-like structure of plasma-deposited OD films.[11] Notably, the authors analyzed a much smaller film area (4 μm^2) than that analyzed here (1×10^5 μm^2). Thus, Akhavan et al. may not have accurately captured the larger scale features present in plasma-deposited OD films. Alternatively, films deposited using the treatment conditions and/or reactor setup employed by Akhavan and coworkers may yield smoother and more uniform films than those fabricated in the present work.

Heat map data are supported by RMS roughness (R_q) values (Table 8.4), demonstrating data that wafers treated using 4 W plasmas for shorter times (<8 min), as well as the wafer treated using a 25 W plasma for 1 min, had similar R_q values when compared to unmodified Si wafers (Table 8.4). All R_q values for wafers treated with 4 W OD plasmas in the coil are <10 nm regardless of treatment time. This is also the case for wafers treated with 25 W plasmas 19 cm downstream for 1 and 5 min. Longer treatment times, however, typically resulted in rougher and less homogenous films (as demonstrated by larger experimental error values in Table 8.4).

Initial profilometry results prompted preparation of replicate OD plasma-modified substrates to gauge deposition reproducibility. Replicate samples prepared using 4 W OD plasmas, as well as those prepared using 25 W OD plasmas for short treatment times (<10 min) were similar to data shown in Figure 8.7 and Table 8.4. Films deposited using 25 W plasmas for longer treatment times, however, had substantially different morphologies and R_q values than those in Figure 8.7e and f. Specifically, film morphology resembled that presented in Figure 8.7d with correspondingly lower R_q values (<10 nm). One reason for morphological inconsistences in preparing replicate samples under high power/long treatment time conditions may be differences in plasma coupling between depositions. Notably, OD plasmas are relatively dim, even at the highest power utilized in this study (25 W). Thus, it is challenging to both identify and remediate coupling issues in OD systems. Another reason may be differences in environmental factors (e.g., humidity) between depositions. For example, previous work in the Fisher group with carbon nitride PECVD systems resulted in deposition of films with similar morphologies to that in Figure 8.7f.[14] In those systems, the resulting morphology was attributable to humidity/moisture effects. A more detailed evaluation of the reason behind inconsistencies in film deposition using 25 W plasmas, however, remains an area for future investigation.

Altogether, the OD parameter space evaluation demonstrates our ability to control the properties of deposited films (e.g., thickness, wettability, and roughness) by varying applied power, position in reactor, and treatment time. Substrates treated further downstream at lower powers are more hydrophilic, suggesting the absence of a hydrocarbon film. Indeed, this is confirmed with VASE data, and likely results from deposition species generated in the coil region not reaching the substrate before recombining, decaying to the ground state, or by other plasma processes. When applied power is increased, however, substrates placed downstream of

the coil are more hydrophobic. This is likely because the amount of deposition species increases, as well as their energies, which may result in the formation of metastable deposition species with longer lifetimes than those generated at lower applied powers. Thus, film deposition occurs downstream of the coil. The plasma parameter space study presented here enhances our knowledge of the OD precursor, and this knowledge can aid in building a library of biomedical polymeric constructs.

8.6 Summary

In this chapter, initial efforts toward building a library of polymeric biomaterials were presented. Work presented included exploration of fabrication and characterization of PCL/PLA polymer films, electrospun fibers, and scaffolds, including an analysis of their surface properties and morphology. Additionally, a valuable tool that could provide a quantitative analysis route for plasma-modified fiber mats was discussed. This tool would allow for a direct comparison of fibers modified using different plasma precursors and with different treatment conditions, and could thus be used in a wide range of future work with plasma-treated electrospun fibers. Furthermore, one of the plasma precursors systems utilized for polymer construct modification (OD) was evaluated under different deposition conditions. The OD parameter space evaluation revealed that film deposition is controlled by power and position relative to the coil region, and furthermore, that film thickness varies linearly as a function of treatment time. Moving forward, this knowledge of these plasma systems, their interactions with polymer constructs, and methods of construct analysis will promote a more holistic understanding of how polymer materials interact with complex biological systems.

REFERENCES

1. Abrigo, M.; Kingshott, P.; McArthur, S. L., Bacterial Response to Different Surface Chemistries Fabricated by Plasma Polymerization on Electrospun Nanofibers. *Biointerphases* **2015,** *10* (4), 04A301.
2. Martinez, J. S.; Kelly, K. D.; Ghoussoub, Y. E.; Delgado, J. D.; Keller III, T. C.; Schlenoff, J. B., Cell Resistant Zwitterionic Polyelectrolyte Coating Promotes Bacterial Attachment: An Adhesion Contradiction. *Biomater. Sci.* **2016,** *4* (4), 689-698.
3. Rieger, K. A.; Porter, M.; Schiffman, J. D., Polyelectrolyte-Functionalized Nanofiber Mats Control the Collection and Inactivation of Escherichia coli. *Materials* **2016,** *9* (4), 297.
4. Cools, P.; Morent, R.; De Geyter, N., *Advances in Bioengineering*. InTech: 2015; p 117-148.
5. Modi, S.; Koelling, K.; Vodovotz, Y., Miscibility of Poly(3-hydroxybutyrate-co-3-hydroxyvalerate) with High Molecular Weight Poly (lactic acid) Blends Determined by Thermal Analysis. *J. Appl. Polym. Sci.* **2012,** *124* (4), 3074-3081.
6. Hotaling, N. A.; Bharti, K.; Kriel, H.; Simon, C. G., DiameterJ: A Validated Open Source Nanofiber Diameter Measurement Tool. *Biomaterials* **2015,** *61*, 327-338.
7. Hotaling, N. DiameterJ. http://imagej.net/DiameterJ.
8. Öner, D.; McCarthy, T. J., Ultrahydrophobic Surfaces. Effects of Topography Length Scales on Wettability. *Langmuir* **2000,** *16* (20), 7777-7782.
9. Quéré, D., Wetting and Roughness. *Annu. Rev. Mater. Sci.* **2008,** *38*, 71-99.
10. Palumbo, F., Wettability Characterization of Plasma Texturing of Polymers. *Plasma Process. Polym.* **2015**.
11. Akhavan, B.; Jarvis, K.; Majewski, P., Evolution of Hydrophobicity in Plasma Polymerised 1, 7-octadiene Films. *Plasma Process. Polym.* **2013,** *10* (11), 1018-1029.
12. Hawker, M. J.; Pegalajar-Jurado, A.; Fisher, E. R., Innovative Applications of Surface Wettability Measurements for Plasma-modified Three-dimensional Porous Polymeric Materials: A Review. *Plasma Process. Polym.* **2015,** *12* (9), 846-863.
13. France, R. M.; Short, R. D.; Duval, E.; Jones, F. R.; Dawson, R. A.; MacNeil, S., Plasma Copolymerization of Allyl Alcohol/1, 7-octadiene: Surface Characterization and Attachment of Human Keratinocytes. *Chem. Mater.* **1998,** *10* (4), 1176-1183.
14. Stillahn, J. M.; Trevino, K. J.; Fisher, E. R., Deposition of Amorphous CN_x Materials in BrCN Plasmas: Exploring Adhesion Behavior as an Indicator of Film Properties. *ACS Appl. Mater. Interfaces* **2011,** *3* (5), 1402-1410.

CHAPTER 9

RESEARCH SUMMARY AND FUTURE DIRECTIONS

Part I of this dissertation concludes with a summary of major aspects and themes of the research presented in Chapters 3-8, as well as a presentation of outlooks and implications for future lines of inquiry. The broader impacts of this body of work are discussed in the context of the biomedical device field.

9.1 Research Summary

9.1.1 Emergent themes. Broadly speaking, research in this dissertation is connected by three central themes. First, the application of novel plasma modification strategies for polymeric biomaterials, which encompasses PECVD (both single-precursor and plasma copolymerization) and functional group implantation strategies. For example, we demonstrated the ability to customize surface properties of two different NO-releasing polymer films via water plasma treatment, enhancing the surface wettability through implanting alcohol functionality (Chapter 4). The second theme establishes the need for comprehensive analysis strategies, including materials characterization and performance evaluation. This theme is explored in Chapter 3, which provides a review of wetting behavior assessment strategies for complex materials as well as in materials characterization strategies developed and utilized throughout Chapters 4-8. The third theme connects the first two by emphasizing the importance of the interplay between synthetic biomaterial properties and construct interactions in biological systems. For example, Chapters 5 and 6 report our ability to create non-bioreactive and bioreactive three-dimensional polymeric scaffolds, respectively, by tuning surface properties using plasma modification. Chapter 8 builds on this work, describing initial steps in the development of a library with

systematically varied surface/bulk properties with the ultimate intention of evaluating the bioreactivity of this collection of constructs in multiple biological environments (described in more detail in Section 9.2.1). This theme is also prevalent throughout Chapter 7, where TEG evaluation of 3D scaffolds with disparate surface properties demonstrates significant differences in coagulation behavior. Although the third emergent theme represents a variation on the property/function relationship that runs throughout the discipline of materials science, the research in this dissertation provides a unique approach, targeting fundamental surface property/biological response questions. The broader impact of this approach is further described in Section 9.1.2.

9.1.2 Broader impact and outlook. Research presented in this dissertation includes several original scientific contributions to the plasma modification of biomaterials field. One such contributions includes the utilization of PECVD to conformally modify porous polymeric constructs, effectively establishing strategies for translating PECVD from 2D construct architectures to those having more complex geometries. This work includes careful selection of plasma precursors to impart specific functionality (e.g., fluorocarbon, nitrogen-containing, oxygen-containing). Notably, such an approach provides numerous opportunities to design synthetic biomaterials with a collection of properties to elicit a particular biological response and, thus, target a specific application. Of equal importance to selecting and/or modifying characterization methodologies for 3D porous materials is developing fabrication and plasma modification strategies such constructs. Both pieces are required to obtain a comprehensive understanding of how materials are being modified, as well as their performance as biomedical devices. In this dissertation research, such efforts included translating both traditional surface characterization and biological assessment techniques to materials with complex geometries. The

research approach of evaluating polymer construct surface properties, bulk properties, and their relationships with biological response has improved our fundamental understanding of plasma processing of polymer constructs for biomedical applications. Collectively, this dissertation research provides a platform for creating tailored polymeric devices through systematically controlling device bulk and surface properties. Taken to the ideal, one could envision this work extending to the creation and deployment of customized, patient-specific synthetic biomaterial devices. More globally, a comprehensive understanding of device performance in biological settings presents numerous opportunities for application to numerous personalized point-of-care diagnostic strategies.

9.2 Future Directions

Research summarized in Section 9.1 represents foundational work that includes key steps for building a fundamental understanding of fabrication, plasma modification, and characterization of polymer constructs for biomedical device applications. This work establishes a platform for future lines of inquiry, both in terms of immediate next steps and long-term goals. This section includes a discussion of each classification of future work, differentiated by four categories: biological testing, plasma modification strategies, fabrication methods, and characterization technique development.

9.2.1 Evaluation of construct library in complex biological systems. Initial proof-of-concept biological experiments presented in this dissertation (e.g., with human dermal fibroblasts, *E. coli*, and blood plasma) are important for establishing methods for interfacing 3D polymer constructs with biological environments. Integrating materials in biomedical devices, however, requires a more sophisticated evaluation in more complex biological environments. To this extent, the groundwork established in this dissertation provides natural extensions for

exploring interactions between 3D porous polymer materials and a wide range of biological species. For example, the TEG technique presented in Chapter 7 offers the opportunity to facilitate investigating coagulation response with whole blood in addition to blood plasma. This exploration more closely mimics the biological environment of a blood-contacting device, and thus provides a more realistic performance assessment for this class of materials. Furthermore, TEG analysis is applicable for evaluating coagulation response of the biomaterials library developed throughout this dissertation, including plasma-modified polymer films and electrospun fiber mats. Such an assessment would provide a direct comparison of coagulation response between surface modifications as well as other construct geometries. Long-term goals in this area should focus on inoculating polymer constructs with different types of mammalian cells (e.g., epithelial, osteoblastic) and bacterial strains (e.g., *Staphylococcus aureus*, *Pseudomonas aeruginosa*). In this area, the biological species (or multiple biological species) would be selected based on a targeted application and 3D polymer matrix properties. For example, tissue engineering for bone regeneration would require a relatively stiff polymer matrix seeded with osteoblast cells, whereas a wound dressing to prevent a hospital acquired infection requires a flexible polymer matrix that is resistant to multiple bacterial strains. More specific aspects of materials fabrication related to these examples are further discussed in Section 9.2.3.

9.2.2 Expanding plasma modification strategies. Research in this dissertation has employed six plasma precursors (two of which were used as monomers for plasma copolymerization). A large portion of the parameter space remains unexplored despite utilizing multiple processing parameters across this collection of six precursors. For example, knowledge gained from the plasma copolymerization work (Chapter 6) and octadiene parameter space exploration (Chapter 8) aids in establishing additional routes to plasma copolymerization using

octadiene as a monomer. Previous studies utilized octadiene as a plasma copolymerization precursor, most commonly with allylamine[1-5] or acrylic acid.[5-11] Although some of these studies used plasma copolymerization strategies to customize interactions with biological species,[3, 10-11] they also focused on fabricating thin films on 2D substrates and subsequent evaluation in biological environments. Thus, potential exists to utilize our current understanding of OD-containing plasma copolymerization systems to modify three-dimensional polymer networks, effectively customizing chemical functionality and wettability.

An additional line of inquiry with regard to plasma modification strategies includes creating layered (i.e., composite) materials by depositing films with distinct properties to tune biological response. For example, depositing a thin film on the surface of a polymer construct using acrylic acid PECVD could produce a water soluble film with alcohol functionality. After acrylic acid treatment, the polymer construct could be plasma-modified using allyl alcohol, depositing a water-insoluble film with alcohol functionality. Alternating plasma treatments with the two precursors provides a platform for controlling release of a pharmaceutical or antibacterial agent, providing a more active strategy to control biological response. Furthermore, such research builds upon previous work in the group with gradient films created using PECVD with hydrocarbon and fluorocarbon functionality.[12]

9.2.3 Developing additional fabrication methods for three-dimensional porous polymer materials. Because of their desirable bulk properties (i.e., bioresorbability, mimicking extracellular matrices), model polyester constructs, including scaffolds and electrospun fibers fabricated using PCL and/or PLA have been the primary substrates of choice for this work. Although these model materials provide a useful foundation for establishing plasma modification and characterization strategies for porous polymer constructs, several avenues exist to expand the

collection of constructs presented in Chapters 3-8. One natural progression includes extending initial work with 50/50 PCL/PLA mixtures (Chapter 8) through fabricating constructs with varying polymer composition. One motivation for fabricating constructs with different polymer compositions was to lay groundwork to create different synthetic extracellular matrix mimics. This concept is especially relevant from an application perspective as extracellular matrices can vary widely with respect to mechanical properties depending on the type of tissue (e.g., brain vs. bone).[13-16] In the case of different PCL/PLA copolymers, constructs would vary in terms of crystallinity, and thus mechanical properties (e.g., strength, plasticity, Young's modulus) and degradation rate. Although mimicking a specific class of extracellular matrices was not a primary focus of this dissertation research, this is a fruitful area of work that could be more deeply explored in the future.

Additional routes to control construct bulk properties could expand on fabrication methods presented in this dissertation to create different polymer network geometries. For example, future work could build on the porogen leaching method by utilizing different porogen sizes and adjusting the polymer:porogen ratio. This approach could yield a series of scaffolds with systematically varied porosity and thus, systematically varied mechanical properties. Along these lines, different network geometries could be fabricated using experimental techniques other than those presented in this dissertation. For example, more ordered construct networks could be created using direct and soft template methods,[17-18] as well as numerous additive design strategies. One particularly promising route includes interfacing 3D printing technology with polyesters, which could offer precise control over construct geometry. Although challenges exist for establishing methods for 3D printing polyesters (e.g., polymer curability), some initial proof-of-concept studies demonstrate promise in this area.[19-22]

9.2.4 Developing additional characterization methods for three-dimensional porous polymer materials. In addition to pursing a broader range of 3D construct fabrication routes, a deep understanding of the interplay between material properties and biological environment will require developing and improving characterization strategies. One such strategy is time-of-flight secondary ion mass spectrometry (ToF-SIMS) depth profiling, which would provide complementary surface chemical functionality data to the XPS methods developed for work presented in this dissertation. These data would provide a detailed picture of functionality throughout a plasma-modified 3D network without disrupting the polymer network (i.e., freeze fracturing), which offers a distinct advantage over cross-sectional XPS data collection. A newly established collaboration with Dr. Lara Gamble and Dr. Dan Graham at University of Washington has yielded preliminary ToF-SIMS data on the exterior surface of unmodified and C_3F_8 plasma-treated PCL scaffolds. Figure 9.1 shows a summary of principal component analysis of positive ion ToF-SIMS data collected on scaffold tops, demonstrating that unmodified scaffolds have positive scores, while C_3F_8 plasma-treated scaffolds have negative scores (Figure 9.1a). These scores correspond to positive and negative loadings, respectively (Figure 9.1b), demonstrating that loading differences are attributed to presence of fluorinated peaks on the surface of C_3F_8 plasma-treated scaffolds. ToF-SIMS images overlaying the $C_6H_{11}O_2^+$ and CF_2^+ signals (Figure 9.2) provide further support for this finding as the CF_2^+ signal (associated with the fluorocarbon coating) is only observed on C_3F_8 plasma-treated scaffolds. Altogether, these preliminary data demonstrate that ToF-SIMS is a powerful technique for providing spatially-resolved surface chemical information on plasma-modified 3D materials. Data collection pertaining to the sputter rate of PCL and fluorocarbon films is currently

underway, which we hope to expand to depth profiling experiments on 3D constructs in the near future.

Fabricating materials with systematically varied bulk properties (such as those discussed in Section 9.2.3) will require a more rigorous porous network characterization than those utilized in this dissertation (SEM and ImageJ). Such characterization will allow for a quantitative comparison of construct geometries, and could include porosimetry or Brunauer-Emmett-Teller analysis. Additionally, mechanical properties testing could be performed using any number of commercially available materials testing systems to establish construct response under tension and/or compression. Notably, employing these methods would likely involve non-trivial optimization in terms of interfacing the technique with a 3D polymeric network. Another line of inquiry connected with PCL/PLA construct data presented in Chapter 8, as well as future directions outlined in Section 9.2.3, includes evaluating construct degradation behavior in biological media.

Future directions for collaborations with Dr. Melissa Reynolds' group (adding to work presented in Chapter 4) could include coupling plasma diagnostic strategies with plasma modification of nitric oxide-releasing polymers. The Fisher group has a long-standing expertise using optical emission spectroscopy (OES) to identify excited-state plasma species, as well as measure rotational and vibrational temperatures of said species. Specifically, we have used OES to identify excited-state nitric oxide (NO) in plasmas formed from water vapor-containing plasmas.[23] Combining this knowledge with our newly-established time-resolved OES capabilities could provide an in situ measurement of NO release from the surface of NO-containing polymer films during water vapor plasma modification. Additional extensions of the NO releasing polymer film projects include incorporating NO releasing polymers into 3D constructs and

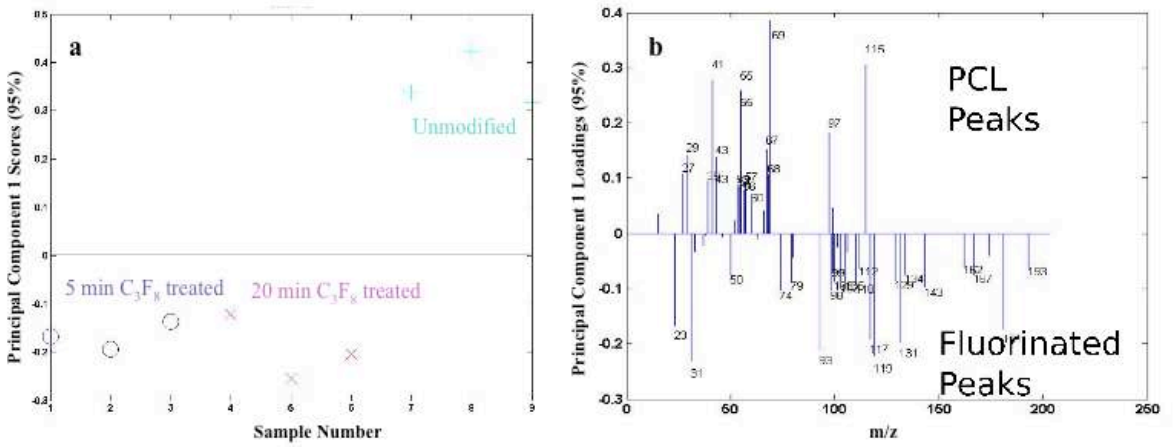

Figure 9.1. Results from principal component analysis of ToF-SIMS positive ion data collected on unmodified (n = 3), 5 min C_3F_8 plasma-treated (n = 3) and 20 min C_3F_8 plasma-treated (n = 3) PCL scaffold tops. (a) principal component scores for each spot analyzed, and (b) corresponding principal component loadings.

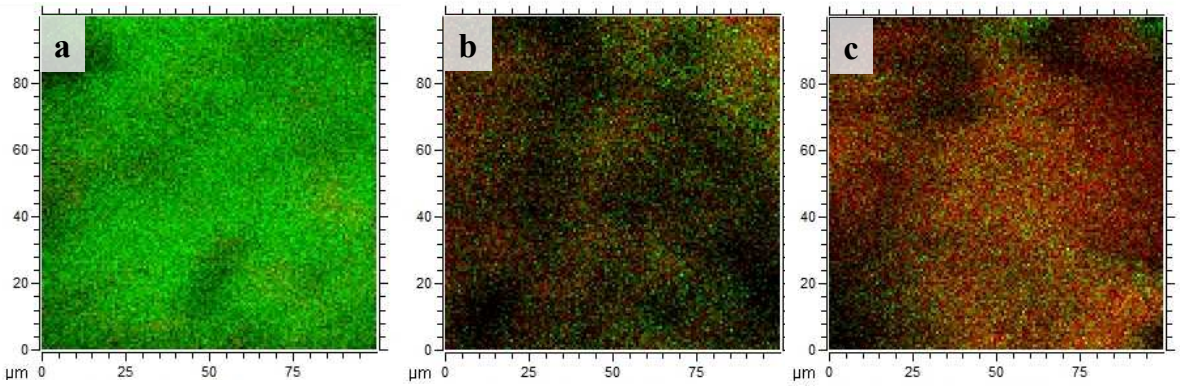

Figure 9.2. Representative overlays of the $C_6H_{11}O_2^+$ (green) and CF_2^+ (red) signals measured via ToF-SIMS on (a) unmodified (b) 5 min C_3F_8 plasma treated and (c) 20 min C_3F_8 plasma treated PCL scaffold tops.

incorporating additional drugs into polymer networks. The latter will require utilizing and/or developing methodologies to measure temporal drug release for drugs other than NO – an aspect that has yet to be explored in this dissertation research.

Collectively, research presented in Part I of this dissertation built a fundamental understanding of how polymer biomaterial properties affect the interplay between materials and biological environments. A comprehensive experimental approach was utilized, including fabrication, plasma modification, materials characterization, and performance evaluation with biological species. This approach resulted in the fabrication of constructs with customizable properties and therefore, tunable biological response. Immense potential exists to expand and apply these strategies to next-generation biomaterial construct development.

REFERENCES

1. Ruiz, J. C.; Taheri, S.; Michelmore, A.; Robinson, D. E.; Short, R. D.; Vasilev, K.; Förch, R., Approaches to Quantify Amine Groups in the Presence of Hydroxyl Functional Groups in Plasma Polymerized Thin Films. *Plasma Process. Polym.* **2014,** *11* (9), 888-896.
2. Coad, B. R.; Bilgic, T.; Klok, H.-A., Polymer Brush Gradients Grafted from Plasma-Polymerized Surfaces. *Langmuir* **2014,** *30* (28), 8357-8365.
3. Zuber, A. A.; Robinson, D. E.; Short, R. D.; Steele, D. A.; Whittle, J. D., Development of a Surface to Increase Retinal Pigment Epithelial Cell (ARPE-19) Proliferation Under Reduced Serum Conditions. *J. Mater. Sci. - Mater. Med.* **2014,** *25* (5), 1367-1373.
4. Photjanataree, P.; Liu, Z.; Jones, F. R., The Role of a Nanoscale Interphase from Plasma Polymers on the Micromechanics of Fiber Composites. *Macromol. Mater. Eng.* **2012,** *297* (6), 523-531.
5. Liu, Z.; Zhao, F.; Jones, F. R., Optimising the Interfacial Response of Glass Fibre Composites with a Functional Nanoscale Plasma Polymer Coating. *Compos. Sci. Technol.* **2008,** *68* (15), 3161-3170.
6. Sugihara, H.; Jones, F., Promoting the Adhesion of High-performance Polymer Fibers using Functional Plasma Polymer Coatings. *Polym. Compos.* **2009,** *30* (3), 318-327.
7. Parry, K. L.; Shard, A.; Short, R.; White, R.; Whittle, J.; Wright, A., ARXPS Characterisation of Plasma Polymerised Surface Chemical Gradients. *Surf. Interface Anal.* **2006,** *38* (11), 1497-1504.
8. Lopattananon, N.; Hayes, S.; Jones, F., Stress Transfer Function for Interface Assessment in Composites with Plasma Copolymer Functionalized Carbon Fibres. *J. Adhesion* **2002,** *78* (4), 313-350.
9. Haddow, D. B.; Goruppa, A.; Whittle, J.; Short, R.; Kahle, O.; Uhlig, C.; Bauer, M., Application of Variable-temperature Ellipsometry to Plasma Polymers: The Effect of Addition of 1,7-octadiene to Plasma Deposits of Acrylic Acid. *Chem. Mater.* **2000,** *12* (4), 866-868.
10. Haddow, D.; France, R.; Short, R.; MacNeil, S.; Dawson, R.; Leggett, G.; Cooper, E., Comparison of Proliferation and Growth of Human Keratinocytes on Plasma Copolymers of Acrylic Acid/1, 7‐octadiene and Self‐assembled Monolayers. *J. Biomed. Mater. Res. A* **1999,** *47* (3), 379-387.
11. Daw, R.; Candan, S.; Beck, A.; Devlin, A.; Brook, I.; MacNeil, S.; Dawson, R.; Short, R., Plasma Copolymer Surfaces of Acrylic Acid/1, 7-octadiene: Surface Characterisation and the Attachment of ROS 17/2.8 Osteoblast-like Cells. *Biomaterials* **1998,** *19* (19), 1717-1725.
12. Tompkins, B. D.; Fisher, E. R., Plasma Synthesis of Hydrocarbon/Fluorocarbon Thin Films with Compositional Gradients. *Plasma Process. Polym.* **2013,** *10* (9), 779-791.
13. Badylak, S. F.; Freytes, D. O.; Gilbert, T. W., Extracellular Matrix as a Biological Scaffold Material: Structure and Function. *Acta Biomater.* **2009,** *5* (1), 1-13.
14. Wu, S.; Liu, X.; Yeung, K. W.; Liu, C.; Yang, X., Biomimetic Porous Scaffolds for Bone Tissue Engineering. *Mater. Sci. Eng., R* **2014,** *80*, 1-36.
15. Banerjee, A.; Arha, M.; Choudhary, S.; Ashton, R. S.; Bhatia, S. R.; Schaffer, D. V.; Kane, R. S., The influence of hydrogel modulus on the proliferation and differentiation of encapsulated neural stem cells. *Biomaterials* **2009,** *30* (27), 4695-4699.

16. Ghosh, K.; Pan, Z.; Guan, E.; Ge, S.; Liu, Y.; Nakamura, T.; Ren, X.-D.; Rafailovich, M.; Clark, R. A., Cell Adaptation to a Physiologically Relevant ECM Mimic with Different Viscoelastic Properties. *Biomaterials* **2007,** *28* (4), 671-679.
17. Liu, Q.; Tang, Z.; Ou, B.; Liu, L.; Zhou, Z.; Shen, S.; Duan, Y., Design, Preparation, and Application of Ordered Porous Polymer Materials. *Mater. Chem. Phys.* **2014,** *144* (3), 213-225.
18. Lee, J.; Cuddihy, M. J.; Kotov, N. A., Three-dimensional Cell Culture Matrices: State of the Art. *Tissue Eng. Part B* **2008,** *14* (1), 61-86.
19. Hoque, M. E.; San, W. Y.; Wei, F.; Li, S.; Huang, M.-H.; Vert, M.; Hutmacher, D. W., Processing of Polycaprolactone and Polycaprolactone-based Copolymers into 3D Scaffolds, and their Cellular Responses. *Tissue Eng. Part A* **2009,** *15* (10), 3013-3024.
20. Sobral, J. M.; Caridade, S. G.; Sousa, R. A.; Mano, J. F.; Reis, R. L., Three-dimensional Plotted Scaffolds with Controlled Pore Size Gradients: Effect of Scaffold Geometry on Mechanical Performance and Cell Seeding Efficiency. *Acta Biomater.* **2011,** *7* (3), 1009-1018.
21. Seyednejad, H.; Gawlitta, D.; Kuiper, R. V.; de Bruin, A.; van Nostrum, C. F.; Vermonden, T.; Dhert, W. J.; Hennink, W. E., In vivo Biocompatibility and Biodegradation of 3D-printed Porous Scaffolds Based on a Hydroxyl-functionalized Poly (ε-caprolactone). *Biomaterials* **2012,** *33* (17), 4309-4318.
22. Domingos, M.; Intranuovo, F.; Russo, T.; De Santis, R.; Gloria, A.; Ambrosio, L.; Ciurana, J.; Bartolo, P., The First Systematic Analysis of 3D Rapid Prototyped Poly (ε-caprolactone) Scaffolds Manufactured Through BioCell Printing: The Effect of Pore Size and Geometry on Compressive Mechanical Behaviour and in vitro hMSC Viability. *Biofabrication* **2013,** *5* (4), 045004.
23. Morgan, M. M.; Cuddy, M. F.; Fisher, E. R., Gas-phase Chemistry in Inductively Coupled Plasmas for NO Removal from Mixed Gas Systems. *J. Phys. Chem. A* **2010,** *114* (4), 1722-1733.

PART II: EXPLORING GENERAL CHEMISTRY STUDENTS' METACOGNITIVE MONITORING ON EXAMINATIONS

CHAPTER 1

INTRODUCTION OF CHEMISTRY EDUCATION FOCUSED RESEARCH

"Ignorance more frequently begets confidence than does knowledge"
— Charles Darwin (*The Descent of Man,* 1871)

This chapter presents an exploration of the importance of judgment accuracy to chemistry student learning framed through the lens of metacognitive skillfulness. Definitions of metacognition and its constituents are included, as well as previous work on evaluating metacognitive monitoring in classroom contexts.

1.1 Motivation: Metacognitive Skillfulness and Judgment Accuracy

Improving students' awareness of their own learning is an important area of research within the education community because of its necessity in the development of students as independent learners. Central to students' awareness of their learning is the concept of metacognition, or, thinking about one's own thinking.[1] Metacognitive skills are recognized for their important role in learning.[2, 3] For example, in one study, metacognitive skillfulness accounted for approximately 40% of the variance in learning outcomes.[4] In a meta-analysis focused on factors that influence student achievement, metacognitive strategies comprise one of the most influential elements (effect size = 0.69).[5] Thus, to improve student learning in a specific content area such as chemistry, it is critical to understand students' metacognitive skillfulness in the content area and how instructional methods in the content area can improve students' metacognitive skillfulness.

There are two components of metacognition: knowledge of cognition and regulation of cognition.[1, 3, 6-8] Knowledge of cognition is defined as a collection of declarative, procedural, and

conditional knowledge.[9] Regulation of cognition is defined as adjustments that learners make to control learning, including planning, monitoring, and evaluating strategies. Metacognitive monitoring is the focus of this dissertation work because of its crucial role in student learning, where monitoring includes assessing one's current knowledge, understanding, and abilities, the task at hand, and task difficulty.[2, 10] Regulation of cognition activities are sometimes referred to as metacognitive skills,[11] although there is some discrepancy in the literature related to the "metacognitive skills" terminology. Namely, whether it is most appropriate to refer to these as "skills" or "strategies". Veenman proposed that metacognitive strategies are those that are consciously executed by the learner, whereas metacognitive skills may be partially automated.[11] Following this distinction, research presented in Chapter 2 of this dissertation focuses more on metacognitive skills, whereas that presented in Chapter 3 focuses more on metacognitive strategies (specifically via metacognitive strategy training).

1.2 Metrics for Evaluating Metacognitive Monitoring

Metacognitive monitoring processes cannot be directly assessed because they occur internally; thus, indirect evaluations must be utilized. The most commonly reported measures of monitoring relate to an individual's judgments, including indirect (confidence-based) and direct (prediction of numerical/percentile score) judgments. Judgments could be based on either individual item (local) or overall (global) performance on a given task,[12] and quantitatively assessed in terms of accuracy, bias, scatter, and discrimination.[13-19]

The accuracy of performance judgments is referred to as *calibration*, defined as the degree to which an individual's judgment of task performance corresponds to actual performance of that task.[20-21] Here, judgments could consist of pre- and/or post-dictions, where a postdiction is a judgment made after completing a task. Although calibration accuracy likely comprises

numerous cognitive and metacognitive processes, a central component includes metacognitive monitoring processes because the individual making the judgment must assess what s/he knows about a specific skill and judge knowledge of that skill against one or more criteria.[21] Generally speaking, people's abilities to pre- or postdict their performance on a task (i.e., their pre- or postdiction calibration) is found to be poor.[22] It is important to note, however, that pre- and postdiction accuracy is related to task difficulty.[22]

1.3 Overview of Research

Work presented in Chapter 2 focuses on postdiction calibration accuracy of general chemistry students' exam performance postdictions. Studies that employ pre- or postdictions of absolute exam performance have been performed in undergraduate educational psychology,[8, 15, 18, 23] education,[13] cognitive psychology,[16] developmental psychology,[24] introductory physics[25] and organic chemistry courses;[26] high-school biology[27, 28] and psychology classrooms;[29] and upper-elementary classrooms.[30] Many studies conclude that many students are well-calibrated when it comes to making postdictive judgments of exam performance.[8, 18, 27-28] A notable exception is the study carried out in organic chemistry, in which the majority of students overestimated their exam performance.[26] Studies that explored relationships between performance and calibration found that higher-performing students were better calibrated on exam postdictions than lower-performing students.[8, 13, 18, 23] Also relevant to the present research were studies that included analyses to determine changes in students' calibration accuracy over time. Here, findings indicate that students became more accurate in some cases where there was an explicit intervention designed to improve students' metacognitive monitoring throughout the course.[13, 15-16, 18, 23]

Work presented in Chapter 3 is inspired by general chemistry exam score postdiction findings (Chapter 2), and includes the experimental design of a protocol for a series of general chemistry metacognitive strategy training workshops. The intervention design includes the comparison of exam score postdiction data with data from an instrument entitled the Metacognitive Assessment Inventory (MAI), which is used to measure metacognitive skillfulness. The MAI, first developed by Schraw and Dennison,[6] is a validated questionnaire instrument that has been used in a variety of education contexts.[31-32] The MAI includes 52 items intended to measure adults' metacognitive awareness, where items are grouped into two categories influenced by proposed components of metacognition discussed in Section 1.1: knowledge of cognition (sub-processes: declarative, procedural, and conditional knowledge) and regulation of cognition. Sub-processes included in regulation include information management and debugging strategies in addition to the three components presented above (planning, monitoring, and evaluation), which resulted from factor analysis involved in the instrument development.[6] The total MAI score, as well as individual scores on questions pertaining to knowledge of cognition (17 questions) and regulation of cognition (35 questions) are typically reported. Notably, the MAI is not exempt from concerns associated with any self-report instrument.[33] This instrument, however, provides a measure of pre/post-intervention metacognitive awareness that is easily adaptable for a relatively large population of students. In the original development report of the MAI, Schraw and Dennison explored the convergent validity of the instrument against pre-test monitoring (i.e., students' self-reports of monitoring abilities), test performance, and the ability to accurately monitor test performance (i.e., individual item confidence judgments). These findings demonstrated significant relationships between knowledge of cognition MAI score/test performance, pre-test monitoring/total MAI

score, and pre-test monitoring/test performance. Research in Chapter 3 expands upon Schraw and Dennison's findings by exploring the relationship between MAI score and *global* monitoring accuracy (as measured by postdictions).

Altogether, the chemistry education research presented in the next two chapters provides insight regarding student learning in chemistry courses through explorations of calibration phenomena in exam score contexts. Calibration accuracy serves as the basis for the design of a metacognitive strategy training intervention, which generates an even deeper knowledge base regarding general chemistry students' metacognitive monitoring. This research represents one of the few explorations of metacognitive monitoring in undergraduate general chemistry courses, and thus, provides an increased understanding of the connections between student judgment accuracy and performance. This research thereby contributes to the growing number of educational studies exploring metacognition in science education classrooms, which can be used to make more informed pedagogical decisions that target metacognitive skillfulness.

REFERENCES

1. Flavell, J. H., Metacognition and Cognitive Monitoring: A New Area of Cognitive-Developmental Inquiry. *Am. Psychol.* **1979,** *34* (10), 906–911.
2. Flavell, J. H.; Miller, P. H.; Miller, S. A., *Cognitive Development*. 4 ed.; Prentice-Hall Englewood Cliffs, NJ: 2002.
3. Zohar, A.; Barzilai, S., A Review of Research on Metacognition in Science Education: Current and Future Directions. *Stud. Sci. Educ.* **2013,** *49* (2), 121-169.
4. Veenman, M. V., *Meta-cognition: A Recent Review of Research, Theory, and Perspectives*. Nova Science Publishers, Inc.: New York, 2008; p 207-220.
5. Hattie, J., *Visible learning: A synthesis of over 800 meta-analyses relating to achievement*. Routledge: 2008.
6. Schraw, G.; Dennison, R. S., Assessing Metacognitive Awareness. *Contemp. Educ. Psychol.* **1994,** *19* (4), 460-475.
7. Brown, A., *Metacognition, Executive Control, Self-regulation, and Other More Mysterious Mechanisms*. Lawrence Erlbaum Associates: Hillsdale, New Jersey, 1987; p 65-116.
8. Nietfeld, J. L.; Cao, L.; Osborne, J. W., Metacognitive Monitoring Accuracy and Student Performance in the Postsecondary Classroom. *J. Exp. Educ.* **2005**, 7–28.
9. Jacobs, J. E.; Paris, S. G., Children's Metacognition About Reading: Issues in Definition, Measurement, and Instruction. *Educ. Psychol.* **1987,** *22* (3-4), 255-278.
10. Nelson, T. O.; Narens, L., *Metamemory: A Theoretical Framework and New Findings*. Academic Publishers San Diego, CA, 1990; Vol. 26, p 125–141.
11. Veenman, M. V.; Alexander, P., *Learning to Self-monitor and Self-regulate*. Routledge: New York, 2011.
12. Mathabathe, K. C.; Potgieter, M., Metacognitive Monitoring and Learning Gain in Foundation Chemistry. *Chemistry Education Research and Practice* **2014,** *15* (1), 94-104.
13. Bol, L.; Hacker, D. J.; O'Shea, P.; Allen, D., The Influence of Overt Practice, Achievement Level, and Explanatory Style on Calibration Accuracy and Performance. *J. Exp. Educ.* **2005,** *73* (4), 269–290.
14. Dunlosky, J.; Metcalfe, J., *Metacognition*. Sage Publications: 2008.
15. Hacker, D. J.; Bol, L.; Bahbahani, K., Explaining Calibration Accuracy in Classroom Contexts: the Effects of Incentives, Reflection, and Explanatory Style. *Metacognition Learn.* **2008,** *3* (2), 101–121.
16. Miller, T. M.; Geraci, L., Training Metacognition in the Classroom: the Influence of Incentives and Feedback on Exam Predictions. *Metacognition Learn.* **2011,** *6* (3), 303–314.
17. Pieschl, S., Metacognitive Calibration—an Extended Conceptualization and Potential Applications. *Metacognition Learn.* **2009,** *4* (1), 3-31.
18. Hacker, D. J.; Bol, L.; Horgan, D. D.; Rakow, E. A., Test Prediction and Performance in a Classroom Context. *J. Educ. Psychol.* **2000,** *92* (1), 160–170.
19. Schraw, G., A Conceptual Analysis of Five Measures of Metacognitive Monitoring. *Metacognition Learn.* **2009,** *4* (1), 33-45.
20. Lin, L. M.; Zabrucky, K. M., Calibration of Comprehension: Research and Implications for Education and Instruction. *Contemp. Educ. Psychol.* **1998,** *23* (4), 345–391.

21. Hacker, D. J.; Bol, L.; Keener, M. C., *Metacognition in Education: A Focus on Calibration*. 2008; p 429-455.
22. Burson, K. A.; Larrick, R. P.; Klayman, J., Skilled or Unskilled, but Still Unaware of it: How Perceptions of Difficulty Drive Miscalibration in Relative Comparisons. *J. Pers. Soc. Psychol.* **2006,** *90* (1), 60.
23. Nietfeld, J. L.; Cao, L.; Osborne, J. W., The Effect of Distributed Monitoring Exercises and Feedback on Performance, Monitoring Accuracy, and Self–efficacy. *Metacognition Learn.* **2006,** *1* (2), 159–179.
24. de Carvalho Filho, M. K., Confidence Judgments in Real Classroom Settings: Monitoring Performance in Different Types of Tests. *Int. J. Psychol.* **2009,** *44* (2), 93–108.
25. Galloway, R. K.; Bates, S. P.; Parker, J.; Usoskina, E. In *The Effect of Research-based Instruction in Introductory Physics on a Common Cognitive Bias*, 2012 Physics Education Research Conference, AIP Publishing: 2013; pp 138-141.
26. Karatjas, A. G., Comparing College Students' Self–Assessment of Knowledge in Organic Chemistry to Their Actual Performance. *J. Chem. Educ.* **2013,** *98* (8), 1096–1099.
27. Bol, L.; Hacker, D. J.; Walck, C. C.; Nunnery, J. A., The Effects of Individual or Group Guidelines on the Calibration Accuracy and Achievement of High School Biology Students. *Contemp. Educ. Psychol.* **2012,** *37* (4), 280–287.
28. Snyder, K. E.; Nietfeld, J. L.; Linnenbrink-Garcia, L., Giftedness and Metacognition A Short–Term Longitudinal Investigation of Metacognitive Monitoring in the Classroom. *Gifted Child Quart.* **2011,** *55* (3), 181–193.
29. Gillström, Å.; Rönnberg, J., Comprehension Calibration and Recall Prediction Accuracy of Texts: Reading Skill, Reading Strategies, and Effort. *J. Educ. Psychol.* **1995,** *87* (4), 545–558.
30. Labuhn, A. S.; Zimmerman, B. J.; Hasselhorn, M., Enhancing Students' Self-regulation and Mathematics Performance: The Influence of Feedback and Self-evaluative Standard. *Metacognition Learn.* **2010,** *5* (2), 173–194.
31. Seraphin, K. D.; Philippoff, J.; Kaupp, L.; Vallin, L. M., Metacognition as Means to Increase the Effectiveness of Inquiry-Based Science Education. *Science Education International* **2012,** *23* (4), 366-382.
32. Sperling, R. A.; Howard, B. C.; Staley, R.; DuBois, N., Metacognition and self-regulated learning constructs. *Educational Research and Evaluation* **2004,** *10* (2), 117-139.
33. Richardson, J. T., Methodological Issues in Questionnaire-based Research on Student Learning in Higher Education. *Educ. Psychol. Rev.* **2004,** *16* (4), 347-358.

CHAPTER 2

INVESTIGATING GENERAL CHEMISTRY STUDENTS' METACOGNITIVE MONITORING OF THEIR EXAM PERFORMANCE BY MEASURING POSTDICTION ACCURACIES OVER TIME

This chapter focuses on examining general chemistry students' metacognitive monitoring, one aspect of metacognition that plays a key role in learning, in the context of exam score judgments. As discussed in Chapter 1, an aspect of metacognitive monitoring can be measured by comparing a student's prediction or postdiction of performance (a judgment made before or after completing the relevant task) with the student's actual performance. In this study, we investigated students' postdiction accuracies for a series of exams within a two-semester general chemistry course. The research questions addressed include: 1) How accurate are general chemistry students at postdicting their exam scores? Are there gender differences in postdiction accuracy?, 2) How do general chemistry students' postdiction accuracies relate to their exam performance?, and 3) How do general chemistry students' postdiction accuracies and metacognitive monitoring of their exam performance change over time?

This chapter, and corresponding supplementary tables in Appendix I, is reproduced with permission from an article published in *Journal of Chemical Education* by Morgan J. Hawker, Lisa Dysleski, and Dawn Rickey [*93* (5), pp 832-840 Copyright 2016 American Chemical Society].[1] This work was supported by the National Science Foundation (award number 0942448). I want to acknowledge and thank the general chemistry students and instructors who participated in the study, as well as Ellen Fisher, Matthew Rhodes, Melonie Teichert and anonymous reviewers for insightful comments on drafts of the manuscript.

2.1 Introduction

As discussed in Chapter 1, evaluating metacognitive monitoring is critical to developing a more detailed understanding of student learning in STEM courses (and more specifically, in chemistry courses). Here, we focus on students' metacognitive monitoring in a general chemistry course. In the context of general chemistry courses, monitoring research has primarily focused on students' abilities to judge their performance on problems outside of exam situations. For example, in two studies, investigators asked students to report their confidence in their abilities to solve particular chemistry problems, but the students did not actually work the problems presented to them.[2, 3] Another study examined the relationship between students' confidence judgments regarding individual stoichiometry questions and their performance on these questions.[4] In one study that did investigate students' judgments of performance on general chemistry exams, students were asked to judge how they performed on exams relative to the average student in the class (without any knowledge of the class average or other students' exam scores).[5] Such relative judgments are fundamentally different tasks compared with the absolute judgments of individual performance examined here.

In this study, we examine general chemistry students' abilities to monitor their examination performance. We investigate students' judgments of their own performance on exams within a two-semester general chemistry course. Our research questions are: 1) How accurate are general chemistry students at postdicting their exam scores? Are there gender differences in postdiction accuracy?, 2) How do general chemistry students' postdiction accuracies relate to their exam performance?, and 3) How do general chemistry students' postdiction accuracies and metacognitive monitoring of their exam performance change over time?

One relationship of interest for work presented in this chapter was that between gender and postdiction accuracy. Previous work has explored differences in male and female postdiction accuracies on informal knowledge tests. In particular, Beyer[6] and Beyer & Bowden[7] found that, although there were no significant differences between male and female undergraduate students in postdiction accuracy on "neutral" tasks (e.g., tests of common knowledge) or "feminine-gender-typed" tasks (e.g., trivia from movies and TV shows with primarily female audiences), females significantly underestimated their performance and exhibited poorer calibration relative to males on "masculine-gender-typed" tasks (e.g., football, basketball, and baseball trivia). In studies that asked undergraduate students to rate their performance relative to that of other students, Kruger and Dunning did not find any gender differences in postdiction accuracy on tests of humor, logical reasoning, or English grammar.[8] Finally, Beyer explored gender differences in accuracy of students' exam postdictions in the context of cognitive psychology, social psychology, and computer science courses.[9] In this study, gender differences were only observed for postdictions in the social psychology course. Results from these prior studies prompted us to explore connections between gender and postdiction accuracy in a general chemistry course setting.

2.2 Methods

We collected data from students enrolled in a two-semester general chemistry sequence (General Chemistry I and General Chemistry II) for science and engineering majors at a large, public university. Although each course included multiple sections and instructors (Table 2.1), common exams were administered to all students. The instructors for the spring General Chemistry II course were a subset of the instructors for the fall General Chemistry I course. For each semester-long course, five multiple-choice exams were administered at three-week intervals,

Table 2.1. Summary of course characteristics

Semester	Sections	Instructors	Students Enrolled[a]	Students in Study
Fall	5	4	1075	925
Spring	3	2	696	491

[a] Total enrollment at the end of each course

including one comprehensive final exam. The first four exams were not comprehensive. Example exam questions are shown in Figure 2.1. Students in both fall and spring semesters had the option to use their final exam percentage as a replacement for one previous exam percentage in the calculation of their final course grade.

All exams included the postdiction question, *What percentage score do you expect to earn on this exam? A) 100%–90%, B) 89%–80%, C) 79%–70%, D) 69%–60%, E) < 60%."* This question appeared as the last or second-to-last question on each exam,[1] such that each student was asked to make a judgment of his or her own score on the exam immediately after taking the exam. We collected students' answers to all exam questions via optical mark recognition (i.e., Scantron®) forms. Each student who answered a postdiction question received credit amounting to 1–2% of the total points for the exam regardless of whether or not his or her postdiction was accurate. No interventions intended to improve students' metacognitive monitoring of exam performance were implemented in these courses. Students who were missing a postdiction response or exam score for any exam were excluded from the study, resulting in the final cohorts indicated in Table 2.1. In addition, we performed separate analyses for the students who took both the General Chemistry I course in the fall and the General Chemistry II course the following spring (Fall & Spring, N=343), and those who took the General Chemistry II course in the spring, but not the General Chemistry I course in the fall (Spring Only, N=148). The Spring Only students took the General Chemistry I course in a different semester or at a different institution, or were exempt from the first-semester course because they had Advanced Placement credit or tested out of the course. To conduct the calibration analyses, we coded each student's actual exam scores and exam postdictions using the categories that were available as answer choices to

[1] On the fall final exam, the last question was: "What letter grade do you expect to earn in [this course]?" A) A+, A or A– B) B+, B or B– C) C+ or C D) D E) F

First Semester
D and E are elements whose identities are unknown. Given that a neutral atom of D has a larger atomic radius than a neutral atom of E, and that the relationships between D and E are consistent with the periodic trends discussed in class, which must be true?

a. Element D is closer to the bottom of the periodic table than element E.
b. An atom of D has more electrons than an atom of E.
c. Element E has a higher first ionization energy than element D.
d. The most stable ion formed from D has a larger atomic radius than the most stable ion formed from E.
e. Both B and D must be true.

Second Semester
Substance A (grey) decomposes into two other substances, B (black) and C (white) according to a zero-order reaction. The molecular scenes below show a portion of the reaction mixture at two times. What is the average rate of disappearance of A during the interval 1 – 2 minutes?

A → B + C

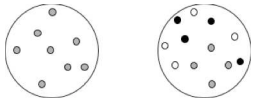

0 minutes 1 minute

(a) 2 min^{-1} (b) 4 min^{-1} (c) 8 min^{-1} (d) 0.25 min^{-1} (e) 12 min^{-1}

Figure 2.1. Sample questions from first- and second-semester general chemistry exams.

the postdiction questions. We converted each exam score category and corresponding postdiction to a numerical value on a 4-point scale as follows: 100%–90% = 4, 89%–80% = 3, 79%–70% = 2, 69%–60% = 1, < 60% = 0. Finally, we determined the postdiction calibration for each student on each exam by calculating the difference between his or her postdiction category and his or her exam score category (equation 2.1).

$$\textit{postdiction calibration} = \textit{postdiction category} - \textit{exam score category} \quad (2.1)$$

A student with positive postdiction calibration postdicted that his or her exam score would be higher than it actually was (*overpostdicted*), whereas a student with negative postdiction calibration postdicted that his or her exam score would be lower than it actually was (*underpostdicted*). A student with postdiction calibration of zero accurately postdicted the score category into which his or her actual exam score would fall (*perfectly calibrated*). We used the absolute value of the postdiction calibration (|calibration|) for each student to determine the average magnitudes of calibration for groups of students. To characterize students' postdiction accuracies in the context of our research questions, we employed the complementary measures of |calibration| and the percentage of students who were perfectly calibrated (% accurate).

To examine relationships between calibration and exam performance, we also established two performance groups of students. One group of consistently “high-performing students", or those who earned exam scores greater than ½ standard deviation above the exam mean on every exam, and one group of consistently “low-performing students," or those who earned exam scores lower than ½ standard deviation below the exam mean on every exam. These performance groups did not encompass all students in the course, as many students did not consistently score within a single performance group for all exams in a given course.

For both the fall and spring semesters, we calculated descriptive statistics for student exam scores, postdictions, calibration, and the percentage of accurate postdictions for the student groups of interest. We used independent samples t-tests to test for significant differences in exam score means of different student groups, except for a case in which the homogeneity of variance assumption was violated for which we used nonparametric Mann-Whitney U tests (two-tailed). Additionally, we performed Mann-Whitney U tests to compare the |calibration| and exam score category distributions for different groups. We determined the appropriate effect sizes, with Cohen's d effect sizes corresponding to t-tests and r effect sizes corresponding to Mann-Whitney U and Wilcoxon signed rank tests. r effect sizes were calculated according to equation 2.2, where *x* is the Mann-Whitney U or Wilcoxon signed rank test Z-score and N is the sample size.[10-11]

$$r = \frac{x}{\sqrt{N}} \tag{2.2}$$

Effect sizes of 0.1, 0.3, and 0.5 are considered to be small, medium, large, respectively.[12]
In addition, we utilized Fisher's exact to test for the significance of differences in % accurate postdictions.[13] We applied the Bonferroni adjustment to correct for multiple comparisons in each semester, resulting an α level of 0.01.[14] We performed all statistical analyses using SPSS version 20.0 software (SPSS Inc., Chicago, IL).

2.3 Results and Discussion

2.3.1 Postdiction accuracy. Figures 2.2 and 2.3 present bubble plots of postdiction category versus exam score category for each exam in fall and spring, respectively. The size of each bubble corresponds to the number of students who fell into a specific combination of exam score category and postdiction category. Bubbles that fall on the dashed diagonal lines in the plots represent students who were perfectly calibrated. In each case, a minority of students fall along the line of perfect calibration, with the percentage of students accurately postdicting their

exam score category ranging from 9.1% to 31.4% (also see Table 2.2). Figure 2.2A shows that for Fall Exam 1, only 9.1% of students were perfectly calibrated, whereas the vast majority of students (89.3%) overpostdicted. In fact, more students made overpostdictions than under- or accurate postdictions for all exams analyzed.

The mean absolute calibration (|calibration|) for each exam (Table 2.2) indicates how close students' postdictions were to their actual performance categories on average. Throughout the two-semester general chemistry course, the accuracy of students' postdictions was low, averaging one to two exam score categories away from their actual performance. (Changes in postdiction accuracy over time are disscussed in Section 2.3.3.) We also note that for the comprehensive final exams for both semesters, larger percentages of students overpostdicted, and mean |calibration| was less accurate than in all other cases except for Fall Exam 1. In addition to the more comprehensive nature of the final exams (which increased the difficulty), student postdictions may have been more optimistic than usual because many students hoped to obtain a higher score on their final exam to replace a previous low exam score. Finally, as discussed in more detail later, the lower the exam mean, the less accurate students' mean |calibration| tended to be. We also compared % accurate postdictions and mean |calibration| for male and female students on each exam. Although female students had consistently higher rates of % accurate postdictions compared with male students, none of the differences are statistically significant (Appendix I, Table AI.1).

With respect to mean |calibration|, female students were significantly more accurate on average than male students for three of the five fall-semester exams (exam 2, exam 4, and the final exam), with small effect sizes of about 0.1, whereas in the spring semester there were no significant differences in mean |calibration| between male and female students (Appendix I,

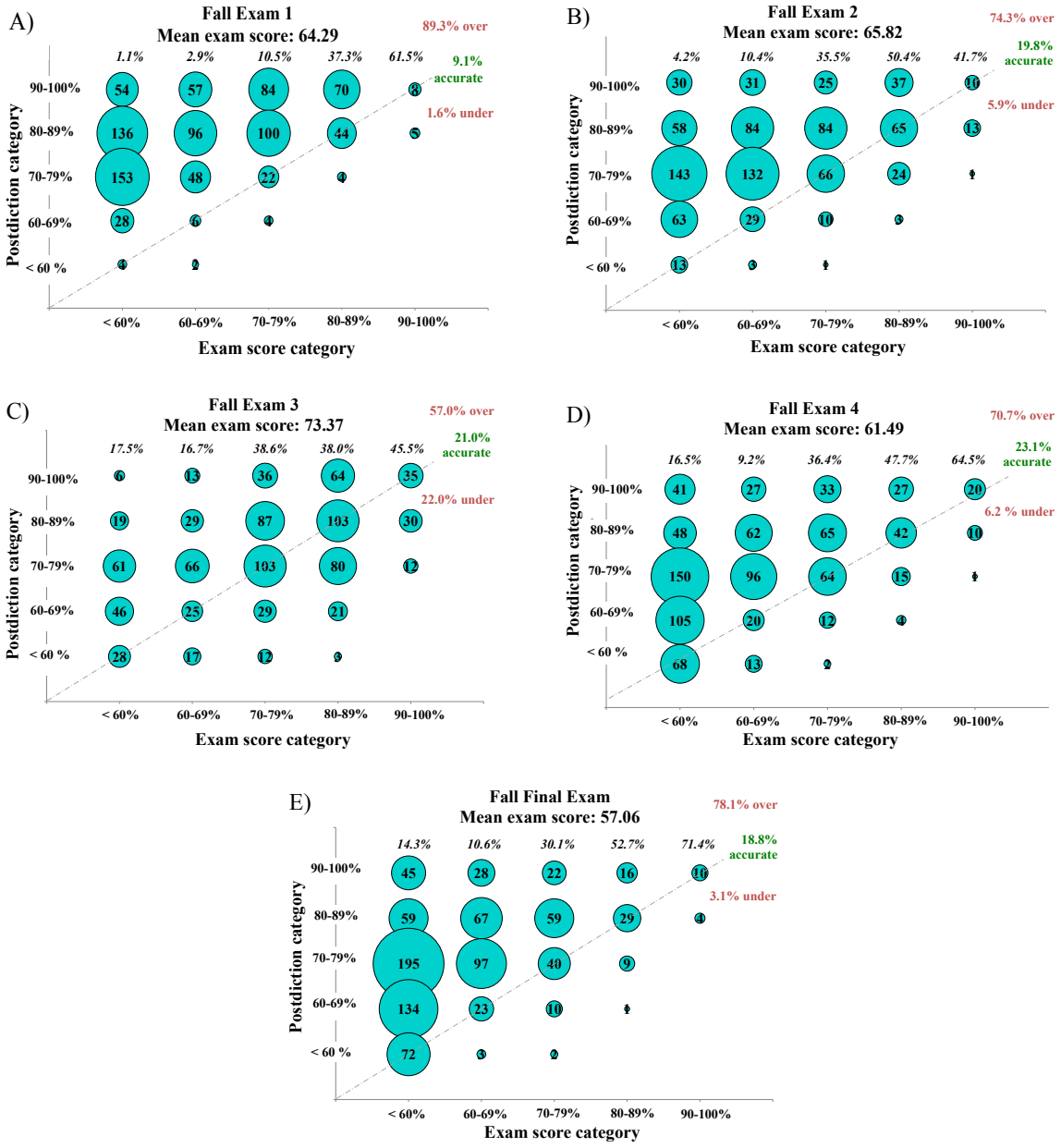

Figure 2.2. Bubble plots of student exam postdiction score category versus exam score category for each exam in the fall semester (N=925). Bubble size is proportional to the number of students with a given exam score category and postdiction. In each case, the dashed diagonal line indicates perfect calibration. Overall percentages of overpostdicting, underpostdicting, and perfectly accurate students are included on the right side of each panel. The percentages of perfectly calibrated students in each exam score category are included at the top of the corresponding columns (italicized).

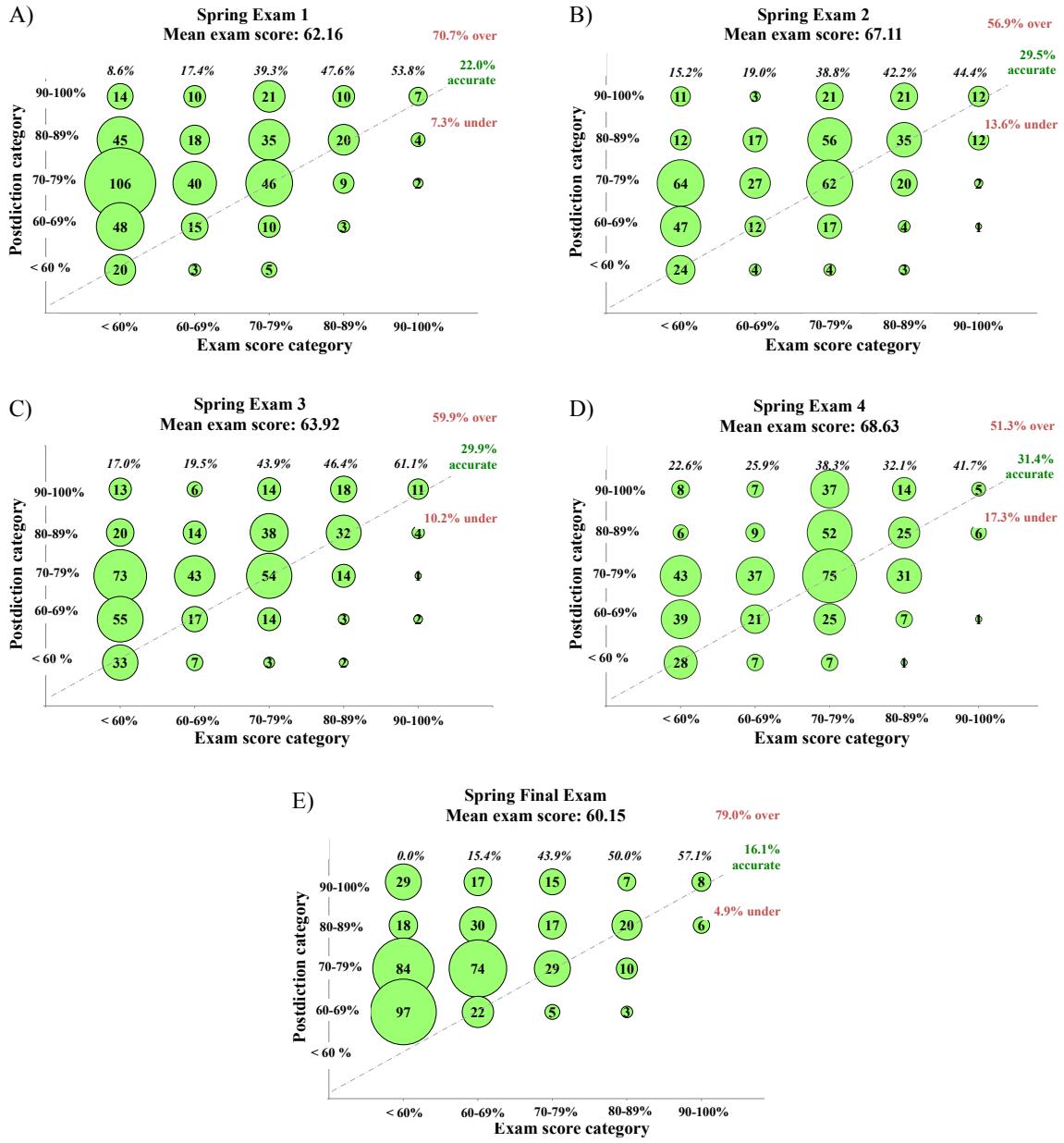

Figure 2.3. Bubble plots of student exam postdiction category versus exam score category for each exam in the spring semester (N=491). Bubble size is proportional to the number of students with a given exam score category and postdiction. In each case, the dashed diagonal line indicates perfect calibration. Overall percentages of overpostdicting, underpostdicting, and perfectly accurate students are included on the right side of each panel. The percentages of perfectly calibrated students in each exam score category are included at the top of the corresponding columns (italicized).

Table 2.2. Performance and calibration statistics for Fall and Spring semesters

Exam	Mean exam score %,[a] *M*	Mean score category[a]	Mean postdiction category[a]	Mean |calibration|[a]	% accurate postdictions
Fall (N = 925)					
Exam 1	64.29 (15.25)	1.12 (1.12)	2.95 (0.87)	1.86 (1.03)	9.1
Exam 2	65.82 (13.86)	1.23 (1.13)	2.47 (0.94)	1.37 (1.01)	19.8
Exam 3	73.37 (13.70)	1.95 (1.22)	2.36 (1.10)	0.96 (0.84)	21.0
Exam 4	61.49 (15.54)	1.04 (1.15)	2.23 (1.16)	1.34 (1.05)	23.1
Final	57.06 (15.86)	0.76 (1.00)	2.15 (1.12)	1.45 (1.05)	18.8
Spring (N = 491)					
Exam 1	62.16 (13.82)	1.01 (1.14)	2.23 (1.04)	1.40 (1.04)	22.0
Exam 2	67.11 (15.88)	1.51 (1.25)	2.24 (1.10)	1.08 (0.94)	29.5
Exam 3	63.92 (15.45)	1.25 (1.22)	2.10 (1.13)	1.12 (0.99)	29.9
Exam 4	68.63 (12.26)	1.54 (1.10)	2.12 (1.14)	1.01 (0.89)	31.4
Final	60.15 (15.59)	0.92 (1.08)	2.24 (1.01)	1.43 (1.03)	16.1

[a] Values for one standard deviation are included in parentheses.

Table AI.1). There were no significant performance differences between males and females for any of the exams across the two-semester general chemistry sequence (Appendix I, Table AI.2).

These findings regarding general chemistry students' postdiction accuracy are consistent with the results of the previously-mentioned exam calibration study conducted in organic chemistry courses, where about 60% of students overestimated their exam scores.[15] The exam calibration accuracy results from the studies in chemistry courses differ substantially from results of exam calibration studies conducted in undergraduate psychology courses,[16-20] in which students were generally found to be well-calibrated. Likely explanations include differences in the nature of the exams, the courses, and the student populations.[21] Differences in the nature of tasks are known to influence judgment accuracy[21, 22] and thus, it is likely that the differences between chemistry and psychology courses and exams influences students' abilities to make accurate exam postdictions. For example, questions on the general chemistry exams often required multi-step problem solving that was quantitative in nature. This differs from example exam questions reported for the psychology course calibration studies, which consisted of questions that required recall and application of declarative knowledge.[18, 20] In addition, some of the student populations studied in the psychology courses were upper-level educational psychology students,[18, 20] and the psychology courses in two studies emphasized the importance of making accurate judgments and how those judgments relate to metacognition throughout the courses.[18, 23]

2.3.2 Relationships between student exam postdiction accuracy and performance. In Figures 2.2 and 2.3, the percentages of perfectly calibrated students in each exam score category are included at the top of the corresponding columns. We observe that larger percentages of higher performing students tended to be perfectly accurate in their postdictions compared with

lower performing students for every exam across the two semesters. To further explore the relationships between postdiction accuracy and exam performance, we compared the exam scores of students who were relatively well calibrated (calibration = 0, ±1) with those who were not well calibrated (calibration = ±2, ±3, ±4) (Table 2.3). (Appendix I, Table AI.3 shows the sample sizes for each group of students.) Mann Whitney U tests indicate that the exam score distributions in the two groups are statistically different for every exam, with medium-to-large effect sizes for most exams (Table 2.3),[12] providing further evidence that students who were better calibrated tended to earn higher exam scores than those who were less accurately calibrated. In addition, we compared the distributions of |calibrations| of the consistently high-performing and low-performing student groups for each exam (Appendix I, Tables AI.4 and AI.5). The distributions differ significantly, with high performers achieving lower mean |calibration| than low performers for all exams, with medium-to-large effect sizes for most exams (Appendix I, Table AI.4). In the fall semester, the average mean |calibration| across all exams was 0.68 for high performers and 1.62 for low performers; in the spring semester, it was 0.65 for high performers and 1.45 for low performers (Appendix I, Table AI.4).

These findings regarding postidiction accuracy and performance are consistent with previous exam calibration studies[18, 20, 23-24] and models of metacognition, which predict that students who are more proficient at monitoring their understanding while studying would make more accurate judgments regarding what they should focus on to enhance their understanding (exercising better metacognitive control), potentially leading to better exam performance. Being better prepared for exams would also allow students to judge their exam performance more accurately.

2.3.3 Changes in postdiction accuracy and metacognitive monitoring over time. We also explored changes in students' exam postdiction accuracies and whether or not students' metacognitive monitoring changed over time. Previous studies have examined changes in postdiction accuracy across one-semester education and psychology courses.[17-19, 23-24] Hacker et. al. compared the R^2 values for the best fit regression lines for actual score versus postdicted score data for each exam, and asserted that an increase in R^2 values over time indicated improved postdiction accuracy over time.[5] However, we concur with the critique by Nietfeld et. al. that "…accounting for increasing amounts of variance does not necessarily mean that the relationship is in the expected direction" (p. 23).[20] Thus, it is unclear that the results of the Hacker et. al. study regarding changes in postdiction accuracy over time are valid. Other studies compared students' mean |calibration| for exams or quizzes over time for one-semester psychology courses to examine changes in postdiction accuracy.[17, 19, 23-24] For our study, in examining trends in mean |calibration| over time (Table 2.2), we observed that when exam means increase, mean |calibration| improves (values decrease). Since a large proportion of students overpostdicted on each exam, higher exam means may be associated with more accurate postdictions regardless of whether or not students are more accurately monitoring their performance. While Nietfeld et. al noted similar changes in postdiction accuracy with changing exam difficulty, the range of exam means (76-81%) was narrower compared with our study (57-73%), and they did not adjust for changes in exam means over time.[20]

Specifically focusing on the pairs of exams for which mean |calibration| improved from one exam to the next (Table 2.2), we developed a method to determine whether or not it was likely that students' improvements in mean |calibration| were because of increases in exam means. In Table 2.4, we compare each exam with the one immediately following it. For each exam pair,

Table 2.3. Exam scores of students who were well calibrated and those who were not.

Exam	Mean exam score [a]		U statistic [b]	Effect size (r) [c]
	Well-calibrated students (calibration = 0, ±1)	Not well-calibrated students (calibration = ±2, ±3, ±4)		
Fall (N= 925)				
Exam 1	75.26 (12.89)	57.76 (12.58)	30226	0.59
Exam 2	71.51 (12.77)	57.51 (10.88)	39075	0.53
Exam 3	75.58 (12.74)	65.93 (12.23)	67522	0.30
Exam 4	65.31 (16.56)	55.70 (11.72)	64515	0.32
Final	60.49 (17.78)	52.91 (11.95)	76490	0.24
Spring (N= 491)				
Exam 1	67.07 (14.29)	56.32 (10.61)	17758	0.41
Exam 2	70.57 (15.29)	58.63 (14.03)	15620	0.36
Exam 3	67.20 (15.40)	56.54 (12.86)	13526	0.35
Exam 4	70.59 (11.56)	62.97 (12.51)	14372	0.26
Final	64.41 (16.78)	55.24 (12.08)	15208	0.27

[a] Values for one standard deviation are included in parentheses. [b] Mann-Whitney U tests compare exam scores; population information can be found in Appendix I, Table AI.3.
[c] p-values <0.0001.

we calculated the effect sizes (r, see equation 2.2) for the change in |calibration| ($r_{|calibration|}$) and the change in exam score category (r_{exam}). For the cases in which students' mean |calibration| improved from one exam to the next, we calculated the ratio $r_{|calibration|}/r_{exam}$. If the magnitude of the effect size of students' decrease in |calibration| is larger than the magnitude of the effect size of the increase in mean exam score category, then the ratio $r_{|calibration|}/r_{exam}$ would be greater than 1, indicating that the improvement in students' calibration accuracy may not be fully explained by a higher exam mean.

As seen in Table 2.4, the only pair of consecutive exams for which students' mean |calibration| improves and $r_{|calibration|}/r_{exam}$ is greater than 1 is for Fall Exams 1 and 2, with $r_{|calibration|}/r_{exam} = 3.41$. This suggests that students may have improved their metacognitive monitoring of their exam performance on Fall Exam 2 relative to Exam 1. For the other three pairs of exams for which students' mean |calibration| improved over time, the $r_{|calibration|}/r_{exam}$ ratios are less than 1, indicating that the effect sizes for the change in mean exam score categories increased to a greater extent than the corresponding effect sizes of the change in mean |calibration|. This suggests that students' metacognitive monitoring of their performance may not have improved across those exams.

For the four other pairs of exams, exam means decreased from one exam to the next and students' mean calibration accuracy decreased, but with a smaller effect size than the mean exam score category decrease in each case. Thus, the only time for which this analysis indicates that students' metacognitive monitoring of their exam performance may have improved is for Fall Exam 2 relative to Exam 1. Of course, Fall Exam 1 is unique in that it is the first exam of the general chemistry course, and also the first college-level chemistry exam for many of the students. Therefore, Exam 1 provided students with a new, particularly relevant experience to

consider in their future judgments of their general chemistry exam performance. In addition, students' mean |calibration| on Exam 1 of 1.86 (an average of almost two exam score categories away from their actual exam score categories) was especially poor. Therefore, students may have adjusted their postdictions between Fall Exams 1 and 2 more than between any other pair of exams in part due to the experience of being miscalibrated by such a large margin for their Exam 1 performance. Previous studies in the psychology laboratory indicate that relevant experience alters the factors people use to make judgments of difficulty.[25, 26]

If it was the case in the fall that students' postdiction accuracy improved in part because experience with the first general chemistry exam informed their future judgments of exam performance, then we would expect to see a similar pattern in the spring for the students who did not take the corresponding first-semester general chemistry course at the same institution in the fall (Spring Only, N=148) to a greater extent than for the students who had the experience of the preceding fall course (Fall & Spring, N=343). Spring Only students took a first-semester general chemistry course at another institution, took the course in a different semester, or tested out of the course, and therefore, while these students had taken general chemistry exams before, most had no previous experience with the spring instructors' course and assessment styles or with making exam postdictions. As expected, Spring Only students' mean |calibration| improved from Spring Exam 1 to Spring Exam 2 with $r_{|calibration|}/r_{exam} = 1.16$, while $r_{|calibration|}/r_{exam} = 0.69$ for the students who had completed the fall course (Appendix I, Tables AI.7– AI.10). The Spring Only students' improvement in postdiction accuracy that may be attributed to enhanced metacognitive monitoring is also smaller than that described earlier for all students in the fall cohort ($r_{|calibration|}/r_{exam} = 3.41$) for which many students were new to college-level chemistry.

Table 2.4. Effect sizes (r) for comparisons between exam score category (r_{exam}) and |calibration| values ($r_{|calibration|}$) for students in Fall and Spring courses.

Exam pair	r_{exam}	$r_{\|calibration\|}$	$r_{\|calibration\|}/r_{exam}$
Fall (N=925)			
Exam 1/Exam 2	0.11	0.38	3.41
Exam 2/Exam 3	0.53	0.34	0.64
Exam 3/Exam 4	0.72	0.32	— [a]
Exam 4/Final	0.36	0.11	— [a]
Spring (N=491)			
Exam 1/Exam 2	0.35	0.27	0.78
Exam 2/Exam 3	0.25	0.04	— [a]
Exam 3/Exam 4	0.33	0.10	0.31
Exam 4/Final	0.57	0.34	— [a]

[a] Only calculated for pairs of exams where mean |calibration| improved.

We also conducted these analyses for high- and low-performing student groups (Appendix I, Table AI.6) and students who took both semesters of general chemistry consecutively (Appendix I, Table AI.10). In terms of changes in postdiction accuracy and metacognitive monitoring over time, the patterns observed for these subgroups are similar to that of the larger groups. Results indicate that both high- and low-performing students improved in postdiction accuracy and monitoring of their exam performance for Fall Exam 2 relative to Exam 1.

Unlike mean |calibration|, which consistently varied inversely with exam mean, the percentage of students who were perfectly calibrated increased across each semester's exams until the final exam (Table 2.2). The only statistically-significant pairwise increases in % accurate students from one exam to the next (Fisher's exact $p < 0.01$) were from the first exam to the second exam in each semester. Adjusting for changes in exam difficulty over time, our findings are generally consistent with previous work indicating that – without an intervention intended to improve student monitoring – students' calibration accuracy did not change much across multiple exams.[17-19, 23-24] However, it appears that the students in our study, including both high and low performers, may have improved in metacognitive monitoring of their performance on Exam 2 relative to Exam 1 in general chemistry courses that were new to them.

2.4 Limitations

A limitation of this study was that student postdictions were collected using optical mark recognition (i.e., Scantron®) forms with only five possible answer choices rather than an open-ended format. This method was chosen to facilitate data collection from larger numbers of students than have been included in previous postdiction calibration studies (more than 1000 students compared with less than 100 students in previous studies), but it also reduced the

sensitivity for detecting differences in students' postdictions as well as the precision of the calibration results relative to an open-ended postdiction format. In addition, the postdiction categories we chose were not equal in range. In particular, the < 60% postdiction answer choice spanned a 60-point range whereas the additional four categories spanned only 10-point ranges. Given that the exam means ranged from 57–73%, it may have been preferable to select consistently wider ranges for the postdiction answer choices (e.g., a 20-point range for each). Of course, this would have also had the effect of making it easier for higher-performing students to be better calibrated. Even though our selection of postdiction answer choices in this study theoretically made it easier for lower-performing students to be better calibrated, results illustrated that they were nevertheless significantly less accurate than higher-performing students. Finally, to the extent that postdictions are random guesses not informed by other information, people who perform closer to the middle of a performance scale have a better chance of more accurate |calibration| than those who perform closer to the extremes of the scale.

2.5 Conclusions and Implications

In this study, we explored aspects of first- and second-semester general chemistry students' metacognitive monitoring of their exam performance by measuring their postdiction accuracies over time. In addition, we determined how postdiction accuracy relates to exam performance. First, we found that a large proportion of students in both semesters of general chemistry were miscalibrated in that they consistently overpostdicted their exam scores. Considering exams 2-4, during which students' postdiction accuracies were the most accurate and most stable, the average mean |calibrations| were 1.2 in the fall and 1.1 in the spring, which indicates an average miscalibration of more than one exam score category. The extent to which students were miscalibrated is particularly striking because, unlike predictions of performance

made without knowledge of the test questions, students made their postdictions immediately after completing each exam while the exam was still in their possession. Our results differ from previous findings in the context of psychology course exam postdiction accuracies, where students were typically found to be well calibrated, but are consistent with a study carried out in organic chemistry courses.[15] We attribute this to course and exam characteristics that are more similar for general and organic chemistry, but differ substantially between general chemistry and psychology courses. Second, we found that general chemistry students who earned higher exam scores also tended to be more accurately calibrated, which is consistent with the findings from previous studies in other courses as well as models of metacognition.[18, 20, 23-24] Finally, although we observed improvements in students' postdiction accuracy between some pairs of exams, in all cases the improvements in calibration were seen for cases where the exam mean also increased. Thus, we realized that this could be due to students' tendency to overpostdict as opposed to improvements in their metacognitive monitoring of their exam performance. We developed a method to determine whether or not improvements in mean |calibration| from one exam to the next were likely due to improvements in students' metacognitive monitoring. Results indicated that, although students who were new to a general chemistry course appeared to improve in their metacognitive monitoring on the second course exam compared with the first, monitoring did not significantly improve after that initial adjustment. Thus, our results are generally consistent with postdiction studies in other domains in which monitoring did not change much without a specific intervention targeted at improving students' monitoring of their exam performance.[17-19, 23-24] Notably, Bol et al. employed an intervention in which students practiced making pre- and postdictions on quizzes and no significant differences were observed in calibration accuracy on the final exam between intervention and control groups.[24] Interventions that have led to

improvements in monitoring exam performance have included offering extra credit for more accurate judgments,[17] and having students complete self-reflection questionnaires that included topics such as how well concepts were grasped, identifying strengths/weaknesses, and confidence ratings regarding ability to answer content questions.[27]

Overall, our results show that general chemistry students' perceptions of their own performance do not typically match their actual performance, especially for lower-performing students, and that in the absence of any intervention to improve monitoring, student monitoring of exam performance does not improve much across a year-long general chemistry course. Given the importance of metacognitive monitoring for student learning of chemistry, these findings suggest that further research and development of interventions to improve the metacognitive monitoring of introductory chemistry students is warranted. Increasing chemistry instructors' awareness of both the importance of metacognitive monitoring and the possibility that their students are miscalibrated may encourage them to test their students' calibration accuracy, and design and implement interventions intended to improve student monitoring. Another direction for future research in this area is the exploration of the strategies and reasoning chemistry students use in making judgments of their performance.

REFERENCES

1. Hawker, M. J.; Dysleski, L.; Rickey, D., Investigating General Chemistry Students' Metacognitive Monitoring of Their Exam Performance by Measuring Postdiction Accuracies over Time. *J. Chem. Educ.* **2016,** *93* (5), 832-840.
2. Lindsey, B. A.; Nagel, M. L., Do Students Know What They Know? Exploring the Accuracy of Students' Self-assessments. *Phys. Rev. Phys. Educ. Res.* **2015,** *11* (2), 020103.
3. Bell, P.; Volckmann, D., Knowledge Surveys in General Chemistry: Confidence, Overconfidence, and Performance. *J. Chem. Educ.* **2011,** *88* (11), 1469-1476.
4. Mathabathe, K. C.; Potgieter, M., Metacognitive Monitoring and Learning Gain in Foundation Chemistry. *Chem. Educ. Res. and Pract.* **2014,** *15* (1), 94-104.
5. Pazicni, S.; Bauer, C. F., Characterizing Illusions of Competence in Introductory Chemistry Students. *Chem. Educ. Res. Pract.* **2014,** *15*, 24–34.
6. Beyer, S., Gender Differences in the Accuracy of Self-evaluations of Performance. *J. Pers. Soc. Psychol.* **1990,** *59* (5), 960.
7. Beyer, S.; Bowden, E. M., Gender Differences in Seff-perceptions: Convergent Evidence From Three Measures of Accuracy and Bias. *Pers. Soc. Psychol. B.* **1997,** *23* (2), 157-172.
8. Kruger, J.; Dunning, D., Unskilled and Unaware of it: How Difficulties in Recognizing One's Own Incompetence Lead to Inflated Self–assessments. *J. Pers. Soc. Psychol.* **1999,** *77* (6), 1121–1134.
9. Beyer, S., Gender Differences in the Accuracy of Grade Expectancies and Evaluations. *Sex Roles* **1999,** *41* (3-4), 279-296.
10. Fritz, C. O.; Morris, P. E.; Richler, J. J., Effect Size Estimates: Current Use, Calculations, and Interpretation. *J. Exp. Psychol.-Gen.* **2012,** *141* (1), 2.
11. Cohen, J., *Statistical Power Analysis for the Behavioral Sciences*. Lawrence Erlbaum Associates, Inc: 1977.
12. Coolican, H., *Research Methods and Statistics in Psychology*. Psychology Press: 2014; p 498.
13. Upton, G. J., Fisher's Exact Test. *J. Roy. Statist. Soc. Ser. A* **1992**, 395-402.
14. Bland, J. M.; Altman, D. G., Multiple Significance Tests: the Bonferroni Method. *BMJ* **1995,** *310* (6973), 170.
15. Karatjas, A. G., Comparing College Students' Self–Assessment of Knowledge in Organic Chemistry to Their Actual Performance. *J. Chem. Educ.* **2013,** *98* (8), 1096–1099.
16. de Carvalho Filho, M. K., Confidence Judgments in Real Classroom Settings: Monitoring Performance in Different Types of Tests. *Int. J. Psychol.* **2009,** *44* (2), 93–108.
17. Hacker, D. J.; Bol, L.; Bahbahani, K., Explaining Calibration Accuracy in Classroom Contexts: the Effects of Incentives, Reflection, and Explanatory Style. *Metacognition Learn.* **2008,** *3* (2), 101–121.
18. Hacker, D. J.; Bol, L.; Horgan, D. D.; Rakow, E. A., Test Prediction and Performance in a Classroom Context. *J. Educ. Psychol.* **2000,** *92* (1), 160–170.
19. Miller, T. M.; Geraci, L., Training Metacognition in the Classroom: the Influence of Incentives and Feedback on Exam Predictions. *Metacognition Learn.* **2011,** *6* (3), 303–314.
20. Nietfeld, J. L.; Cao, L.; Osborne, J. W., Metacognitive Monitoring Accuracy and Student Performance in the Postsecondary Classroom. *J. Exp. Educ.* **2005**, 7–28.

21. Schraw, G.; Roedel, T. D. B., Test Difficulty and Judgment Bias. *Mem. Cognition* **1994,** *22* (1), 63–69.
22. Pulford, B. D.; Colman, A. M., Overconfidence: Feedback and Item Difficulty Effects. *Pers. Indiv. Differ.* **1997,** *23* (1), 125–133.
23. Nietfeld, J. L.; Cao, L.; Osborne, J. W., The Effect of Distributed Monitoring Exercises and Feedback on Performance, Monitoring Accuracy, and Self–efficacy. *Metacognition Learn.* **2006,** *1* (2), 159–179.
24. Bol, L.; Hacker, D. J.; O'Shea, P.; Allen, D., The influence of Overt Practice, Achievement LEvel, and Explanatory Style on Calibration Accuracy and Performance. *J. Exp. Educ.* **2005,** *73* (4), 269–290.
25. Koriat, A., Monitoring One's Own Knowledge During Study: A Cue-utilization Approach to Judgments of Learning. *J. Exp. Psych.* **1997,** *126* (4), 349.
26. Kelley, C. M.; Jacoby, L. L., Adult Egocentrism: Subjective Experience Versus Analytic Bases for Judgment. *J. Mem. Lang.* **1996,** *35* (2), 157-175.
27. Bol, L.; Hacker, D. J.; Walck, C. C.; Nunnery, J. A., The Effects of Individual or Group Guidelines on the Calibration Accuracy and Achievement of High School Biology Students. *Contemp. Educ. Psychol.* **2012,** *37* (4), 280–287.

CHAPTER 3

DESIGN OF METACOGNTIVE-BASED EXAM AND STUDY PREPARATION WORKSHOPS TO PROMOTE GENERAL CHEMISTRY STUDENT METACOGNITIVE AWARENESS

This chapter details the design of a series of workshop interventions inspired by the findings presented in Chapter 2, namely that general chemistry students' metacognitive monitoring on exams is largely inaccurate. Broadly, we hoped to glean a more complete understanding of the relationships between general chemistry student participation in metacognition-based exam preparation workshops and students' metacognitive monitoring and awareness. The research design described in this chapter involves two groups of general chemistry students. One group participated in exam preparation workshops (metacognition-based) and another group participated in traditional test-taking strategy workshops (non-metacognition-based). Several pre- and post-workshop metrics were planned to explore relationships between student workshop participation and student outcomes related to metacognition.

Section 3.1 includes an introduction regarding the importance of metacognitive skill development and a brief review of previously-reported interventions that target such development. Section 3.2 provides an overview of the intervention design. Section 3.3 discusses the pilot study that was conducted with students in the Fall 2014 semester. Although the pilot study did not include a large enough sample size to yield meaningful quantitative and qualitative comparisons as was intended in the original design, it provided several useful considerations for future studies (Section 3.4).

Information presented in this chapter is based on a protocol prepared by Morgan Hawker, Lisa Dysleski, and Dawn Rickey submitted to the Institutional Review Board (IRB) at Colorado State University entitled *General Chemistry Students' Metacognitive Awareness: Before and After Metacognition-based Exam and Study Preparation Workshops*. This IRB protocol was approved on September 16th, 2014 and renewed on October 22nd, 2015.

3.1 Introduction

Preparing for examinations is a critical component of student learning. Students' ability to actively participate in the process of preparing for and taking exams is critical for success in academic settings. Through this process, students have opportunities to make decisions to guide their learning in a specific content area. As can be deduced from postdiction data presented in Chapter 2, many students are underprepared for the examination process. This includes both preparing for, taking, and reflecting on the exam. One way that may help students become better prepared for exams is by applying metacognitive skills, including planning and evaluating (discussed in Chapter 1).[1-3] A different method that may help to increase students' preparedness utilizes more traditional multiple-choice test-taking strategy instruction. The work presented here centers on comparing a metacognitive-focused exam preparation intervention with a test-taking strategies intervention for undergraduate learners, implemented within the general chemistry student population at Colorado State University. This population comprises mainly first-semester freshmen who typically view general chemistry as a rigorous course. Providing scaffolds for exam preparation and test taking may improve student learning outcomes for students who may otherwise have underdeveloped skills relative to the examination process at the undergraduate level. The study was designed to evaluate possible relationships between aspects of students' metacognitive awareness and learning outcomes in the context of preparing for and taking

general chemistry exams. I am not aware of similar studies (e.g., that involving metacognitive and test-taking strategy training workshops) performed in an undergraduate general chemistry setting. Thus, this study is expected to enrich our understanding of student metacognitive skill development and test-taking strategies as they relate to general chemistry exam preparation.

Metacognitive skill development, an important component of the present study, is discussed in more detail in Chapter 1 (Part II of this dissertation). Briefly, metacognitive monitoring is a central metacognitive skill that involves assessing one's current knowledge and understanding.[1] One way to measure monitoring ability is to evaluate the accuracy of postdictions of performance (Chapter 2). Student learning outcomes (e.g., exam scores) are correlated with exam score postdictions, and related to metacognitive monitoring.[4-6] Therefore, metacognitive monitoring of tasks is related to task performance (e.g., monitoring during exam studying is related to performance on exams). Arguably, it is important to provide undergraduate instruction in the form of metacognitive training within the scientific field.[7] There is some evidence that presenting metacognitive training, in the form of study skills, is more beneficial in the context of course content rather than as a stand-alone course.[8] Thus, teaching students to apply study skills using their general chemistry course content may improve student learning outcomes both within that course and more broadly. Past studies in the context of metacognitive skill development, often referred to as *strategy training*, include an undergraduate mathematics classroom[9] and upper elementary classrooms.[10-11] In each of these course settings, students who received strategy training in monitoring demonstrated improved performance over a control group(s). Only one of these studies, however, demonstrated a relationship between strategy training and monitoring accuracy, where the task evaluated was mathematical probability question sets.[9] An additional metacognitive strategy training study that took place as a stand-

alone course in reading comprehension (e.g., outside of a formal undergraduate course setting) demonstrated a significant improvement between the intervention group's pre- and post- reading comprehension performance, as well as for their general metacognitive awareness.[12] Strategy training methods implemented these studies included presenting self-questioning strategies, modeling those strategies through think-aloud protocols and practicing strategies in small groups. Because of the demonstrated effect of such methods in non-chemistry course domains, a combination of these approaches were integrated into the intervention described in this chapter. Self-questioning strategies included in this work were influenced by the cyclic plan/model/reflect framework, originally proposed by Bandura[13] and summarized later by Tanner,[14] as it was directly translatable to chemistry course activities proposed in the intervention.

Although sample questions have been proposed for use in strategy training with the aim of promoting student metacognitive monitoring in science courses,[14] to my knowledge, a monitoring intervention based in an undergraduate science classroom setting has yet to be performed. Amzil discussed the lack of such strategy training/monitoring interventions at the undergraduate level in general, especially those taking place over a "short" (< 1 semester) time span.[12] The exam preparation strategies intervention discussed here was intended to address this gap in the literature.

Regarding the test-taking strategy training intervention, there have been limited reports of multiple-choice test-taking strategy training at the undergraduate level. The few studies on this topic confirm, however, that test-taking strategy instruction is effective in raising students' scores on multiple-choice exams.[15-18] Notably, these reports have only focused on multiple choice exam strategy training within undergraduate education course settings. Exploring the generalizability of multiple choice exam strategy training in an undergraduate chemistry setting

will provide new insight regarding the translation of this strategy training methodology to other testing modes, as well as to other disciplines, and therefore address this gap in the literature.

3.2 Intervention Design and Implementation

This work is classified as early-stage/exploratory research, and involves a between-subjects control study design.[19] As such, the purposes of this study included examination of associations between learning outcomes (e.g., exam scores/course grades) and "malleable factors" (e.g., metacognitive monitoring, metacognitive awareness), as well as "opportunities for new interventions or strategies and challenges to their adoption, with the goal of informing policy, practice, and future design or development" as stated in the Common Guidelines for Education Research and Development developed by the Institute of Education Sciences and the National Science Foundation.[19] Here, it is important to re-emphasize that the remainder of Section 3.2 is adapted from the original IRB protocol. Appendix II contains corresponding supplemental information for Section 3.2, and is referred to where relevant. Notably, this protocol was designed in the context of the General Chemistry I (CHEM 111) course at Colorado State University but could be generalized to additional chemistry courses at CSU or other universities in the future.

3.2.1 Overview of the proposed study design. The timeline outlining the four main components of this study is depicted in the Gantt chart in Figure 3.1. All students answered questions from the Metacognitive Awareness Inventory (MAI, see Chapter 1) and made exam postdictions on each of 5 exams. The pre- and post- MAI were administered as a Likert scale survey via the course management website (Appendix II). The survey was opened for one week during each of the two administered time periods such that all students enrolled in CHEM 111 could participate, and all students who completed the MAI received a small amount of CHEM

111 course credit (<1% of the final course grade). Students had alternative means to earn this course credit if they chose not to complete the MAI.

The workshop components of this study included two groups of volunteers: the test-taking strategies group (non-metacognition focused) and the exam preparation strategies group (metacognition-focused). Each of these workshops comprised three one-hour sessions, and participants were assigned to groups controlling for exam 1 score (i.e., ranking by their exam 1 score and then assigning groups ensuring that the exam 1 performance distribution is as even as possible between the two groups).

The first two one-hour sessions consisted of an activity involving a set of eight relevant general chemistry multiple-choice content questions (exam-like questions, see Appendix II). The test-taking strategies group and exam preparation group were, however, given different tasks with respect to these content question sets. The final one-hour session focused on skill generalizability, either focused on metacognitive skills or test-taking strategies, depending on the workshop group. An overview of the specific workshop activities students participated in is outlined in Figure 3.2, and more detail is provided in Sections 3.2.2 and 3.2.3.

At the beginning of session #1 and the end of session #3, students in both groups participated in a clicker question activity, in which they answered these questions:

1) Did you have a study plan for Exam 1/3? (yes/no)
2) Were you able to carry out your study plan for Exam 1/3? (yes/no/I didn't have one)
3) Do you intend to change your study plan for Exam 2/4? (yes/no)

Students also performed a short writing task pertaining to the following questions:

1) What was your study plan for Exam 1/3?
2) What made your study plan successful or unsuccessful?
3) How will you change your study plan for Exam 2/4?

These clicker questions and writing prompts served as a pre/post assessment, in addition to the

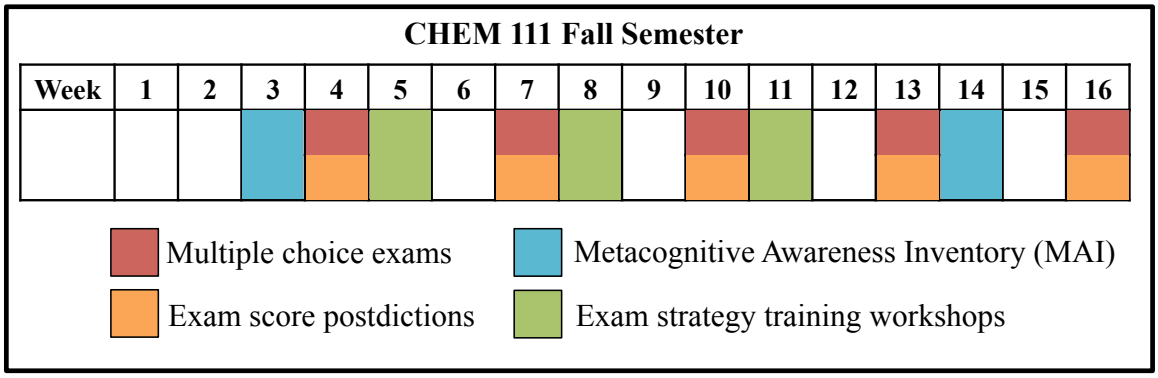

Figure 3.1. Gantt chart representing the planned workshop timeline during the fall semester.

MAI and exam score postdictions, providing additional comparisons between the test-taking strategies group and the exam preparation group.

3.2.2 Test-taking strategies group ("traditional") activities. Each of the first two sessions began with students answering the first four multiple-choice questions in groups, followed by reviewing the questions in such a way that focused on test-taking strategies (discussed below with examples in Appendix II). This process was then repeated with the remaining four questions, where each eight-question set was written to promote similar strategies.

Session # 1: Focused on reading the question completely (e.g., questions phrased as "which is true" versus "which is false") and eliminating unreasonable answer choices based on the problem context. These questions were based on Exam 2 material, including, electron configurations, quantum numbers, and naming compounds. Students were encouraged to study in a spaced manner for Exam 2.

Session #2: Focused on distractor answer awareness via common misconceptions/errors. These questions were based on Exam 3 material, including, mole calculations, periodic trends, Lewis structures/hybridization, and VSEPR. At the end of session #2, students received a template of the test-taking strategies covered in sessions #1 and #2 and categorize questions under specific strategies that they came across during one study session for Exam 3 (Appendix II).

Session #3: The review in session #3 focused on generalizability of test-taking strategies to other courses/exam formats to mirror the exam preparation strategies group reflection component in session #3. This included comparing and contrasting multiple-choice to different exam formats (true/false and essay/short answer) by group brainstorming.

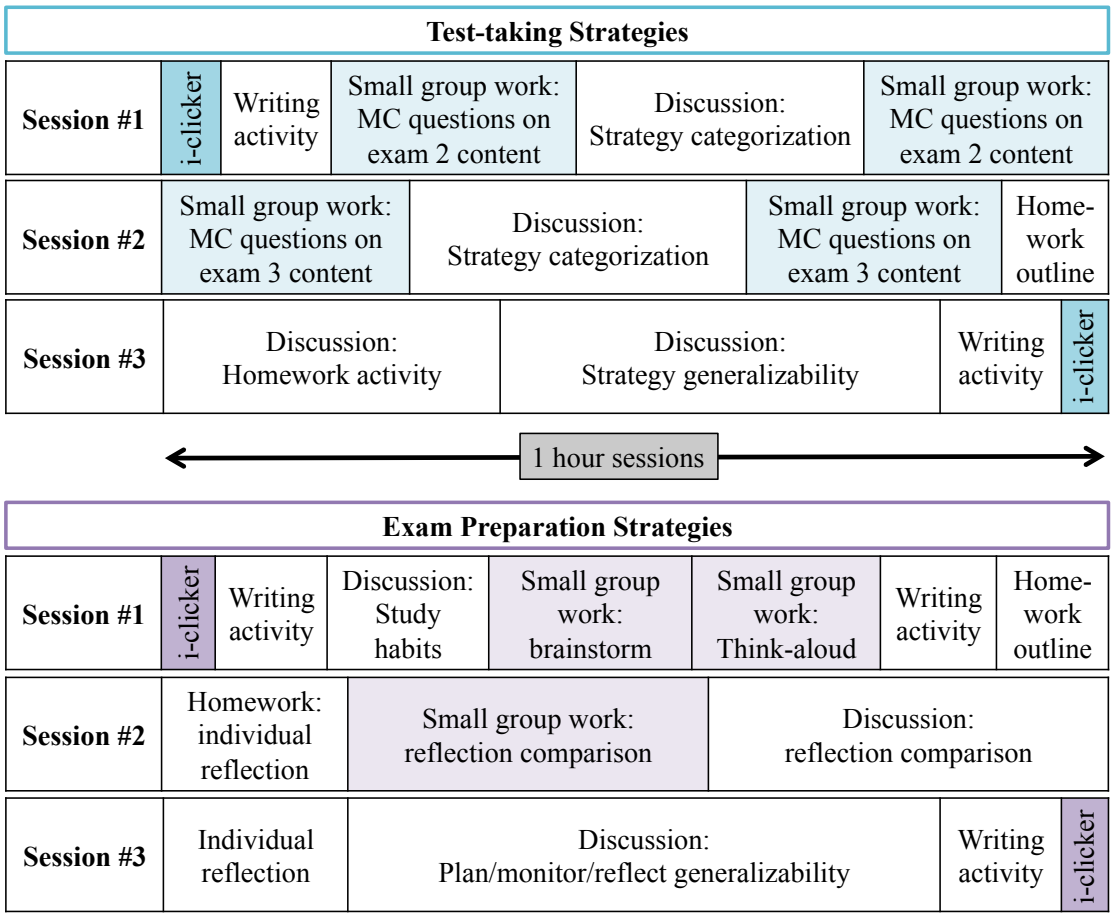

Figure 3.2. Outline of workshop activities for test taking ("traditional") and exam preparation ("metacognitive") strategy groups [MC: multiple choice].

3.2.3 Exam preparation strategies group ("metacognitive") activities. Session #1: After the initial clicker question/writing activity outlined above, the workshop leader facilitated a student discussion that centers on student ideas about the importance of paying attention to one's study habits, and potential benefits of doing such. The discussion involved discussing planning, monitoring, and reflecting in both educational and non-educational contexts (i.e., the plan/model/reflect cycle).[13-14] Self-questioning was modeled for students during this introductory activity via a think-aloud, with the purpose of motivating students to use this strategy when preparing for academic tasks. Before students were presented with the same eight-question set as the test-taking strategies group, they were informed that they needed to prepare to study for a "quiz" with CHEM 111 exam-like questions. In groups of three, students brainstormed questions that they could ask themselves, both when planning for such a task (planning) and when working on the task (monitoring), and then each group presented a question from each category to the whole class. Students then considered the eight-question set and actively monitor their thinking processes via a think-aloud in groups. Group members alternated between "thinking through" the question set one question at a time. This activity intended to scaffold self-questioning behavior (i.e., participate in a think-aloud where one verbalizes thoughts that come to mind while participating in a particular task). To conclude session #1, students responded to the following prompt in writing:

- Will you change your study plan when studying for Exam 2? If yes, how and why will you change it? If no, why not?

Students received a template that contained a few planning, monitoring, and reflection questions (see Appendix II). They filled out this questionnaire during one study session for Exam 2 and brought the filled out questionnaire with them to discuss in session #2.

Session #2: Students began session #2 by independently reflecting on their previously developed study plans, as well as on Exam 2 as a whole. They were presented with reflection prompts (Appendix II), discussed their reflections in small groups, and were prompted to note any similarities and differences between their planned and actual study sessions. The small groups then shared responses with the larger group. This tiered activity intended to highlight similarities between student study plans, specifically common successes and necessary improvements. After this reflection activity, students worked individually to modify their study plan. They then received the same set of eight content questions as the test-taking strategies group, again to ensure that the test-taking strategies group did not have an unfair advantage with exposure to practice material. Students were encouraged to use this question set as a practice test for Exam 3, although no direct follow-up occurred with students regarding what they have done with these questions.

Session #3: The planned activities for session #3 were as follows: 1) a similar reflection activity as session #2, whereby students reflected on what worked/did not work in terms of using their study plan to prepare for Exam 3, as well as reflected on Exam 3 itself; 2) A group discussion regarding the generalizability of the plan/monitor/reflect cycle for other activities that they came across before or may come across in the future. This discussion would center on the questions of whether the students found this approach helpful, why it was/was not helpful, and what could make it more helpful in terms of maximizing their study habits and learning outcomes. Notably, and as discussed in more detail in section 3.3, the third workshop was not implemented because of the lack of student participants.

3.2.4 Student exam data and postdiction data collection. The last question of each CHEM 111 multiple-choice exam (i.e., the "postdiction question") was identical to that presented in Chapter 2:

> *What percentage score do you expect to earn on this exam?*
> *A) 100%–90%*
> *B) 89%–80%*
> *C) 79%–70%*
> *D) 69%–60%*
> *E) < 60%*

Student answers to the postdiction question were compared to their exam score for each individual exam to determine students' calibration for each exam. Postdiction responses and exam scores were retrieved via instructors' electronic gradebooks, and precautions to protect students' identities were taken (see Section 3.2.6).

3.2.5 Student recruitment plan. Undergraduate general chemistry students are an ideal population for the proposed study because the majority of these students are first-semester freshman. Incoming freshman may not have developed metacognitive skills to the extent necessary for excelling in undergraduate courses, and this intervention may jumpstart this skill development. Based on the ~1100 students taking CHEM 111 in Fall 2014, we recruited a sample of approximately 80 students total (40 to participate in the test-taking strategies group and 40 students to participate in the exam preparation strategies workshops). This sample size was calculated via an estimation of the Mann-Whitney test statistic (U), which is non-parametric (i.e., assumes a non-normal ordinal data distribution). At sample sizes greater than 20, U conforms to a normal distribution such that a z statistic can be calculated. In this instance, a sample size of 80 assumes an effect size (Cohen's d) of 0.6, a power level of 0.8, and a p-value of 0.05. Self-selection effects were present, but this group of students can be considered an "ideal population". Therefore, this work can be considered efficacy research.[19]

Initial recruitment occurred by a researcher visiting the CHEM 111 courses (General Chemistry 1 courses at Colorado State University) during the lecture immediately following Exam 1, during which an announcement was made regarding the volunteer opportunity (Appendix II). All students enrolled in CHEM 111 received a follow-up email after the 3rd week of the Fall 2014 semester (Appendix II). Volunteers were included in this study if they were enrolled in CHEM 111 in Fall 2014 and were available to meet during all advertised meeting times, as specified in the recruitment email. Students who are not available to meet during all advertised meeting times were excluded from the study. Total approximate time commitment for all participants was 3.5 hours, including 3 one-hour workshops and time to complete one activity during a study session outside of the workshops.

The original design indicated that student data would only be analyzed for those who attended all assigned sessions, completed the pre- and post- MAI, and completed all exams, including postdiction questions. Data analysis for postdiction data was similar to that presented in Chapter 2. Pre-post MAI data for the two different workshop groups (i.e., test-taking strategies vs. exam preparation strategies) were analyzed by calculating so-called gain scores (i.e., where gain is defined as the post score minus the pre score) and groups were using an independent samples t-test (with the Mann-Whitney U test as a non-parametric option). Notably, there is an extensive body of literature devoted to comparing the gain scores method with the analysis of covariance (ANCOVA) method, where there is substantial debate on which method is more appropriate for pre-post data analysis (a few representative examples are included as references here).[20-24] Notably, these methods test different hypotheses and, thus, have somewhat different focuses. Gain scores focus on the change between the pre- and post-test, but may be challenging to interpret if pre-test differences exist between groups. ANCOVA focuses on post-test

differences rather than changes between pre- and post-test. Gain scores were used to analyze pilot data because it was of interest to evaluate changes between the pre- and post-test MAI results.

3.2.6 Procedures to maintain confidentiality. Volunteer privacy was protected by keeping volunteer emails on an account that is accessible only to the researchers. For electronic data, student names were removed for analyses, and data were grouped by students' eIDs for analyses. For paper data, student names were removed and replaced with codes. Code keys were kept electronically (i.e., separated from the paper data). Paper consent forms were given to students at the start of the first workshop meeting, and consent forms as well as written data from students (i.e., filled out study plans, test-taking strategy forms) were collected at the end of the second intervention session. Only researchers from our group had access to this office, the computers in it (and data stored on them), as well as to the cabinets (including filing cabinets).

3.3 Pilot Study Summary

A pilot study following the protocol described above was conducted in the Fall 2014 semester in all sections of CHEM 111. Initially, 84 volunteers were recruited such that 42 were assigned to each workshop group. This sample size was very close to our original request in the protocol (n = 80). Participant population in each workshop (Table 3.1), however, demonstrated substantial attrition as the semester progressed, making it challenging to draw conclusions from the limited amount of student data collected. Attrition may have occurred because of the volunteer nature of the study, which is further discussed in Section 3.4.

Although data analysis from the pilot study is not the focus of this chapter, sample qualitative and quantitative data are included for the purpose of providing insight into how students interacted with workshop materials. Figure 3.3 includes student responses to the writing

Table 3.1. Volunteer attendance throughout the intervention pilot study in Fall 2014.

Group	Initial recruitment	Session #1	Session #2	Session #3
Test-taking strategies	42	25	7	2
Metacognition strategies	42	18	6	0

activity that took place in the first workshop. Student 1 participated in the test-taking strategies workshop, and Student 2 participated in the exam preparation strategies workshop. These responses were chosen to exemplify ways that students interpreted the reflection questions that were posed to them and are not intended to be representative. Responses demonstrate that these two students were able to reflect on their study plan for Exam 1 and were able to articulate how they plan to modify their study plans for Exam 2 with the given prompt. Both students list specific strategies that they employed when studying for Exam 1 and that they had planned when studying for Exam 2. In addition to these qualitative data, quantitative pre- and post-MAI data (Table 3.2) were tabulated for student participants in each workshop series, as well as for CHEM 111 students who did not participate in any workshops. Comparing the difference between average pre- and post-workshop MAI scores provides a quantitative gain score metric referred to as "delta" in Table 3.2 [included for the overall MAI score as well as the knowledge of cognition (KC) and regulation of cognition (RC) sub-scores]. Positive delta values indicate an increase in score between the two instances in which the MAI was administered (Figure 3.1), whereas negative values indicate a decrease in score. Differences between pre and post MAI scores were not statistically significant for any group. This may be because of the small sample size and corresponding low statistical power, or because the interventions did not influence metacognitive awareness. Table 3.2 shows a non-statistically significant improvement in MAI score for the exam preparation strategies group (delta = 5.0), with concomitant non-statistically significant increases in both the KC and RC sub-scores (delta = 6.0 and 6.7, respectively). A negative delta value is observed for test-taking strategies group MAI score (delta = −1.8), as well as for the RC sub-score (delta = −1.6). Altogether, findings from MAI data presented here are preliminary and warrant further data collection for a larger sample size in future iterations of this study.

Student 1 (Exam 1 score: 37%, Exam 2 score: 57%)

1) What was your study plan for Exam 1?

"I made sure to review the past exam example, I went through the handouts that were given at recitation, I completed all of the ALEKS topics and understood them."

2) What made your study plan successful or unsuccessful?

"I believe that because a lot of the problems that I was studying were all worded in a particular way that I understood and when they were different on the exam it was like I didn't know how to even start more than half of the questions"

3) Will you change your study plan when studying for Exam 2? If yes, how and why will you change it? If no, why not?

"I do need to change the fact that I do not look at the problems in different ways. That was my biggest downfall. I also need to reread questions and make sure that I am answering what the question is asking. I also need to eliminate the distractor questions first. This will definitely help."

Student 2 (Exam 1 score: 43%, Exam 2 score: 67%)

1) What was your study plan for Exam 1?

"I made flash cards for the material we needed to memorize. I also planned to go over the book work and review the objectives in ALEKS. I also took the exam from last year that was posted online and went over those answers. I also went to all of the study sessions."

2) What made your study plan successful or unsuccessful?

"My study plan was unsuccessful because I did not leave myself enough time to do all of the things I planned. I starting studying the weekend before the exam which only gave me about 4 days to do it as well as study for two other exams I had that week. My flashcards however were successful in helping me to memorize the material we were supposed to memorize. Everything else though was done too quickly for me to actually learn the material."

3) Will you change your study plan when studying for Exam 2? If yes, how and why will you change it? If no, why not?

"Yes I will actually go over book problems and write questions about problems I am unsure of and ask the professor during office hours. I will also start studying now rather than saving everything until the end. I will do flashcards for vocab. I will also go to the study sessions again."

Figure 3.3. Sample student responses from the writing activity administered during workshop #1.

Table 3.2. Pre- and post- measures from the MAI for students who did not participate in the workshop, those in the test-taking strategies group, and those in the exam preparation strategies group.

Group	Mean MAI score (SD) [a]	Mean KC score (SD) [b]	Mean RC score (SD) [c]
No intervention (n=358)			
Pre-Exam 1	194.0 (20.5)	61.2 (7.0)	124.8 (14.2)
Post-Exam 4	191.9 (21.0)	65.2 (7.9)	126.7 (15.0)
delta	**–2.1**	**4.0**	**1.9**
Test-taking strategies (n=8)			
Pre-Exam 1	189.1 (21.8)	58.0 (8.2)	123.5 (13.7)
Post-Exam 4	187.3 (27.0)	65.4 (11.1)	121.9 (16.8)
delta	**–1.8**	**7.4**	**–1.6**
Exam preparation strategies (n=7)			
Pre-Exam 1	197.6 (35.7)	62.1 (8.5)	127.7 (25.2)
Post-Exam 4	202.6 (28.9)	68.1 (9.1)	134.4 (20.6)
delta	**5.0**	**6.0**	**6.7**

[a] Total MAI score (maximum = 260)
[b] Knowledge of cognition score (maximum = 85)
[c] Regulation of cognition score (maximum = 175)

Anecdotally, several students in both workshop groups spoke with me (as the facilitator) at the end of the first workshop and expressed that participating was informative and the workshop provided tools they felt were useful. Thus, it is possible that participants felt that they received enough information after the first workshop such that they did not feel compelled to attend future sessions, although there was no formal survey following the intervention.

3.4 Reflections and Alterations for Future Studies

Designing this intervention provided valuable insight regarding performing education research in an undergraduate course context. Working with such a large course (over 1000 students enrolled) meant access to a large population, but also required navigating logistics with multiple instructors within course schedule confines. Altogether, the design process was a productive experience, and the CHEM 111 student participants were positive and receptive to learning about their own learning.

A critical feature in the next iteration of this study is the inclusion of student-led focus groups to identify metacognitive skills and strategies used by general chemistry students during the exam preparation process. This may be more of a case-study based approach in comparison with the pilot study. Focus groups could include semi-structured interviews with think-aloud prompts, followed by qualitative coding of student responses. This knowledge could be used as a basis for designing the next iteration of intervention workshops, and would ideally make sessions more targeted and relatable for workshop participants (i.e., include skills that successful general chemistry students have employed in the past).

In future studies, it will also be important to incentivize participation to ensure student retention. This will likely introduce a new set of challenges and require more resources (e.g., workshop facilitators, coordination with course instructors for the integration of incentives

and/or the workshops themselves into the course structure). Furthermore, high-achieving students may already successfully utilize metacognitive skills in general chemistry and may not see the need for workshop participation. Thus, designing a different supplemental course activity by which these students could receive an equal incentive would be necessary. These challenges would need to be addressed before deploying the next iteration of workshops. Furthermore, follow-up surveys to collect student perspectives would be useful to integrate into further studies. Such surveys could be used as design tools to maximize workshop session utility to general chemistry students. Altogether, these alterations could provide an expanded understanding of preliminary data collected in the pilot study, further contributing to our knowledge of student metacognition in general chemistry settings.

REFERENCES

1. Flavell, J. H.; Miller, P. H.; Miller, S. A., *Cognitive Development*. 4 ed.; Prentice-Hall Englewood Cliffs, NJ: 2002.
2. Veenman, M. V.; Alexander, P., Learning to Self-monitor and Self-regulate. *Handbook of Research on Learning and Instruction* **2011**, 197-218.
3. Zohar, A.; Barzilai, S., A Review of Research on Metacognition in Science Education: Current and Future Directions. *Stud. Sci. Educ.* **2013,** *49* (2), 121-169.
4. Hacker, D. J.; Bol, L.; Horgan, D. D.; Rakow, E. A., Test Prediction and Performance in a Classroom Context. *J. Educ. Psychol.* **2000,** *92* (1), 160–170.
5. Nietfeld, J. L.; Cao, L.; Osborne, J. W., Metacognitive Monitoring Accuracy and Student Performance in the Postsecondary Classroom. *The Journal of Experimental Educational* **2005**, 7–28.
6. Nietfeld, J. L.; Cao, L.; Osborne, J. W., The Effect of Distributed Monitoring Exercises and Feedback on Performance, Monitoring Accuracy, and Self–efficacy. *Metacogn. Learn.* **2006,** *1* (2), 159–179.
7. Brewer, C. A.; Smith, D., Vision and Change in Undergraduate Biology Education: A Call to Action. *American Association for the Advancement of Science, Washington, DC* **2011**.
8. Anderson, J. R.; Greeno, J. G.; Reder, L. M.; Simon, H. A., Perspectives on Learning, Thinking, and Activity. *Educ. Res.* **2000,** *29* (4), 11-13.
9. Nietfeld, J. L.; Schraw, G., The Effect of Knowledge and Strategy Training on Monitoring Accuracy. *J. Exp. Educ.* **2002,** *95* (3), 131–142.
10. Paris, S. G.; Cross, D. R.; Lipson, M. Y., Informed Strategies for Learning: A Program to Improve Children's Reading Awareness and Comprehension. *J. Educ. Psychol.* **1984,** *76* (6), 1239.
11. Delclos, V. R.; Harrington, C., Effects of Strategy Monitoring and Proactive Instruction on Children's Problem-solving Performance. *J. Educ. Psychol.* **1991,** *83* (1), 35.
12. Amzil, A., The Effect of a Metacognitive Intervention on College Students' Reading Performance and Metacognitive Skills. *J. Educ. Dev. Psychol.* **2014,** *4* (1), 27.
13. Bandura, A., Social Cognitive Theory of Self-regulation. *Organ. Behav. Hum. Dec.* **1991,** *50* (2), 248-287.
14. Tanner, K. D., Promoting Student Metacognition. *CBE Life Sci. Educ.* **2012,** *11* (2), 113-120.
15. Dolly, J. P.; Williams, K. S., Teaching Testwiseness. In *1st Annual Meeting of the Northern Rocky Mountain Educational Research Association*, Jackson Hole, WY, 1983.
16. Dolly, J. P.; Williams, K. S., Using Test-taking Strategies to Maximize Multiple-choice Test Scores. *Educ. Psychol. Meas.* **1986,** *46* (3), 619-625.
17. Stough, L. M., The Effects of Test-Taking Strategy Instruction on the Processing of Test Items. In *Annual Meeting of the Southwest Educational Research Association*, Huston, TX, 1992.
18. Stough, L. M., Research on Multiple-Choice Questions: Implications for Strategy Instruction. In *71st Annual Convention of the Council for Exceptional Children* San Antonio, TX, 1993.
19. Institute of Education Sciences, U.S. Department of Education, and the National Science Foundation. Common Guidelines for Education Research and Development. **August 2013**.

20. Cattell, R. B., The Clinical Use of Difference Scores: Some Psychometric Problems. *Multivariate Experimental Clinical Research* **1983**.
21. Overall, J. E.; Woodward, J. A., Unreliability of Difference Scores: A Paradox for Measurement of Change. *Psychological Bulletin* **1975,** *82* (1), 85.
22. Gardner, R.; Neufeld, R. W., Use of the Simple Change Score in Correlational Analyses'. *Educ. Psychol. Meas.* **1987,** *47* (4), 849-864.
23. Knapp, T. R.; Schafer, W. D., From Gain Score t to ANCOVA F (and vice versa). *Practical Assessment, Research & Evaluation* **2009,** *14* (6), 1-7.
24. Dimitrov, D. M.; Rumrill Jr, P. D., Pretest-posttest Designs and Measurement of Change. *Work* **2003,** *20* (2), 159-165.

APPENDIX I: TABLES CORRESPONDING TO PART I1, CHAPTER 2

Table AI.1. Calibration statistics, Mann-Whitney U test results, and postdiction accuracy for male and female students from the Fall and Spring semesters.

Exam	Mean |calibration| [a]		U statistic (comparing |calibration|)	Effect size (r)	% accurate postdictions		Fisher's Exact *p value*
Fall	Male (N = 483)	Female (N = 442)			Male	Female	
Exam 1	1.95 (1.02)	1.77 (1.04)	97300	0.08	6.6	11.8	0.335
Exam 2	1.48 (1.02)	1.25 (0.98)	93535 [b]	0.11	16.4	23.5	0.216
Exam 3	1.03 (0.91)	0.89 (0.76)	99696	0.06	29.6	32.4	0.878
Exam 4	1.46 (1.09)	1.20 (1.00)	92284 [b]	0.12	20.5	26.0	0.409
Final	1.59 (1.08)	1.31 (1.00)	91483 [b]	0.13	15.3	22.6	0.207
Spring	Male (N = 207)	Female (N = 284)					
Exam 1	1.35 (1.03)	1.45 (1.05)	27822	0.05	15.9	16.9	1.000
Exam 2	1.19 (0.93)	1.00 (0.93)	25791	0.11	23.7	33.8	0.161
Exam 3	1.16 (0.96)	1.00 (1.02)	27739	0.05	27.5	31.7	0.540
Exam 4	1.02 (0.84)	0.99 (0.93)	28098	0.04	29.5	34.9	0.546
Final	1.40 (1.04)	1.45 (1.03)	28416	0.03	16.9	15.5	1.000

[a] Values for one standard deviation are included in parentheses. [b] Significant at the $\alpha = 0.01$ level.

Table AI.2. Exam performance data for male and female students from the Fall and Spring semesters.

Exam	Mean exam score[a]		Independent samples t statistic	Independent samples t-test p-value	Effect size (d)
Fall	Male (N = 483)	Female (N = 442)			
Exam 1	64.56 (15.12)	63.28 (15.63)	+ 0.995	0.320	+ 0.08
Exam 2	65.31 (13.60)	65.82 (14.37)	– 0.982	0.326	– 0.04
Exam 3	72.35 (13.69)	73.72 (13.88)	– 1.906	0.057	– 0.10
Exam 4	61.16 (15.34)	60.98 (15.78)	– 0.351	0.725	+ 0.01
Final	56.43 (15.60)	57.12 (16.00)	– 1.116	0.265	– 0.01
Spring	Male (N = 207)	Female (N = 284)			
Exam 1	63.07 (14.21)	61.51 (13.51)	+ 1.236	0.217	+ 0.01
Exam 2	67.60 (16.10)	66.76 (15.73)	+ 0.576	0.565	+ 0.05
Exam 3	64.13 (15.86)	63.77 (15.18)	+ 0.257	0.797	+ 0.02
Exam 4	67.93 (13.05)	69.15 (11.64)	– 1.085	0.278	– 0.10
Final	59.54 (16.34)	60.59 (15.03)	– 0.736	0.462	– 0.07

[a] Values for one standard deviation are included in parentheses.

Table AI.3. Sample sizes for students who were well calibrated and those who were not. [a]

Exam	Well-calibrated students (calibration = 0, ±1)	Not well-calibrated students (calibration = 0, ±2, ±3)
Fall		
Exam 1	345	580
Exam 2	549	376
Exam 3	713	212
Exam 4	557	368
Final	506	419
Spring		
Exam 1	267	224
Exam 2	349	142
Exam 3	340	151
Exam 4	365	126
Final	295	196

[a] Populations correspond to results presented in Table 3.

Table A1.4. Performance and calibration statistics for the high-performing and low-performing groups for the Fall and Spring semesters.

Exam	Mean exam score % [a] *M*	Mean exam score category [a]	Mean postdiction category [a]	Mean |calibration| [a]	% accurate postdictions
Fall					
Exam 1, mean = 64.29 [b]					
High-performing (N=88)	85.43 (5.45)	2.90 (0.61)	3.63 (0.69)	0.82 (0.58)	27.2
Low-performing (N=107)	44.23 (9.53)	0.00 (0.00)	2.22 (0.76)	2.22 (0.76)	0.4
Exam 2, mean = 65.82 [b]					
High-performing (N=88)	85.21 (6.03)	2.98 (0.62)	3.17 (0.76)	0.56 (0.54)	46.5
Low-performing (N=107)	47.00 (9.85)	0.06 (0.23)	1.90 (0.87)	1.84 (0.89)	6.5
Exam 3, mean = 73.37 [b]					
High-performing (N=88)	89.73 (4.33)	3.53 (0.50)	3.32 (0.70)	0.58 (0.56)	45.5
Low-performing (N=107)	53.52 (10.89)	0.35 (0.48)	1.53 (1.18)	1.36 (0.98)	18.7
Exam 4, mean = 61.49 [b]					
High-performing (N=88)	83.97 (7.59)	2.95 (0.77)	3.22 (0.81)	0.69 (0.67)	42.0
Low-performing (N=107)	40.75 (8.64)	0.00 (0.00)	1.32 (1.12)	1.32 (1.12)	23.4
Final, mean = 57.06 [b]					
High-performing (N=88)	80.84 (7.32)	2.58 (0.83)	3.19 (0.72)	0.75 (0.79)	43.1
Low-performing (N=107)	37.77 (6.98)	0.00 (0.00)	1.36 (1.14)	1.36 (1.14)	23.4
Spring					
Exam 1, mean = 62.16 [b]					
High-performing (N=41)	83.31 (7.78)	2.85 (0.76)	3.07 (0.87)	0.80 (0.71)	36.6
Low-performing (N=49)	45.25 (7.83)	0.00 (0.00)	1.63 (0.99)	1.63 (0.99)	14.3
Exam 2, mean = 67.11 [b]					
High-performing (N=41)	87.58 (6.52)	3.24 (0.66)	3.12 (0.90)	0.66 (0.79)	48.7
Low-performing (N=49)	44.94 (9.79)	0.06 (0.24)	1.14 (1.06)	1.39 (1.02)	20.4
Exam 3, mean = 63.92 [b]					
High-performing (N=41)	85.08 (6.76)	2.98 (0.65)	3.10 (0.89)	0.56 (0.67)	53.6
Low-performing (N=49)	42.92 (9.79)	0.00 (0.00)	1.22 (0.92)	1.22 (0.92)	24.5

Exam 4, mean = 68.63[b]					
High-performing (N=41)	84.89 (6.15)	2.93 (0.69)	3.02 (0.82)	0.59 (0.67)	53.6
Low-performing (N=49)	51.99 (7.01)	0.08 (0.28)	1.27 (0.95)	1.22 (0.96)	24.5
Final, mean = 60.15[b]					
High-performing (N=41)	84.81 (8.08)	2.95 (0.84)	3.12 (0.78)	0.66 (0.69)	46.3
Low-performing (N=49)	40.17 (8.40)	0.00 (0.00)	1.78 (0.94)	1.78 (0.94)	0.0

[a] Values for one standard deviation are included in parentheses. [b] Exam mean for the entire population.

Table AI.5. Mann-Whitney U test results comparing exam scores and |calibration| of high and low performing students.

Exam	U statistic (comparing exam score) [a]	Effect size (r)	U statistic (comparing |calibration|)	Effect size (r) [a]
Fall				
Exam 1	0	0.86	804	0.75
Exam 2	0	0.86	1144	0.68
Exam 3	0	0.86	2551	0.42
Exam 4	0	0.86	3202	0.29
Final	0	0.86	3235	0.28
Spring				
Exam 1	0	0.86	526	0.43
Exam 2	0	0.86	570	0.39
Exam 3	0	0.86	781	0.39
Exam 4	0	0.86	616	0.35
Final	0	0.86	358	0.59

[a] p-values ≤ 0.0001.

Table AI.6. Effect sizes (r) for comparisons between exam score category ($r_{\text{exam score category}}$) and |calibration| values ($r_{|\text{calibration}|}$) for high and low performing students

Exam pair	$r_{\text{exam score category}}$	$r_{|\text{calibration}|}$	$r_{|\text{calibration}|}/r_{\text{exam score category}}$
Fall: High performers (N=88)			
Exam 1/Exam 2	0.03	0.31	10.83
Exam 2/Exam 3	0.54	0.03	— [a]
Exam 3/Exam 4	0.62	0.14	— [a]
Exam 4/Final	0.34	0.05	— [a]
Fall: Low performers (N=107)			
Exam 1/Exam 2	0.23	0.34	1.48
Exam 2/Exam 3	0.43	0.43	0.99
Exam 3/Exam 4	0.75	0.01	0.02
Exam 4/Final	0.31	0.02	— [a]
Spring: High performers (N=41)			
Exam 1/Exam 2	0.44	0.14	0.32
Exam 2/Exam 3	0.29	0.11	0.37
Exam 3/Exam 4	0.01	0.06	— [a]
Exam 4/Final	0.04	0.09	— [a]
Spring: Low performers (N=49)			
Exam 1/Exam 2	0.01	0.29	— [a]
Exam 2/Exam 3	0.17	0.13	0.78
Exam 3/Exam 4	0.57	0.04	— [a]
Exam 4/Final	0.78	0.48	— [a]

[a] Only calculated for pairs of exams where mean |calibration| improved.

Table AI.7. Performance and calibration statistics for students who took the Spring course only (n=148).

Exam	Mean exam score %[a] *M*	Mean exam score category[a]	Mean postdiction category[a]	Mean |calibration|[a]	% accurate postdictions
Exam 1	59.66 (14.01)	0.85 (1.10)	2.24 (1.03)	1.45 (0.98)	19.6
Exam 2	63.26 (15.41)	1.20 (1.18)	2.13 (1.13)	0.93 (1.20)	29.1
Exam 3	59.61 (15.10)	0.92 (1.14)	1.91 (1.18)	1.10 (0.98)	30.4
Exam 4	65.08 (12.79)	1.26 (1.09)	1.97 (1.12)	1.04 (0.90)	31.1
Final	55.57 (14.67)	0.65 (0.86)	2.12 (1.05)	1.51 (0.98)	10.8

[a] Values for one standard deviation are included in parentheses.

Table AI.8. Effect sizes (r) for comparisons between exam score category ($r_{\text{exam score category}}$) and |calibration| values ($r_{|\text{calibration}|}$) for students who took the Spring course only (n=148).

Exam pair	$r_{\text{exam score category}}$	$r_{|\text{calibration}|}$	$r_{|\text{calibration}|}$/ $r_{\text{exam score cateogry}}$
Exam 1/Exam 2	0.24	0.27	1.16
Exam 2/Exam 3	0.27	0.02	0.07
Exam 3/Exam 4	0.37	0.05	0.13
Exam 4/Final	0.60	0.37	— [a]

[a] Only calculated for pairs of exams where mean |calibration| improved.

Table AI.9. Performance and calibration statistics for students who took both Fall and Spring courses.

Exam	Mean exam score % [a] *M*	Mean exam score category[a]	Mean postdiction category[a]	Mean |calibration|[a]	% Accurate Postdictions
Fall (N=343)					
Exam 1	69.87 (13.34)	1.51 (1.11)	3.15 (0.76)	1.67 (1.03)	11.9
Exam 2	71.68 (11.95)	1.67 (1.12)	2.64 (0.86)	1.17 (0.94)	24.8
Exam 3	78.95 (10.17)	2.44 (1.05)	2.59 (1.03)	0.84 (0.75)	34.7
Exam 4	67.79 (13.50)	1.45 (1.19)	2.45 (1.04)	1.22 (0.93)	23.0
Final	64.42 (13.93)	1.15 (1.10)	2.41 (0.96)	1.36 (0.97)	19.8
Spring (N=343)					
Exam 1	63.24 (13.61)	1.38 (1.06)	2.23 (1.05)	1.38 (1.06)	23.0
Exam 2	68.78 (15.80)	1.05 (0.90)	2.29 (1.09)	1.05 (0.90)	29.7
Exam 3	65.77 (15.25)	0.84 (0.75)	2.19 (1.09)	0.84 (0.75)	34.7
Exam 4	70.16 (11.71)	0.99 (0.89)	2.19 (1.15)	0.99 (0.89)	22.7
Final	62.12 (15.58)	1.39 (1.05)	2.29 (0.98)	1.39 (1.05)	19.8

[a] Values for one standard deviation are included in parentheses.

Table AI.10. Effect sizes (r) for comparisons between exam score category ($r_{\text{exam score category}}$) and |calibration| values ($r_{|\text{calibration}|}$) for students who took both Fall and Spring courses.

Exam pair	$r_{\text{exam score category}}$	$r_{|\text{calibration}|}$	$r_{|\text{calibration}|}$/ $r_{\text{exam score cateogry}}$
Fall (N=343)			
Exam 1/Exam 2	0.15	0.40	2.70
Exam 2/Exam 3	0.58	0.27	0.47
Exam 3/Exam 4	0.72	0.33	— [a]
Exam 4/Final	0.31	0.14	— [a]
Spring (N=343)			
Final (Fall)/ Exam 1	0.12	0.02	— [a]
Exam 1/Exam 2	0.39	0.27	0.69
Exam 2/Exam 3	0.24	0.06	0.25
Exam 3/Exam 4	0.32	0.13	— [a]
Exam 4/Final	0.55	0.33	— [a]

[a] Only calculated for pairs of exams where mean |calibration| improved.

APPENDIX II: SUPPLEMENTAL MATERIAL CORRESPONDING TO PART I1, CHAPTER 3

Metacognitive Awareness Inventory (MAI) (reproduced from Schraw and Dennison, 1994)

52 items on a 5-point likert scale (strongly agree → strongly disagree). 260 points total

35 Regulation of cognition (175 points possible)

Regulation of cognition (RC): planning (P), information management strategies (IMS), monitoring (M), debugging strategies (DS), and evaluation (E).

17 Knowledge of cognition (85 points possible)

Knowledge of cognition (KC): declarative knowledge (DK), procedural knowledge (PK), and conditional knowledge (CK).

Question	Strongly agree	Agree	Neural	Disagree	Strongly disagree
1. I ask myself periodically if I am meeting my goals.					
2. I consider several alternatives to a problem before I answer.					
3. I try to use strategies that have worked in the past.					
4. I pace myself while learning in order to have enough time.					
5. I understand my intellectual strengths and weaknesses.					
6. I think about what I really need to learn before I begin a task.					
7. I know how well I did once I finish a test.					
8. I set specific goals before I begin a task.					
9. I slow down when I encounter important information.					
10. I know what kind of information is most important to learn.					
11. I ask myself if I have considered all options when solving a problem.					
12. I am good at organizing information.					
13. I consciously focus my attention on important information.					
14. I have a specific purpose for each strategy I use.					
15. I learn best when I know something about the topic.					
16. I know what the teacher expects me to learn.					
17. I am good at remembering information.					
18. I use different learning strategies depending on the situation.					
19. I ask myself if there was an easier way to do things after I finish a task.					
20. I have control over how well I learn.					
21. I periodically review to help me understand important relationships.					
22. I ask myself questions about the material before I begin.					
23. I think of several ways to solve a problem and choose the best one.					
24. I summarize what I've learned after I finish.					
25. I ask others for help when I don't understand something.					
26. I can motivate myself to learn when I need to.					
27. I am aware of what strategies I use when I study.					
28. I find myself analyzing the usefulness of strategies while I study.					
29. I use my intellectual strengths to compensate for my weaknesses.					
30. I focus on the meaning and significance of new information.					
31. I create my own examples to make information more meaningful.					
32. I am a good judge of how well I understand something.					
33. I find myself using helpful learning strategies automatically.					
34. I find myself pausing regularly to check my comprehension.					
35. I know when each strategy I use will be most effective.					
36. I ask myself how well I accomplish my goals once I'm finished.					
37. I draw pictures or diagrams to help me understand while learning.					
38. I ask myself if I have considered all options after I solve a problem.					
39. I try to translate new information into my own words.					

40. I change strategies when I fail to understand.					
41. I use the organizational structure of the text to help me learn.					
42. I read instructions carefully before I begin a task.					
43. I ask myself if what I'm reading is related to what I already know.					
44. I reevaluate my assumptions when I get confused.					
45. I organize my time to best accomplish my goals.					
46. I learn more when I am interested in the topic.					
47. I try to break studying down into smaller steps.					
48. I focus on overall meaning rather than specifics.					
49. I ask myself questions about how well I am doing while I am learning something new.					
50. I ask myself if I learned as much as I could have once I finish a task.					
51. I stop and go back over new information that is not clear.					
52. I stop and reread when I get confused.					

1. I ask myself periodically if I am meeting my goals. **(M) RC**
2. I consider several alternatives to a problem before I answer. **(M) RC**
3. I try to use strategies that have worked in the past. (PK) **KC**
4. I pace myself while learning in order to have enough time. **(P) RC**
5. I understand my intellectual strengths and weaknesses. (DK) **KC**
6. I think about what I really need to learn before I begin a task. **(P) RC**
7. I know how well I did once I finish a test. **(E) RC**
8. I set specific goals before I begin a task. **(P) RC**
9. I slow down when I encounter important information. **(IMS) RC**
10. I know what kind of information is most important to learn. (DK) **KC**
11. I ask myself if I have considered all options when solving a problem. **(M) RC**
12. I am good at organizing information. (DK) **KC**
13. I consciously focus my attention on important information. **(IMS) RC**
14. I have a specific purpose for each strategy I use. (PK) **KC**
15. I learn best when I know something about the topic. (CK) **KC**
16. I know what the teacher expects me to learn. (DK) **KC**
17. I am good at remembering information. (DK) **KC**
18. I use different learning strategies depending on the situation. (CK) **KC**
19. I ask myself if there was an easier way to do things after I finish a task. **(E) RC**
20. I have control over how well I learn. (DK) **KC**
21. I periodically review to help me understand important relationships. **(M) RC**
22. I ask myself questions about the material before I begin. **(P) RC**
23. I think of several ways to solve a problem and choose the best one. **(P) RC**
24. I summarize what I've learned after I finish. **(E) RC**
25. I ask others for help when I don't understand something. **(DS) RC**
26. I can motivate myself to learn when I need to. (CK) **KC**
27. I am aware of what strategies I use when I study. (PK) **KC**
28. I find myself analyzing the usefulness of strategies while I study. **(M) RC**
29. I use my intellectual strengths to compensate for my weaknesses. (CK) **KC**
30. I focus on the meaning and significance of new information. **(IMS) RC**
31. I create my own examples to make information more meaningful. **(IMS) RC**
32. I am a good judge of how well I understand something. (DK) **KC**
33. I find myself using helpful learning strategies automatically. (PK) **KC**
34. I find myself pausing regularly to check my comprehension. **(M) RC**
35. I know when each strategy I use will be most effective. (CK) **KC**
36. I ask myself how well I accomplish my goals once I'm finished. **(E) RC**
37. I draw pictures or diagrams to help me understand while learning. **(IMS) RC**
38. I ask myself if I have considered all options after I solve a problem. **(E) RC**
39. I try to translate new information into my own words. **(IMS) RC**
40. I change strategies when I fail to understand. **(DS) RC**
41. I use the organizational structure of the text to help me learn. **(IMS) RC**
42. I read instructions carefully before I begin a task. **(P) RC**
43. I ask myself if what I'm reading is related to what I already know. **(IMS) RC**
44. I reevaluate my assumptions when I get confused. **(DS) RC**

45. I organize my time to best accomplish my goals. **(P) RC**
46. I learn more when I am interested in the topic. (DK) **KC**
47. I try to break studying down into smaller steps. **(IMS) RC**
48. I focus on overall meaning rather than specifics. **(IMS) RC**
49. I ask myself questions about how well I am doing while I am learning something new. **(M) RC**
50. I ask myself if I learned as much as I could have once I finish a task. **(E) RC**
51. I stop and go back over new information that is not clear. **(DS) RC**
52. I stop and reread when I get confused. **(DS) RC**

Multiple Choice Question Sets

Question set #1: Focus on distractor answer awareness (via common misconceptions/errors). These questions will be based on Exam 2 material, including electron configurations, quantum numbers, and naming compounds (assuming no change from Fall 2013 curriculum order).

1. What is the electron configuration for Kr?
A) $1s^2 2s^2 2p^6 3s^2 3p^4 3d^{10} 4s^2 4p^6$
B) $1s^2 2s^2 2p^6 3s^2 3p^6 4s^2 3d^{10} 4p^5$
C) $1s^2 2s^2 2p^6 3s^2 3p^6 4s^2 3d^{10} 4p^6$
D) $1s^2 2s^2 2p^6 3s^2 3p^2 4s^2 3d^{10} 4p^6$
E) none of the above

2. A tunicate is a marine invertebrate with blood that contains the transition metal vanadium (V). Which best represents the electron configuration of vanadium?

A) [Ne] 

B) [Ne] 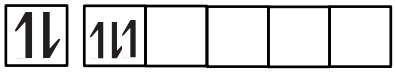

C) [Ne] 

D) [Ar] 

E) [Ar] 

3. As orbitals are filled with electrons, which correctly lists the subshells in order of increasing energy?
A) $1s < 2p < 2s$
B) $3s < 2p < 4s$
C) $4s < 4d < 4p$
D) $4d < 4p < 4s$
E) $4s < 3d < 4p$

4. How many unpaired electrons are in a ground-state carbon atom?
A) 12
B) 6
C) 4
D) 2
E) none of the above

5. Which element has the electron configuration of $1s^1 2s^2 2p^6 3s^2 3p^5$ and what column of the periodic table contains elements with similar properties?

A) O, halogens
B) Cl, halogens
C) F, halogens
D) O, noble gases
E) Cl, noble gases

6. How many valence electrons must a phosphorous atom gain in order to have a full valence shell?

A) 0
B) 1
C) 2
D) 3
E) 5

7. Each individual orbital in the "d" subshell can hold a maximum of _____ electrons.

A) 2
B) 5
C) 6
D) 10
E) none of the above

8. The size of an atom generally increases

A) down a group and from right to left across a period.
B) up a group and from left to right across a period.
C) down a group and from left to right across a period.
D) up a group and from right to left across a period.
E) up a group and diagonally across the Periodic Table.

Question set #2: Focus on reading the question completely (e.g., which is true versus which of the following is false) and eliminating unreasonable answer choices based on the problem context. These questions will be based on Exam 3 material, including mole calculations, periodic trends, Lewis structures/hybridization, and VSEPR (assuming no change from Fall 2013 curriculum order).

1. In comparing a balloon containing 25 grams of nitrogen to a balloon containing 25 grams of oxygen, which one of the statements is TRUE?

A) Each balloon has an equal number of atoms.
B) The oxygen balloon has more atoms.
C) The nitrogen balloon has more atoms.
D) This scenario cannot happen because gases have no mass.
E) none of the above

2. How many N atoms are in 2.25 moles of nitrogen gas?

A) 6.022×10^{23}
B) 9.03×10^{23}
C) 18.98
D) 2.71×10^{24}
E) none of the above

3. What is the electron geometry of a molecule with 3 electron groups around the central atom?
A) linear
B) trigonal planar
C) tetrahedral
D) trigonal pyramidal
E) not enough information

4. Atoms with small atomic radii tend to have _____ ionization energies, while atoms with large atomic radii tend to have _____ ionization energies.
A) high, low
B) low, high
C) low, low
D) high, high
E) None of the above

5. How many moles of Pt are in a 455 mg ring of pure platinum?
A) 2.33 mol
B) 2.33×10^{3} mol
C) 2.33×10^{-3} mol
D) 8.88×10^{4} mol
E) 88.8 mol

6. How many moles of water are needed to react with 2.2 moles of Li_2O?

Given: $Li_2O + H_2O \rightarrow 2\ LiOH$

A) 4.4
B) 2.2
C) 1.5
D) 1.1
E) 1.0

7. As orbitals are filled with electrons, which incorrectly lists the subshells in order of increasing energy?
A) $1s < 2s < 2p$
B) $2s < 2p < 3s$
C) $3s < 3p < 4s$
D) $3p < 3d < 4s$
E) $4p < 5s < 3d$

8. The second ionization energy of sodium (Na) is much higher than the first ionization energy because:

A) The second electron is removed from an already-stable noble gas core
B) The second electron is a valence electron
E) Na^+ has a larger radius than Na
D) The second ionization energy of Na not higher than the first ionization energy of Na.
E) None of the above

Reflection Activity: Test taking strategies

Exam 1: Reflect

1) What test taking strategies worked well for me that I should remember to use next time?

2) What test taking strategies did not work so well for me that I should change for next time?

3) Comment on your overall use of test taking strategies on Exam 1. Do you feel that these strategies help you on Exam 2? Why or why not?

4) Will you change the way that you use test-taking strategies on Exam 2? If yes, how and why will you change? If no, why not?

Writing Assignment: Workshop #1

Directions: Respond to the following questions in as much detail as you can in the allotted time period.

1) What was your study plan for Exam 1?

2) What made your study plan successful or unsuccessful?

3) Will you change your study plan when studying for Exam 2? If yes, how and why will you change it? If no, why not?

Study session template for test-taking strategies group

CHEM 111 study session guide

This guide is intended for your use when taking the posted practice exam for CHEM 111 Exam 2, ideally carried out individually. Please provide detailed answers in complete sentences. You may write on the back or on an attached sheet of paper if you need more room.

Please read all questions before you begin.

Provide an example of 2 multiple-choice questions from the practice exam in which you eliminated "distractor" answers. Please copy the questions on to this sheet of paper.

A)

B)

Copy 4 multiple-choice questions (different than the above two questions) from the practice exam on to this paper. Describe how you solved each question, detailing any strategies that you used in order to arrive at the final answer.
A) Question

How I solved this question

B) Question

How I solved this question

C) Question

How I solved this question

D) Question

How I solved this question

Study session template for exam preparation strategies group
(Questions adapted from Tanner (2014))

CHEM 111 study session guide

This guide is intended for your use during a single CHEM 111 Exam 2 study session of your choosing, ideally carried out individually. Please provide detailed answers in complete sentences. You may write on the back or on an attached sheet of paper if you need more room.

Please read all questions before you begin.

PLAN: Before you begin your study session, please answer these questions.

1) What are my goals for this study session, and what are all the things I need to do to successfully them?

2) Which aspects of the Exam 2 material should I spend more or less time on, based on my current understanding of what has been covered in lecture thus far?

MONITOR: At some point during your study session, please answer these questions:

3) What other resources could I be using to complete this task, and what action should I take to get them?

4) What is most challenging for me about this study session? Most confusing?

REFLECT: After your study session, please answer these questions:

5) Which of my confusions have I clarified during this study session, and *how* was I able to get them clarified?

6) Which confusions remain and *how* am I going to get them clarified?

Research Flyer

Are you struggling with CHEM 111 exams?

Participate in a 3-session exam preparation workshop, designed specifically for CHEM 111 exams.

Participants must be available between 7:00 pm and 9:00 pm on ALL of the following dates:

Wednesday, 9/24/14	**Piñon Hall, 131**
Wednesday, 10/15/14	**Piñon Hall, 131**
Wednesday, 11/05/14	**Piñon Hall, 131**

You will be randomly assigned to either a 7:00 pm – 8:00 pm or a 8:00 pm – 9:00 pm group.

Total time commitment is 3 ½ hours and is open to all students enrolled in CHEM 111. Space is limited (first-come, first-serve).

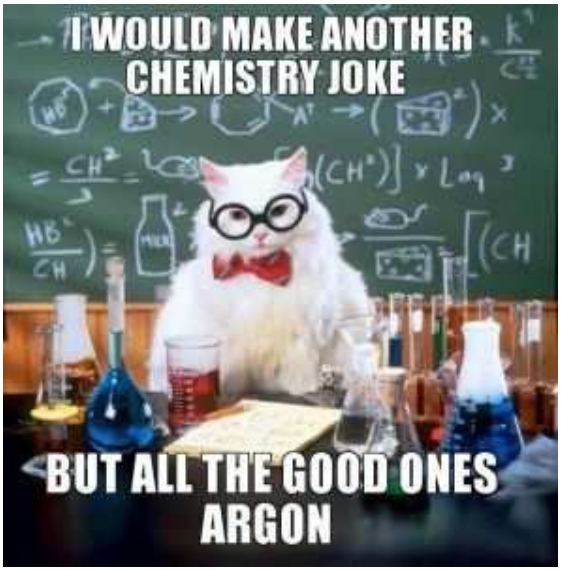

Recruitment E-mail

Dear CHEM 111 student,

I am writing to let you know about a series of exam preparation workshops for CHEM 111, available to all Fall 2014 CHEM 111 students. The main goal of these workshops is to help students to improve their exam preparation skills with regards to general chemistry exams.

Workshops will run on Wednesday evenings between the hours of 7:00 and 9:00 pm on the following dates (you will be randomly assigned to either a 7:00 pm-8:00 pm group or an 8:00 pm-9:00 pm group): 09/24/14, 10/15/14, and 11/05/14 in Piñon Hall, room 131. You will be expected to attend all three workshop dates.

Wednesday	9/24/14	7:00–9:00 pm	Piñon 131
Wednesday	10/15/14	7:00–9:00 pm	Piñon 131
Wednesday	11/05/14	7:00–9:00 pm	Piñon 131

Total volunteer time for participating in these workshops will be approximately 3 hours, plus an additional 30-minute activity, for a total of 3 ½ hours.

If you wish to volunteer or have any questions that pertain to this opportunity, please respond to this e-mail, or send me an e-mail (Morgan.Hawker@colostate.edu) by Wednesday, September 17th, 2014 at 11:59 pm.

Space in the workshops will be limited, and volunteers will be chosen on a first-come, first-serve basis.

Sincerely,
Morgan Hawker
Graduate Student
CSU Chemistry Department

LIST OF ABBREVIATIONS

PART I

2D	Two-dimensional
3D	Three-dimensional
ABS	Acrylonitrile butadiene styrene
ACS	American Chemical Society
AFM	Atomic force microscopy
allylNH	Allylamine
allylOH	Allyl alcohol
ANOVA	Analysis of variance
C/N (or N/C)	Carbon-to-nitrogen (or nitrogen-to-carbon) ratio
C/O (or O/C)	Carbon-to-oxygen (or oxygen-to-carbon) ratio
C_{1s}	Carbon 1s (XPS spectrum)
C_2H_4	Ethylene
C_3F_8	Octofluoropropane
CA	Contact angle
CAD	Computer assisted drafting
$CHCl_3$	Chloroform
CO_2	Carbon dioxide
CW	Continuous wave
d.c.	Duty cycle
DCM	Dichloromethane
E. coli	Escherichia coli
ECM	Extracellular matrix
EDS	Energy dispersive x-ray spectroscopy
F	Flow rate
F/C	Fluorine-to-carbon ratio
FC	Fluorocarbon
FTIR	Fourier transform infrared spectroscopy
FWHM	Full width at half maximum
GSNO	*S*-nitrosoglutathione
GSNO20	Tygon® film with 20% *S*-nitrosoglutathione incorporated (w/w)
GSNO5	Tygon® film with 5% *S*-nitrosoglutathione incopororated (w/w)
H_2	Diatomic hydrogen
H_2O	Water
HDF	Human dermal fibroblasts
HFPO	Hexafluoropropylene oxide

HMPA	2,2-bis(hydroxymethyl propionic acid)
IEP	Isoelectric point
IRB	Institutional Review Board
LTP	Low-temperature plasma
MA	Maximum amplitude (TEG)
M_n	Number average molecular weight
MeOH	Methanol
MRTG	Maximum rate of thrombus generation (TEG)
N_2	Diatomic nitrogen
NaCl	Sodium chloride
NBM	Nutrient broth media
NH_3	Ammonia
NO	Nitric oxide
NTC	Non-tissue culture (polystyrene)
O/N	Oxygen-to-nitrogen ratio
O•	Oxygen radical
OD	1,7-octadiene
OES	Optical emission spectroscopy
OH•	Hydroxide radical
P	Applied plasma power
p	Pressure
PBS	Phosphate buffered saline
PC	Polycarbonate
PCL	Polycaprolactone
PE	Polyethylene
PECVD	Plasma-enhanced chemical vapor deposition
PES	Polyethersulfone
PET	Polyethylene terephthalate
PGA	Polyglycolic acid
PI	Propidum iodide
PLA	Polylactic acid
PLGA	Polylactic-co-glycolic acid
PLGH	Carboxyl-functionalized polymer prepared from L-lactide, glycolide and 2,2-bis(hydroxymethyl propionic acid)
PPP	*Plasma Processes and Polymers*
PSF	Polysulfone
PTFE	Polytetrafluoroethylene
PVC	Polyvinyl chloride
R	Reaction time (TEG)
R_a	arithmetic average roughness

rf	Radio frequency
RMS	Root mean squared
R_q	Root mean square roughness
RSNO	*S*-nitrosothiol
SEM	Scanning electron microscopy
t	Time (associated with dynamic contact angle measurements)
TC	Tissue culture (polystyrene)
TEG	Thromboelastography
TMA	Time to maximum amplitude (TEG)
TMRTG	Time to maximum rate of thrombus generation (TEG)
ToF-SIMS	Time-of-flight secondary ion mass spectrometry
TTG	Total thrombus generation (TEG)
VASE	Variable angle spectroscopic ellipsometry
WCA	Water contact angle
XPS	X-ray photoelectron spectroscopy
$\theta_{advancing}$	Advancing water contact angle
$\theta_{receding}$	Receding water contact angle
θ_{static}	Static water contact angle

PART II

ANCOVA	Analysis of covariance
CHEM 111	General chemistry 1 course at Colorado State University
KC	Knowledge of cognition
M	Mean exam score
MAI	Metacognitive Awareness Inventory
$r_{\|calibration\|}$	Effect size of absolute calibration
r_{exam}	Effect size of exam score
RC	Regulation of cognition
STEM	Science, technology, engineering, and mathematics
VSEPR	Valence-shell electron-pair repulsion